MODELS FOR THE EVOLUTION OF THE CAROLINA TROUGH AND THEIR LIMITATIONS

by

BERNARD CELERIER

Ingenieur Civil des Mines
Ecole des Mines de Paris
(1979)

Submitted to the Department of Earth,
Atmospheric, and Planetary Sciences
in Partial Fulfillment of the
Requirements of the Degree of

DOCTOR OF PHILOSOPHY

at the

MASSACHUSETTS INSTITUTE OF TECHNOLOGY

March 1986

©Massachusetts Institute of Technology

Signature of Author . . . . . .
Department of Earth, Atmospheric, and Planetary Sciences
March 1986

Certified by . . . . . .
John G. Sclater
Thesis Supervisor

Accepted by . . . . . .
Chairman, Department Committee on Graduate Students

MASS. INST. TECH.
JUN 17 1986
LIBRARIES
WITHDRAWN FROM MIT LIBRARIES

MODELS FOR THE EVOLUTION OF THE CAROLINA TROUGH AND THEIR LIMITATIONS

by

BERNARD CELERIER

Submitted to the Department of Earth,
Atmospheric, and Planetary Sciences
in Partial Fulfillment of the
Requirements for the Degree of Doctor of Philosophy

ABSTRACT

This thesis applies extensional model to the Carolina trough in order to predict the evolution of this basin where only seismic stratigraphy is available. The validity of these predictions is estimated by studying the effect of data uncertainties and model assumptions. A very simple model is applied first. Further complications are then introduced in order to better account for the data.

The simplest model is applied in order to obtain first order results and evaluate the error range due to data uncertainty. It is a one dimensional uniform extension model, which uses McKenzie's (1978) analytical formulae for the thermal evolution, coupled with a local isostatic response to the sedimentary load. Lateral transfer of heat and sediment thermal blanketing effects are ignored. The results show that the amount of extension is poorly constrained landward of the hinge zone due to data uncertainties. The predicted crustal thickness is not compatible with gravity data; the early predicted paleowaterdepths do not look very realistic and are not compatible with the inferred shelf environment especially landward of the hinge zone. Overall predicted Cretaceous water depths tend to be too deep but to analyze this secondary problem further would require more information about the amount of sediments eroded during the evolution of the Carolina trough.

The next model is applied in order to correct the problems encountered before. It is a two dimensional uniform extension model, where the thermal evolution is numerically simulated (Sawyer, 1982), coupled with a flexural response to the load. Lateral heat flow and thermal blanketing are taken into account and the flexural plate thickness is controlled by the depth to a relaxation temperature T_R. For a value of 350°C for T_R, the predicted crustal thickness is reasonably compatible with gravity data and the predicted paleowaterdepth and stratigraphy look more realistic. However the early paleowaterdepth predictions are still too deep landward of the hinge zone, suggesting higher initial heat input than accounted by uniform extension. As for the one dimensional model there is a secondary problem of overall too deep predicted Cretaceous water depth. The effect of

lateral heat flow and thermal blanketing are significant but small compared to the effect of data uncertainties; the major contributor to the better account of the data is the introduction of flexural rigidity.

The final model is applied in order to correct the paleowaterdepth problem encountered landward of the hinge zone and in order to obtain an upper bound on the initial amount of heat which could affect thermal predictions. It is a two dimensional two layer extension model, also based on Sawyer's (1982) simulation, where the initial conditions are modified for two layer extension (Royden and Keen, 1980; Sclater et al., 1980). Inverting for a deep thermal anomaly on which there is no direct control raises a few difficulties. However it can be concluded that the inferred paleowaterdepth landward of the hinge zone of the Carolina trough can be explained in that framework only by assuming a much larger subcrustal heat input than predicted by uniform extension.

The validity of the predicted thermal evolution, for which no independent check is available, is estimated by comparing the results of the different models. Most of the differences occur during the early evolution of the basin (less than 30 MY after end of rifting) and fade away after. The flexural plate thickness which initially varies a lot laterally becomes uniform 80 MY after end of rifting. The sediment thermal history depends on the timing of their burial. If buried soon enough (less than 30 MY after rifting) they are sensitive to model assumptions. If buried later they are more sensitive to the equilibrium thermal state. As a result the present degree of hydrocarbon maturation of synrift and early post-rift sediment is model dependent and varies from mature to overmature. The present shallowest limit of maturation is more dependent on the present geotherm which remains to be measured; this limit roughly follows the top Callovian (163 MYBP) reflector but may reach the Kimmeridgian (152 MYBP) if a large radiogenic heat generation is assumed for the sediments.

Thesis Supervisor: Dr. John G. Sclater

Title: Associate Director
Institute for Geophysics
University of Texas at Austin

CONTENT

ACKNOWLEDGMENTS

John Sclater initiated this project and provided encouragment to keep it (me) going. He reminded me, as many times as I forgot it, that the trees I was studying were part of a forest and he fully demonstrated to me that a Scottish ghost can be alive and well.

Dale Sawyer introduced me to continental margin modeling and provided the simulation for a good part of this thesis (Chapters 5,6 & 7).

Kim Klitgord provided the stratigraphy, which is the main constraint on the models, guided my review of the geology of the East Coast continental margin (Chapter 3) and helped clear away administrative problems.

Debby Hutchinson showed me how to modify her gravity model for the purpose of this study; the program used in that gravity modeling was written by Evelyn Wright.

Discussions with Luce Fleitout, Steve Hellinger and Dale Sawyer were helpfull in assessing the geodynamic concepts of basin formation (Chapter 2).

My understanding of the geology of the East Coast continental margin was developed through discussions with Bill Dillon, John Grow, Wylie Poag, Peter Popenoe and Anne Swift and critical reviews (of Chapter 3) by James Austin, Debby Hutchinson, Kim Klitgord and John Schlee.

Wiki Royden, Dale Sawyer, John Sclater, Mike Steckler and Tony Watts influenced the modeling (Chapter 4,5,6) through stimulating comments. Discussions with Steve Daly helped sort out the confusion created by heat diffusion in two layer extension.

Reviews of this thesis and earlier drafts by Cindy Ebinger, Debby Huchinson, Jack Jemsek, Kim Klitgord, Barry Parsons, Wiki Royden, Dale Sawyer, John Sclater and Dick Von Herzen improved the style.

This and earlier drafts were typed by Dorothy Frank and Lee Mortimer.

Many other people at MIT, at the Woods-Hole USGS Branch as well as at the USGS Denver and Reston Multics systems helped in many ways. Even if a few were only doing their job, I am gratefull to those who did it cheerfully and efficiently. I believe that they know it and therefore will not take the risk of making an uncomplete list. However, Jimmy, who cleaned my office and let me in when I was locked out during all these years, may not be aware of his contribution and I wish to thank him.

Funding for this project was provided by the USGS and my first nine months at MIT were supported by a fellowship from the French " Ministere des affaires etrangeres ".

I am also deeply indebted to all the people, fellow students, scientists and staff (not forgetting the tuff schists) who brought human warmth inside work, at MIT, at the USGS, or on occasionnal trips. If their input was not directly related to this thesis, to be among them was one of the main motivations during the years spent working on it.

Above all, this thesis is dedicated to those who enriched these last years with their affection.

"La grandeur d'un métier est, peut-être, avant tout, d'unir les hommes: il n'est qu'un luxe véritable, et c'est celui des relations humaines"

A. de Saint Exupery, Terre des hommes.

J'ai l'esprit tout ennuye
D'avoir trop etudie
Les Phenomenes d'Arate :
Il est temps que je m'ebatte
Et que j'aille aux champs jouer.
Bons Dieux ! qui voudrait louer
Ceux qui colles sur un livre
N'ont jamais souci de vivre ?

Que nous sert d'etudier,
Sinon de nous ennuyer
Et soin dessus soin accroitre
A nous, qui serons peut-etre
Ou ce matin, ou ce soir,
Victime de l'Orque noir,
De l'Orque qui ne pardonne,
Tant il est fier, a personne !

Corydon, marche devant;
Sache ou le bon vin se vend;
Fait rafraichir ma bouteille,
Cherche une fueilleuse treille
Et des fleurs pour me coucher;
Ne m'achete point de chair,
Car tant soit elle friande,
L'ete je hais la viande.

Achete des abricots,
Des pompons, des artichauts,
Des fraises et de la creme :
C'est en ete ce que j'aime
Quand sur le bord d'un ruisseau
Je la mange au bruit de l'eau,
Etendu sur le rivage
Ou dans une antre sauvage.

Ores que je suis dispos,
Je veux rire sans repos,
De peur que la maladie
Un de ces jours ne me die,
Je t'ai maintenant vaincu :
Meurs galant, c'est trop vecu.

Pierre de Ronsard , 1554

CHAPTER I

INTRODUCTION

Resist beginnings

Ovid, Remediorum amoris

1.1 THE PROBLEM

The goal of this thesis is to apply extensional models to predict the evolution of the Carolina trough which is a basin of the Eastern United States Continental margin where no deep well has been drilled but where seismic stratigraphy is available.

Because the data suffer from a significant uncertainty range it appeared necessary to evaluate the effect of these uncertainties on the predictions. It also appeared necessary to evaluate the effect of model assumptions on the predictions because both the data uncertainties and the lack of information about pre- and syn-rift conditions left these assumptions underconstrained.

1.2 STRATEGY

The simplest model (one-dimensional model) is applied first because, aside from economy of means, it is the easiest to constrain. In addition it best allows us to trace the effect of assumptions on predictions.

Both because the effect of different assumptions need to be studied and because the data are not fully accounted for by the simplest model, more and more complicated models are then introduced. As complexity increases so does the degree of freedom of the models. As a result, they tend to become less and less constrained and to account for the data more and more. Such a procedure allows us to estimate the effect of each extra complication by comparing the results of a given model with the one obtained by the next simpler model. The last applied model (two dimensional two layer model) exhausted the constraints and reasonably accounted for most available data.

We also introduce extreme data sets to evaluate the effect of data error (Chapter 3).

This results in a series of models differing either in data sets or model assumptions [Table 1.1].

1.3 THESIS OUTLINE

Chapter 2 summarizes the evolution of ideas on basin genesis and the problems associated with current models. It also explains how we choose and implemented suitable models for the Carolina trough.

Chapter 3 reviews the geology of the Carolina trough in order to justify the use of extensional models and sort out constraint on them. The standard constraining data set (basement depth and sediment properties) is completed by extreme data sets to evaluate the prediction error range.

The simplest model is applied in Chapter 4 (technical details in Appendix A and B) in order to obtain preliminary results where first order effects can be easily sorted out and in order to evaluate the prediction error range due to data uncertainties. The tectonic model is a one dimensional uniform extension model and uses McKenzie's (1978a) analytical formulae. It therefore neglects lateral heat transfer and the sediment thermal blanketing effect. The loading response is assumed to satisfy local isostasy. The constraint on the model is the present total subsidence (obtained through basement and water depth) which determine the amount of extension, β, once the loading effect is removed. The independent checks are the gravity data and inferred paleowaterdepth.

The next model (Chapter 5 and Appendix C) is a two dimensional uniform extension model which includes the effect of lateral heat flow and sediment thermal blanketing. The loading response is that of an elastic plate; the bottom of the plate is defined as the depth where the relaxation temperature, T_R is reached. This model relies on a finite difference simulation for the basin evolution developed by Sawyer (1982). The constraints on the model are the tectonic subsidence which determines β and the gravity data which determine T_R. The independent checks are the inferred paleowaterdepth.

The last model (Chapter 6 and Appendix D) is a modification of the previous one in order to incorporate two layer extension (Royden and Keen, 1980; Sclater *et al.*, 1980) in the two dimensional simulation of Sawyer (1982). The loading response remains the same as in the previous case. The constraints on the model are the tectonic subsidence which determine the crustal extension factor, β_c, the gravity data which determine T_R, and the inferred early paleowaterdepth which determine the subcrustal extension

factor, βsc. This model therefore exhausted the constraints and there is no independent check on it.

Whereas in chapter 4 to 6, I concentrate on predictions which can be checked: mainly crustal extension factor which can be checked against gravity data and subsidence data which can be checked against geologically inferred paleogeography, Chapter 7 concentrates on the thermal predictions for which there is no direct check. I then concentrate on the comparison between the different models predictions in order to evaluate their variability. These thermal predictions are then used to estimate the degree of hydrocarbon maturation of the sediments.

Table 1.1

MODELS DEVELOPED IN THIS THESIS

extension (**) type	thermal calculations: dimension	blanketing	origin time	loading response T_R (°C)	data set (***)		Chapter
uniform	1-D	no	200	local	n	ϕ	4
uniform	1-D	no	200	local	n	ϕ_{max}	4
uniform	1-D	no	200	local	n	ϕ_{min}	4
uniform	1-D	no	200	local	b	ϕ	4
uniform	1-D	no	200	local	b	ϕ_{max}	4
uniform	1-D	no	200	local	b	ϕ_{min}	4
uniform	1-D	no	200	local	h	ϕ	4
uniform	1-D	no	200	local	h	ϕ_{max}	4
uniform	1-D	no	200	local	h	ϕ_{min}	4
uniform	1-D	no	175	local	n	ϕ	4
uniform	1-D	no	175	local	n	ϕ_{max}	4
uniform	1-D	no	175	local	n	ϕ_{min}	4
uniform	1-D	no	175	local	b	ϕ	4
uniform	1-D	no	175	local	b	ϕ_{max}	4
uniform	1-D	no	175	local	b	ϕ_{min}	4
uniform	1-D	no	175	local	h	ϕ	4
uniform	1-D	no	175	local	h	ϕ_{max}	4
uniform	1-D	no	175	local	h	ϕ_{min}	4
uniform	2-D	yes	200	0 (local)	n	ϕ	5
uniform	2-D	yes	200	200	n	ϕ	5
uniform	2-D	yes	200	250	n	ϕ	5
uniform	2-D	yes	200	300	n	ϕ	5
uniform	2-D	yes	200	200(*)	n	ϕ	5
uniform	2-D	yes	200	250(*)	n	ϕ	5
uniform	2-D	yes	175	0	n	ϕ	5
uniform	2-D	yes	175	250	n	ϕ	5
uniform	2-D	yes	175	300	n	ϕ	5
uniform	2-D	yes	175	350	n	ϕ	5
uniform	2-D	yes	175	350	b	ϕ_{max}	5
uniform	2-D	yes	175	350	h	ϕ_{min}	5
uniform	2-D	yes	175	400	n	ϕ	5
2L model 0	2-D	yes	175	400	n	ϕ	6
2L model 12	2-D	yes	175	400	n	ϕ	6
2L model 23	2-D	yes	175	400	n	ϕ	6
2L model 31	2-D	yes	175	400	n	ϕ	6

(*) :models where synrift sediments are also compensated flexurally (in all other models synrift sediment are compensated locally)
(**) :2L refers to two layer extension
(***):n = normal basement estimate
h = shallowest basement estimate
b = deepest basement estimate
ϕ = normal porosity estimate
ϕ_{max} = maximal porosity estimate
ϕ_{min} = minimal porosity estimate

CHAPTER II

BACKGROUND: MODELS OF PASSIVE MARGIN EVOLUTION

> No theory is good except on condition that one uses it to go beyond.
>
> A. Gide, Journals, 1918

2.1 IDEAS ON BASINS

When the idea that sediment loading alone could not explain the subsidence of a sedimentary basin (see Scheidegger and O'Keefe, 1967; Watts and Ryan, 1976) was accepted, gravity data and the concept of Airy isostasy with compensation below the Moho suggested that the crust under sedimentary basins must be thinner or denser than normal (Hsu, 1958). That it is thinner was later confirmed by seismological work (see, for example, Sheridan, 1969). That compensation occurs at much greater depth than the Moho (100 km as opposed to 40 km) suggested that slight variations of density within the mantle could also account for subsidence; these variations of densities could be related to thermal expansion (Hsu, 1965). Ocean-floor studies strengthened that idea (Vogt and Ostenso, 1967) and analysis of well data showed that the eastern United States continental margin subsidence could be explained by thermal cooling of the lithosphere with a time constant similar to that of the ocean floor (Sleep, 1971).

However a thermal anomaly alone would lead to initial uplift and, as it decays, to a return to the initial elevation with no net subsidence. Therefore the development of a sedimentary basin requires the occurrence of another event which either thins (Sleep, 1971) or increases the density of the crust (Falvey, 1974). These two events, crustal change and deeper heat input, do not have to be synchronous (Hsu, 1965; Sleep, 1973; Sengor and Burke, 1978; Sclater et al., 1980), to involve the same spatial scales (Hellinger and Sclater, 1983) or to occur over the same time scales.

From these observations and concepts, two main models have been developed (Sengor and Burke, 1978).

The first one, "active rifting" considers that the original and determinant event is the thermal anomaly. This implies that the early phase of rifting is characterized by a regional uplift (Sleep, 1971; Falvey, 1974; Falvey and Middleton, 1981). The crustal event posed a problem since it was argued that the thermal event could not generate enough tensile stresses to stretch the crust (Artemjev and Artyushkov, 1971, Salveson, 1978, Fitton, 1983). It was then suggested that the crust was thinned either by subaerial erosion (Sleep, 1971), but the amounts involved appeared unrealistic, or by subcrustal erosion or delamination (Artyushkov, 1981). Deep metamorphism could also increase the crust

density (Falvey, 1974; Falvey and Middleton, 1981). More recent work claims that crustal extension actually can be produced by thermal anomalies at depth (Artyushkov, 1973; Fleitout and Froidevaux, 1982).

The second model, "passive rifting", considers extension as the primary phenomenon; the thermal anomaly is then viewed as the result of passive upwelling of hot mantle by isostatic response (Artemjev and Artyushkov, 1971; Tapponnier and Francheteau, 1978; Salveson, 1978; McKenzie, 1978a). This simple model, the uniform extension model, allowed for a lot of quantitative predictions (McKenzie, 1978a). One of the sharpest differences with the "active" model is that here the initiation is characterized by an isostatic adjustment which produces quick and eventually large initial subsidence instead of uplift. It is followed by a long-term subsidence due to thermal contraction of the cooling lithosphere as that of Sleep (1971). This model was quickly and widely applied to back arc basins (McKenzie, 1978b; Angelier, 1981), continental basins (Sclater and Christie, 1980; Sclater et al., 1980; Steckler and Watts, 1980; Brunet and LePichon, 1982; Wood and Barton, 1983) and continental margins (Steckler and Watts, 1978; Watts and Steckler, 1979, 1981; Royden and Keen, 1980; Royden et al., 1980; Watremez, 1980; Cochran, 1981; Keen et al., 1981; LePichon and Sibuet, 1981; Sawyer et al., 1982a, 1982b; Sawyer, 1982; Beaumont et al., 1982) and found to be reasonably compatible with the data. Its popularity was further reinforced by the observation of crustal extension (Profett, 1977; McKenzie, 1978b; Salveson, 1978; DeCharpal et al., 1978; LePichon and Sibuet, 1981; Bally et al., 1981; Wernicke et al., 1982a,b).

However, evidence against large initial subsidence (Royden and Keen, 1980; Sclater et al., 1980; Royden et al., 1983), the existence of marginal uplift (Hellinger and Sclater, 1983; Steckler, 1985) and evidence of differential extension at depth (Camus, 1981; Avedik et al., 1982; Chenet et al., 1982; Ginzburg et al. 1985) led to a third model, the non-uniform or two-layer extension model. This model seems to reunite "active" and "passive" rifting by decoupling the crustal extension from the lower lithosphere "extension" which appears as a simple representation of a deep thermal anomaly; according to the relative importance of crustal and subcrustal stretching, initial uplift or subsidence can be predicted. The

lithosphere is considered to be composed of a brittle and a ductile layer (Artemjev and Artyushkov, 1971; Salveson, 1978; Tapponnier and Francheteau, 1978). In this model, the extra heat brought by secondary convection under the flanks of a rift zone can be represented by thinning of the lower lithosphere (Buck, 1984; Fleitout et al., in press, Steckler, 1985). Finally if one sees rifting as controlled by a few active hot spots (Morgan, 1983) then one should expect the relative importance of active and passive mechanisms to vary along strike, as allowed by this model.

2.2 PROBLEMS OF MODELS

2.2.1 Uplift or not?

An essential criteria to consider when selecting models is how much initial uplift or subsidence occurred during the early evolution (20-30 MY after onset of rifting) of basins. Unfortunately this early evolution is recorded in the deepest, therefore least known, sediments of most basins. Hence the continuing arguments for and against the existence of an uplift phase (Kent, 1980). In most cases it is not clear whether the "post rift unconformity" occurs during emergence (Falvey, 1974) or under deep water (De Charpal et al., 1978). It could be an indication either of uplift or of a change in structural style from fault controlled subsidence to more regional subsidence. Moreover, uplift, as long as confined to the periphery of a basin, can be accommodated within an extensional framework by effects of lateral heat transfer (Watremez, 1980; Watts et al., 1982), flexural response (Watts et al., 1982) or non-uniform extension (Hellinger and Sclater, 1983; Steckler, 1985).

2.2.2 Loading response

The models discussed above deal with the "tectonic subsidence" only, i.e., the subsidence that a basin would undergo if it were not filled with sediments. They must then be combined with a model for the loading response of the lithosphere in order to be compared with the observed total subsidence. This loading response is poorly understood (Watts, et al., 1982) but its contribution to the total subsidence is of the same order of magnitude as that of tectonic models. Any comparison relating data to the tectonic model is done after correcting with a poorly known loading response model.

2.3 CHOOSING A MODEL FOR THE CAROLINA TROUGH

Both the geology of the east coast continental margin of the United States (Chapter 3) and previous work concentrating on the Baltimore Canyon trough and Georges Bank basin where both well and seismic reflection data are available, show that extension models are a useful framework of investigation (Steckler and Watts, 1978, Watts and Steckler, 1979, 1981; Sawyer, 1982; Sawyer et al., 1982a, 1982b).

In this thesis, I apply these models to the Carolina trough, also located on the East coast continental margin, where seismic stratigraphy is available but where no deep well has been drilled, in order to obtain predictions on its tectonic and thermal evolution. The linear geometry of this basin makes it particularly suitable for two dimensional modeling (Hutchinson et al., 1982).

I concentrate on the uniform extension model (McKenzie, 1978a) for two reasons. First, previous work in other basins of the Eastern United States continental margin (Watts and Steckler, 1981; Sawyer, 1982; Sawyer et al., 1982a, 1982b) found it reasonably compatible with subsidence data from up to 140 MYBP even though the oldest data deviate from it. Second, the lack of reliable early paleowaterdepth data within the Carolina trough make it difficult to constrain the extra degree of freedom brought in by non uniform extension. Moreover the extension coefficient obtained by uniform extension should be very similar to the crustal extension that would be predicted by two layer extension in a basin as old as the Carolina trough. I will, however, also consider non uniform extension, as underconstrained as it will be, as a mean of evaluating the sensitivity of the results to this assumption.

Rifting started onshore 225 MYBP at the earliest and finished 175 MYBP with the onset of oceanic spreading (see Chapter 3). Rifting may then have lasted a maximum of 50 MY, but a duration of 20 MY might be more appropriate for the offshore basins (Schlee and Klitgord, in press). I prefer to use the instantaneous extensional model (McKenzie, 1978a) instead of the finite extension rate model (Jarvis and McKenzie, 1980) firstly because the range of possible durations of rifting is too wide to exploit the extra information brought by the latter model, secondly because it is simpler, and thirdly because the difference between these two models, assuming the longest rifting duration, remains acceptable though not negligible. I will evaluate the error involved by that approximation by considering two different origin times: 200 MYBP and 175 MYBP.

2.4 APPLICATION OF THE EXTENSION MODEL TO A MARGIN

McKenzie (1978a) studied the evolution of a column of lithosphere which is uniformly stretched (Appendix A), and where initial and thermal subsidence can be computed analytically by assuming a local isostatic response. However, in a continental margin the amount of stretching should vary from the continent to the ocean, as well as we expect the response of the lithosphere to the sediment loading to increase the subsidence. We then model the evolution of such a margin by the three following steps:

2.4.1 Pre-rift stage

We consider the lithosphere to be divided into a series of columns (Fig. 2.1a) which are assumed to be of the same thickness and to be in thermal equilibrium. These two assumptions are debatable: the last Appalachian orogenic events, the Alleghenian events, are Permian and occurred 50 to 80 MY before rifting started (Chapter 3).

2.4.2 Rift stage: initial subsidence

Each column undergoes a different amount of stretching (Fig. 2.1b). We assume that the isostatic response is local as did McKenzie (1978a) so that the subsidence of each column can be treated independently from the others. This simplification is also arguable since the flexural rigidity of the thinned lithosphere affects the initial configuration by adding a slight doming effect to the main subsidence effect, as shown for mid-oceanic ridges (Tapponnier and Francheteau, 1978).

The model considers the "rift stage" crust (see Hutchinson et al., 1982) as stretched continental crust. This concept cannot be extended to the oceanic crust which is generated in a different fashion. Neither can one consider that the oceanic part corresponds to an infinite stretching since that would not leave any crust. I therefore define the initial oceanic lithosphere to have a finite crustal thickness and a thermal state compatible with mid-oceanic ridge observations and to be isostatically balanced with the unstretched continental lithosphere. The boundary between the two models, stretched continent and ocean, will be taken at the East Coast Magnetic Anomaly which marks edge of the oceanic crust (Chapter 3). The details of this procedure are given in Appendix A.

2.4.3 Post-rift stage: thermal subsidence and loading

The sediment loading and the slow disappearance of the thermal anomaly (Fig. 2.1c) which corresponds to the drifting of the continent away from the spreading center increase the subsidence. This subsidence can be evaluated in two different ways:

In the first way, the one dimensional model (Chapter 4 and Appendix A), we assume that the behavior of each column is not influenced by its neighbors. We then assume Airy pointwise isostasy for the loading response (Appendix B) and neglect the effect of the lateral heat flow in the thermal calculations. We can then apply McKenzie's (1978a) analytical solutions to evaluate the thermal subsidence. This approach does not take into account the thermal blanketing effect of the sediments.

In the second way, the two dimensional model (Chapter 5 and Appendix C), we will take into account both the flexural rigidity of the lithosphere for the loading response, and the effect of lateral heat flow and thermal blanketing by the sediments for the thermal calculation. The schematized cross section of the margin (Fig. 2.1b) is treated as a whole; McKenzie's (1978a) analytical formula can no longer be applied and is replaced by a finite difference computer simulation designed by Sawyer (1982) which solves the heat equation numerically. This simulation, besides predicting the subsidence history, allows us to keep track of the temperature history of any packet of deposited sediments, which can be applied to predicting hydrocarbon maturity (Royden et al., 1980).

In this two dimensional framework, I also will apply a non uniform extension model (Chapter 6 and Appendix D) which appears just as a different setting of the initial conditions.

The simpler one dimensional model is used first to give first order results and to evaluate various sources of errors in these predictions. The more complex 2-D simulation is used to give more detailed subsidence and thermal predictions. Non-uniform extension is used to estimate the effect on the thermal predictions of extra subcrustal heat suggested by the early paleogeography of the basin. Since these models do not take into account the actual geometry of stretching by normal faults, they will be acceptable only if we are interested in features which have a longer wavelength than the spacing between faults. This is probably valid for the thermal and loading parts of the subsidence but may not be valid for the initial subsidence.

Figure Caption

Fig. 2.1. Application of extensional models to a margin (we only represent the crustal part).

2.1a: Before extension we consider the future margin as a set of blocks.

2.1b: Each block has been extended by a different amount β.

2.1c: The blocks have subsided thermally and have been loaded by sediments.

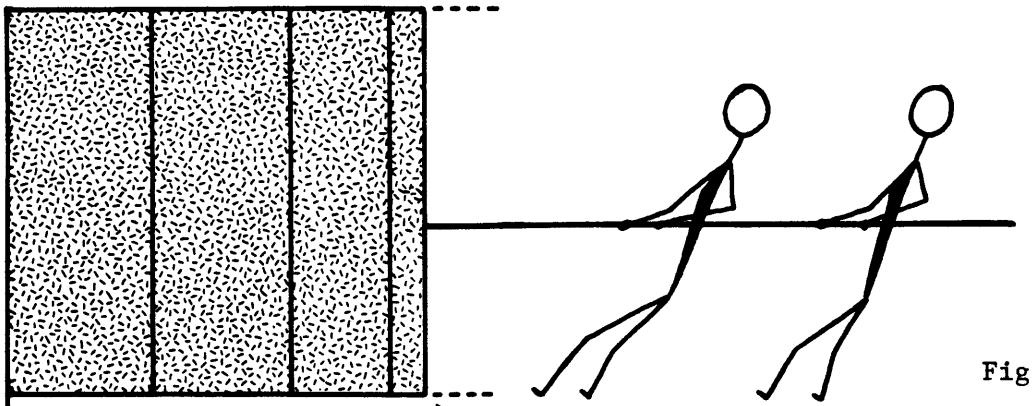

Fig. 2.1a

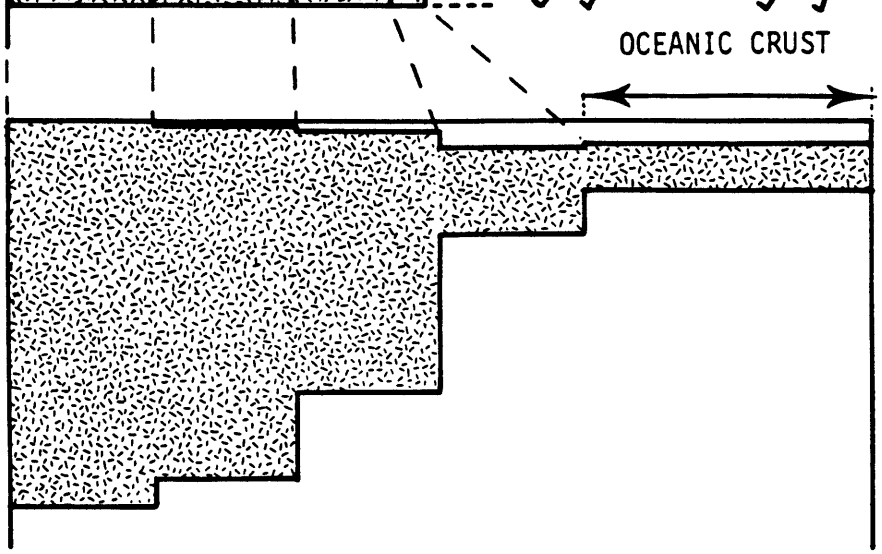

Fig. 2.1b

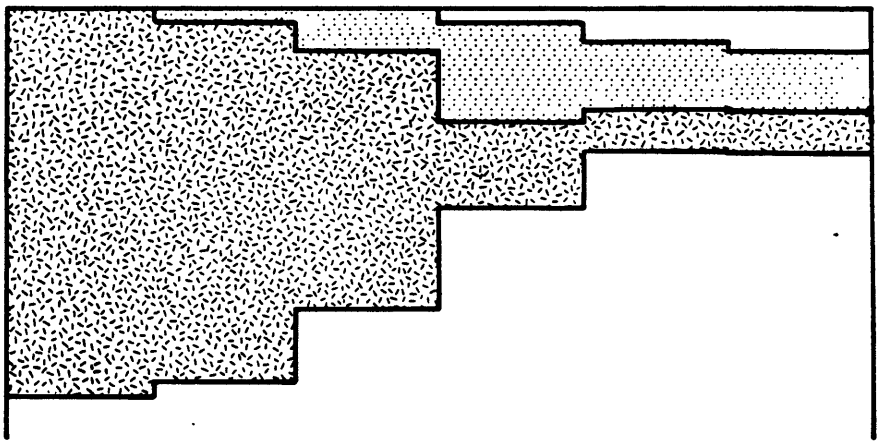

Fig. 2.1c

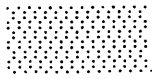

Sediments

Crust

CHAPTER III

BACKGROUND: THE CAROLINA TROUGH

> It is a capital mistake to theorize before one has data
>
> Sir Conan Doyle, "Scandal in Bohemia", 1891

3.1 INTRODUCTION

This section has four main goals.

First, to show that the regional geology and the seismic stratigraphy within the Carolina trough support an extensional origin for that basin despite the lack of definite evidence of extension in it.

Second, to evaluate the rifting duration and the origin time of thermal decay since these factors are crucial in establishing initial condition for our model.

Third, to also evaluate the paleogeography since it is the only truly independent check that we have on the rates of subsidence that our model is going to predict. The early paleogeography is the most crucial since it strongly constrains the amount of heat input; unfortunately, it also happens to be the least known.

Fourth, to describe the constraints that we derive from the data for the modelling: the origin time of thermal decay, the sediment budget, the sediment properties, the total present subsidence.

Because data on the Carolina trough are limited to seismic stratigraphy which is controlled only by wells in neighboring basins, we will have to rely on regional trends. We will then try as much as possible to discuss for each topic not only what is known, and how it is known, but where it is known, which is the best way, in our mind, to estimate the reliability of what remains an extrapolation.

3.2 PHYSICAL DESCRIPTION

The Carolina trough belongs to a series of basins located on the East Coast of North America which are linked with the opening of the Atlantic Ocean (Heezen, 1968, 1974): the Scotian, Georges Bank, Baltimore Canyon, Carolina Trough and Blake Plateau offshore basins and Newark group onshore basins (Klitgord and Behrendt, 1979) (Fig. 3.1).

It is separated from the Blake Plateau basin to the south by the Blake Spur fracture zone and from the Baltimore Canyon trough to the north by the Norfolk fracture zone; it is bounded on its landward side by the Brunswick Magnetic Anomaly [BMA] and on its seaward side by the East Coast Magnetic Anomaly [ECMA] (Klitgord and Behrendt, 1979). Recent COCORP profiles in Georgia suggest that the BMA is associated with a Paleozoic suture (Nelson

et al., 1985). The ECMA is interpreted as the edge of the oceanic crust (Keen, 1969; Klitgord and Behrendt, 1979), an interpretation supported by refraction and gravity studies (Sheridan et al., 1979; Grow et al., 1979a, Hutchinson et al., 1982).

This trough is a deep (more than 11 km of post Paleozoic sediments) and narrow (200 km wide) linear feature which strikes along the axis of opening of the Atlantic ocean (Klitgord and Behrendt, 1979, Grow and Sheridan, 1981, 1982). It is then particularly suitable for two dimensional modeling and is well represented by a cross section (Hutchinson et al., 1982). We show such a cross section (Fig. 3.2) where the stratigraphy (Table 3.1) is interpreted from USGS seismic reflection line 32 (Klitgord, unpublished work) and the Moho depth is estimated by gravity modeling (Fig. 3.3) (Hutchinson et al., 1982). This gravity model is subject to potentially large errors due to the poor control on sediment densities in the deepest part of the basin (Barton, in press).

3.3 TECTONIC HISTORY

3.3.1 Rifting

Regionally, the basement and synrift sediments have been studied in the Newark group of basins (Cornet et al., 1973; Cornet and Traverse, 1975; Van Houten, 1977, 1980; Olsen, 1980; Olsen et al., 1982), and drilled in the Scotian basin (Jansa and Wade, 1975; Given 1977) and the Georges Bank basin (Austin et al., 1980; Scholle and Wenkam, 1982; Poag, 1982a,b; Schlee and Fritsch, 1982; Schlee and Klitgord, in press). Related basins in Morocco yield strikingly similar information (Cousminer and Manspeizer, 1976; Manspeizer et al., 1978).

In all these places the Mesozoic sediments are separated from the basement by a major unconformity which truncates older structures and includes a depositional gap from at least Middle Permian (270 MYBP; time scale from Harland et al., 1982) to Middle Triassic (230 MYBP) (Jansa and Wade, 1975; Given, 1977; Van Houten, 1977, 1980; Manspeizer et al., 1978; Olsen, 1980; Poag, 1982a). The existence of such a gap as well as the fact that deposition starts at the same time in Acadian as in Alleghenian regions as well as in Morocco shows that the Middle Triassic tectonics is not a continuation of the Appalachian orogeny, which ended with the Alleghenian events before Mid-Permian, but a new extensional regime (Van Houten, 1977; Manspeizer et

al., 1978) even if it is influenced by these older structures (Ballard and Uchupi, 1975; Burke, 1976; Van Houten, 1977; Given, 1977). The basal unconformity is then considered as the rift onset unconformity (Falvey, 1974; Given, 1977). From the published observations, it is not clear whether this unconformity is a consequence of uplift (Ballard and Uchupi, 1975; Van Houten, 1980) or stability (Van Houten, 1977); neither is it clear whether, if uplift is considered, this uplift would be generalized or limited to the flanks of the basins and if it would have occurred just before or long before rifting; this latter possibility would relate it to older orogeny.

The oldest synrift sediments have been paleontologically dated as Carnian (231-225 MYBP) in the Newark group (Cornet et al., 1973; Olsen et al., 1982) and on the Grand Banks (Jansa et al., 1980), landward of the hinge zone. Seaward of the hinge zone the oldest sediments are inferred as Middle Triassic (243-231 MYBP) in the Scotian basin (Jansa and Wade, 1975); late Triassic (231-213 MYBP) microfossils have been found in the Georges Bank basin (Poag, 1982a; Cousminer et al., 1984), but these are likely to be reworked sediments (Schlee and Klitgord, in press). These sediments are essentially non-marine in the Newark and Scotian basins (Jansa and Wade, 1975; Van Houten, 1977, 1980; Olsen, 1980) with eventual marine incursions in Georges Bank basin (Poag, 1982a; Valentine, 1982; Cousminer et al., 1984) and suggest a large initial subsidence by their coarse base in the Newark basin (Van Houten, 1977) as well as by their large thickness in the Georges Bank basin (Schlee and Fritsch, 1982).

The deposition is strongly fault controlled in all these places (Sanders, 1963, Cornet et al., 1973; Jansa and Wade, 1975; Ballard and Uchupi, 1975; Given, 1977; Van Houten, 1977, 1980; Austin et al., 1980; Schlee and Fritsch, 1982) and accompanied by a first intense igneous event (Van Houten, 1977; Manspeizer, 1980) which has been radiometrically dated to peak at 191 MYBP (Sutter and Smith, 1979).

It should be noted that reliable ages for the synrift sediments are available only for those basins located landward of the hinge zone (Schlee and Klitgord, in press). The subsequent evolution also seems to differentiate the basins situated on each side of the hinge zone.

Landward, the Newark group stopped subsiding, their youngest sediments being dated as Sinemurian (206-200 MYBP) (Cornet et al., 1973; Olsen et al., 1982) and was uplifted and eroded, while seismic stratigraphy suggests the same evolution for the basins of the Long Island platform located landward of the hinge zone (Hutchinson et al., in press).

Seaward, continuing subsidence and marine invasion is recorded by salt deposits (Jansa and Wade, 1975; Folger et al., 1979; Austin et al., 1980; Poag, 1982a; Schlee and Fritsch, 1982). In the Scotian basin, pollen indicates that the salt can be Carnian (231-225 MYBP) to Liassic (213-188 MYBP) (Walton and Berti, 1978) while in Georges Bank a Late Triassic (231-213 MYBP) age estimate (Poag, 1982a) may also be biased because of reworked sediments (Schlee and Klitgord, in press). These evaporites are synrift for three reasons: firstly they are dated younger than the onset of oceanic spreading in Nova Scotia (Walton and Berti, 1978; Jansa et al., 1980), secondly they are observed only on non-oceanic crust (Van Houten, 1977) except in Nova Scotia (Uchupi and Austin, 1979) where they might have flowed since emplacement (Austin, personal communication); thirdly because they are inferred below the Post Rift Unconformity in the Baltimore Canyon trough (Grow, 1980; Schlee and Jansa, 1981).

In the Carolina trough, a strong seismic reflector (reflector 19, Fig. 3.2) supports the existence of salt (Grow and Markl, 1977; Dillon et al., 1982); it is observed only between the hinge zone and the ECMA, thus on non-oceanic crust. Below that reflector it is difficult to trace any coherent arrival: the basement depth is then only poorly estimated and the nature and thickness of older synrift sediments is unknown. Landward of the hinge zone, a Triassic or older graben is inferred below the Brunswick magnetic anomaly which also corresponds to a negative gravity anomaly and to landward dipping reflectors within the acoustic basement (Klitgord and Behrendt, 1979; Hutchinson et al., 1982). However the existence of that graben remains conjectural since diffraction caused by an eroded basement surface or by an inferred Paleozoic suture zone (Nelson et al., 1985) could also account for these anomalous reflectors. Thus, there is no definite evidence of block faulting of the basement in that basin.

3.3.2 Onset of Oceanic Spreading

The onset of oceanic spreading is estimated at 175 MYBP independently by extrapolation from sea floor magnetic and drilling data (Klitgord and Grow, 1980) and by radiometric dating (Sutter and Smith, 1979) of a second widespread igneous event which is believed to occur at or just before spreading (Scrutton, 1973) as confirmed by paleomagnetism (Smith and Noltimier, 1979).

There are three conspicuous geological records closely related in time to that event: firstly an influx of clastics (Schlee and Jansa, 1981; Uchupi et al., 1982) is observed in the Scotian (Jansa and Wade, 1975) and Georges Bank basins (Austin et al., 1980; Poag, 1982a; Schlee and Fritsch, 1982); secondly, a series of dikes accompanied by normal faults which cut through the synrift sediments (Van Houten, 1977) and which are thought to be related to the opening stress field (May, 1971); thirdly, the Post Rift Unconformity observed in the Scotian (Uchupi and Austin, 1979), Georges Bank (Uchupi and Austin, 1979; Austin et al., 1980; Schlee and Fritsch, 1982), Baltimore Canyon (Grow, 1980; Schlee, 1981) and Carolina trough basins (Dillon et al., 1982; Hutchinson et al., 1982) and interpreted as Falvey's (1974) breakup unconformity.

The Post Rift Unconformity (PRU) has been interpreted as an indication of emergence (Falvey, 1974; Austin et al., 1980; Hutchinson et al., 1982) or of uplift (Ballard and Uchupi, 1975), but observations only show evidence of erosion limited to the landward periphery or to the basement highs of the basins (Given, 1977; Uchupi and Austin, 1979; Austin et al., 1980; Schlee and Jansa, 1981; Grow and Sheridan, 1981; Schlee and Klitgord, in press). Recent seismic interpretation documents that, on the Long Island Platform, uplift and erosion occurred landward of the hinge zone, while seaward of it deposition seems continuous through the PRU (Hutchinson et al., in press). Moreover, when occurring on basement highs, this unconformity is often indistinguishable from the rift onset unconformity which can be related to erosion occuring long before rifting. The oldest sediments overlying this unconformity have been paleontologically dated from Late Early Jurassic (200 to 175 MYBP) in the Scotian basin (Barss et al., 1979) to Bajocian-Bathonian (181-169 MYBP) in Georges Bank (Ascoli, 1983; Schlee and Klitgord, in press).

All this shows that the same geometrical unconformity can be associated with different events at different places and that it may also be time transgressive. In the Carolina trough, landward of the hinge zone, the Post Rift Unconformity (Dillon et al., 1982; Hutchinson et al., 1982) is indistinguishable from the rift onset unconformity except over the inferred Brunswick graben, and may have been associated with some erosion (Hutchinson et al., 1982). Seaward of the hinge zone it is not observed and is therefore assumed to coincide with the top of the inferred synrift salt.

3.3.3 Post rift sedimentation

Regionally, the post-rift are more evenly distributed than the synrift sediments (Burke, 1976; Folger et al., 1979; Schlee and Fritsch, 1982). A fault controlled Cenozoic depocenter on the Florida-Hatteras shelf appears to be an exception (Paull and Dillon, 1980).

The seismic data suggest that a paleoslope developed in the late Jurassic in the Carolina trough and that from late Jurassic to present, sedimentation occurred at shallow depth landward of this slope as observed in the Blake Plateau to the south (Dillon et al., 1985), and in northern basins (Austin et al., 1980; Schlee and Jansa, 1981; Schlee, 1981; Schlee and Fritsch, 1982).

During the Jurassic, the inferred setting for the Carolina trough is a shallow water carbonate platform bordered seaward by a reef which controlled the position of the slope as observed in northern basins (Schlee et al., 1979; Austin et al., 1980; Schlee and Jansa, 1981; Grow and Sheridan, 1982; Schlee and Fritsch, 1982). However the existence of that reef has not been proven and it may have been eroded during the Cenozoic.

In the northern basins the Cretaceous started with a regression and was marked by a growing influx of clastics which buried the reef (McIver, 1972; Jansa and Wade, 1975; Given, 1977; Austin et al., 1980; Schlee and Jansa, 1981; Uchupi et al., 1982; Schlee and Fritsch, 1982). By the late Cretaceous, the water depth above the shelf may have increased (Popenoe, 1985) as observed in the Southeast Georgia Embayment (Poag and Hall, 1979) and in the Blake Plateau (Pinet and Popenoe, 1985; Dillon et al., 1985).

The Cenozoic is marked by major erosions (Grow and Markl, 1977; Grow et al., 1979b; Dillon et al., 1979, 1985; Schlee et al., 1979; Folger et al., 1979; Austin et al., 1980; Uchupi et al., 1982; Schlee and Fritsch, 1982; Popenoe, 1985). These events can be correlated not only with a major mid-Oligocene sea level drop (Vail et al., 1977) but also with the onset of two currents during the Eocene: the shallower Gulf Stream flowing to the North and the deeper cold Western Boundary Undercurrent (Uchupi et al., 1982; Mountain and Tucholke, 1985; Popenoe, 1985) due to the opening of Arctic water to the Atlantic (Burke, 1977, 1979). The Gulf Stream eroded the shelf during sea level high stand and the upper slope during sea level low stand while the Western Boundary Undercurrent eroded the slope and rise (Popenoe, 1985). As a result the slope in the Carolina trough was cut back by about 30 km (Grow and Markl, 1977). In the Carolina trough these erosions were followed by an intense Miocene and younger sedimentation on the continental rise which pushed the slope seaward again (Grow and Markl, 1977).

3.3.4 Conclusion

(1) Rifting started around 225 MYBP (Carnian) onshore and eventually later, during the Triassic, offshore since it seems to have shifted from the former to the latter location (Sanders, 1963; Van Houten, 1977; Schlee and Fritsch, 1982; Klitgord et al., 1983; Hutchinson et al., in press). While rifting stopped and may have been followed by an episode of uplift onshore, continuing subsidence led to marine invasion and evaporite deposition offshore.

The whole evolution is qualitatively compatible with a model which predicts a fault controlled initial subsidence due to crustal extension, and eventual uplift on the flanks due to either flexural response, lateral heat transfer or more intense subcrustal "extension".

(2) Spreading started 175 MYBP (Bathonian) and was followed by a slower subsidence, also more regular in space, compatible with the thermal subsidence predicted by extensional models. The major perturbations to the sedimentation can be attributed to sea level changes or oceanic currents rather than to local tectonic events.

3.4 PALEOWATERDEPTH

Past subsidence predictions can be checked by past sediment thickness and paleowaterdepth. The seismic stratigraphy gives some estimate of past paleowaterdepth across the Carolina trough (Klitgord, unpublished work). For that, we divide the cross section along line 32 (Fig. 3.2) into 5 parts:

Zone A (Shot Points 800 to 2000):

This zone corresponds today to the shelf: its water depth is less than 50 m. The oldest sediments are late Jurassic which may mean that this area was either emergent or at sea level from rifting until late Jurassic. From Late Jurassic until today deposition occurred in shallow water.

Zone B (Shot Points 2000 to 3100):

This zone extends from the present shelf break up to the basement hinge zone. The oldest sediments are mid-Jurassic hence this area must have been at or above sea level until that time. From then until the Eocene deposition occurred in shallow water. Since the Eocene, the Gulf Stream has eroded this shelf and, as a result, water depth varies from 200 m to 600 m today.

Zone C (Shot Points 3100 to 4200):

This zone extends from the hinge zone to the late Jurassic paleoshelf edge. The oldest sediments are synrift and until late Jurassic the paleowaterdepth is unknown. From late Jurassic until Eocene shelf deposition is inferred (less than 200 m of water depth). Since the Eocene, Gulf Stream erosions increased the water depth which today varies from 700m to 2200m. Also salt tectonics have been active in this zone since the Jurassic (Dillon et al., 1982) and may have altered the total stratigraphic thickness.

Zone D (Shot Point 4200 to 4600):

This zone extends from the Jurassic shelf break to the ECMA. Two markers are present here: the ECMA and a salt diapir. The ECMA represents the oceanward edge of rifted crust, while the salt diapir is believed to mark the oceanward edge of the synrift deposits. Paleowaterdepth is unknown until late Jurassic; from then on it seems to be a continental rise environment.

Zone E (Shot Point 4600 to 5600):

This area is underlain by oceanic crust. Rise environment has prevailed since oceanic spreading began and the oldest sediments would be middle Jurassic in age. Intense sedimentation has occurred since the Miocene.

3.5 CONSTRAINTS ON THE MODELS

We use three sources of information to constrain our models and we evaluate their error ranges.

3.5.1 Origin time of thermal decay

Our model will assume instantaneous rifting even though rifting may have started as early as 225 MYBP or as late as 195 MYBP and terminated with oceanic spreading 175 MYBP.

In order to evaluate the errors involved in that approximation we will consider two cases:

- in the first case we assume an instantaneous rifting and spreading event at 200 MYBP. The synrift sediments are then deposited between 200 MYBP time and 175 MYBP.

- in the second case we assume an instantaneous rifting and spreading event at 175 MYBP. The synrift sediments are then instantaneously deposited at 175 MYBP.

In both cases the post rift sediment will be added progressively after 175 MYBP.

3.5.2 Present total subsidence and sediment budget

The fundamental constraint on all the models that we will discuss is that the tectonic subsidence they predict for today added to the loading effect of the present sediment pile equals exactly the present basement depth. This requires knowing both the present water and basement depth. Moreover, past reconstructions will require us to know the past sediment thickness. All these sediment thicknesses are obtained from the USGS seismic line 32 (Klitgord, unpublished data) which has been chosen as the base of our model because of its good basement reflections. We model the section from SP 800 (40 km from the coastline) to SP 5600 (280 km from the coastline) by 25 columns of equal width (10 km or 200 Shot Points). Estimates of the ages of the reflectors identified on that line are given on Table 3.1 and their depth is shown on Fig. 3.2.

We ignored the Brunswick graben in the modeling that we present here because its existence is still conjectural. It is not known if it is a syn-or pre-rift structure, and its geometry is not well defined. Moreover in

an attempt to include it we realized that the model would attribute its subsidence to a Moho upwarp right below it. This did not appear to be a good assumption because of the implied narrow horizontal scale. A salt diapir located around SP 4400 has also been neglected because our modelling could not simulate the flow of salt through time; the depths of the reflectors which were affected by this diapir have been replaced by values interpolated between neighboring shot points.

Because there is no clear basement reflection between shot points 3400 and 5200: we considered, apart from a standard interpretation taken from Hutchinson et al. (1982), two extreme interpretations. Overall, even when the problem of interpretation is settled, an assumed uncertainty of 10% on seismic velocities led to an extra 10% of error on the depths. This results in 3 sets of basement depth: a best estimate and two extreme estimates (Fig. 3.4).

3.5.3 Sediment physical properties

Because there is no deep well within the Carolina trough, the physical properties of the sediments are not known; therefore we used the properties from the 4 COST wells drilled in the Georges Bank and Baltimore Canyon basins. The porosity can be be represented by an exponential function of depth and the observed range of porosities can be bounded by two extreme exponential laws (Fig. 3.5) (Sawyer, 1982). Even though these extreme laws are conservative estimates for the error range on the entire sedimentary column, we think it is reasonable to use them because we are applying sediment properties from other basins to the Carolina trough where the lithologies are not yet known.

TABLE 3.1

Seismic Reflectors Observed on Line 32
[Klitgord, unpublished work]

SHELF

label	Definition			Datation						Correlation	
	type	explanation	ref	type	explanation	ref	d	Age (geologic)	Age (MYBP) (*)	type	ref
1	2	seafloor	-	-	-	-	-	present	0	-	-
2	1		a	1	COST B2,B3	a	?	top Pliocene	2	1	c
3	1		a	1	COST B2,B3	a	?	top Miocene	5.5	1	c
4	1		a	1	COST B2,B3	a	?	top middle Miocene	11	1	c
555	1		a	1,3	COST B2,B3	a	?	top Oligocene	24.5	2	c
6	1	unconformity	a	1	COST B2,B3	a	?	middle Oligocene	31	1	c
7	1		a	1	COST B2,B3	a	?	Cretaceous top (Kt)	65	1	c
8	1		a	1	COST B2,B3	a	?	top Coniacian	87.5	2	c
10	1		a	1	COST B2,B3	a	?	top lower Cretaceous	97.5	1	c
11	1		a	1	COST B2,B3	a	?	top Neocomian	125	1	c
12	1		a	1	COST B2,B3	a	?	Jurassic top (Jt)	144	1	c
13	1		a	1	COST B2,B3	a	?	Tithonian	145	2	c
14	1,2		b	1	COST G1,G2	b	?	Kimmeridgian	152	2,4	c
15	1,2		b	1	COST G1,G2	b	?	top Callovian	163	2,4	c
16	1,2		b	1,3	COST G1,G2	b	?	top Bathonian	169	3,4	c
19	1,2	PRU-Salt top	b	1	COST G1,G2	b	?	Bathonian	175	3,4	c
20	2	Basement	b	-	COST G1,G2	b	y	-	-	-	c

DEEP SEA

label	Definition			Datation						Correlation	
	type	explanation	ref	type	explanation	ref	d	Age (geologic)	Age (MYBP) (*)	type	ref
1	2	seafloor	-	-	-	-	-	present	0	-	-
2	1	blue	d	1	DSDP	d	?	top Pliocene	2	1	c
3	1		d	1	DSDP	d	?	top Miocene	5.5	3	c
4	1	marlin	d	1	DSDP	d	?	top middle Miocene	11	1	c
5	1	X	d	1	DSDP	d	?	middle lower Miocene	22	1	c
555	1		d	1	DSDP	d	?	top Oligocene	24.5	3	c
6	1	A^u	d	1	DSDP	d	?	middle Oligocene	31	1	c
7	1	A^*	d	1	DSDP	d	?	Cretaceous top (Kt)	65	1	c
8	1		d	1	DSDP	d	?	top Coniacian	87.5	3	c
10	1		d	1	DSDP	d	?	top lower Cretaceous	97.5	3	c
11	1	β	d	1	DSDP	d	?	top Neocomian	125	1	c
12	1,2	J1	e	1,2	DSDP	e	?	Jurassic top (Jt)	144	1	c
15	2	J2	e	2	-	e	?	top Callovian	163	1	c
16	2	J3	e	2	-	e	?	top Bathonian	169	1	c
20	2	Basement	-	-	-	-	y	-	-	-	c

Definition types: Where and how is the reflector defined
(1): Observed at a given depth in a well
(2): Observed at a given time on a seismic line

Datation types: How the age of the reflector is estimated
(1): By fossils in a well
(2): By pinch-out on magnetically dated oceanic crust
(3): By correlation with "global unconformities" (Vail et al., 1977)

Correlation types: How is the reflector on line 32 linked to the place where it was defined.
(1) Traced continuously through seismic line network from definition area to USGS line 32
(2) Traced discontinuously but with confidence
(3) Traced discontinuously with doubts
(4) Correlated by sequence similarity

d : diachronous or not (y/n) ?

* Age from Harland et al. (1982)

References: a: Poag, 1985
b: Poag, 1982b; Ascoli, 1983
c: Klitgord, unpublished work
d: Tucholke & Mountain, 1979
& Mountain & Tucholke, 1985
e: Klitgord & Grow, 1980

Figure Captions

Fig. 3.1. Western Atlantic continental margin (modified after Klitgord and Behrendt, 1979).

Fig. 3.2. Simplified stratigraphy of line 32.
For modeling purpose, the depth to the reflectors [from Klitgord, unpublished work] are taken every 10 km on a 25 column grid. As a result the detailed geometry of the contacts is not faithfully represented. Age of reflectors are given in Table 3.1. Dashed line corresponds to absence of clear reflections. Zone A, B, C, D, E correspond to different paleoenvironment histories.

Fig. 3.3. Gravity model along USGS seismic line 32 (Hutchinson et al.,1982).

Fig. 3.4. Uncertainties on the basement depth.
Standard estimate, Interpretation range and Range including interpretation range and velocity error (Extreme range) are shown.

Fig. 3.5. Porosity versus depth for all lithologies from core samples in the COST B2, B3, G1 and G2 Wells (from Sawyer, 1982). The porosity versus depth relationship will be taken of the form: $\phi(Z) = \phi(0) \exp(-CZ)$, where $\phi(Z)$ is the porosity at sub-bottom depth Z. The average behavior of these sediments can be represented by: $\phi(0) = 55\%$ and $C = 0.43$ km^{-1}, while two extreme behavior would be obtained for: $\phi(0) = 25\%$ and $C = 0.6$ km^{-1} and $\phi(0) = 75\%$ and $C = 0.3$ km^{-1}. The density of the matrix will be assumed to be: $\rho_r = 2.7$ g/cm^3.

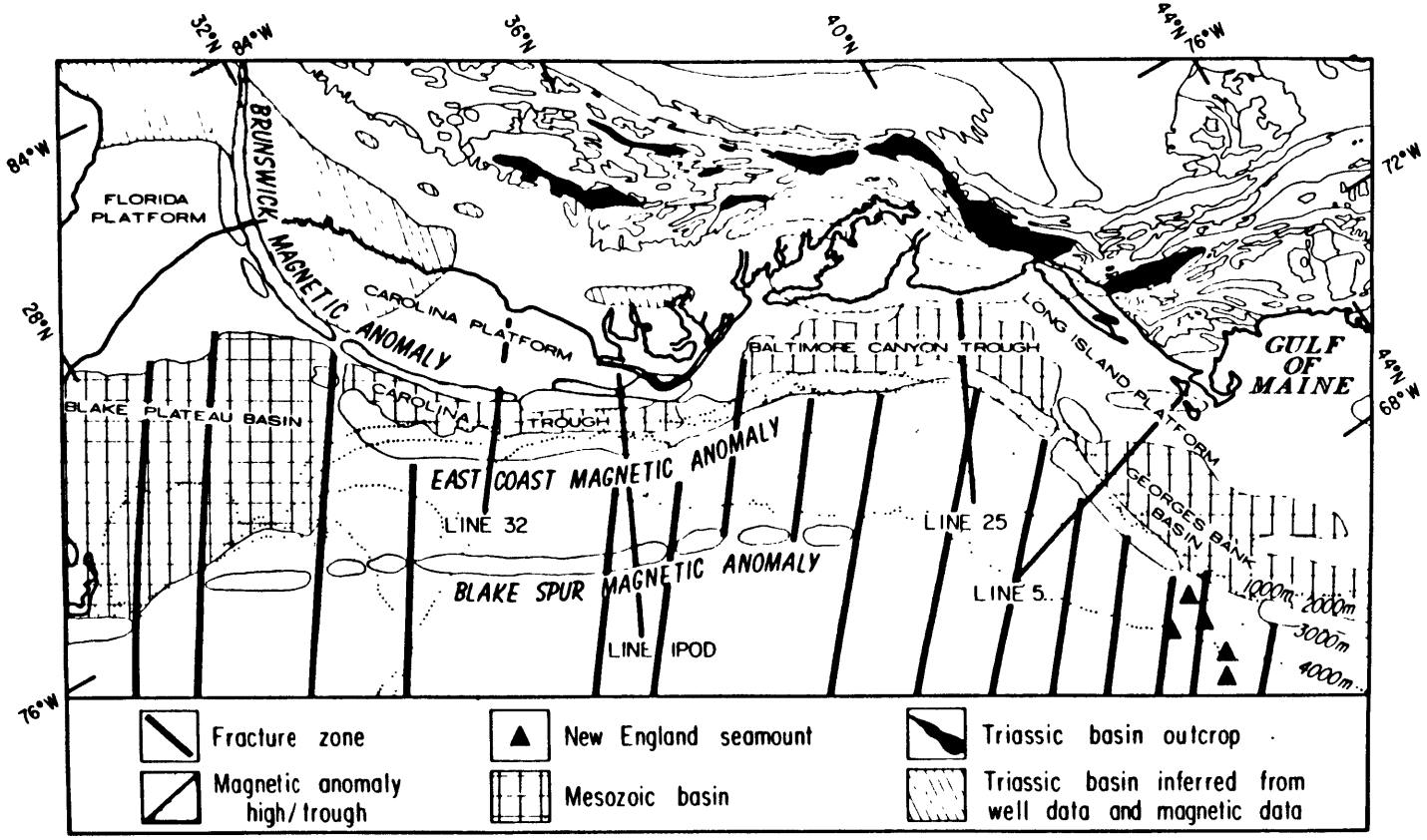

Figure 3.1 Index map showing the major structural elements and magnetic anomalies of the U.S. Atlantic continental margin and the locations of lines IPOD, 32, 5, and 25 (modified from Klitgord and Behrendt, 1979). Bathymetry in meters is shown by dotted lines.

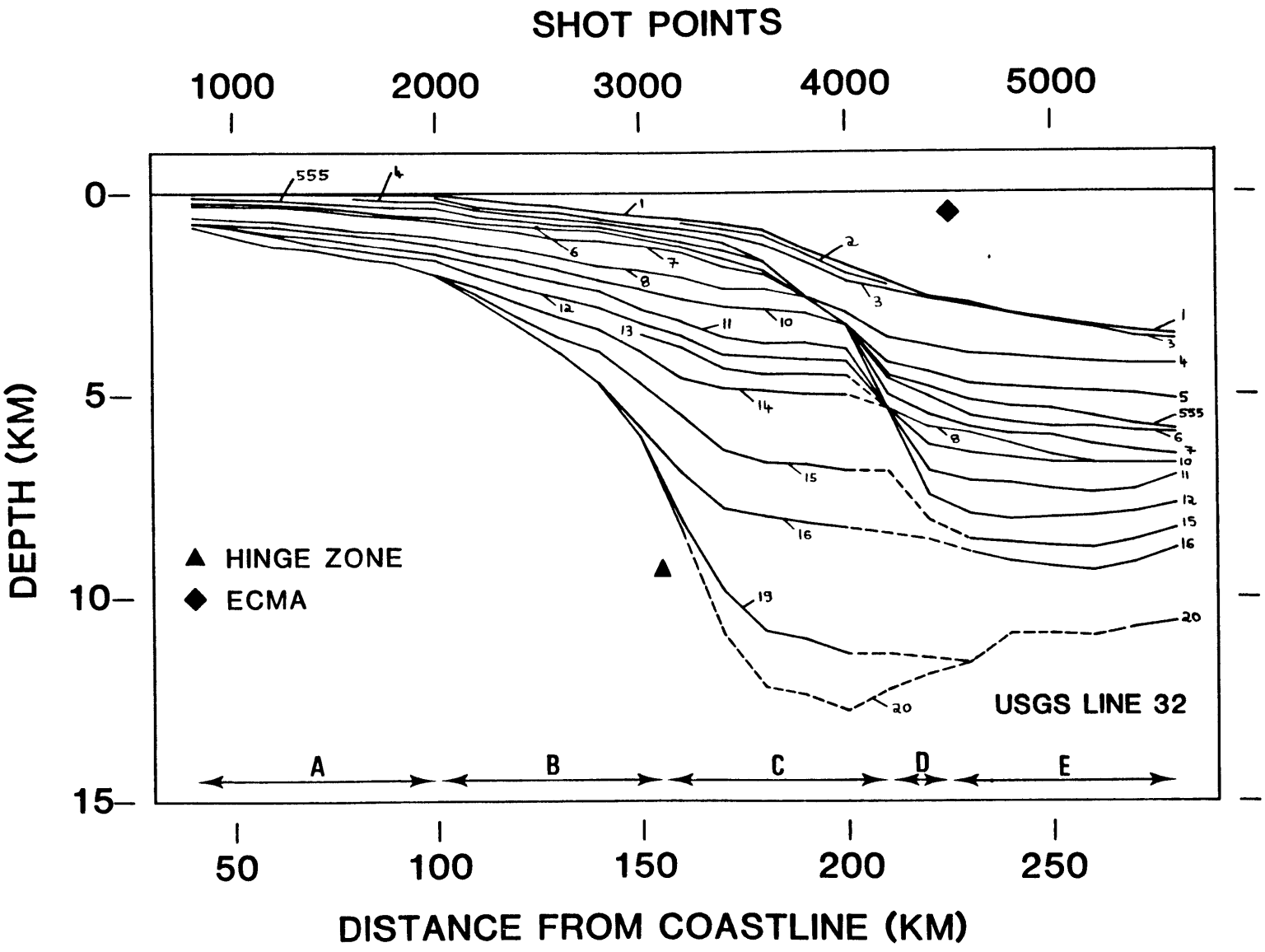
SHOT POINTS
1000
2000
3000
4000
5000
DEPTH (KM)
0
5
10
15
HINGE ZONE
ECMA
USGS LINE 32
A
B
C
D
E
50
100
150
200
250
DISTANCE FROM COASTLINE (KM)

Fig. 3.2

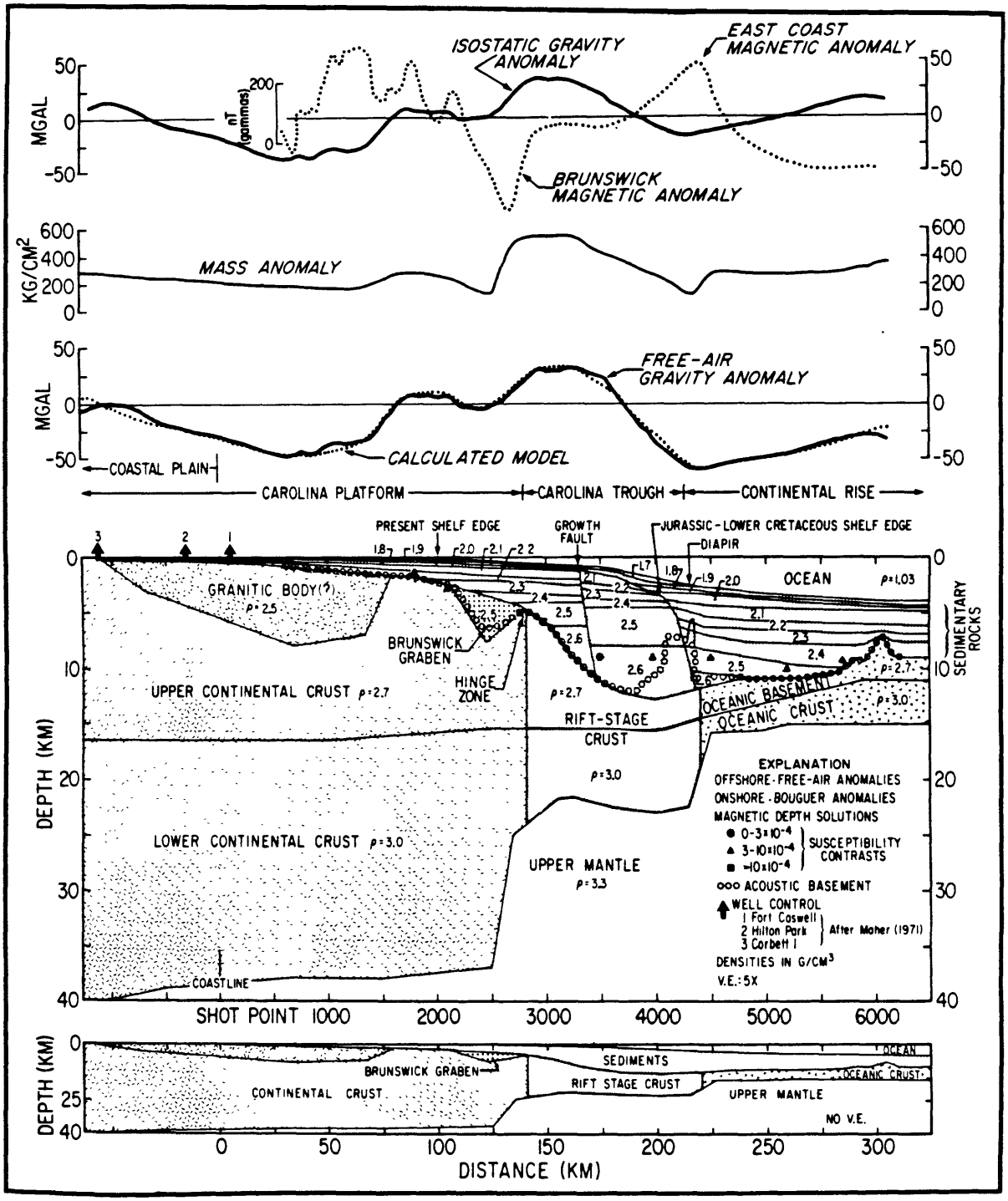
ISOSTATIC GRAVITY ANOMALY
EAST COAST MAGNETIC ANOMALY
BRUNSWICK MAGNETIC ANOMALY
MGAL
nT (gammas)
MASS ANOMALY
KG/CM2
FREE-AIR GRAVITY ANOMALY
CALCULATED MODEL
COASTAL PLAIN
CAROLINA PLATFORM
CAROLINA TROUGH
CONTINENTAL RISE
PRESENT SHELF EDGE
GROWTH FAULT
JURASSIC-LOWER CRETACEOUS SHELF EDGE
DIAPIR
GRANITIC BODY(?)
BRUNSWICK GRABEN
HINGE ZONE
OCEAN
SEDIMENTARY ROCKS
UPPER CONTINENTAL CRUST
OCEANIC BASEMENT
OCEANIC CRUST
RIFT-STAGE CRUST
LOWER CONTINENTAL CRUST
UPPER MANTLE
COASTLINE
EXPLANATION
OFFSHORE-FREE-AIR ANOMALIES
ONSHORE-BOUGUER ANOMALIES
MAGNETIC DEPTH SOLUTIONS
SUSCEPTIBILITY CONTRASTS
ACOUSTIC BASEMENT
WELL CONTROL
1 Fort Caswell
2 Hilton Park
3 Corbett 1
After Maher (1971)
DENSITIES IN G/CM3
V.E.: 5X
DEPTH (KM)
SHOT POINT
SEDIMENTS
CONTINENTAL CRUST
RIFT STAGE CRUST
NO V.E.
DISTANCE (KM)

Fig. 3.3

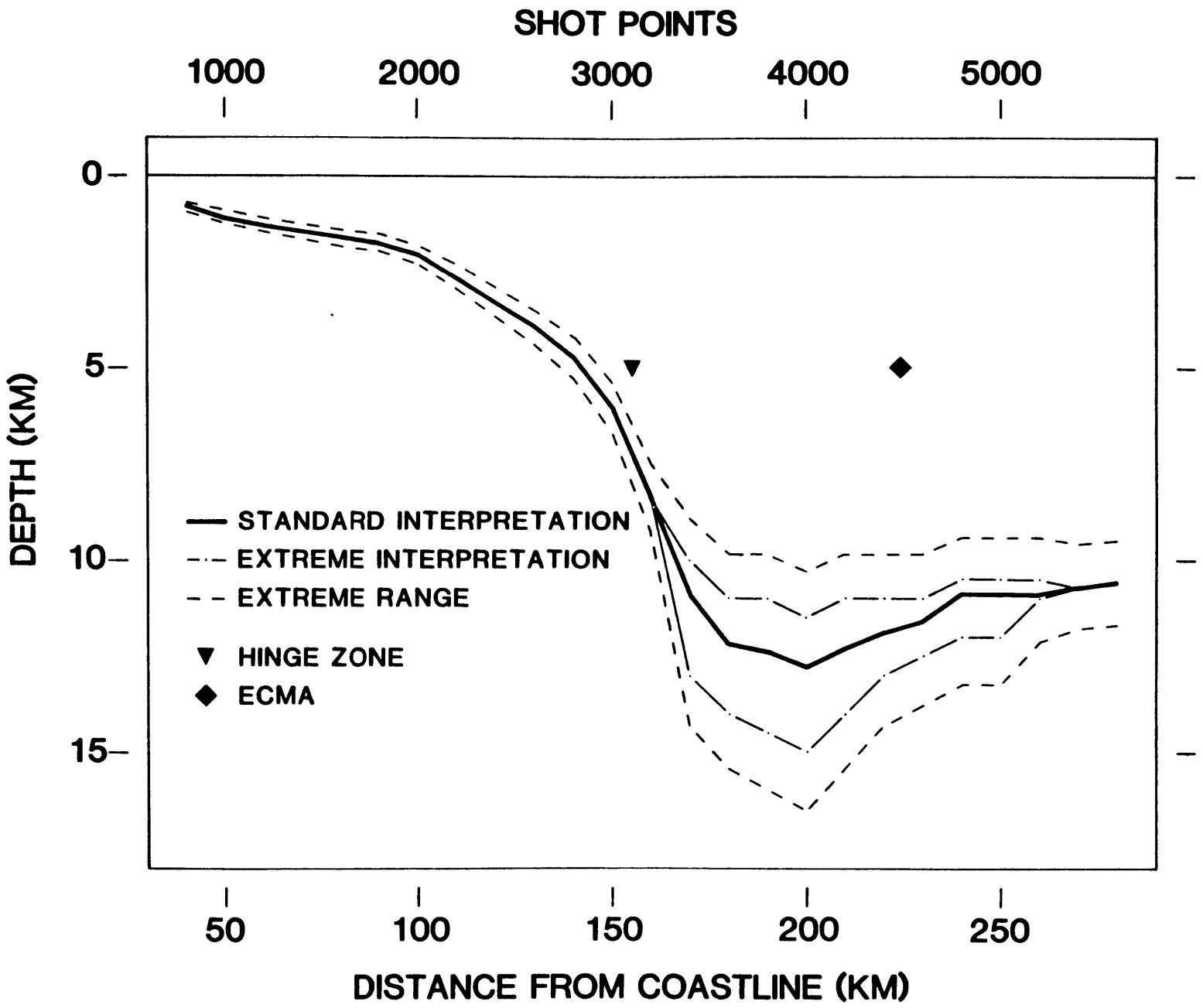
SHOT POINTS
1000
2000
3000
4000
5000
0
5
10
15
DEPTH (KM)
STANDARD INTERPRETATION
EXTREME INTERPRETATION
EXTREME RANGE
HINGE ZONE
ECMA
50
100
150
200
250
DISTANCE FROM COASTLINE (KM)

Fig 3.4

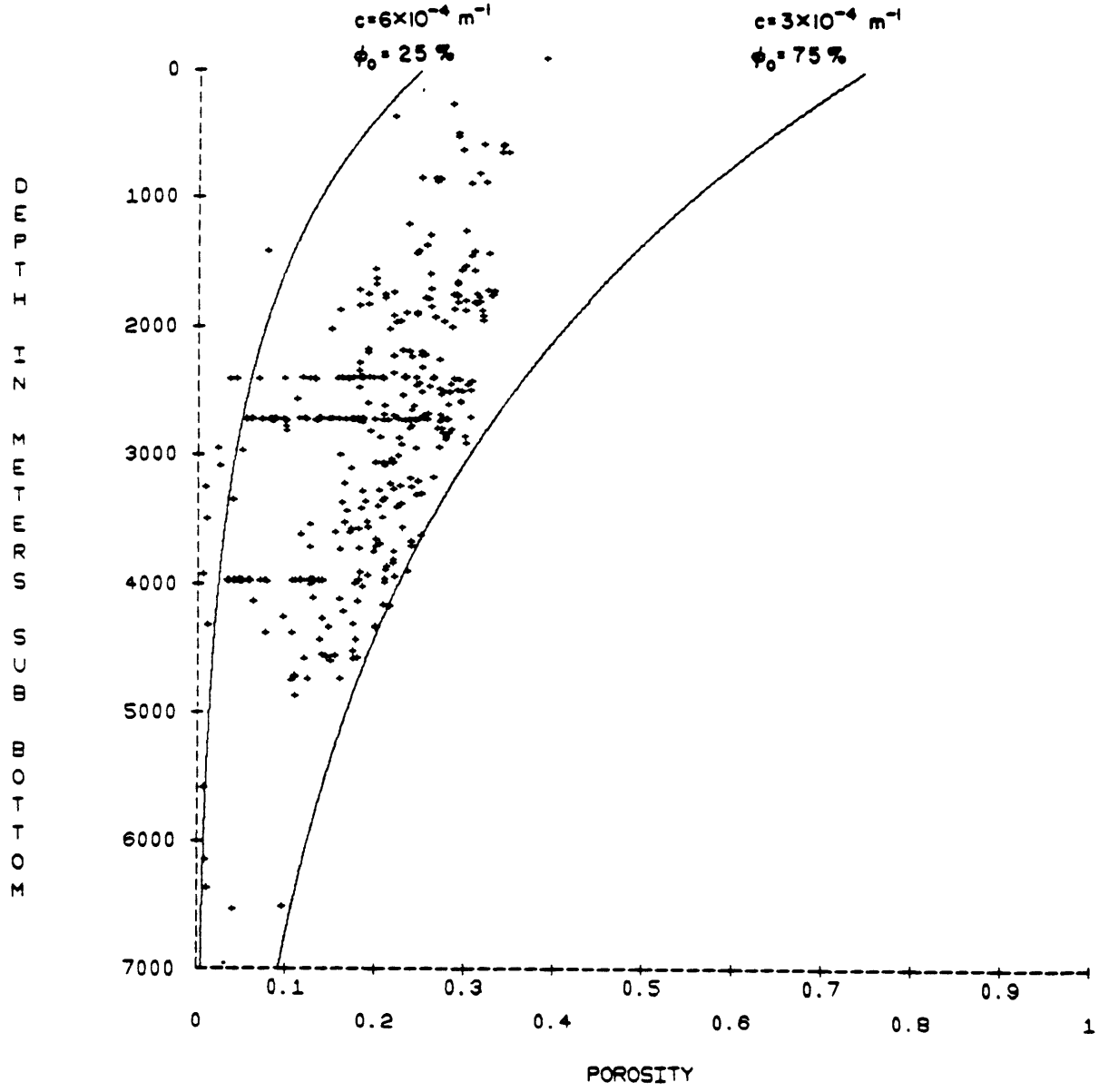
c=6×10⁻⁴ m⁻¹
φ₀ = 25 %
c=3×10⁻⁴ m⁻¹
φ₀ = 75 %
DEPTH IN METERS SUB BOTTOM
0
1000
2000
3000
4000
5000
6000
7000
0
0.1
0.2
0.3
0.4
0.5
0.6
0.7
0.8
0.9
1
POROSITY

Fig. 3.5

CHAPTER IV

ONE DIMENSIONAL UNIFORM EXTENSION MODEL

Science is always wrong. It never solves a problem without creating ten more.

G. B. Shaw

4.1 INTRODUCTION

The purpose of this chapter is to determine whether the one-dimensional extension model coupled with a local isostatic response to the load can account for the observed total subsidence, gravity and paleowaterdepth within the Carolina trough. Since the model set up is described in Appendix A, we just recall that the procedure is in two steps (Section A.5, Appendix A).

First, the model is constrained to predict the observed present total subsidence (obtained from basement and water depth data). This determines the extension factor β across the profile.

Second, crust thickness and past basin configuration are calculated, using the extension factor β. The predicted crust thickness is then used to compute gravity that can be compared with data while past basin configuration can be compared to geological inferences.

The error due to uncertainties are evaluated by using extreme data sets (see Chapter 1, table 1.1 and Chapter 3, section 3.5).

4.2 AMOUNT OF EXTENSION

The extension coefficient, β, for each column is the ratio of the the predicted present crustal thickness to the assumed original crustal thickness; crustal thickness being defined as the difference between the Moho and pre-Mesozoic basement depth (Fig. 4.1). At this stage, setting the origin time at 200 MYBP or at 175 MYBP makes no difference, since the thermal subsidence after 175 MY is negligible.

4.2.1 Error

The error in crustal thickness due to the uncertainties in the sediment properties is large and increases as the sediment thickness increases from the land to the center of the basin where it reaches a maximum of ±40% of the prediction (Fig. 4.1). The error due to the basement depth uncertainties is significant only in the central part of the basin where the basement reflections are missing and where it also reaches ±40% of the predictions. Because of this large error range, our model constrains the crustal thickness seaward of the hinge zone to be between 0 and 20 km ($\beta>2$). Better basement depth location and better knowledge of the sediment physical properties would improve these predictions. However,

even if our absolute determinations of β are poorly constrained, we can still expect our relative values across the basin to be more reliable as long as the data error do not correlate with the distance from coastline. (This is probably true for basement depth errors but geological common sense suggests that variations in sediment properties may correlate with distance from coastline (Watts and Thorne, 1984)).

4.2.2 Comparison with gravity model estimate of crust thickness

Our model was set up to be consistent with Hutchinson's et al. (1982) unstretched continental structure and oceanic structure, hence the good agreement of predicted crustal thickness at these two end points (Fig. 4.1). Yet, between these two end points, our model, which predicts a smooth transition, departs significantly from the gravity model of Hutchinson et al. (1982) (Fig. 4.3) which predicts a two step transition.

At the landward end (40 to 120 km from coastline) the disagreement is within the error range allowed by sediment properties and our prediction falls in between the gravity model (Hutchinson et al., 1982) and seismic refraction estimates (James et al., 1968).

Across the hinge zone and seaward of it (120 to 180 km from coastline) the error range is not sufficient to explain the disagreement. However, the inferred Brunswick graben which was given density contrast with respect to the rest of the crust by Hutchinson et al. (1982) is located on the landward part of this area and may partly affect their crustal model.

Further seaward (180 to 240 km from coastline) the disagreement could be fully accounted for by the effect of uncertainty in the basement depth on our model. The gravity model is also poorly constrained in that area due to poor control on sediment densities (Barton, in press).

4.2.3 Gravity predicted by the extension model

In order to test directly our prediction we computed the gravity from the structure predicted by our model (Fig. 4.2) using the same procedure as Hutchinson et al. (1982) (Fig. 3.3, Chapter 3), the only alteration being the mid-crustal density discontinuity and Moho depth. If the Brunswick graben is given a standard crustal density of 2.7 g/cm^3 (Fig. 4.2) instead of 2.5 g/cm^3 (Fig. 4.2b) as in Hutchinson et al. (1982) a better fit is obtained from 100 to 150 km from the coastline. However, our prediction disagrees with the gravity data further seaward: a more abrupt transition

than predicted by our model is needed across the hinge zone. Introducing a flexural response in our model does predict such a more abrupt transition (Chapter 5), but because this gravity modeling is poorly constrained seaward of the hinge zone (Barton, in press) only refraction data would provide a good test of these estimates.

4.3 THE DIFFERENT CONTRIBUTIONS TO SUBSIDENCE

4.3.1 Present situation

Assuming an origin time of 175 MYBP or 200 MYBP makes no significant difference to the present different contributions to subsidence shown in Fig. 4.3.

In the oceanic part, the tectonic subsidence (initial plus thermal subsidence) is defined as the depth of unloaded seafloor of 175 MY (or 200 MY) of age. Once the loading subsidence is added, a misfit is observed with the basement depth (Fig. 4.3). This misfit (less than 550 m) remains roughly the same as the error on the seismically defined basement depth and becomes smaller (less than 300 m) where the seismic basement is well defined (SP 5200 to 5600). As expected, the fit is also better for standard rather than extreme sediment properties. This misfit can then be attributed to uncertainties in the basement picks, to the error range of 10% on the thermal subsidence amplitude set up which amounts up to 300 m for the oceanic crust (Appendix A, Section A.4.7 and table A-2), and to eventual oceanic basement irregularities which could be linked to the buried seamount observed at the seaward end of line 32, outside the domain modeled in this study.

In the non-oceanic part, the extension factor β was adjusted so that the current tectonic subsidence plus the loading subsidence exactly matches the total subsidence, i.e. the basement depth because zero elevation was assumed prior to rifting. Clearly, many uncertainties in the data or errors in the assumptions can be compensated for by a corresponding error in the value of the extension factor, β. The error range on the tectonic subsidence reaches ± 1.5 km, which is $\pm 25\%$, in the central part of the basin. This error is mainly due to the uncertainty on the sediment properties landward of the hinge zone and equally to the uncertainty of both sediment properties and basement depth seaward of it.

Sediment loading accounts for 40% of the subsidence at the landward edge of the basin, 60% in the central part of the basin, and 45% in the area with oceanic crust. This occurs because two factors are acting against each other. On one hand, compaction causes the average density of the sediments to increase with their thickness, resulting in a greater loading effect, while on the other hand as the water depth increases, the loading effect is less intense. The first effect is dominant across the hinge zone while the second one is dominant across the slope.

The tectonic subsidence accounts therefore for from 40% to 55% of the total subsidence seaward of the hinge zone. This is a large contribution because the basin is not filled with sediments. This tectonic subsidence is equally shared between initial and thermal subsidence except over the oceanic crust where the share is 40% and 60% respectively.

The initial subsidence accounts for up to 30% of the total subsidence landward of the hinge zone. This seems in contradiction with two observations in that area: first there are no deposits of either synrift or early postrift sediments, second it is possible that the PRU was associated with erosion (Hutchinson et al., 1982). Two modifications of the model can be considered to accommodate this factor. First, introducing flexural rigidity would attribute more of the subsidence to the effect of the loading of the central part and less to tectonic causes (Walcott, 1972; Watts and Steckler, 1979), second assuming more subcrustal extension than crustal extension would keep this area more elevated during and early after rifting (Royden and Keen, 1980).

4.3.2 Evolution since rifting

We show (Fig. 4.4) the evolution of tectonic and total (basement depth) subsidence for four different locations across line 32, corresponding to the zone A, B, C and D (as defined in Chapter 3, section 3.4).

In the non oceanic part (A, B and C), the error range on the total subsidence corresponds to the current uncertainty in basement depth while the error range on the tectonic subsidence, of the order of 25%, corresponds to the uncertainty on both sediment properties and, especially seaward of the hinge zone, basement depth. These errors are reflected directly in the early paleowaterdepths because when the amount of deposited sediment is negligible, the water depth is entirely controlled by the

poorly constrained tectonic subsidence. As sediment thickness increases, these sources of error are damped and the water depth becomes the best constrained prediction, as it is today. Independent estimates of early paleowaterdepth and synrift sediment thickness would therefore considerably help reduce the model uncertainty on these predictions.

In the oceanic part (zone D), tectonic subsidence is assumed to be well constrained (Parsons and Sclater, 1977), therefore the error in the data are directly propagated into the waterdepths which are known only for today. This known water depth is not an input of the model, but the prediction for standard sediment properties matches it sufficiently well.

4.4 PALEOWATERDEPTHS

Paleowaterdepth predictions can be compared to interpretations from seismic stratigraphy (described in Chapter 3) in two different fashions: we can look at predicted cross sections of the basin at a fixed time or at the waterdepth evolution at fixed location within the basin through time. Setting rifting at 200 MYBP instead of 175 MYBP results essentially in an increase of the overall waterdepth from rifting until 150 MYBP, we will then discuss the model with rifting at 175 MYBP unless otherwise specified.

4.4.1 Profiles at fixed time

Until the end of Callovian (163 MYBP) the waterdepths are not known within the Carolina trough. Yet the model predictions (Fig. 4. 5a and 4.5b) are suspect for two reasons: first, the initial topography deepens very gradually from land to sea without any significant hinge zone (Fig. 4.5a) which seems to develop later essentially by sediment loading (Fig. 4.5b); second the synrift (Fig. 4.5b) and later (Fig. 4.5c) sediments are not deposited flat and their center of deposition doesn't seem controlled by any topographic boundary; worse, the deposition seems to concentrate on a high in the central part of the basin, leaving a significant trough landward of the hinge zone unfilled.

The same anomalous pattern continues until at least the end of the Jurassic (Fig. 4.5d and 4.5e): Area A and B (as defined in Chapter 3) are 400 m to 300 m too deep compared to area C while the shelf edge is very poorly defined and smears into zone C which is inferred as shelf proper from seismic stratigraphy.

These anomalies tend to decay with time and by the end of the Cretaceous (Fig. 4.5f) the top of sediment dips seaward. However area B and C tend to be too deep for a shelf environment. The shelf edge is still poorly defined, probably because the part which was eroded during the mid-Oligocene is missing in our model.

The situation at mid-Oligocene time (Fig. 4.5g) looks like the Cretaceous one, except that this time it is compatible with the inferred greater depth due to underwater erosions.

4.2.2 Evolution through time

To analyze these water depth problems further, the evolution through time is shown at these locations along line 32 which represents zone A, B and C. In this evolution contrary to what was discussed before the effect of sea level change is included.

Zone A (SP2000, Fig. 4.6)

The predicted waterdepth is too deep until the mid-Oligocene to be compatible with the inferred persistent subaerial to shelf environment. This is especially true soon after rifting where depths of up to 750^{m} are reached (Kimmeridgian).

Zone B (SP2800, Fig. 4.7)

The same pattern as in zone A is predicted. The deepest waterdepths (more than 1 km) are reached soon after rifting (top Bathonian).

Zone C (SP3400, Fig. 4.8)

The early waterdepths are also deep but cannot be checked because early paleodepths are unknown in this zone. The predictions are compatible with the inferred shelf environment during the late Jurassic, but they deepen again during the Cretaceous contrary to the inferred persistence of shelf environment until mid-Oligocene.

4.2.3 Discussion

The predicted waterdepths are too deep and seem incompatible with the inferred environment even if the error range due to uncertainties in sediment properties and basement depths is taken into account. Assuming rifting at 200 MYBP, which predicts an even deeper early environment, is therefore ruled out on that basis. We will distinguish between two aspects of this misfit: first, an overall too great depth in zones A, B and C, from rifting until mid-Oligocene for A and B and from Coniacian to

mid-Oligocene for C; second, a too great depth in area A and B relative to C from rifting to end of Jurassic, which alters the shape of the predicted profile.

The overall offset can be related to two types of approximations. First, we did not take into account the amount of sediments eroded during the evolution of the basin, yet most dated reflectors are erosional unconformities. We then always underestimate the sediment thickness at a given time, except just after an erosion. The predictions are then the envelope of the deepest waterdepth, which are reached just after erosion. This still means that according to our model these erosions would have been active up to 500m under water.

Second, we can take into account the uncertainties on the model parameters, or the model setup (Appendix A, section A.4.7). We can estimate from zone A to C an error varying from 200m to 500m in the initial subsidence, from 200m to 600m in the tectonic subsidence at the end of the Jurassic, from 200m to 700m in the tectonic subsidence since the end of the Cretaceous.

It is also independently inferred that the whole shelf may have been anomalously deep during the Cretaceous (Pinet and Popenoe, 1985; Dillon et al., 1985) which goes in the direction of model predictions. Finally, salt tectonics in zone C does not seem a good explanation for the late Cretaceous depth in that area because assuming a thicker sediment column at that time, because of more salt, would also require assuming a thicker column at the end of the Jurassic; this would raise the elevation in the Jurassic above sea level.

The too great depth landward of the hinge zone (zone and A and B) relative to the area immediately seaward of it (zone C) after early rifting suggests two modifications to the model: assuming a flexural response to the sediment loading (Watts and Steckler, 1979) and/or more active heating represented by greater subcrustal than crustal extension in that area (Royden and Keen, 1980). However, to properly constrain a two-layer model one would need an indication on the paleodepth just after rifting in zone A, B and C: if zone A and B can be assumed at zero depth, paleodepth of zone C remains unconstrained. Shifting the origin time of rifting from 200 MYBP to 175 MYBP in the uniform extension model, as we did, is in some way comparable to introducing extra subcrustal extension: in both cases the early paleowaterdepth is reduced.

4.5 CONCLUSION

This simple model shows that most predictions suffer a large error range seaward of the hinge zone where the basement depth and the properties of the thick sedimentary section are poorly constrained.

Even when that error range is considered, the model cannot account for gravity data and inferred early paleogeography. This suggests that introducing a flexural response to the loading would be appropriate. Inferred early waterdepths may also indicate that more heat was present during rifting than accounted for by the uniform extension model. A lesser concern is that predicted post-Jurassic waterdepths are not very compatible with observations but probably partly because they do not take into account amounts of erosions which are not known; moreover this smaller problem becomes close to the model resolution due to set up uncertainties.

Figure Captions

Fig. 4.1. Crustal thickness along line 32. According to our model this thickness (in km) is equal to $40/\beta$ where β is the extension factor. We compare estimates from seismic refraction (James et al., 1968) and gravity modeling (Hutchinson et al., 1982) with estimates from our extension model with origin time at 175 MYBP. Error range on our model due to sediment property errors only, and to both sediment properties and basement depth errors, are also shown.

Fig. 4.2. Direct gravity calculation of model predicted structure.
4.2a: With Brunswick graben density at 2.7 g/cm^3.
4.2b: With Brunswick graben density at 2.5 g/cm^3.
4.2c: Structure; the extension model predicts the position of the moho and mid-crustal discontinuity; all other densities are from Hutchinson et al (1982) (Fig. 3.3, Chapter 3). B: Brunswick graben.

Fig. 4.3. Different contribution to subsidence along line 32 according to our model starting 175 MYBP.
From top to bottom: predicted initial subsidence (Sinitial), thermal subsidence (Sthermal), and loading effect (Sload). The sum of these three components is the predicted basement depth. The error in each of these estimates due to sediment properties errors only and to both sediment properties and basement depth errors are shown. In the continental part, the predicted basement depth is constrained to fit the data from line 32, therefore the solid line represents both the data and prediction. In the ocean, the basement depth prediction is not adjusted to the data: the star represents the data while the solid line represents the prediction.

Fig. 4.4. Subsidence history at 4 different locations along line 32.
4.4a: model starting at 200 MYBP.
4.4b: model starting at 175 MYBP.
From top to bottom: predicted water depth, tectonic subsidence (Stectonic), basement depth (Stotal); all these predictions are made assuming no variation of sea level. The difference between the upper and lower curve represents then the reconstituted sediment thickness

through time while the difference between the median and lower curve represents the subsidence due to the load.

(a) Standard estimate.

(b) Error range due to sediment properties errors.

(c) Error range due to both sediment properties and basement depths errors.

(d) Observed Waterdepth in the oceanic case.

(e) Observed basement depth in the oceanic case.

(f) Observed basement uncertainty range in the oceanic case.

Jt: Jurassic top; Kt: Cretaceous top;

Fig. 4. 5. Basin reconstruction according to the model starting 175 MYBP without correction for sea level changes using standard estimates for basement depths and sediment porosity. Two surfaces are shown: basement and top of sediments.

4.5a Age = 175 MYBP: Initial subsidence before loading by synrift sediments

4.5b Age = 175 MYBP: Situation after loading by synrift sediments

4.5c Age = 169 MYBP: (top Bathonian)

4.5d Age = 163 MYBP: (top Callovian)

4.5e Age = 144 MYBP: (top Jurassic)

4.5f Age = 65 MYBP: (top Cretaceous)

4.5g Age = 31 MYBP: (mid-Oligocene)

Fig. 4.6. Paleowaterdepths at SP 2000 on line 32.

4.6a: Upper solid curve is sea level according to Vail et al. (1977); lower dashed line is maximum water depth as inferred from seismic stratigraphy (Chapter 3, section 3.4). G: onset of Gulf Stream environment.

4.6b: Model predicted water depth (Model starting 200 MYBP) corrected for sea level. Jt: Jurassic top; Kt: Cretaceous top.

Continuous line: Standard prediction

Dot dash: Range of error due to sediment properties errors.

Dash: Range of error due to both sediment properties and basement depth errors.

4.6c. Same as Fig. 4.6b but model starts 175 MYBP.

Fig. 4.7. Paleowaterdepth at SP 2800.

Fig. 4.8. Paleowaterdepth at SP 3400.

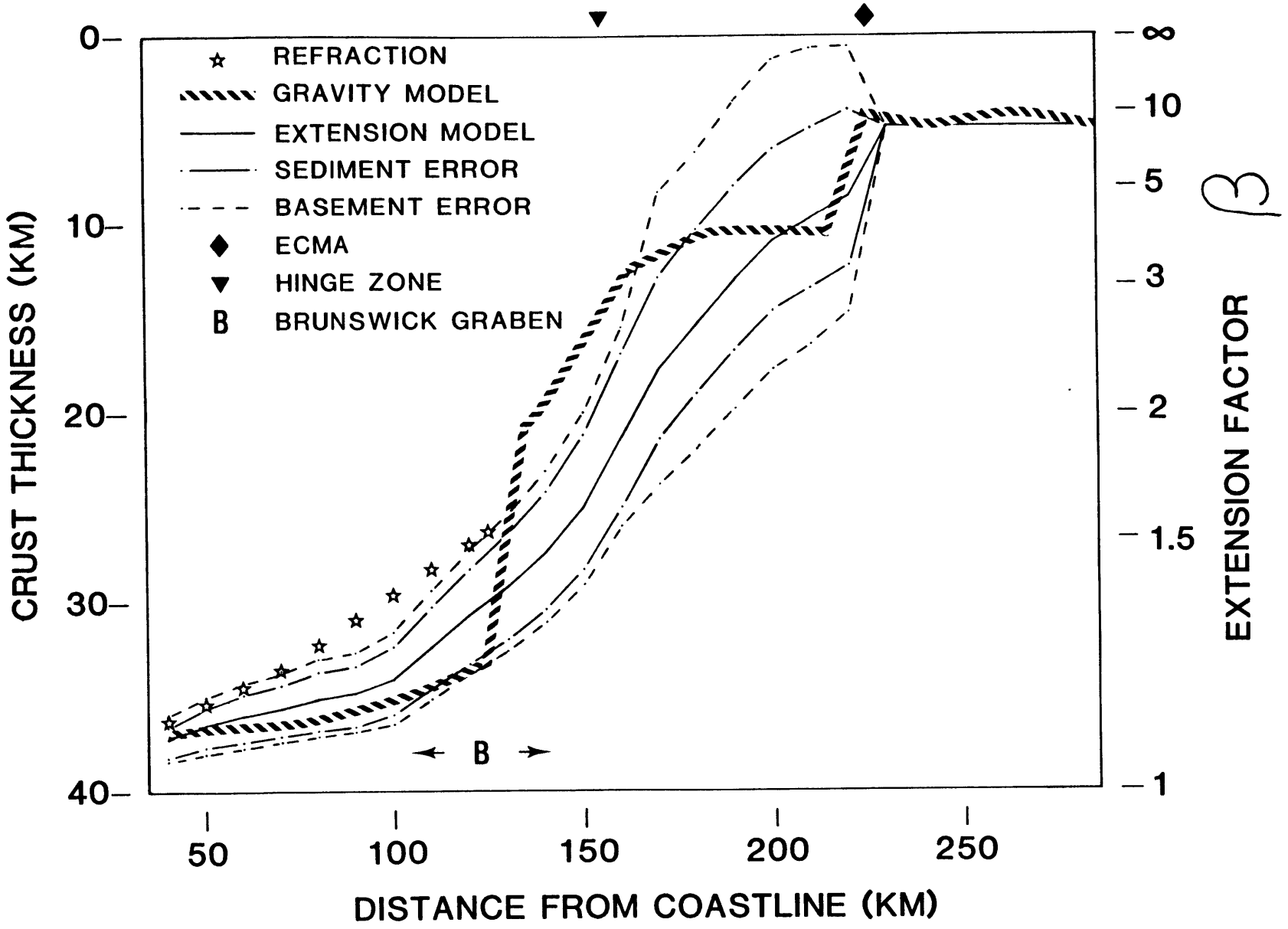
REFRACTION
GRAVITY MODEL
EXTENSION MODEL
SEDIMENT ERROR
BASEMENT ERROR
ECMA
HINGE ZONE
B BRUNSWICK GRABEN
B
CRUST THICKNESS (KM)
0
10
20
30
40
EXTENSION FACTOR
∞
10
5
3
2
1.5
1
50
100
150
200
250
DISTANCE FROM COASTLINE (KM)

Fig. 4.1

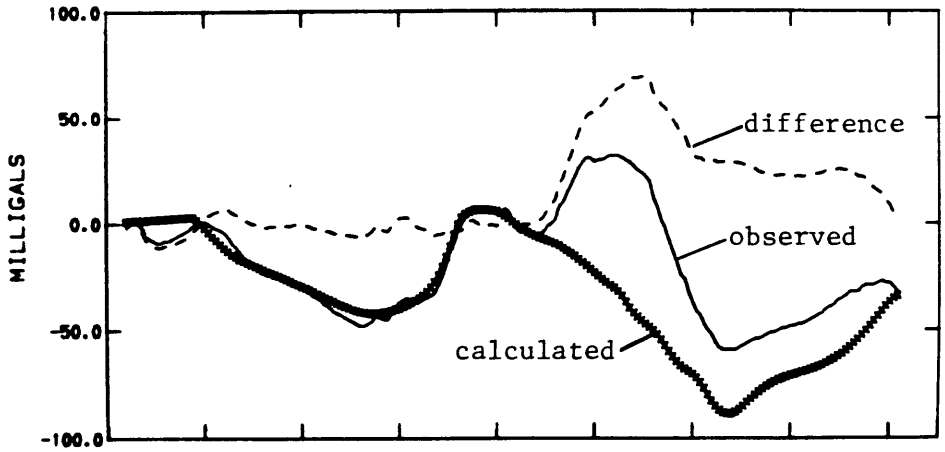

Fig. 4.2a

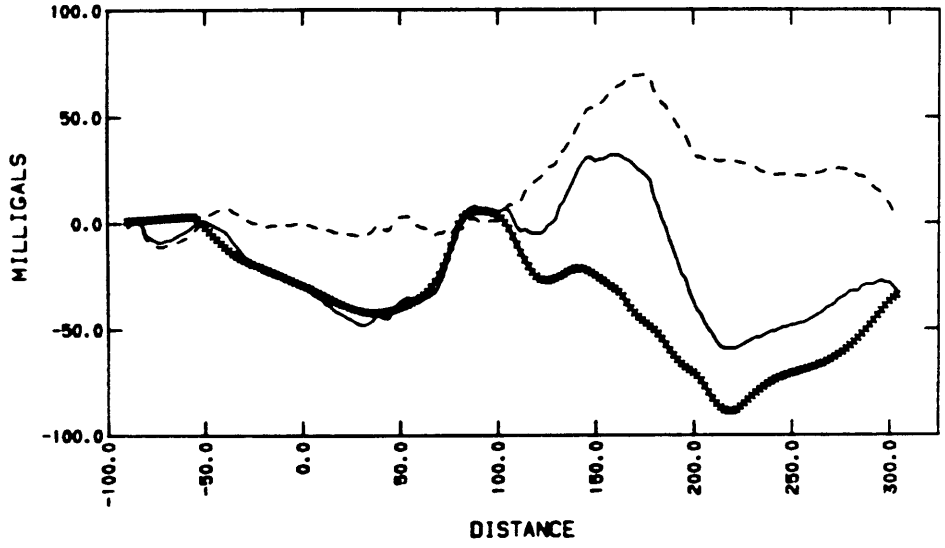

Fig. 4.2b

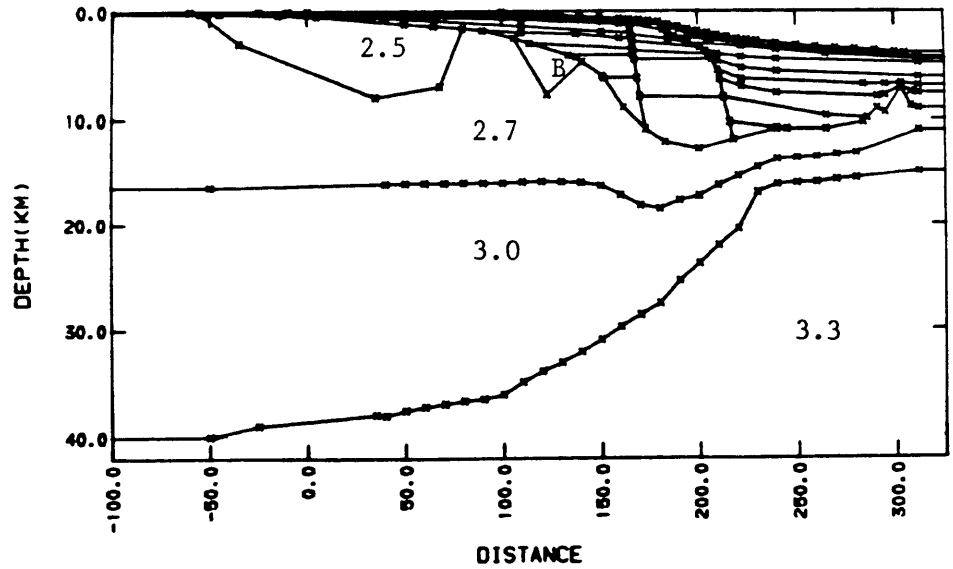

Fig. 4.2c

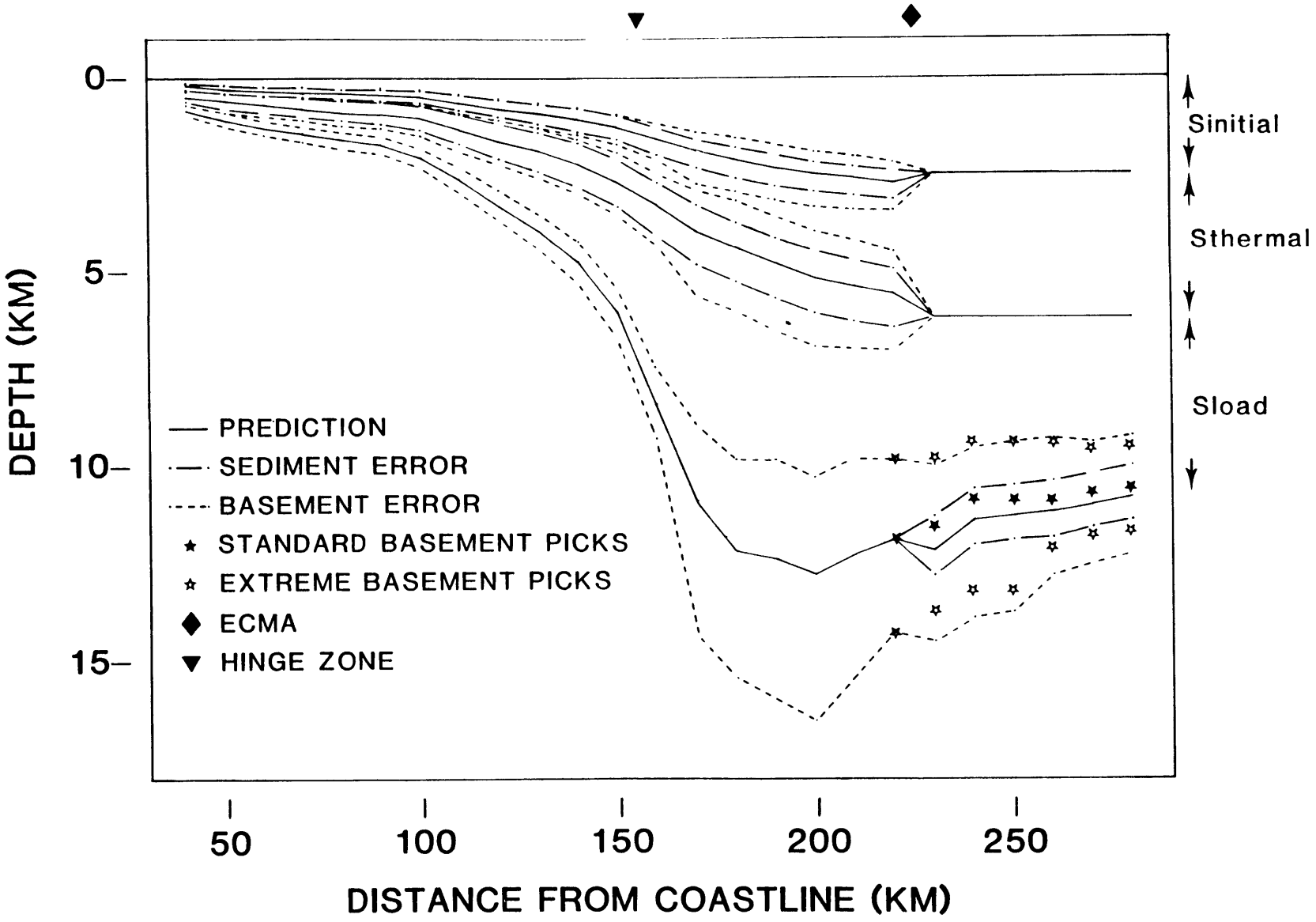
0
5
10
15
DEPTH (KM)
PREDICTION
SEDIMENT ERROR
BASEMENT ERROR
STANDARD BASEMENT PICKS
EXTREME BASEMENT PICKS
ECMA
HINGE ZONE
Sinitial
Sthermal
Sload
50
100
150
200
250
DISTANCE FROM COASTLINE (KM)

Fig. 4.3

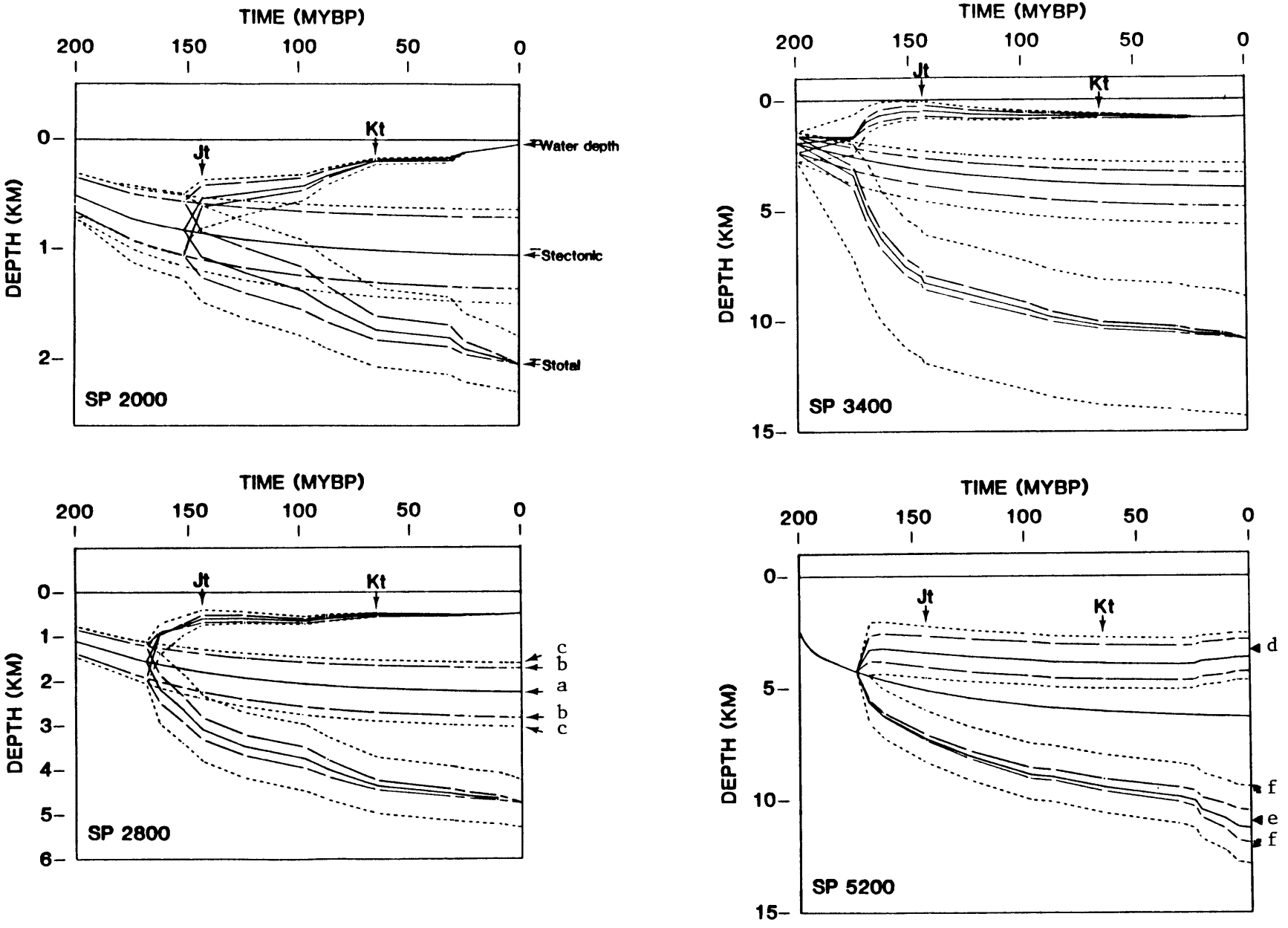
TIME (MYBP)
200
150
100
50
0
DEPTH (KM)
Jt
Kt
Water depth
Stectonic
Stotal
SP 2000
SP 3400
SP 2800
SP 5200
a
b
c
d
e
f

Fig. 4.4a

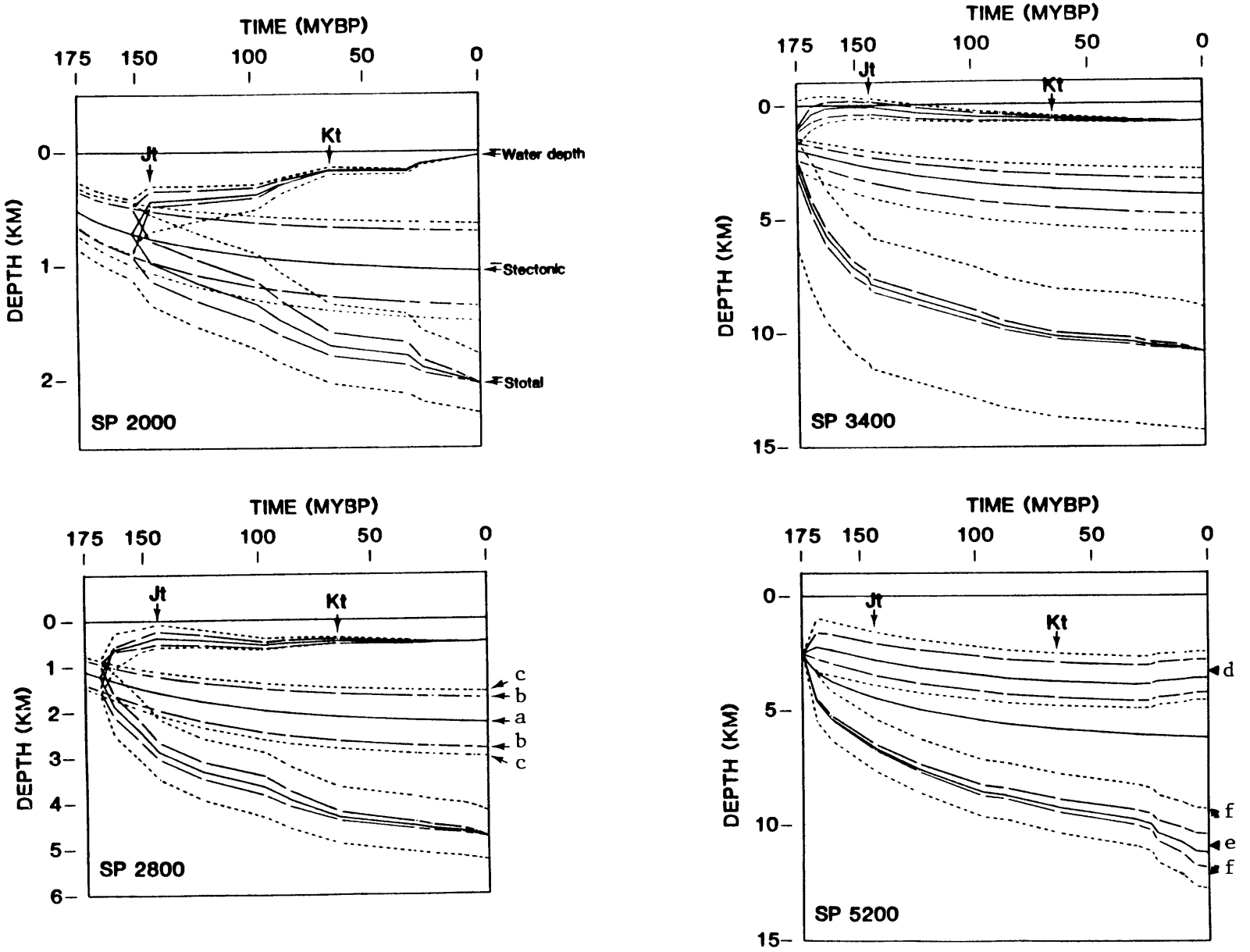
TIME (MYBP)
175
150
100
50
0
Jt
Kt
DEPTH (KM)
Water depth
Stectonic
Stotal
SP 2000
SP 3400
SP 2800
SP 5200
a
b
c
d
e
f

Fig. 4.4b

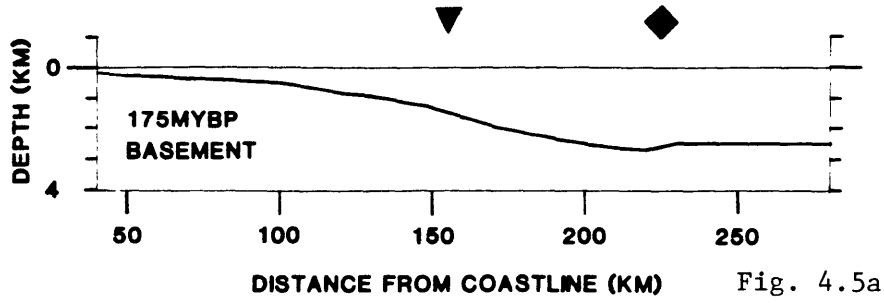

Fig. 4.5a

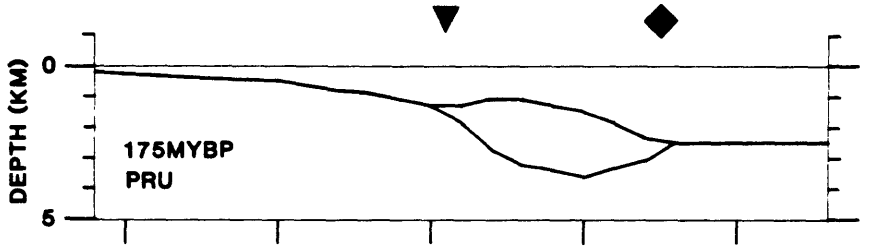

Fig. 4.5b

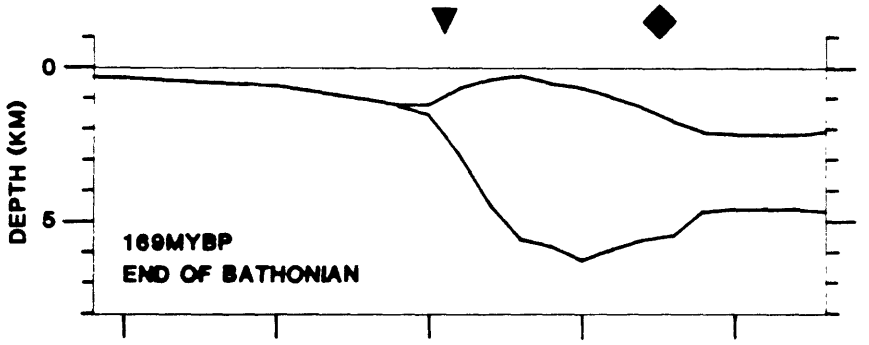

Fig. 4.5c

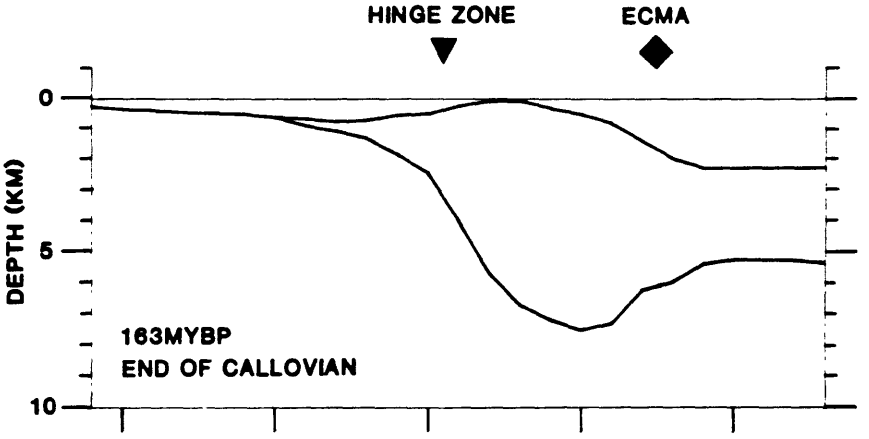

Fig. 4.5d

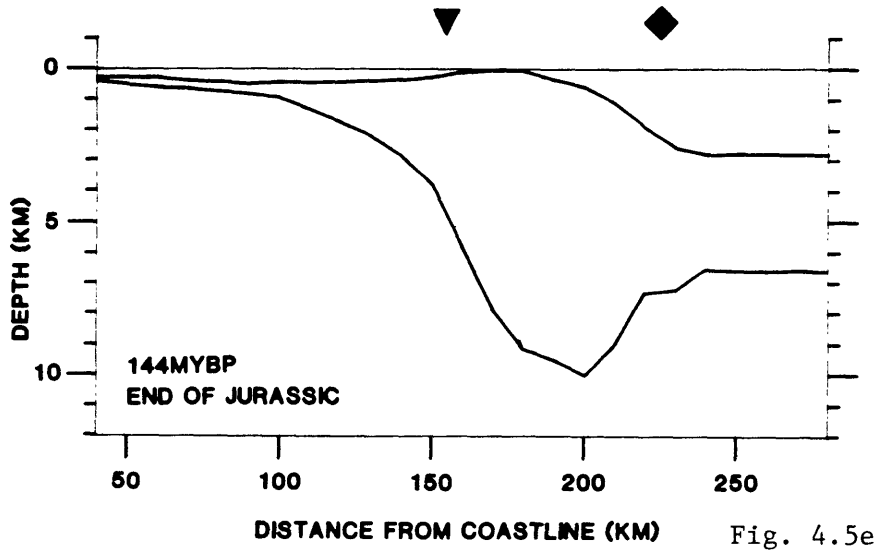

Fig. 4.5e

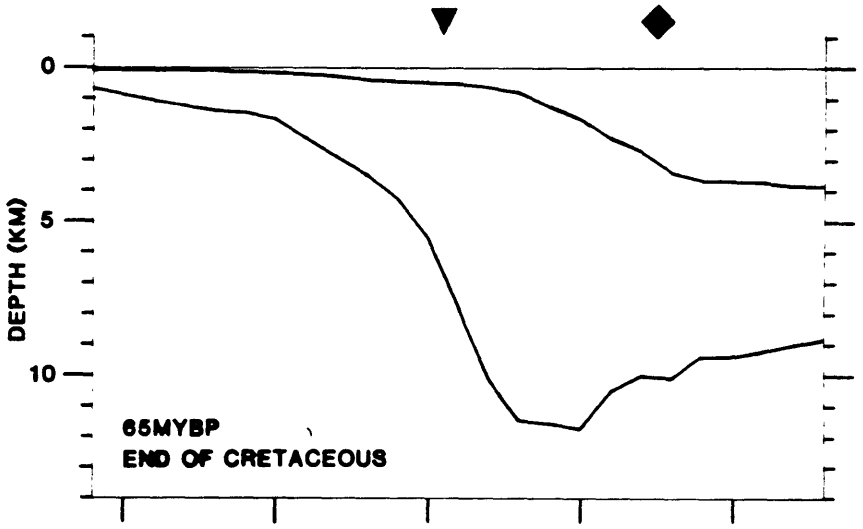

Fig. 4.5f

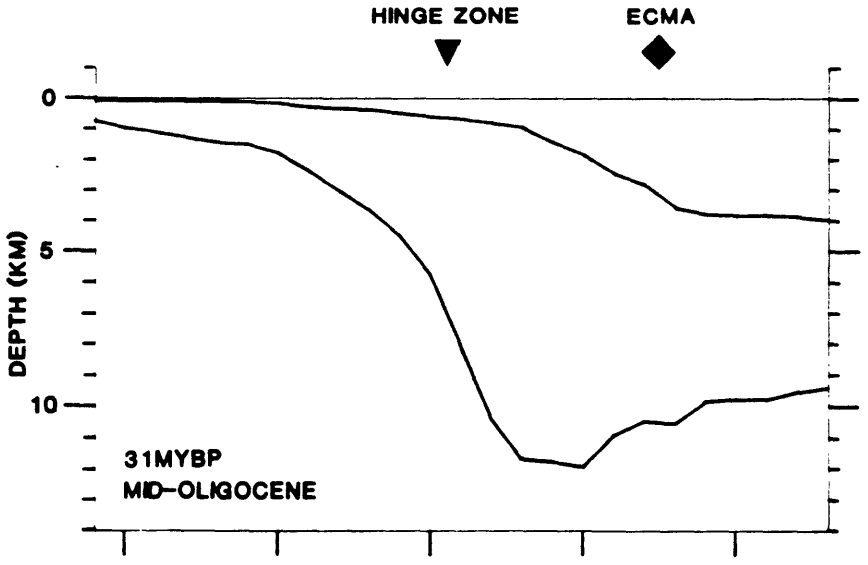

Fig. 4.5g

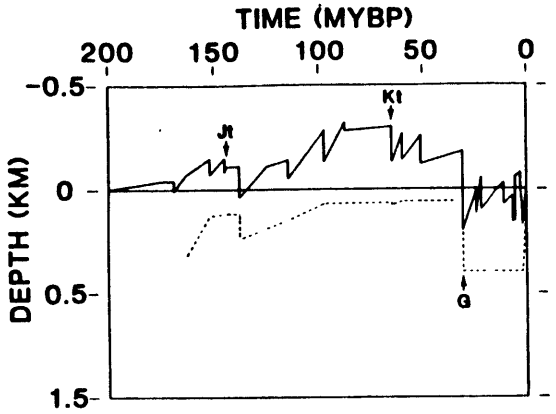

Fig. 4.6a

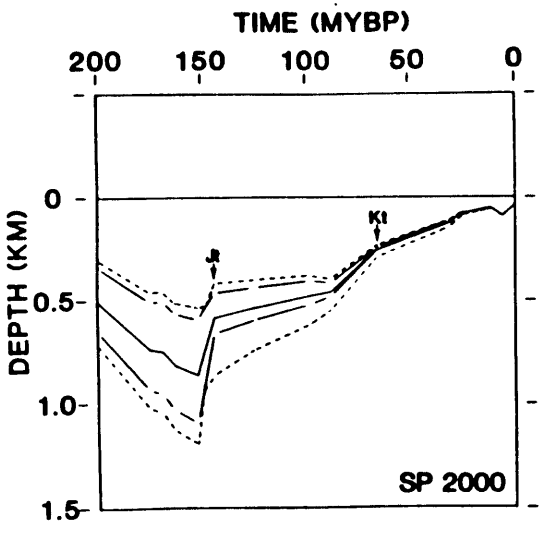

Fig. 4.6b

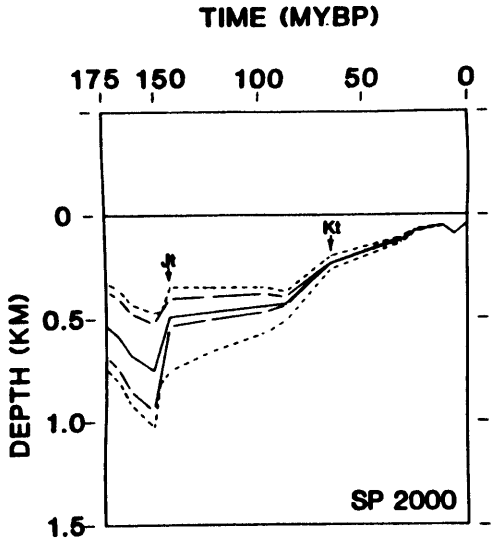

Fig. 4.6c

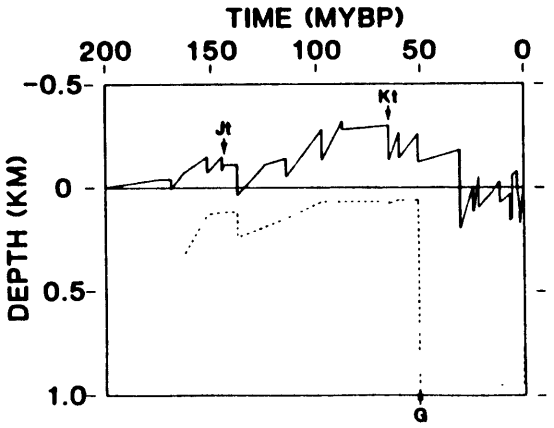

Fig. 4.7a

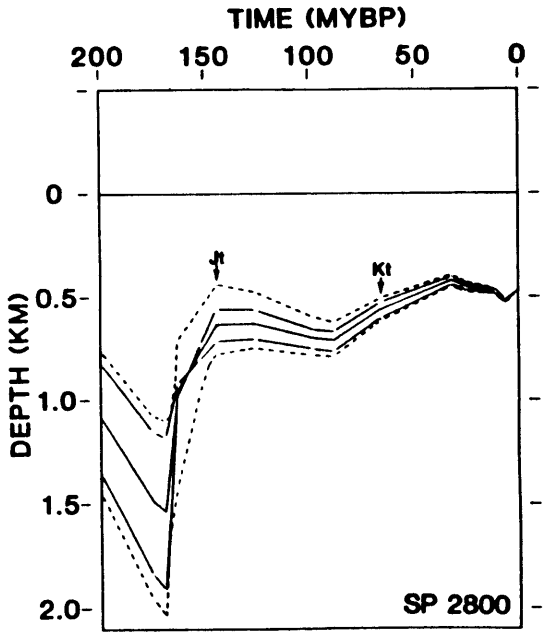

Fig. 4.7b

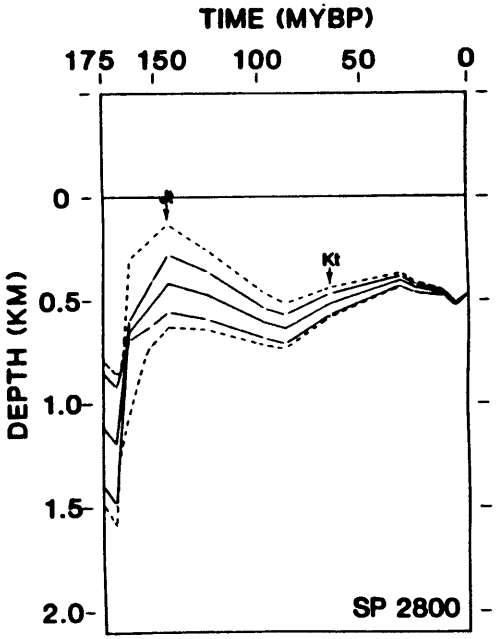

Fig. 4.7c

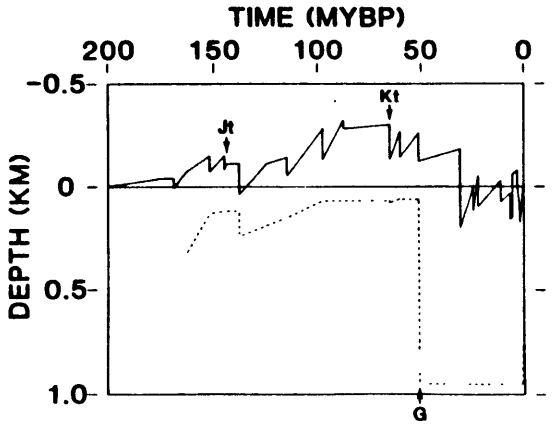

Fig. 4.8a

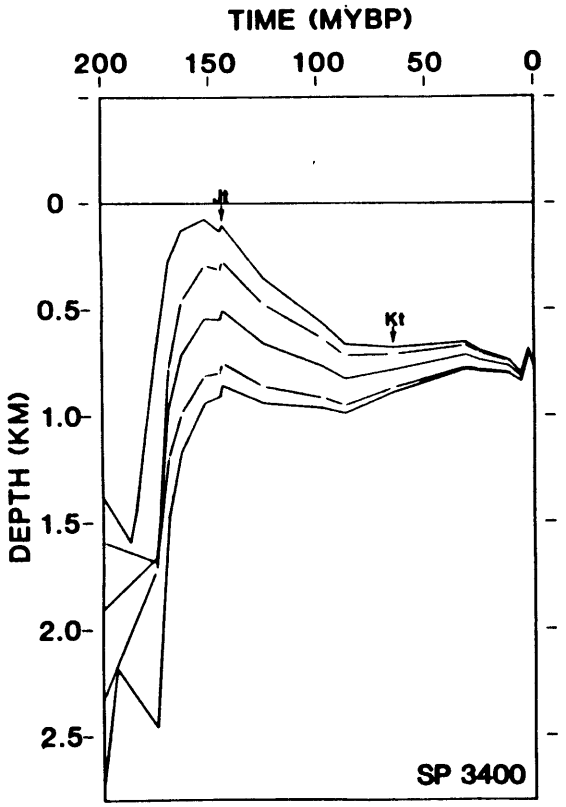

Fig. 4.8b

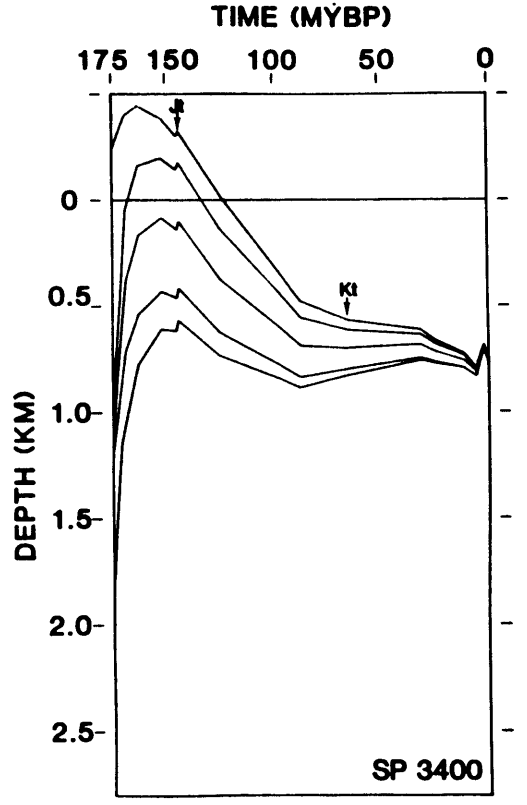

Fig. 4.8c

CHAPTER V

TWO DIMENSIONAL UNIFORM EXTENSION MODEL

'Tis a lesson you should heed,
Try, try again.
If at first you don't succeed,
Try, try again

W.E. Hickson, Try and try again.

5.1 INTRODUCTION

Application of a simple one dimensional model to the Carolina trough (Chapter 4) showed the need for more complete modeling, even when the large error range due to data uncertainties was considered. We here apply a two dimensional model (Appendix C) to evaluate the effect of more complex assumptions. The constraints are the same as in the one dimensional model (Chapter 3, section 3.5) and the major constraint on the extension factor is that present day water depth be correctly predicted landward of the ECMA. This model is based on Sawyer's (1982) finite difference simulation and includes effects of thermal blanketing by sediments, lateral heat flow and flexural response to the load.

In the case of flexural response, the lithosphere is assumed to be composed of an elastic plate above an inviscid fluid. The thickness of the plate is the depth to a relaxation temperature, T_R, and therefore varies both laterally and through time (Watt et al., 1982; Sawyer, 1982). Because of supposed active faulting the synrift sediments are always assumed to be locally compensated for. The postrift sediments are flexurally compensated. For each value of T_R the extension model will predict a crustal structure, from which a gravity model will be computed. The gravity data will then be compared to these models in order to constrain the value of T_R.

Unless otherwise specified the model assumes instantaneous rifting 175 MYBP and immediate synrift deposition between 175 MYBP and 174 MYBP. Another model assuming instantaneous rifting 200 MYBP with synrift deposition until 175 MYBP was also developed but was less successful. It will not be discussed further.

We will discuss in this chapter the predictions that can be tested directly against observations and inferences: crustal thickness and paleowaterdepth and paleostratigraphy. The thermal predictions, for which no independent estimates exist, will be discussed in Chapter 7.

5.2 AMOUNT OF EXTENSION

We represent the coefficient of extension by the predicted current crustal thickness which is proportional to $1/\beta$, for different values of relaxation temperature (Fig. 5.1).

5.2.1 Flexural versus local loading response

There is a clear difference between the prediction obtained by assuming a flexural response to the load, even in the case of a thin plate, as the one controlled by the 250°C isotherm (at most 18 km under cold continental crust and as small as 0 under oceanic crust at rifting time), and the prediction obtained assuming pointwise isostasy. The flexural model predicts a sharp reduction of crustal thickness across the hinge zone: the crust is more than 31 km thick ($\beta<1.3$) 40 km landward of the hinge zone and less than 15 km thick ($\beta>2.7$) immediately seaward of it. The estimate of the extension factor across the hinge zone is therefore very sensitive to the assumption of the loading response of the lithosphere. The hinge zone corresponds to a major change in crustal structure (Watts and Steckler, 1979).

The flexural prediction also appears more compatible with the gravity model estimates (Hutchinson et al., 1982), but offset by about 20 km from it. When the error range is considered, this offset results in a disagreement only in the region from 130 km to 160 km from the coastline. This offset results from the fact that the gravity model predicts a sharp crustal reduction below the inferred Brunswick graben while the extension model predicts it below the hinge zone, 20 km further seaward. We can imagine two reasons for that disagreement. First, the extension model assumes that tectonic subsidence is due to lithospheric thinning right below the area of subsidence, and we may be seeing the limitation of that assumption which may not be valid below a 20 km horizontal scale. Second, if the Brunswick graben is partly synrift it may correspond to some extra crustal thinning. However, the extension model would once again localize this crustal thinning right below it in contrast to the gravity model which puts it seaward from its center (Fig. 3.3, Chapter 3), which sends us back to the same problem of horizontal resolution of the extension model.

5.2.2 Error range

To evaluate the error range due to uncertainties in basement depth and sediment properties we inverted the two extreme sets of data which would give the maximum and minimum estimate of extension: mainly a set where the basement is taken at its deepest estimate and the porosity at its highest estimate and a set where the basement is taken at its shallowest estimate and the porosity at its lowest estimate. This was done for the relaxation temperature of 350°C which is the most compatible with gravity data (section 5.2.3).

The resulting error range shows, as in the 1-D model (Chapter 4), that the extension factor, β, is poorly constrained between the hinge zone and the ECMA (Fig. 5.1). Moreover, in that area the flexural model predicts a large amount of extension, and at large values β becomes very sensitive to tectonic subsidence, therefore in errors in basement depth and sediment properties. This may explain why the predicted crustal thickness is irregular and why it was even more so in other estimates which we made assuming flexural compensation of the synrift sediments, because in the latter case errors in basement depth lead to a greater adjustment of tectonic subsidence and lesser adjustment of loading effect.

Our model could not totally account for these extreme data in several instances:

Landward of the hinge zone, 90 km to 100 km from the coastline, the extreme choice of constraints which corresponds to smallest tectonic subsidence cannot be fully accounted for by setting $\beta=1$ resulting in a topographic misfit of at most 170m. In other words at that location the loading effect alone predicts more subsidence than observed for these extreme hypotheses.

Between the hinge zone and the ECMA, the extreme choice of constraints which corresponds to the largest tectonic subsidence cannot be fully accounted for even by setting $\beta=\infty$, or in other terms by assuming that no crust is left. This results in a topographic misfit of at most 700m.

This shows that assuming extreme basement and porosity estimates together is excessive and results in data which are at the limit of what the extensional model could account for. However, there is no real lower bound for the basement depth on the seismic record between the hinge zone

and the ECMA. Therefore, if the basement was ever proven to be substantially lower than our lower estimate in that area, the extension model would have serious difficulties accounting for the corresponding very large subsidence.

Seaward of the ECMA, the two extreme models misfit the topography by a very large amount (up to 2.3 km). This suggests that these extremes are excessive. Therefore they cannot be accommodated by Parsons and Sclater's (1977) parameters which, after all, were designed to account for the average subsidence of normal seafloor.

In the case of the one-dimensional model, there was no such topographic misfit landward of the ECMA and only a smaller one seaward of it (less than 1.6 km; fig. 4.3 of chapter 4) because more of the anomalies are absorbed in the loading effect in the case of pointwise isostasy than in the case of flexural response.

5.2.3 Gravity predicted by the extensional model

Since different assumptions about the loading response lead to different crustal thickness estimates, an independent source of information is needed to constrain these assumptions. Therefore we compute the gravity predicted by the extensional model structure and compare it with data in order to constrain the value of the relaxation temperature T_R (Fig. 5.2). The gravity calculations are done as in Hutchinson et al. (1982) but for two modifications: the Brunswick graben is given a standard crustal density of 2.7 g/cm^3 and the mid-crustal density discontinuity and Moho are those predicted by the extensional model for different values of T_R. The best fit occurs for T_R between 300°C and 350°C (Fig. 5.2b and 5.2c). This value is in the lower range of the 300°C to 600°C bracket observed for oceanic lithosphere (Watts et al., 1980) but the same trend is observed for the continental margin of Nova Scotia where, using the same modeling techniques as ours, a best value of 250°C is obtained (Beaumont et al., 1982).

The gravity fit is considerably enhanced by the introduction of flexural rigidity (compare Fig. 5.2b with Fig. 5.2a) but the value of T_R remains poorly constrained because of large error both in the gravity modeling due to uncertainties on the sediments densities (Barton, in press) and in the extensional modeling due to uncertainties on basement depth and sediment properties.

Therefore a good test of both approaches and a better constraint on T_R would come from either reduction of these uncertainties or from independent crustal thickness estimates by refraction data.

5.2.4 Thermal blanketing

The two dimensional local model (Fig. 5.1) gives slightly higher estimates of extension than the one dimensional local model (Fig. 4.1 of chapter 4). The maximum difference is about 30% and is reached in the central part of the basin. The main cause for that difference seems to be the effect of thermal blanketing which is included in the two dimensional simulation and neglected in the one dimensional model. This raises the temperature of the basement to 150°C while this temperature is assumed 0°C in the one dimensional model. The effect of the extra heat stored in the lithosphere on depth has then to be compensated for by more extension. Other but less significant causes of difference between the two models include slightly different parameter values and compensation depth [Appendix A and C].

5.3 THE VARIOUS CONTRIBUTIONS TO SUBSIDENCE

The tectonic subsidence is obtained by running the simulation with the same initial condition as the normal run but without adding sediments during the evolution.

5.3.1 Present day situation

Introducing a flexural response modifies the predictions in opposite sense landward and seaward of the hinge zone (Fig. 5.3). The loading effect is less intense seaward of the hinge zone, where the main load is located and more intense landward of it, than in local isostatic estimates. As expected, flexural response tends to spread out the loading effect and reduce its peak. As a result, in order to maintain the same total tectonic subsidence, imposed by the observed basement depth, the flexural model predicts less tectonic subsidence landward of the hinge zone (up to 60% or 700m less) and more seaward of it (up to 20% or 1.1 km more) than the local model.

The flexural model tectonic subsidence shows more irregularities seaward of the hinge zone than does the local isostasy model. There are two reasons for this. First, by smoothing the loading effect in space, the introduction of flexural rigidity increases the irregularity of the tectonic subsidence as the sum of these two effects, which is the observed basement depth, is a constraint on the model. This also accounts for the enhancement of the hinge zone in flexural model. Second, because seaward of the hinge zone, more of the total subsidence is attributed to the tectonic subsidence, the basement irregularities have an enhanced effect on tectonic subsidence. This in turn explains why the predicted crustal thickness is irregular as mentioned earlier.

The initial and thermal subsidence remain of equivalent magnitude as in the one dimensional model. The reduced amount of initial subsidence landward of the hinge zone is more compatible with the absence of synrift deposits and the inferences of early erosion. Yet, the model still predicts this area to be initially submerged.

The two-dimensional local model predicts up to 400m more tectonic subsidence than the one dimensional model in the center of the basin, essentially to compensate for the effect of thermal blanketing by the sediment.

5.3.2 Evolution through time

We show the predicted evolution through time of the water depth, tectonic subsidence and total subsidence by both the local and flexural models at 3 different locations corresponding to the three areas A, B, and C (as defined in Chapter 3,section 3.4).

Zone A (SP2000, Fig. 5.4):

The local model (Fig. 5.4a) predicts a large (500m) initial subsidence which results in a large early water depth. The tectonic subsidence represents between 100% (early) and 55% (late) of the total subsidence and is therefore the major contribution to subsidence. A slight lateral heat flow tends to decrease the tectonic subsidence and therefore to maintain higher elevations during the first 25 MY after rifting but its effect is less than 100m.

The flexural model (Fig. 5.4b) predicts a much smaller (150m) initial subsidence which results in a small initial water depth. However an intense (around 500m) loading effect which corresponds to the filling of zones C and D with a thick Jurassic sequence increases the water depth to 700m during the first 25 MY after rifting. After 25 MY after rifting total subsidence and water depth are similar to those of the local model. However the loading effect which represents between 65% and 75% of the total subsidence remains the major contributor to subsidence until today. The effect of lateral heat flow is larger (up to 200m) and makes the tectonic subsidence curve concave early after rifting. In both cases this area receives extra lateral heat from seaward and this effect is enhanced in the flexural model by the more abrupt transition.

Zone B (SP2800, Fig. 5.5):

This zone, also landward of the hinge zone, follows the same pattern as zone A. The total subsidence and water depth predicted by the local (Fig. 5.5a) and flexural (Fig. 5.5b) models differ only during the first 6 MY after rifting. The local model predicts an initial subsidence of 1.2 km, a tectonic subsidence that is 55% of the total subsidence and a maximum lateral heat flow effect on tectonic subsidence of 200m while the flexural model predicts 600m of initial subsidence, a 35% tectonic share of total subsidence and up to 600m of lateral heat flow effect.

Zone C (SP3400, Fig. 5.6):

The comparisons are reversed as the hinge zone is crossed: the flexural model now predicts a larger initial subsidence (2.8 km) than the local one (2.2 km), a larger share of tectonic to total subsidence (55% versus 40%) and the lateral heat flow tends to increase the early tectonic subsidence (about 250m in local, 350m in flexural) because the heat is now flowing landward towards the colder hinge zone. The water depth and total subsidence (basement depth estimates) of the two models differ only before the top of the Jurassic (31 MY after rifting).

5.4 PALEOWATERDEPTH

5.4.1 Profiles at fixed times

Reconstituted cross sections of the basin are shown for 6 different times for both the local and flexural model (Figs. 5.7 to 5.12). The two dimensional local model has more realistic predictions than the one dimensional model (Chapter 4) for the zone A,B,C. This is mainly due to the lateral heat transfer which keeps zones A and B higher and zone C lower early after rifting. However, the flexural model prediction looks even more realistic in many different respects. First, the hinge zone is present from the end of rifting time (Fig. 5.7b) where it separates shallow zone A (up to 250m deep) and B (300m to 750m deep) from a deep trough (1 to 3 km deep) of zone C; it also controls the deposition of the synrift sediments (Fig. 5.8b) which have an almost flat surface. Second, from the end of the Callovian until the Cretaceous, the shelf edge is sharply defined (see Fig. 5.9b, end of Jurassic, and 10b, end of Cretaceous), especially if one considers that this edge was partly eroded during the mid-Oligocene and that the missing sediments are not included in the reconstruction. Besides predicting too progressive a slope, the local model tends to unrealistically bend landward the reflector below that slope because of differential loading (Fig. 5.9a).

At mid-Oligocene time (Fig. 5.11) both models give similar predictions and the present predicted cross section (Fig. 5.12) was constrained to fit the observations landward of the ECMA (Fig. 3.2, Chapter 3).

Three slight problems can be noticed. First, the flexural model cannot account for a steep oceanic basement bend around the ECMA and this results in a misfit in the present topography (Fig. 5.12b). However this occurs in an area where the basement picks are poorly constrainted (Fig. 3.4, Chapter 3). Second, both the local and flexural models predict waterdepth 300m to 500m below expected on the shelf from the top Callovian to Cretaceous. Third, the slightly convex shape of the shelf for the flexural model at the end of the Jurassic (Fig. 5.9b) suggests that we are close to the upper limit of acceptable flexural plate thickness.

5.4.2 Evolution through time

As discussed with the results of the one dimensional model, (Chapter 4) because the model paleowaterdepth predictions (Fig 5.13) do not take into account erosion phases, they represent the lowest envelope of paleowaterdepth.

Zone A (SP2000):

Even though the flexural model predicts less initial subsidence than the local model, the larger loading effect which comes during the first 23 MY after rifting makes both models predictions very similar by the end of that period. The predicted depths (deepening from 170m initially up to 650m 23 MY after rifting for the flexural model) are therefore too large for an inferred shelf or subaerial environment. Later, from the end of the Jurassic to mid-Oligocene, the depth decreases from ~350m to 200m, which is still slightly deep for a shelf especially if the Cretaceous sea level rise is considered. After mid-Oligocene the current shelf built-up is well represented by the predictions.

Zone B (SP2800):

Here again the flexural and local models, even though predicting different initial subsidence (up to 400m of difference), agree by 6 MY after rifting (top Bathonian). They predict a water depth of more than 1 km for that time which is, again, too large for a shelf environment. From the end of the Jurassic to the end of the lower Cretaceous both predictions are very close and deepen from around 300m to 500m. Later, the flexural model predicts a rise during the Cretaceous and a fall after the mid Oligocene which is consistent with the Cretaceous sea level rise and mid Oligocene erosional event. The local model predictions seem insensitive to these events.

Zone C (SP3400):

Predicted initial subsidence is over 2 km but there is no independent check on it. From the end of Callovian to middle lower Miocene the predicted depth, between 500m and 600m, seems larger than the inferred shelf environment. The further deepening after mid-Oligocene time is consistent with the inferred erosion occurring at that time.

5.4.3 Discussion

These results, when compared with the one dimensional model results, show one clear improvement: the depths of zone A, B, and C relative to each other are correctly predicted. In other words, the shape problem is solved. Yet two problems remain: too great a depth in zone A and B early after rifting (less than 25 MY), and a slightly too great overall depth (400m to 500m too much) from the end of the Jurassic to mid-Oligocene.

The second problem (overall too great depth by around 400 to 500m) can be related to three causes: first, we ignored erosions because the amounts are not known; second, the model set-up error, comparable to the set up error for the one dimensional model (Appendix A; section A.4.7), can account for a significant amount of this misfit (from 200m at the landward edge of zone A to 600m at the seaward edge of zone C); third, because salt tectonics have been active since late Jurassic in zone C, we underestimate past sediment thickness in that area, resulting in an overestimate of waterdepth. It can be noticed that this last explanation which was not acceptable for the one-dimensional model because it would lift the late Jurassic shelf too much, is acceptable now because the late Jurassic shelf depth is not very different from Cretaceous depth in the two dimensional model.

The first problem (too much subsidence in zone A and B early after rifting) seems too large to be accounted for by erosion and model set-up errors. We are then left with two hypotheses: either the initial conditions of near sea level water depth and thermal equilibrium assumed by the model are not correct or there was more heat input during rifting than predicted by uniform extension, suggesting two layer extension. The same early predicted depth problem has been reported in the Nova Scotian basin (Beaumont et al., 1982).

5.5 CONCLUSIONS

Compared to the simple one dimensional model, the two dimensional model gives much more realistic predictions.

The main contributor to these improvements is the introduction of flexural rigidity which leads to a crustal transition more consistent with gravity data and more realistic paleostratigraphy. The estimation of the extension factor, β, appears sensitive to the choice of loading response. However, if flexural response appears a better assumption, the thickness of the plate, or the controlling relaxation temperature, is poorly constrained.

The effect of lateral heat flow improves the early predicted paleogeography but this effect which is enhanced when coupled with flexural response, remains small compared to the influence of the loading response assumption and data uncertainties.

Neglecting thermal blanketing by the sediments results in a slight underestimate of extension factor (30% in the deepest part of the basin where β reaches values around 5). This is also a small effect when compared to loading response assumption and data uncertainties.

The early predicted paleodepth seems too large landward of the hinge zone. Contrary to expectation, flexural response does not improve that prediction very much because attributing subsidence either to loading effect or to tectonic subsidence turns out to predict very fast deepening early after rifting in both cases because the load is applied very soon after rifting. This suggests either different initial conditions than expected or two layer extension. Only independent constraints on the early paleogeography (pre- and synrift) would help resolve this problem. Later paleodepths seem slightly overestimated but a better knowledge of erosion amounts would be necessary to evaluate this further.

Overall the same error range due to data uncertainties as for the one dimensional model is observed in the two dimensional model. Thus the model is poorly constrained, especially seaward of the hinge zone, where the main basin is located. Better control on basement depth, sediment properties, Moho depth, paleoenvironment and amounts of erosion will be necessary before we can fully assess the significance of differences between model predictions and geological inferences.

Figure Captions

Fig. 5.1. Estimates of crustal thickness along line 32.
Gravity model is from Hutchinson et al., (1982). The extensional model predicts the crust thickness to be $40/\beta$ (in km). T_R refers to relaxation temperature; for local model: $T_R = 0°C$; flexural model corresponding to values of 250°C, 300°C, 350°C, and 400°C are shown. The error range on the prediction at $T_R = 350°C$ due to uncertainties on basement depth and sediment properties is also shown.

Fig. 5.2. Gravity calculation of our model predicted structure. Brunswick graben density at 2.7 g/cm^3. All other densities are as those of Fig. 3.3, Chapter 3.
5.2a: $T_R = 0°C$ (local isostasy)
5.2b: $T_R = 300°C$
5.2c: $T_R = 350°C$
5.2d: $T_R = 400°C$

Fig. 5.3. Different causes of subsidence along line 32 according to our model starting 175 MYBP.
From top to bottom: predicted initial subsidence (Sinitial), thermal subsidence (Sthermal), and loading effect (Sload). The sum of these three components is the predicted basement depth. In the oceanic part the basement depth prediction is not adjusted to the data: the star represents the data while the solid line represents the prediction. In the continental part the basement depth predictions were constrained to fit the data, therefore the solid line represents both the data and the prediction.
T_R=0 corresponds to local isostasy while the flexural model is controlled by $T_R = 350°C$

Fig. 5.4. Subsidence history at SP2000 along line 32. From top to bottom at the right hand side: predicted water depth, tectonic subsidence, basement depth; all these predictions are made assuming no variation of sea level. The difference between the upper and lower curve represents then the reconstituted sediment thickness through time while the difference between the median and lower curve represents the subsidence due to the load. Shaded area represents the difference in tectonic subsidence between a 1-D model (parameter as in appendix A) which gives the same present tectonic subsidence as the 2-D model with the 2-D model. This difference is mainly due to lateral heat transfer.
Jt: Jurassic top Kt: Cretaceous top
5.4a: model with local compensation
5.4b: model with flexural compensation, T_R = 350°C

Fig. 5.5. Same as Fig. 5.4 but at SP2800.

Fig. 5.6. Same as Fig. 5.4 but at SP3400.

Fig. 5.7. The Carolina trough 175 MYBP, just after rifting ceased. Same horizontal distance as in Fig. 5.3 [from 40 km to 280 km from coastline].
5.7a Local model
5.7b Flexural model

Fig. 5.8. The Carolina trough 174 MYBP, after deposition of synrift sediment. The horizons correspond to those of Fig. 3.2, Chapter 3.
5.8a Local model
5.8b Flexural model

Fig. 5.9. The Carolina trough at the end of the Jurassic, 144 MYBP
5.9a Local model
5.9b Flexural model

Fig. 5.10. The Carolina trough at the end of the Cretaceous, 65 MYBP
5.10a Local model
5.10b Flexural model

Fig. 5.11. The Carolina trough at mid Oligocene time 31 MYBP
5.11a Local model
5.11b Flexural model

Fig. 5.12. The Carolina trough today as predicted

5.12a Local model

5.12b Flexural model

The main constraint on the model is that this stratigraphy matches the data (Fig. 3.2, Chapter 3). However, the flexural model can not account for sharp oceanic basement bend and therefore predict an incorrect topography at that location.

Fig. 5.13. Predicted paleowaterdepth at 3 different locations along line 32 (SP 2000, 2800 and 3400). Uncorrected for sea level change.

line: Local model

dot-dash: Flexural model with T_R = 350°C

dash: Error range on flexural model due to uncertainties on basement depth and sediment properties

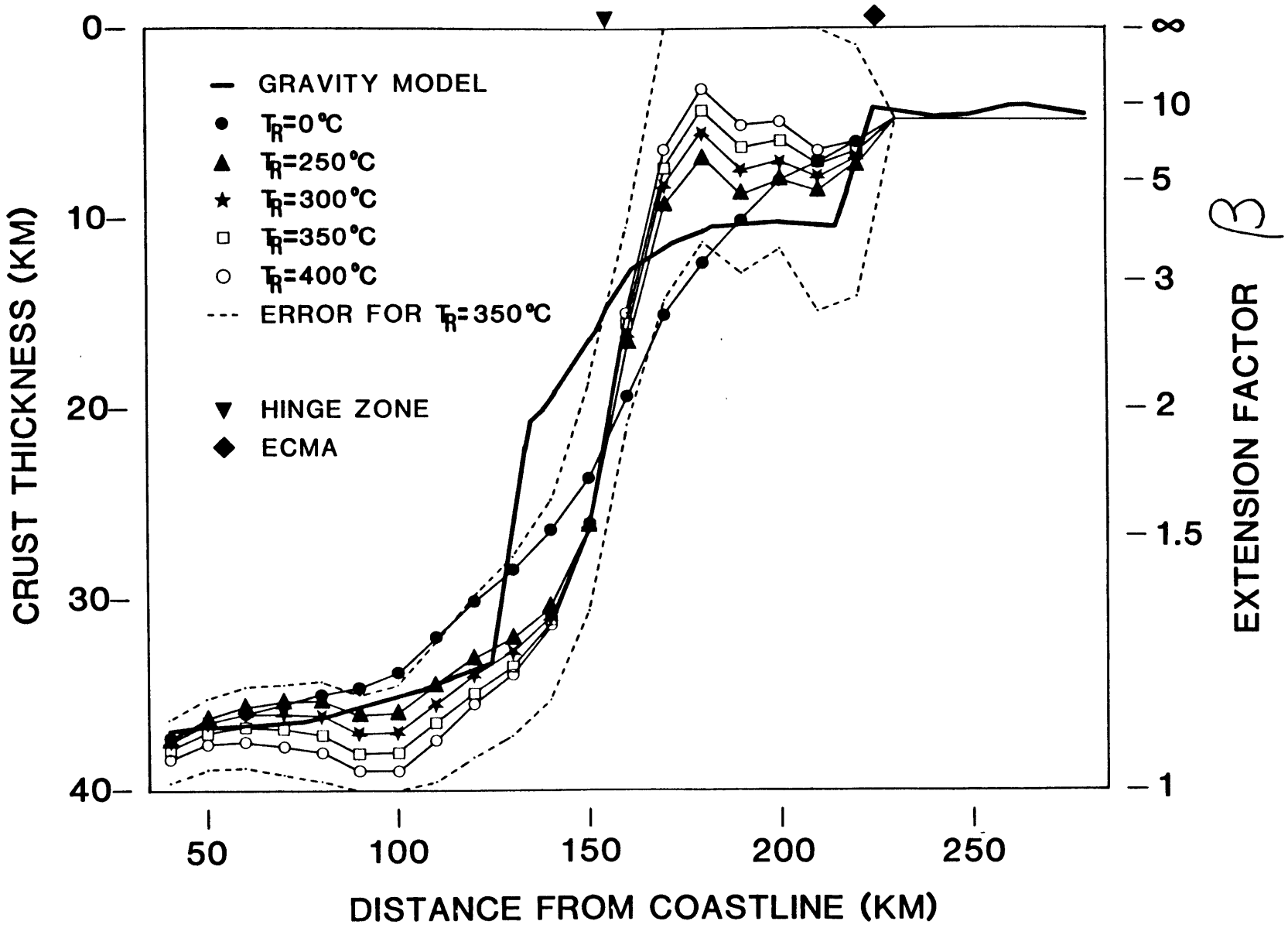
GRAVITY MODEL
T_R=0°C
T_R=250°C
T_R=300°C
T_R=350°C
T_R=400°C
ERROR FOR T_R=350°C
HINGE ZONE
ECMA
CRUST THICKNESS (KM)
0
10
20
30
40
EXTENSION FACTOR
∞
10
5
3
2
1.5
1
β
50
100
150
200
250
DISTANCE FROM COASTLINE (KM)

Fig. 5.1

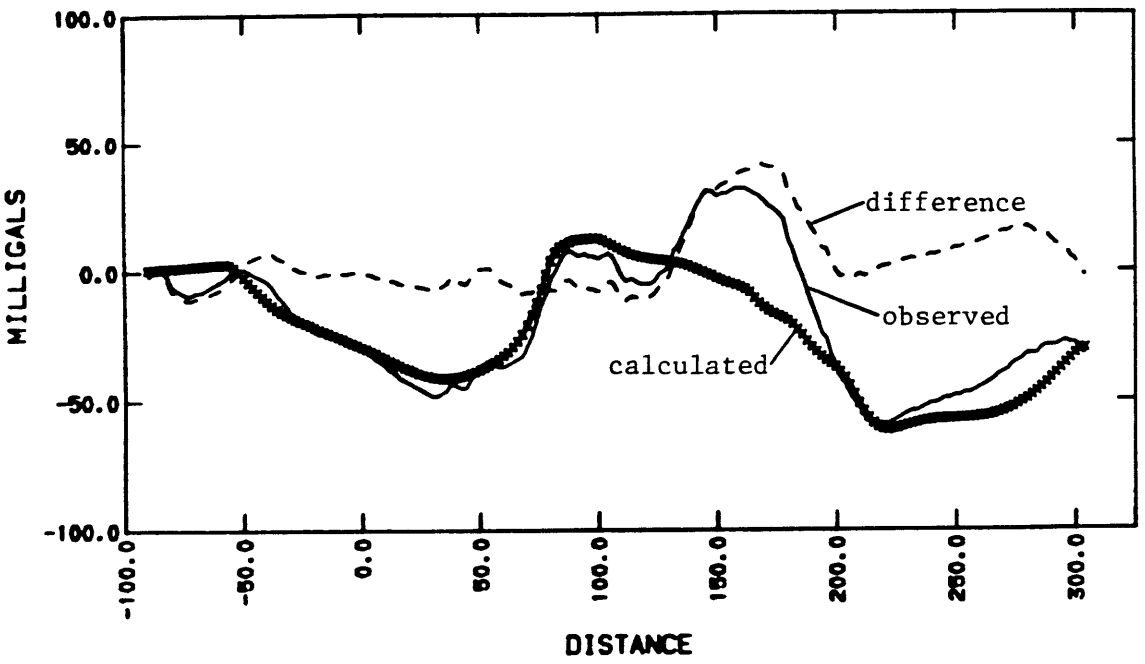
100.0
50.0
0.0
-50.0
-100.0
MILLIGALS
difference
observed
calculated
-100.0
-50.0
0.0
50.0
100.0
150.0
200.0
250.0
300.0
DISTANCE

Tr = 0°C

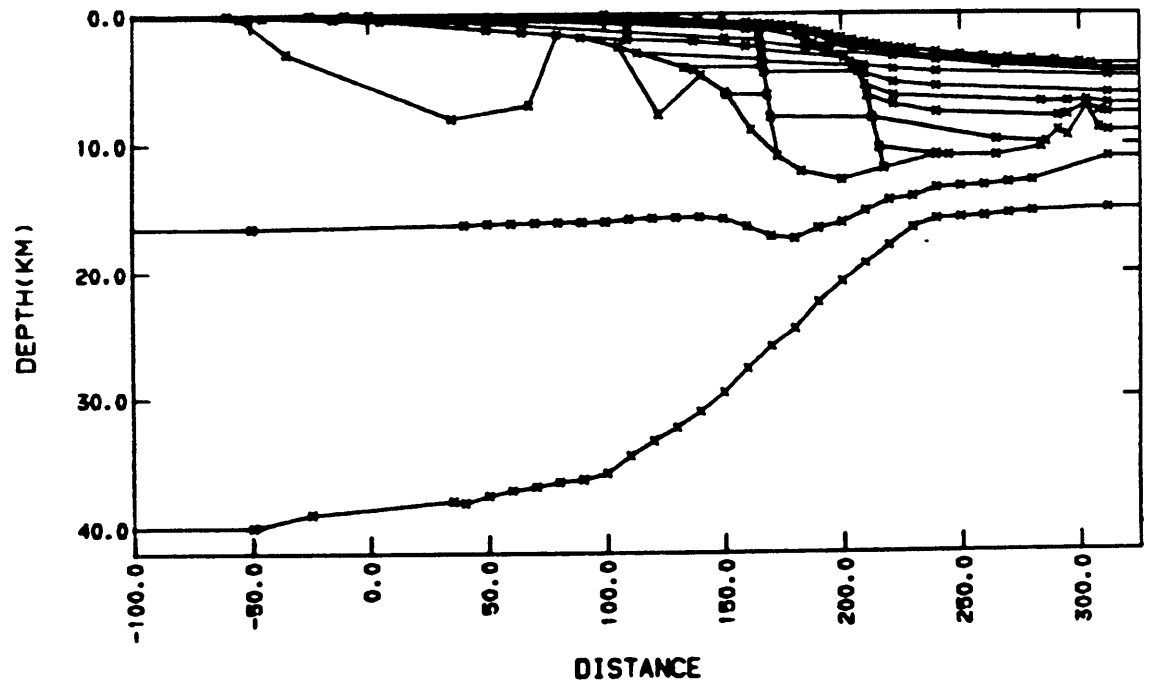
0.0
10.0
20.0
30.0
40.0
DEPTH(KM)
-100.0
-50.0
0.0
50.0
100.0
150.0
200.0
250.0
300.0
DISTANCE

Fig. 5.2a

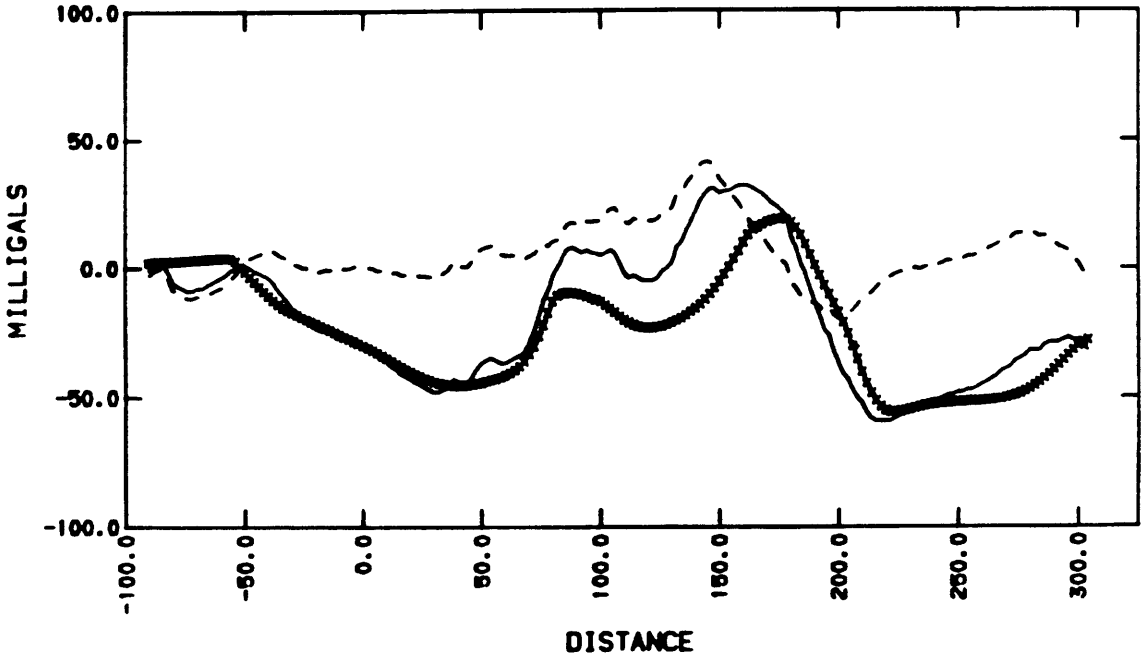

Tr = 300°C

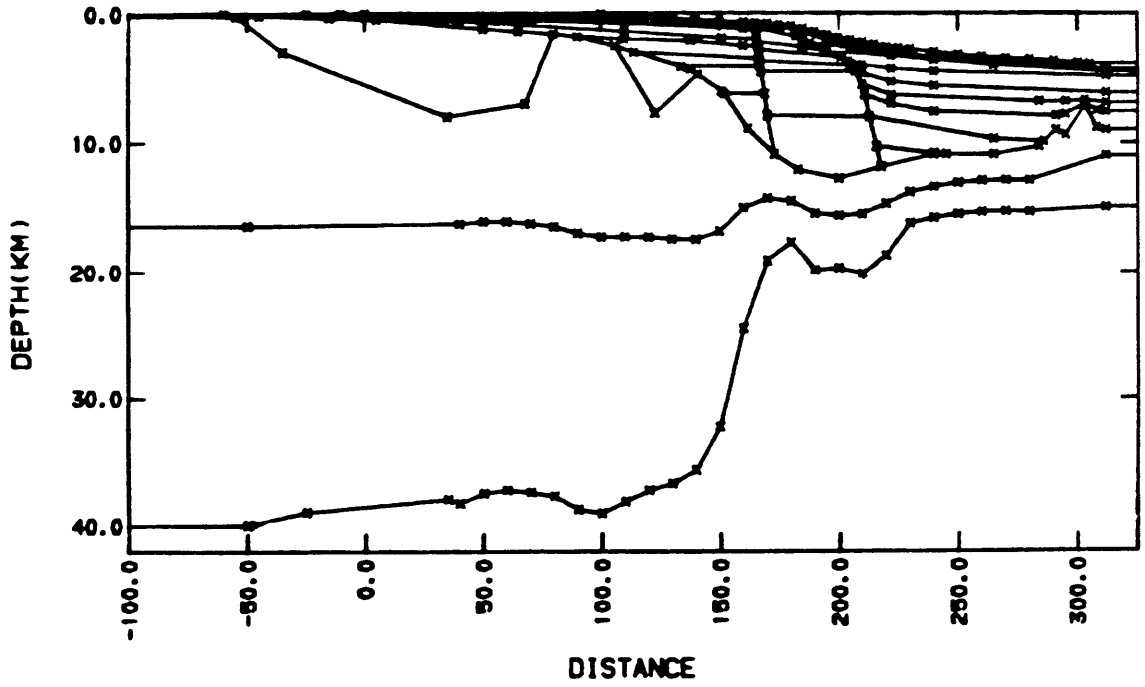

Fig. 5.2b

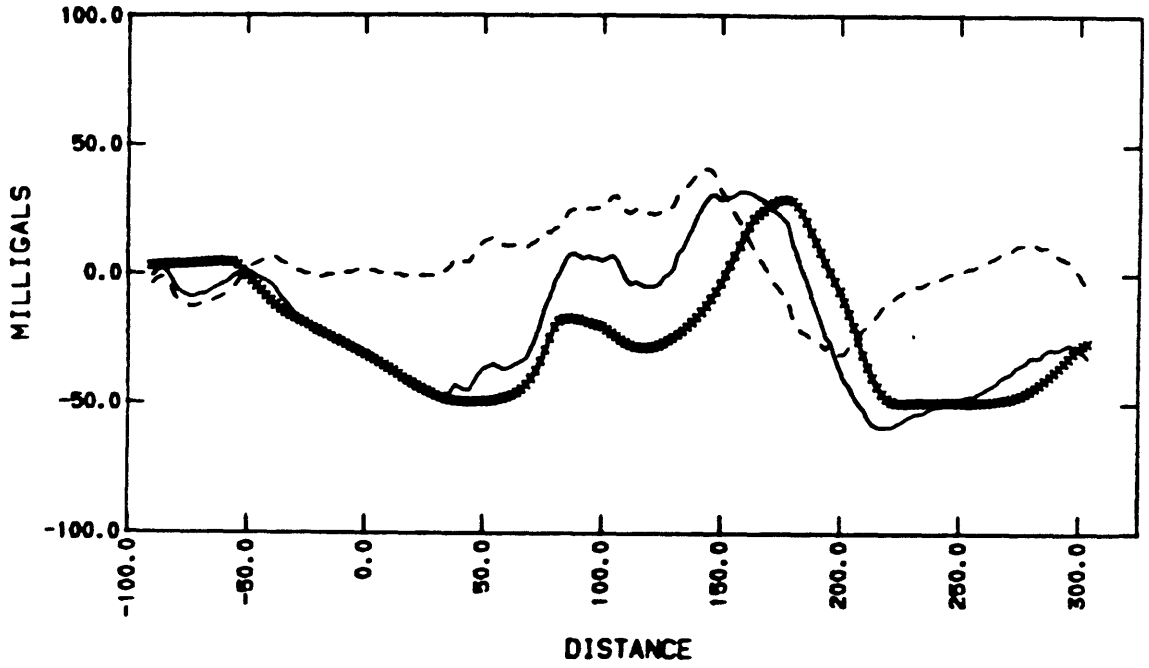

Tr = 350°C

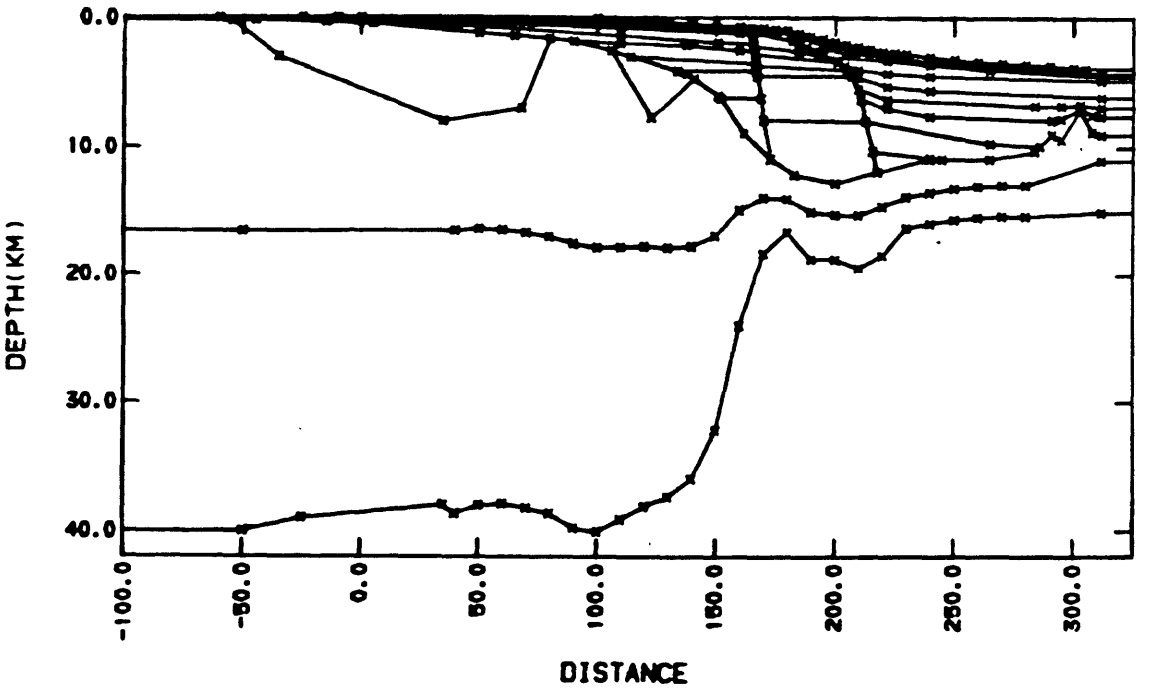

Fig. 5.2c

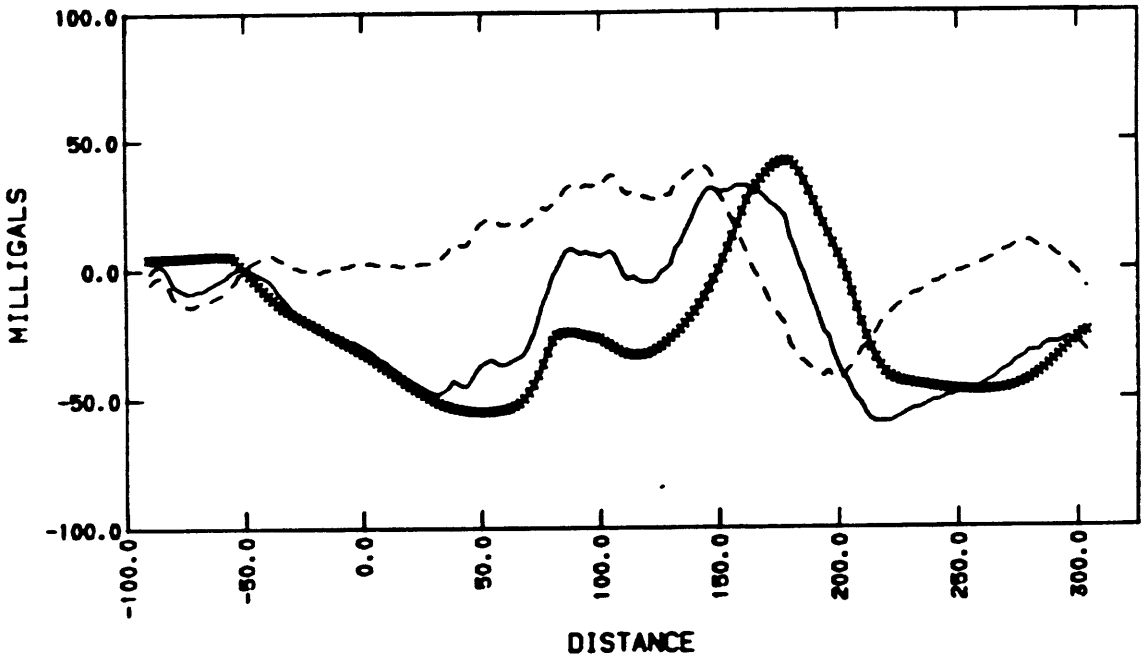

Tr = 400°C

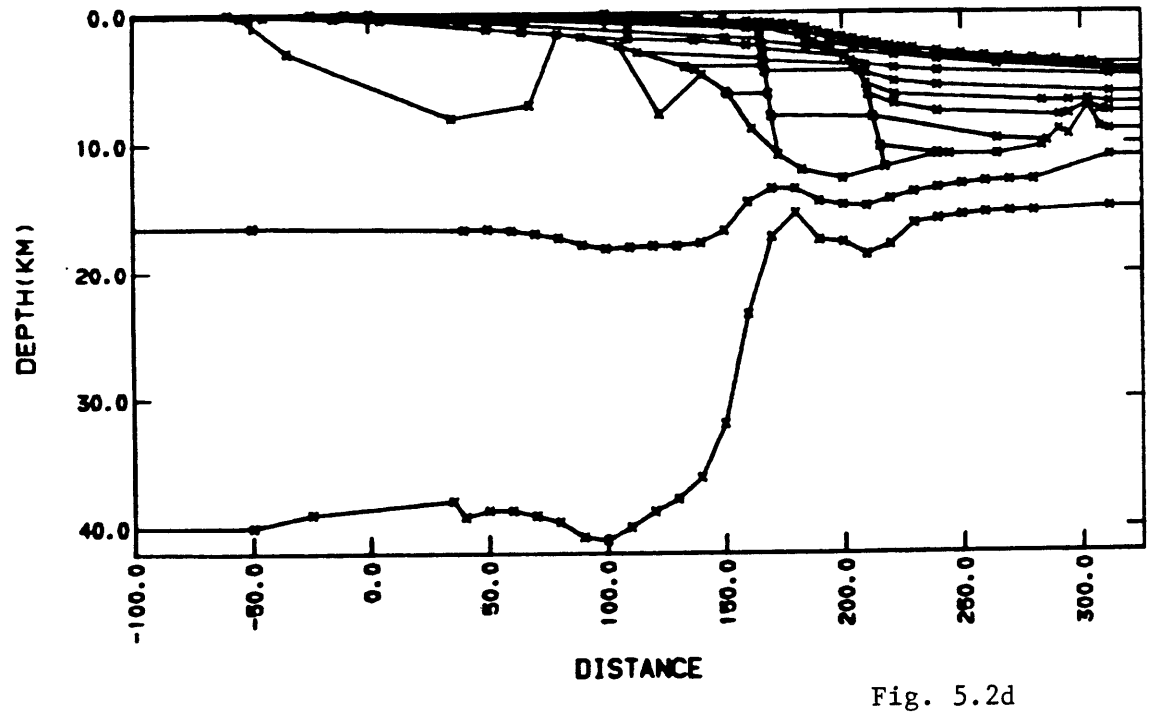

Fig. 5.2d

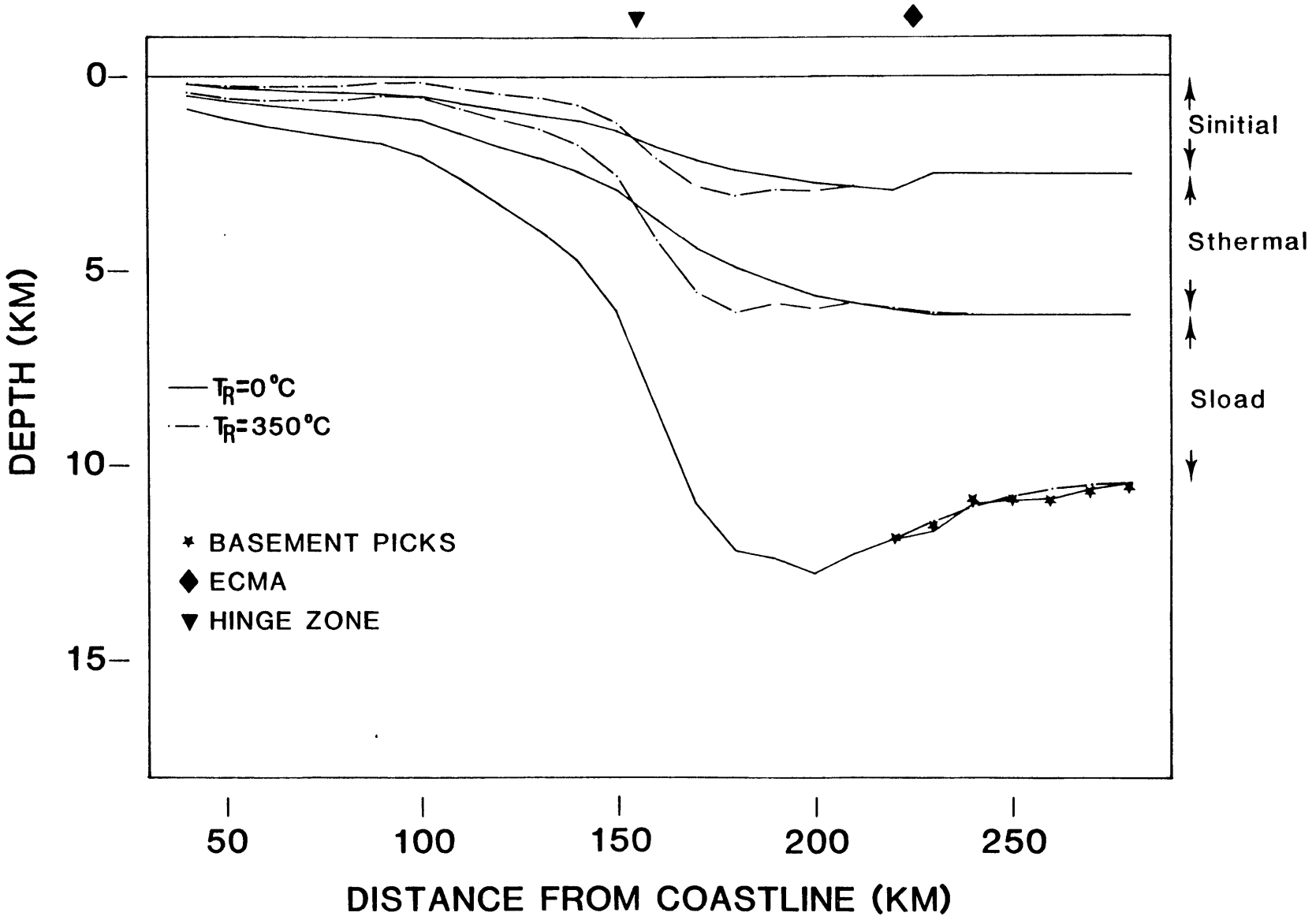
0
5
10
15
DEPTH (KM)
Sinitial
Sthermal
Sload
T_R=0°C
T_R=350°C
BASEMENT PICKS
ECMA
HINGE ZONE
50
100
150
200
250
DISTANCE FROM COASTLINE (KM)

Fig. 5.3

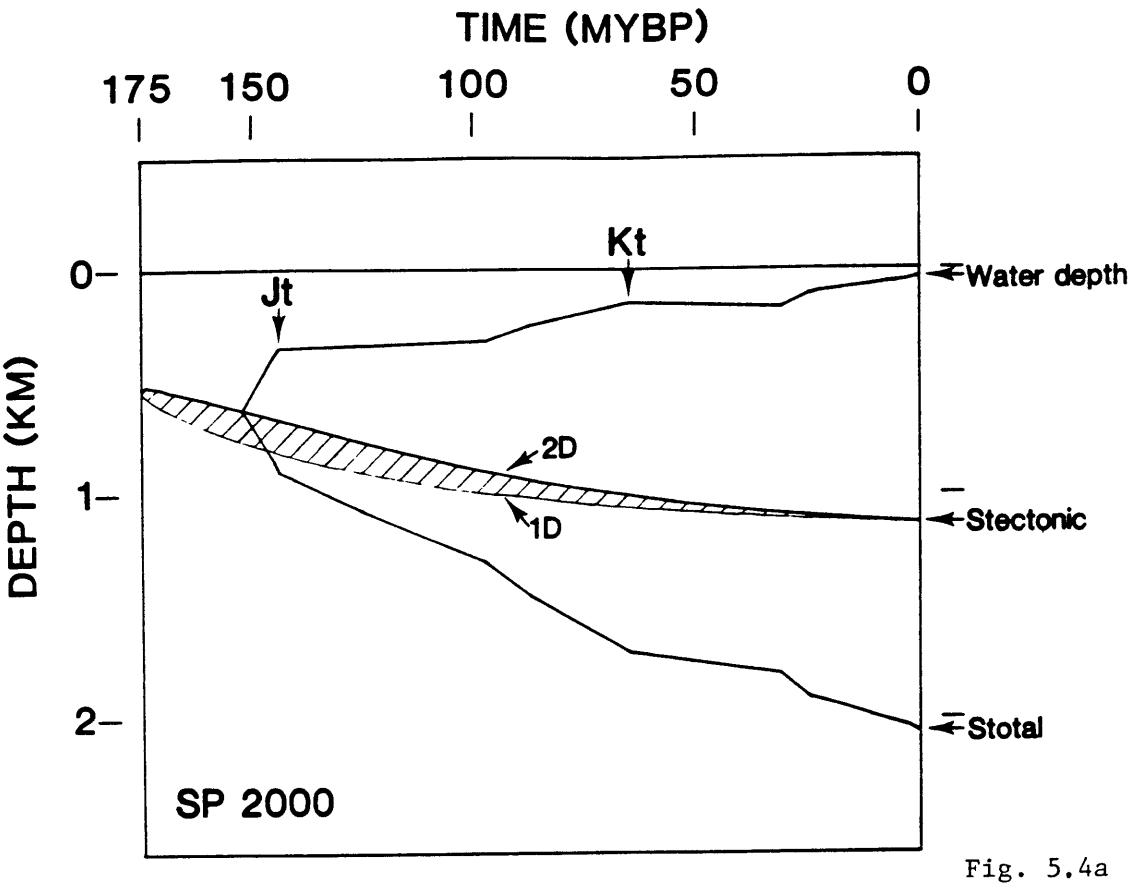

Fig. 5.4a

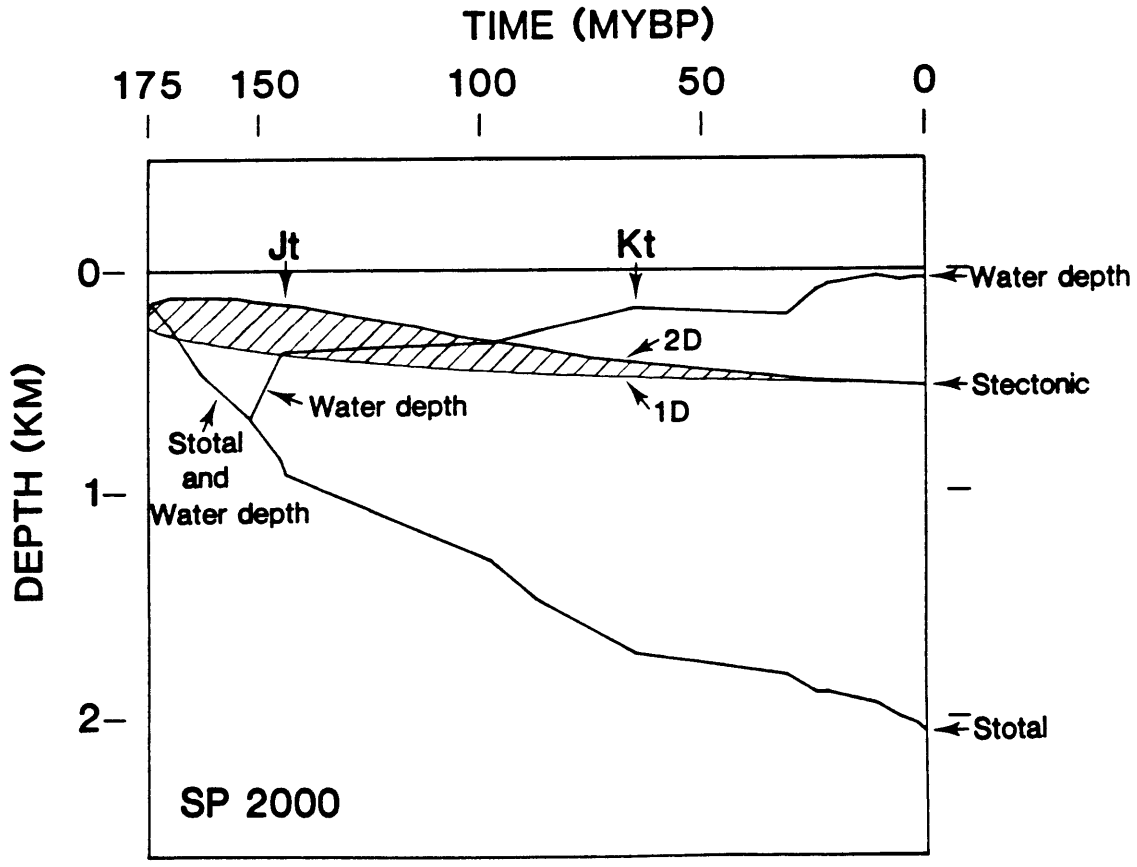

Fig. 5.4b

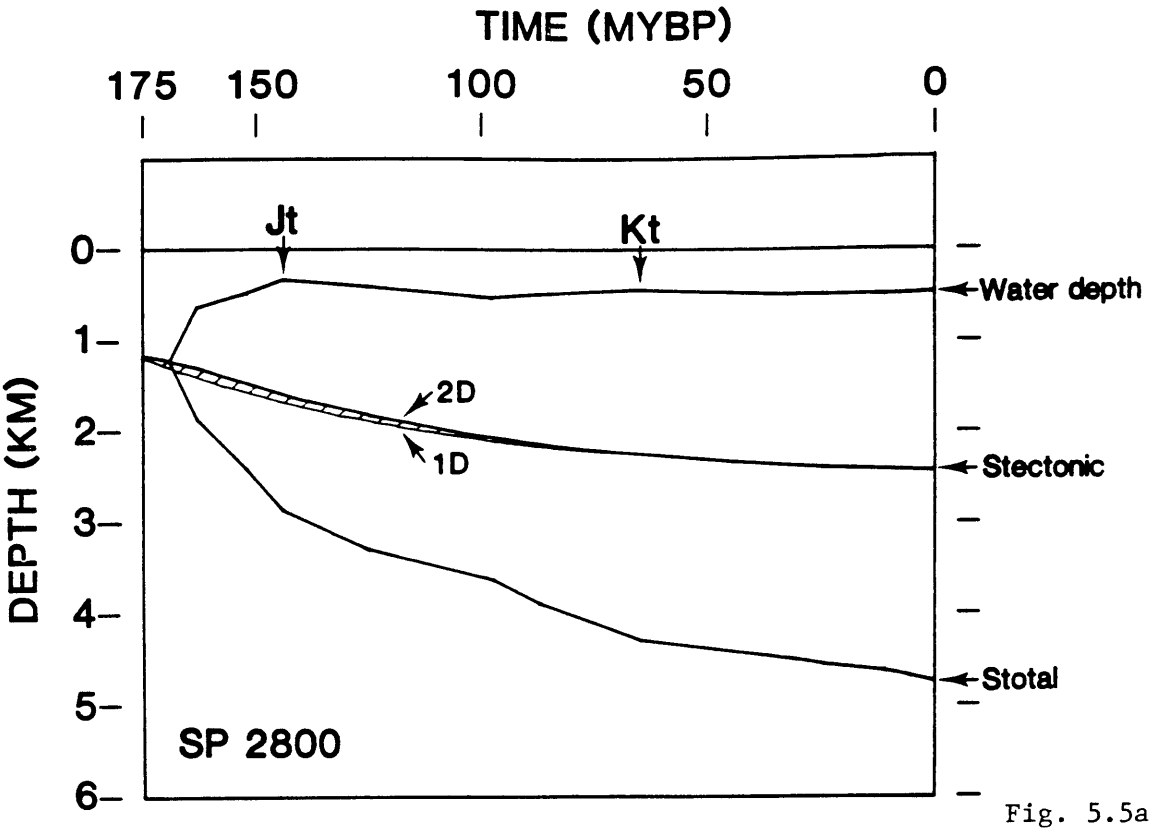

Fig. 5.5a

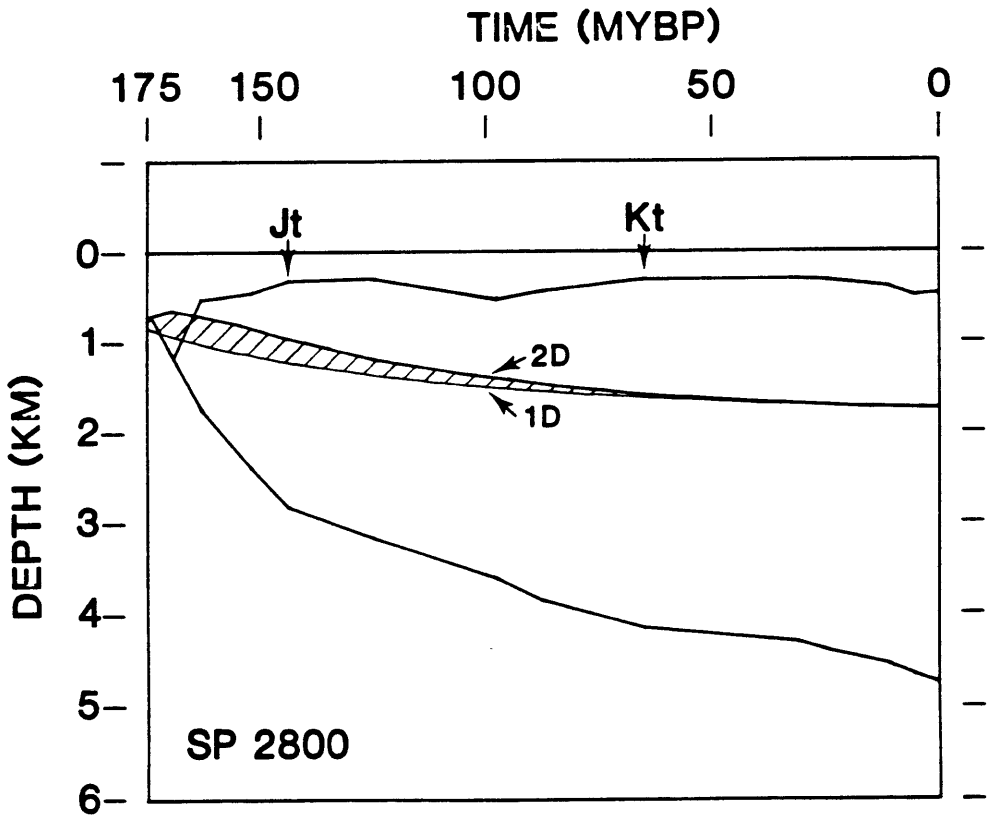

Fig. 5.5b

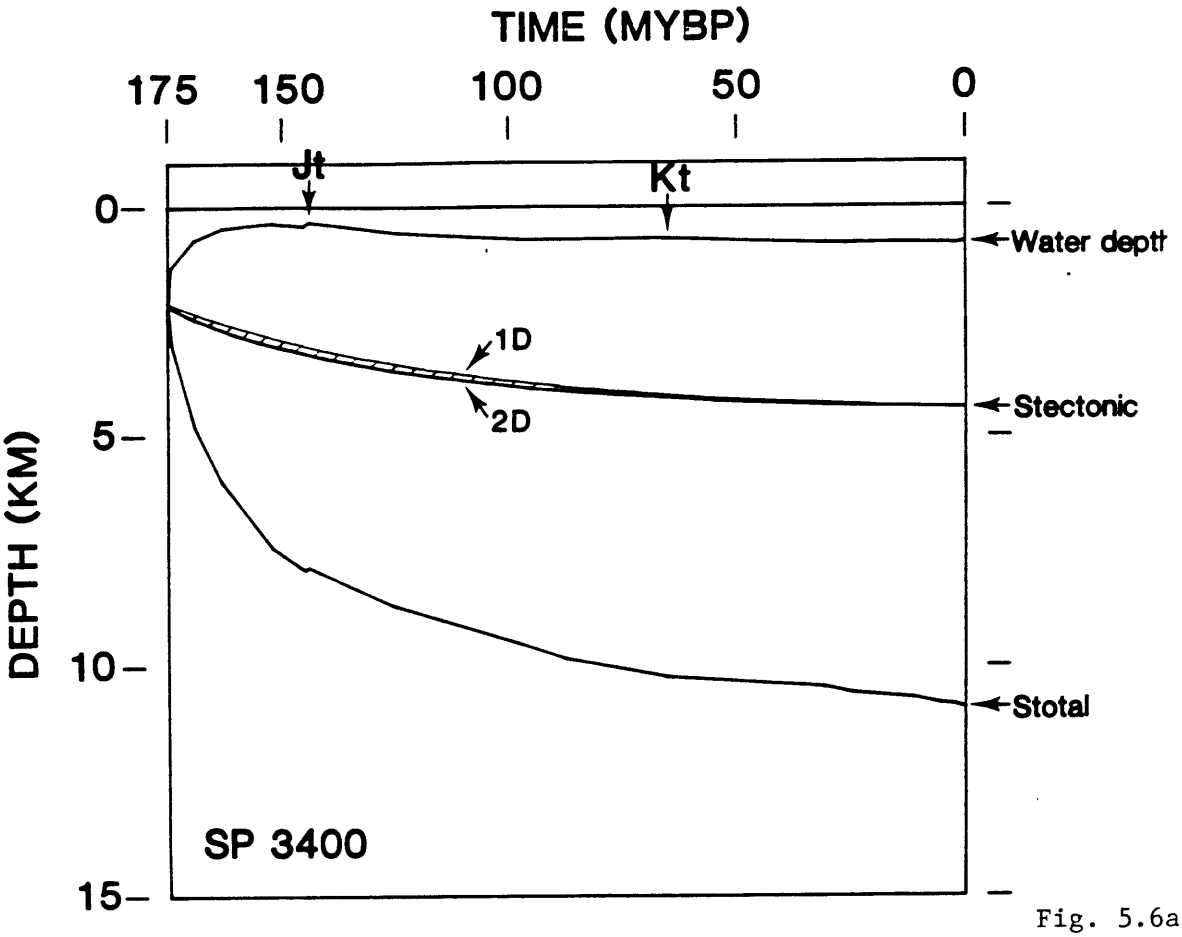

Fig. 5.6a

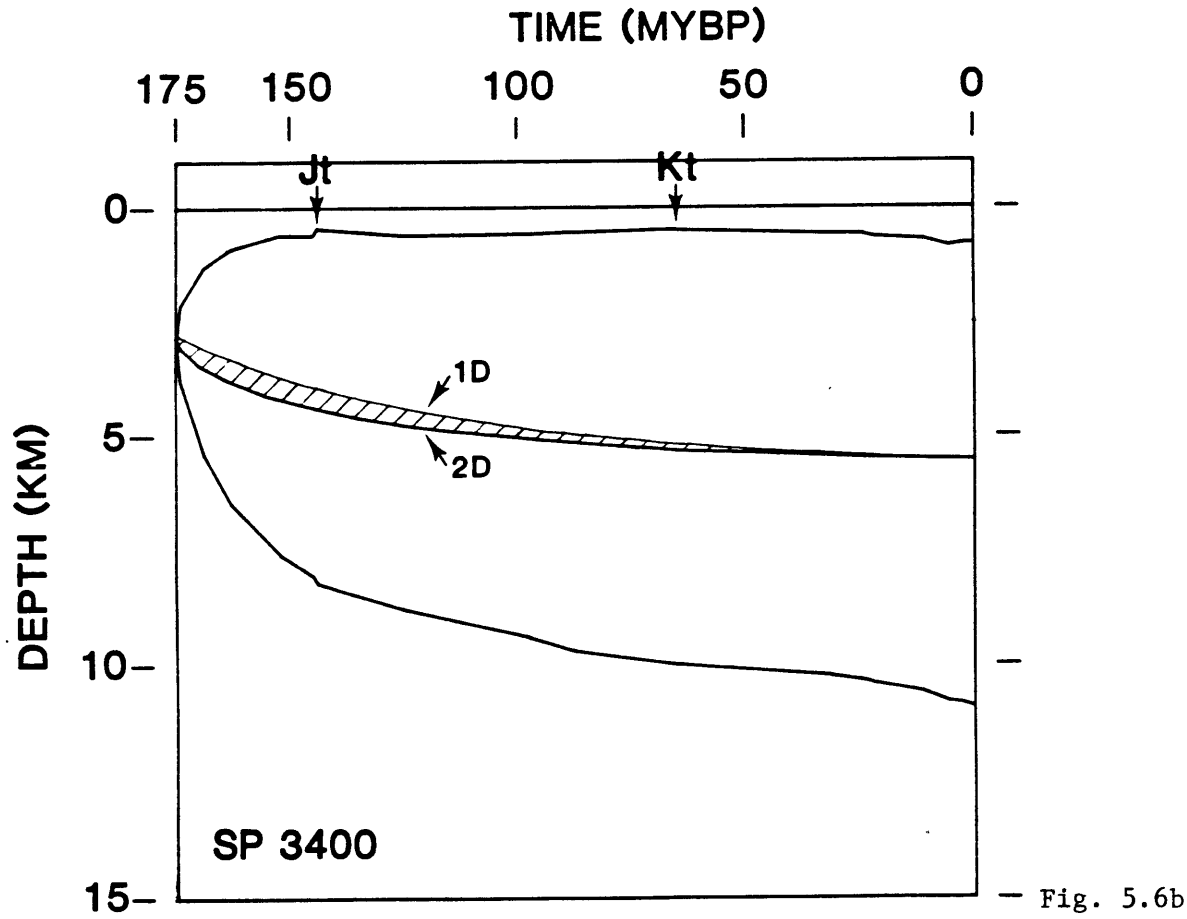

Fig. 5.6b

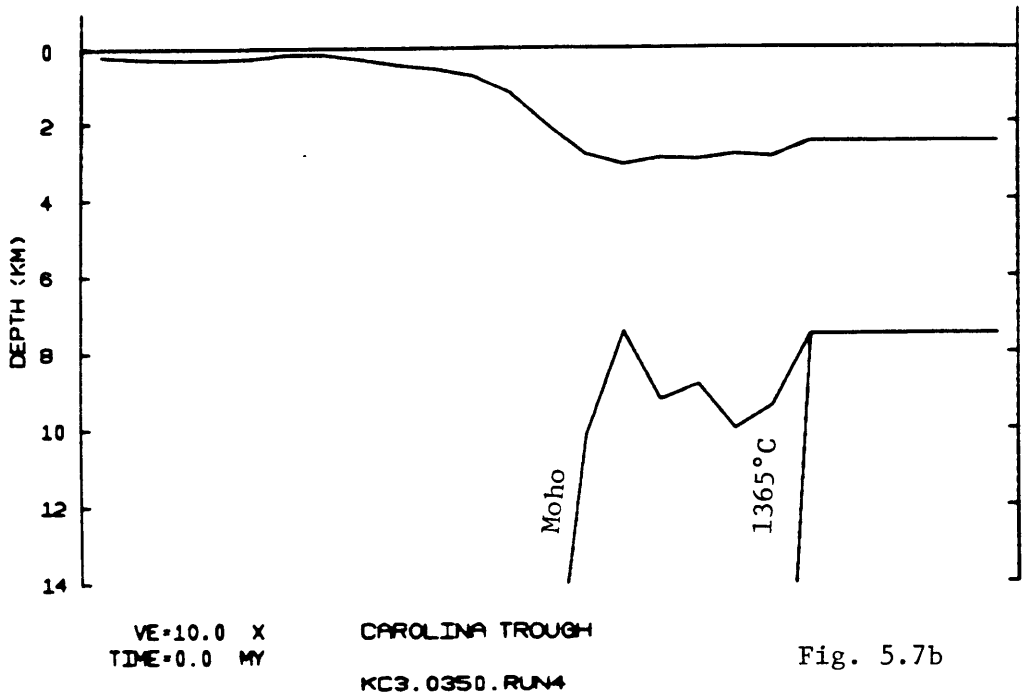

Fig. 5.7b

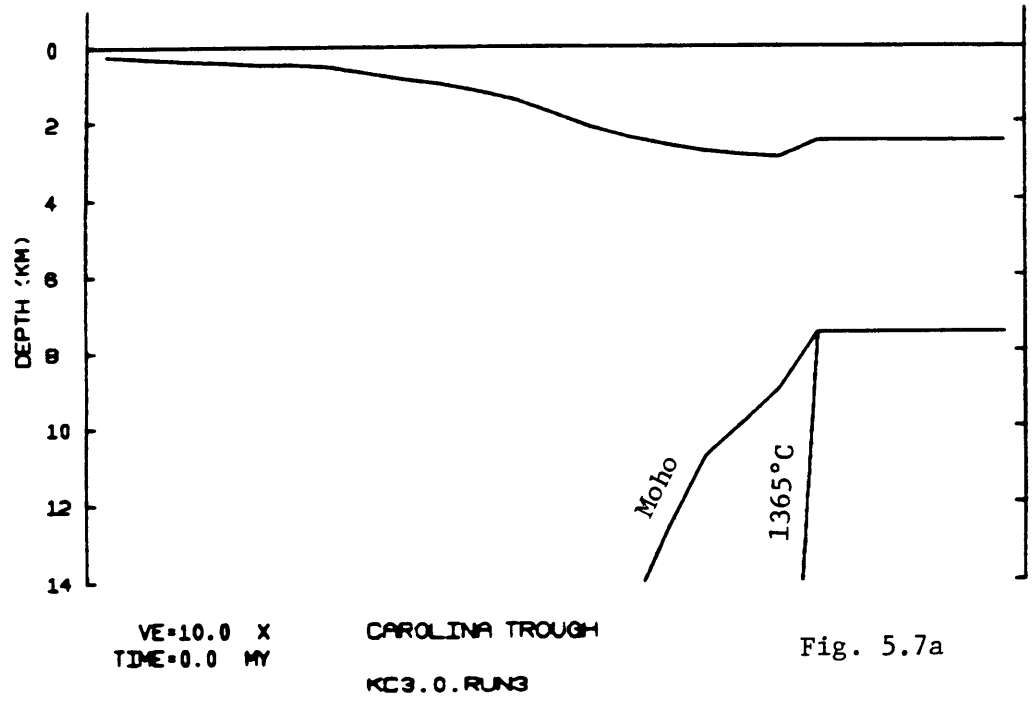

Fig. 5.7a

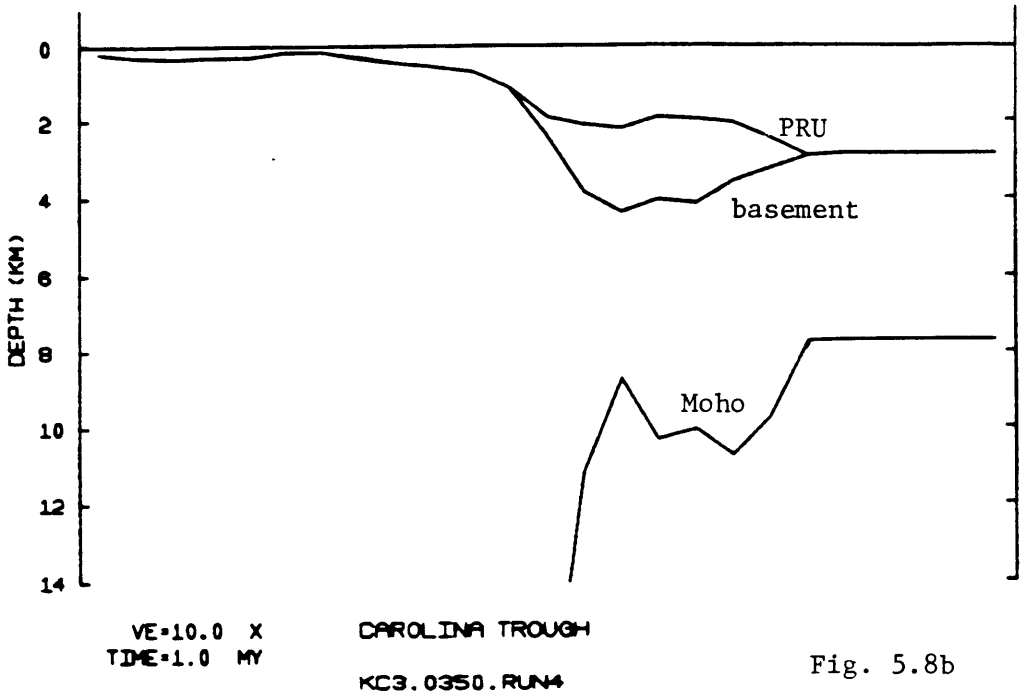

Fig. 5.8b

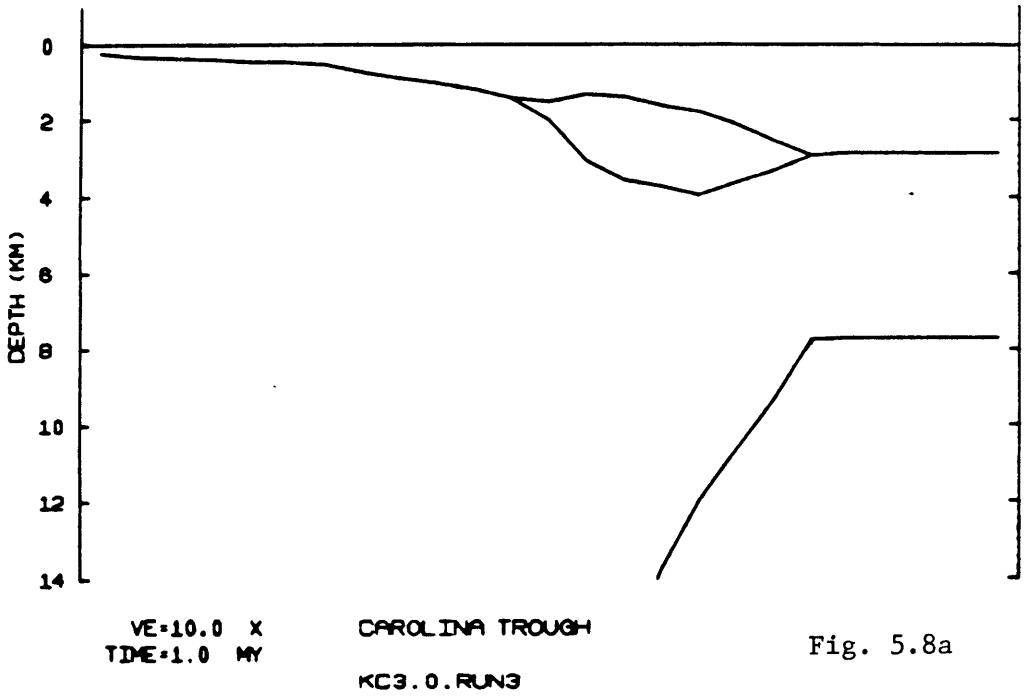

Fig. 5.8a

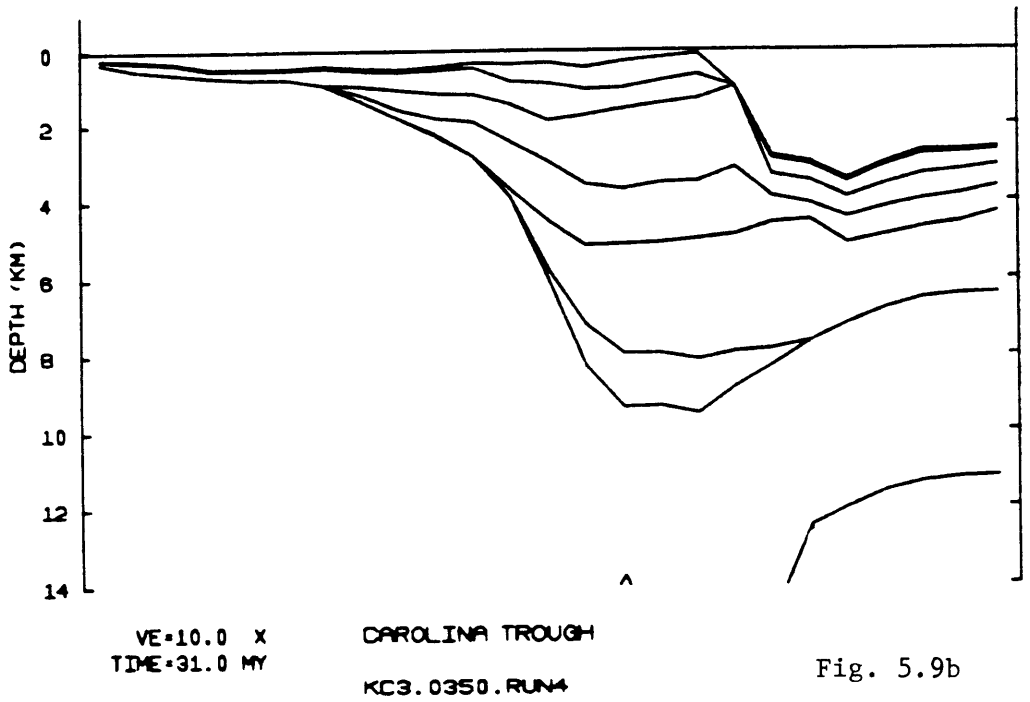

Fig. 5.9b

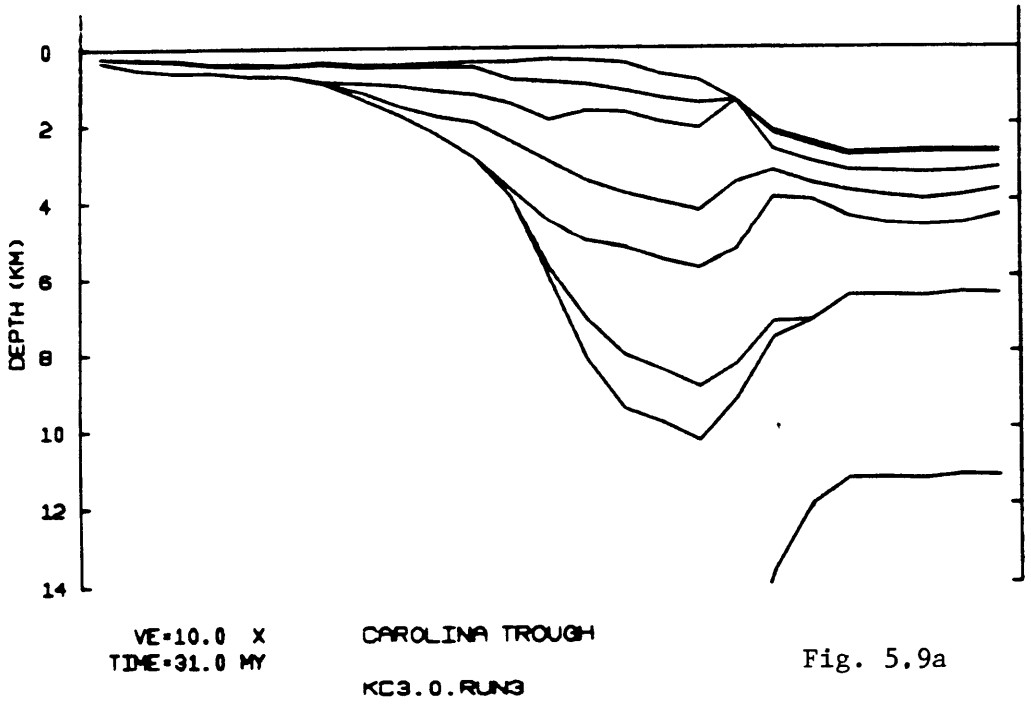

Fig. 5.9a

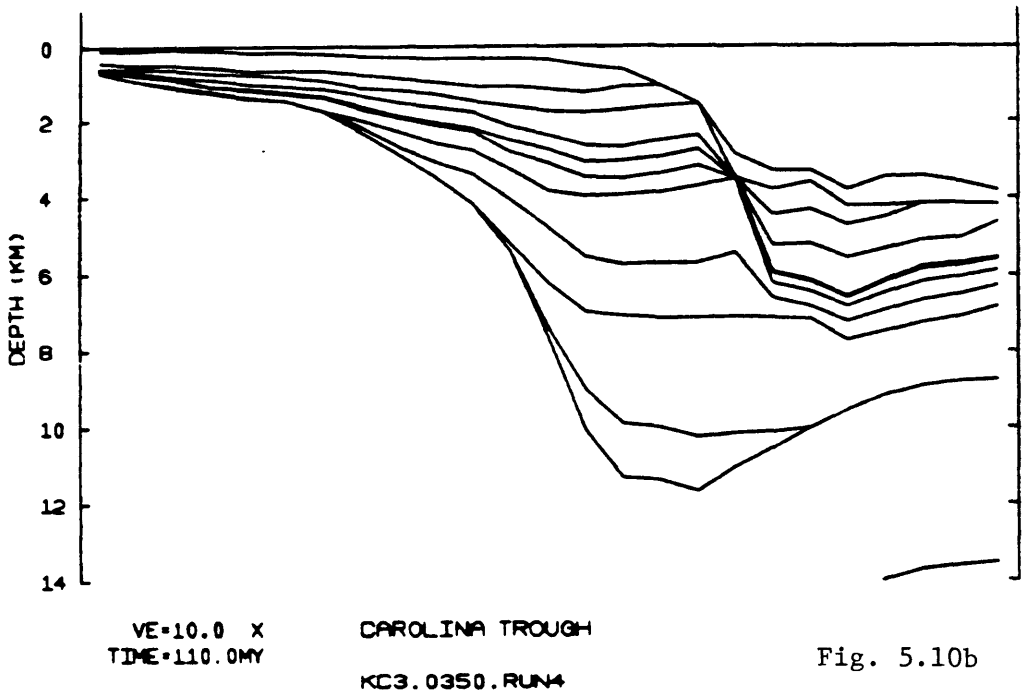

Fig. 5.10b

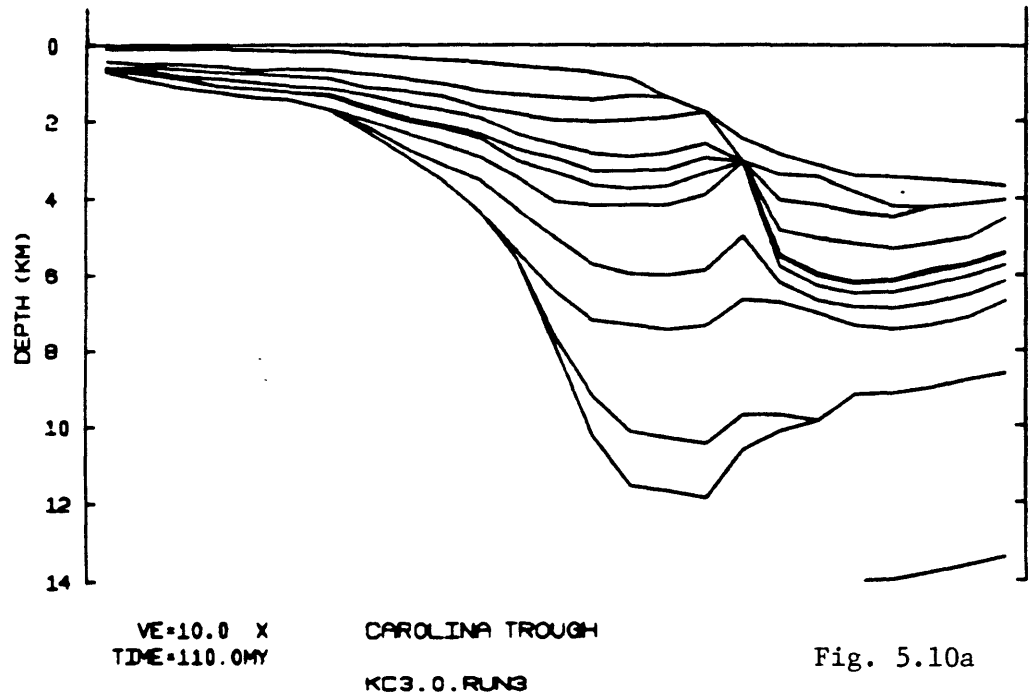

Fig. 5.10a

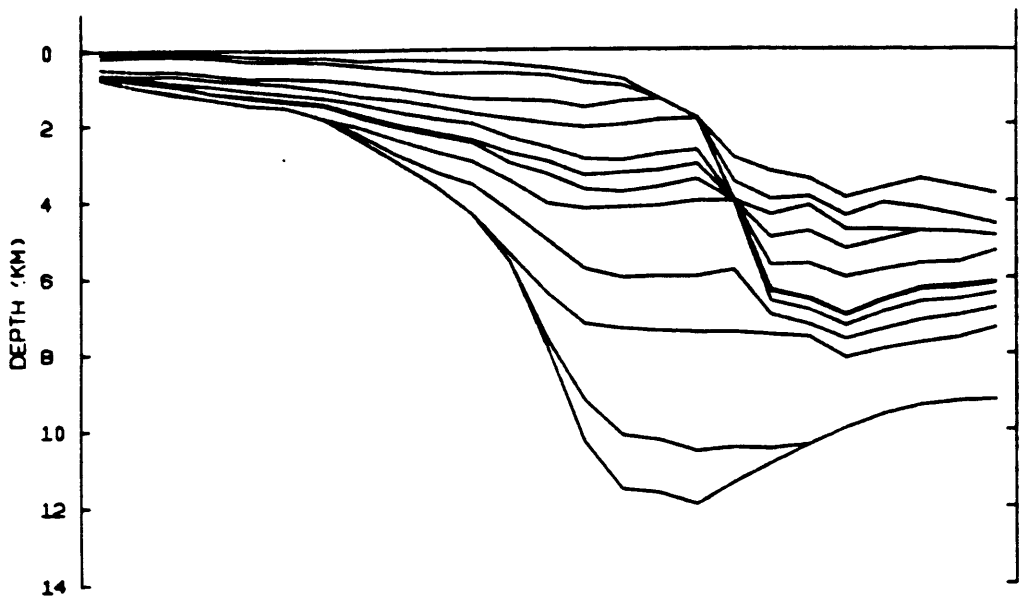

Fig. 5.11b

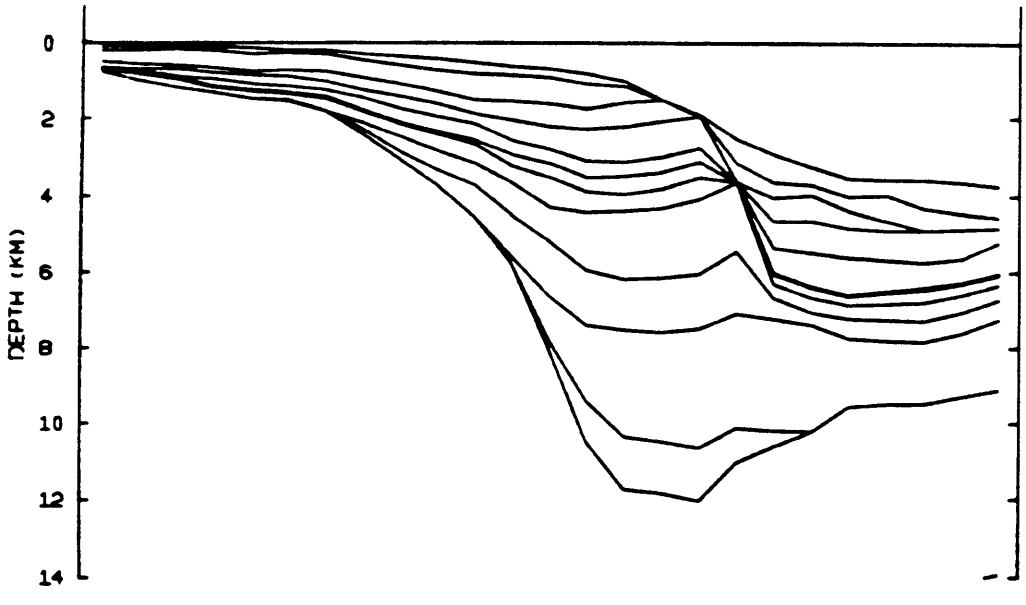

Fig. 5.11a

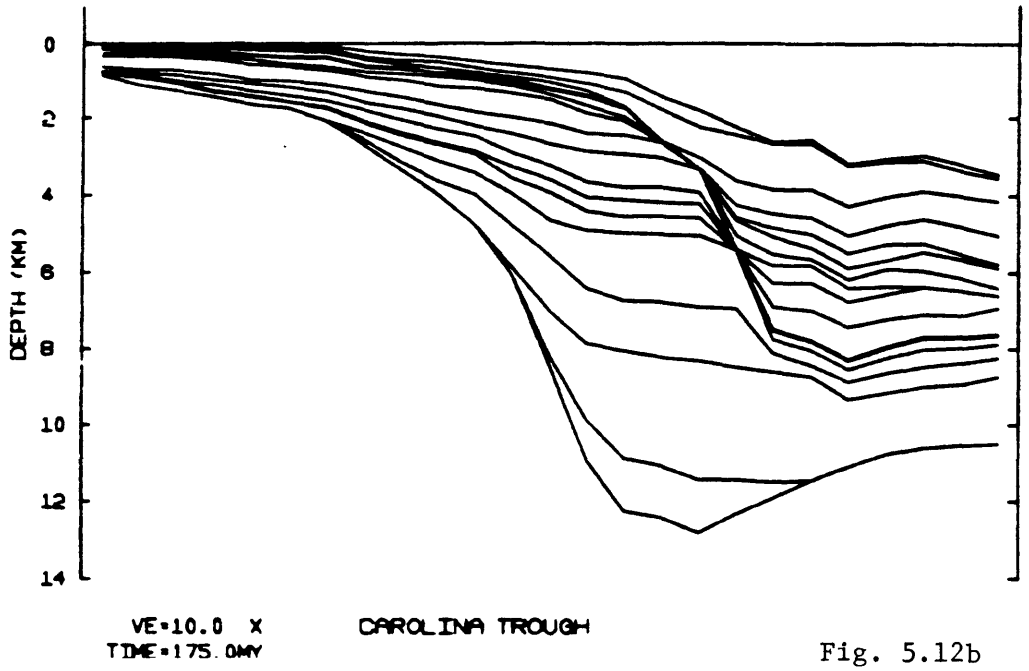

Fig. 5.12b

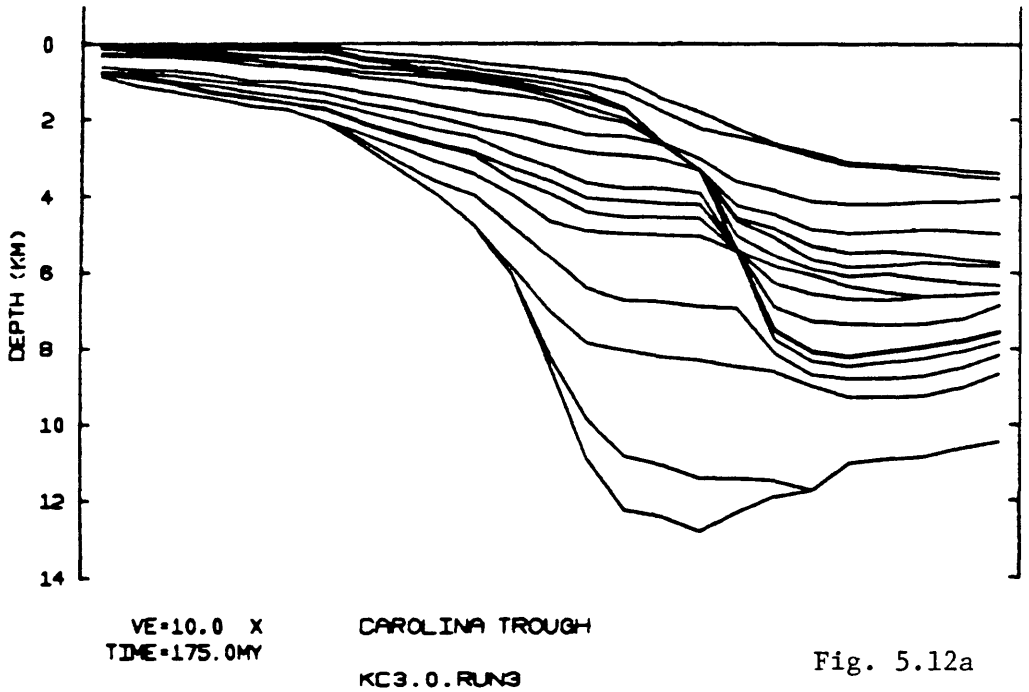

Fig. 5.12a

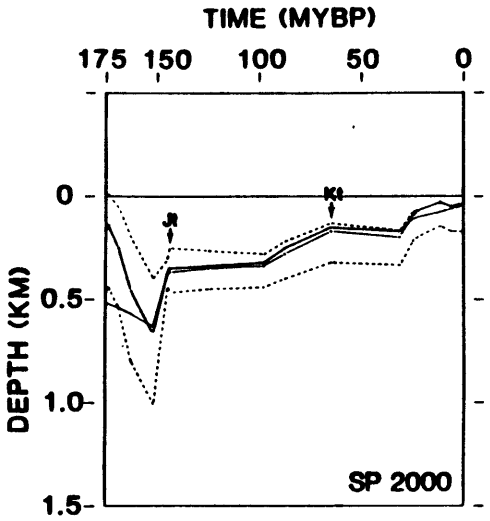

Fig. 5.13a

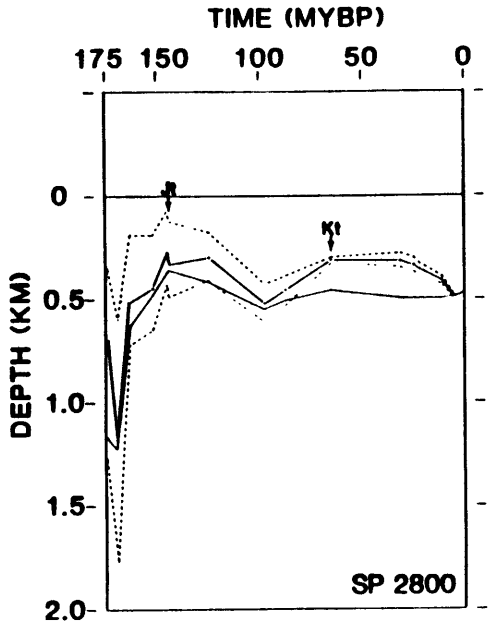

Fig. 5.13b

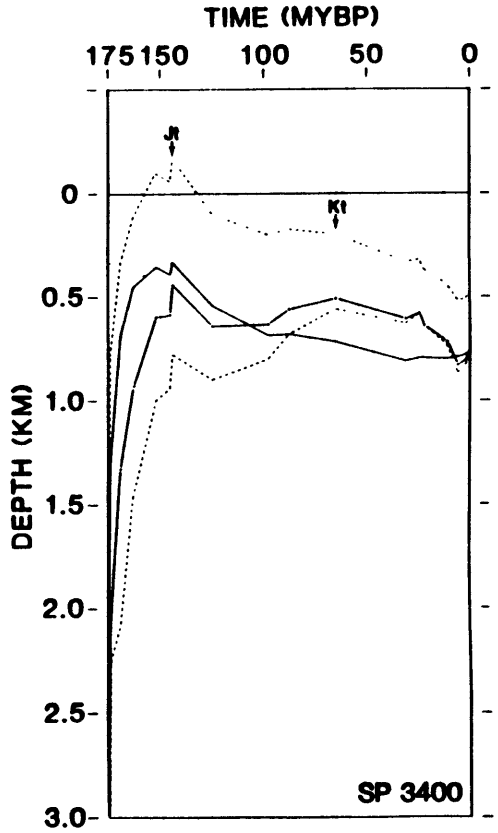

Fig. 5.13c

CHAPTER VI

TWO DIMENSIONAL TWO LAYER EXTENSION MODEL

L'ennui naquit un jour de l'uniformité.
(Boredom was born one day out of uniformity)

Houdar de Lamotte, Fables, 1719

6.1 INTRODUCTION

The uniform extension model (Chapter 4 and 5) predicts too deep a continental shelf shortly after rifting: zones A, B, and C are about 700m below expected between the end of the Callovian (163 MYBP) and the end of the Jurassic (144 MYBP). This indicates that the Carolina trough subsided less at the time than predicted. Since the current total subsidence is constrained by present data, it is the ratio of early (up to 30 MY after rifting) to present tectonic subsidence which needs to be modified.

When confronted with the same problem, Royden and Keen (1980) and Sclater et al. (1980) introduced the non-uniform extension model. The basic idea is that an extra heat input below the crust, may keep an area more elevated than predicted by uniform extension. Uniform extension may then underestimate the total heat input within the Carolina trough. Since this extra amount of heat may influence the thermal history and the degree of hydrocarbon maturation, we will apply, in this chapter, the two layer model in order to obtain an upper bound on this effect.

We will first show how a simple analysis of the data suggest the necessity of such modeling. We will then show that present data are not adequate to constrain such modeling but that an estimate can be made, keeping in mind that we are only looking for an upper bound, not for precise predictions.

6.2 DATA ANALYSIS

Our studies (Chapter 4 and 5) suggest the need for extra subcrustal extension, while similar studies in the Baltimore Canyon did not (Sawyer 1982, Sawyer et al., 1982a, 1982b). We will then see if the data on these two basins suggest such a difference; mainly we want to compare early subsidence versus late subsidence.

Cross sections of the two basins (Fig. 6.1) show that a major difference between them is that the Carolina trough is not filled with sediments as far seaward as is the Baltimore Canyon trough. This difference seems to explain most of the difference in basement depth and part of the difference in basin width. When the effect of sediment loading is removed, the tectonic subsidence between the hinge zone and ECMA are not

very different (from 3 km to 6 km in the Carolina trough, Chapter 4 and 5) and from 2 km to 6 km in the Baltimore Canyon trough (Sawyer, 1982; Sawyer et al. 1982b). However this difference in present water depth is due mainly to Cenozoic erosions in the Carolina trough, therefore does not seem to bear any relationship with the initiation mechanism.

The next simpler analysis of the data is to evaluate the ratio of early sediment thickness to total sediment thickness. The oldest reliable reflector which can be correlated across both basins being the top of the Jurassic (31 MY after rifting) we computed the ratio of pre-Cretaceous to total sediment thickness, allowing for compaction correction (Fig. 6.2). This ratio is indicative of the importance of early subsidence only where Jurassic water depth were uniform, therefore landward of the Jurassic shelf edge. We can distinguish three segments:

1 - between the hinge zone and the Jurassic shelf edge the ratios are comparable for both basins (between 70% and 90%).

2 - seaward of the Jurassic shelf edge the ratio falls off as expected in both basins but more so in the Carolina trough where Miocene sedimentation has been more intense.

3 - landward of the hinge zone we have data only for the Carolina trough where the ratio falls off drastically.

The interesting comparison is then limited to the area between the hinge zone and the Jurassic shelf edge. However in that area the Carolina trough is not filled up while the Baltimore Canyon is, therefore the total sediment thickness does not represent the total subsidence.

We then need to introduce some further processing: we computed the ratio of the pre-Cretaceous sediment thickness to the current tectonic subsidence (i.e., the basement depth if sediment loading were removed as given in Chapter 4 for the Carolina trough and in Sawyer (1982) for the Baltimore Canyon trough; in both cases, pointwise isostasy was assumed). This time (Fig 6.3), a marked difference appears: the average ratio is slightly higher and the peak ratio is much higher in the Baltimore Canyon than in the Carolina trough. This may be regarded as an indication of less early subsidence in that latter basin. Moreover, in the Carolina trough,

the ratio falls off drastically landward (50 km landward of the hinge zone the ratio is 10 times smaller than at peak) which indicates that most subsidence must have been post Jurassic landward of the hinge zone. This, we have already seen (Chapter 5), cannot be accounted for by uniform extension, even when flexural response is considered. Non uniform extension with extra heat input landward of the hinge zone seems a logical answer to that problem (Watts and Thorne, 1984).

6.3 CONSTRAINTS

The crustal extension factor, β_c, governs the present crustal thickness; it then controls the elevations once the thermal anomaly has disappeared. Therefore β_c is best constrained by subsidence data as long as possible after rifting time. In the Carolina trough, the present tectonic subsidence is a very good constraint since 90% of the thermal subsidence has occurred 175 MY after rifting, therefore thermal equilibrium is almost reached. Moreover, because once the thermal anomaly has disappeared both the uniform and the two layer models predict the same evolution, we expect the crustal extension factor to be similar in both cases.

The subcrustal extension factor, β_{sc}, governs the initial subcrustal heat input. It then controls the elevations during and shortly after rifting, before the thermal anomaly disappears. It is therefore best constrained by synrift or end of rifting elevations (Hellinger and Sclater, 1983; Royden et al., 1983). However, no reliable paleodepth estimates are available for zone C of the Carolina trough before the end of the Callovian, after which a shelf environment is inferred. The best we can do is to constrain β_{sc} so that the reflectors top Callovian (12 MY after rifting), Kimmeridgian (23 MY after rifting), and top Jurassic (31 MY after rifting) are deposited near present sea level, since Jurassic sea level was not very different from today's. From the beginning this approach appears to be plagued by a major problem: even at the earliest time (12 MY) a lot of heat will have disappeared and little will be left of the thermal signal in the subsidence data. Since these subsidence data are expected to incorporate some noise, we will be trying to invert with a low signal to noise ratio. We therefore do not expect β_{sc} to be well constrained.

6.4 FIRST APPROACH

Our first inversion will only try to match a zero water depth for the Jurassic shelf at time either 12 MY, 23 MY or 31 MY after rifting resulting in 3 different models (model 12, 23 and 31). For each model we try to match the depth in each column: we adjust β_{sc} at each column so that waterdepth can be as close as possible to zero: if waterdepth is predicted above sea level we will iterate with a smaller β_{sc}, if under sea level with larger β_{sc}.

The results are very unsatisfactory: first, unrealistic variations of β_{sc} are obtained landward of the hinge zone (Fig. 6.4a); second, these β_{sc} values are not very consistent between different models; third, the predicted topography can differ by as much as 200m from zero in most models.

This can be attributed partly to the bad signal/noise ratio already mentioned but also to other causes. First, the two dimensional model tends to propagate and emphasize errors: if an error tends to overestimate β_{sc} in one column, the extra heat will diffuse to the neighboring column, which will have to be compensated for by an underestimation of β_{sc} there. Second, as β_{sc} is modified, not only the amount of heat is modified but also the plate thickness which is controlled by temperature. As a result, two effects are working together at each column: a change in the tectonic subsidence and a change in the loading effect. These two effects go in the same direction at the periphery of the basin but in opposite direction in the center of the basin, where it may create some degree of non-uniqueness.

However a better understanding requires thinking in terms of heat diffusion. If we concentrate on model 12, the predicted top Callovian topography is not flat but shows some short wavelength variations (Fig. 6.5c). In an attempt to cancel these short wavelength variations, the predicted initial topography shows the same variations but inverted (Fig. 6.5a). This attempt fails since most of the initial relief is lost around 6 MY after rifting (Fig. 6.5b). The explanation for this is clear if one looks at the predicted thermal structure: to create the initial topography, huge short wavelength lateral temperature variations are assumed (Fig. 6.6) but these short wavelength variations decay very fast

and 6 MY later none of them remain (Fig. 6.6c). As a consequence the short wavelength lateral variation in subsidence data, which can be seen in the pre-Jurassic sediment thickness (Fig. 6.2a and 6.3a) cannot be accounted for by thermal considerations. Conversely two initial thermal models differing only by short lateral wavelength would give the same predictions after 6 MY after rifting. Therefore β_{sc} cannot be inverted locally. The early lateral variation in sediment thickness may be due to synsedimentary faulting, prerift irregular topography contrary to model assumptions, or to errors in depths to the deep reflectors to which they correspond.

There are two approaches to solve that problem: one is to filter the data so as to eliminate the short wavelength before inverting for β_{sc}. Another is to look for extra constraints on the acceptable model, as we chose to do here.

6.5 SECOND APPROACH

Though β_{sc} cannot be inverted for locally, the regional trend should be easier to estimate.

First, all previous models do agree at the landward end of the model and seaward of the hinge zone. We will then constrain our new model (model 0) to agree with them at these end points too.

Second, a good way to filter the short wavelength out of a function is to integrate it. The sum:

$$H(x) = \int_0^x \gamma(t)dt$$

where $\gamma = 1-1/\beta$ and x is the lateral distance represents the cumulative amount of heat input into the model as one proceeds across it. This function controls the long wavelength topography and we should therefore be able to invert for it. In fact, the three previous models agree reasonably on the estimate of that function (Fig. 6.7). We will then require model 0 to yield a compatible estimate of the amount of heat. Third, the only remaining degree of freedom is the shape of the curve $\gamma(x)$. It could be constrained to follow some simple functions such as linear or gaussian, but we decided instead to only assume that $\gamma(x)$ always increases seaward and to use the remaining degree of freedom to improve the topography fit at 12 MY after rifting.

The regional topography fit is then ensured by the two first conditions, while the more local fit comes only as a very loose secondary constraint in the variation of $\gamma(x)$. The resulting model (model 0), which looks more realistic (Fig. 6.4), gives as acceptable a topography (Fig. 6.5) as the previous ones, and thermally does not differ from them past 6 MY after rifting (Fig. 6.6).

6.6 RESULTS

All four models agree on an amount of heat much larger than the one predicted by uniform extension especially landward of the hinge zone (Fig. 6.7). As a result, landward of the hinge zone, the lithosphere remains hotter than in the uniform extension case over an extended period of time (up to 100 MY after rifting) (Fig. 6.6). They predict paleowaterdepth more compatible with shelf environment from 12 MY after rifting until at least 50 MY after rifting; by 100 MY after rifting, the difference with uniform extension is not significant (Fig. 6.5).

To obtain crustal extension factors (Fig. 6.4b) comparable to the one derived in the uniform extension case with a relaxation temperature of 350°C, we had to assume a relaxation temperature of 400°C for the two layer models. This is easily explained by the fact that the two layer model isotherms are shallower than the one of the uniform extension model. Therefore to conserve plate thickness, one has to increase the relaxation temperature. This shows that loading response and thermal models are not independent but dynamically interacting. As a result what we invert for in one of them depends on what is assumed in the other.

6.7 CONCLUSIONS

The estimation of the subcrustal extension factor, β_{sc}, from topography early after rifting is not straightforward, but has to be considered as an inverse problem. The short wavelength "noise" may be due partly to uncertainties in the data, especially in old basins where the corresponding deeply buried reflectors depths are sometimes imprecise, but also to local geological causes which cannot be reduced just by improving the data quality. The longer wavelength thermal signal component can be enhanced by concentrating on data as close as possible to the peak of thermal activity. This shows that an estimate made from a well should include regional trends around that well in order to separate these two components of the topography. In young basins (less than 30 MY old) heat flow data should help considerably in determining the initial heat input.

In the Carolina trough, even though this inversion is poorly constrained, it appears that only a larger amount of heat than predicted by uniform extension can explain the late Jurassic shelf environment landward of the hinge zone.

Figure Captions

Fig. 6.1. Compared cross sections of the Carolina trough along USGS line 32 (6.1a) with the Baltimore Canyon trough along line 25 (6.1b). The two sections are drafted at the same horizontal and vertical scale. (Baltimore Canyon depth taken from Sawyer (1982) who used Grow's (1980) interpretation). Jt: Jurassic top; Kt: Cretaceous top.

Fig. 6.2. Ratios of pre-Cretaceous sediment thickness to total sediment thickness (solid line: corrected for compaction; dashed line: uncorrected). The horizontal scales are the same for the two basins.
6.2a: Carolina trough
6.2b: Baltimore Canyon trough

Fig. 6.3. Ratio of pre-Cretaceous sediment thickness (reduced to zero porosity) to present tectonic subsidence (i.e., unloaded basement depth assuming local isostasy).
6.3a: Carolina trough (tectonic subsidence from one dimensional model, Chapter 4)
6.3b: Baltimore Canyon trough (tectonic subsidence from Sawyer (1982))

Fig. 6 4. Estimates of extension in the Carolina trough along line 32 according to models 0, 12, 23 and 31.
6.4a: Subcrustal extension
6.4b: Crustal extension

Fig. 6.5. Predicted early topography and stratigraphy according to the uniform extension model with a relaxation temperature of 350°C (Chapter 5) compared to the two-layer extension models 0 and 12.
6.5a: at rifting (175 MYBP)
6.5b: 6 MY after rifting, end of Bathonian.
6.5c: 12 MY after rifting, end of Callovian.
6.5d: 23 MY after rifting, Kimmeridgian.
6.5e: 31 MY after rifting, end of Jurassic.
6.5f: 50 MY after rifting, end of Neocomian.
6.5g: 110 MY after rifting, end of Cretaceous.

Fig. 6.6. Predicted thermal structure according to the three models of Fig. 6.5.

6.6a: at rifting (175 MYBP)

6.6b: 1 MY after rifting

6.6c: 6 MY after rifting

6.6d: 12 MY after rifting

6.6e: 31 MY after rifting

6.6f: 110 MY after rifting

Fig. 6.7. Cumulative amount of heat along line 32. The sum $\sum_{j=1}^{n} \gamma_j$, where j designates the column, is computed starting at the landward end of the model. Past the ECMA, $\gamma=1$, therefore the slope is 1 for each model. Uniform extension refers to the two dimensional model with T_R = 350 °C and standard data.

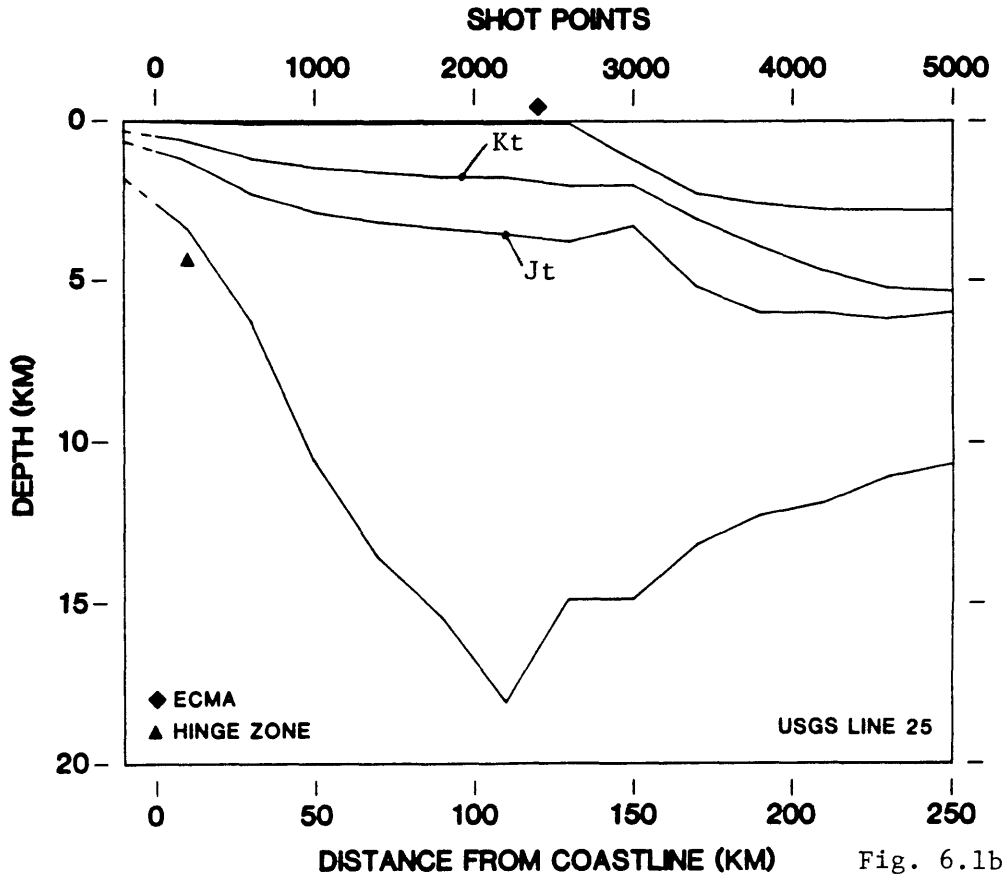

Fig. 6.1b

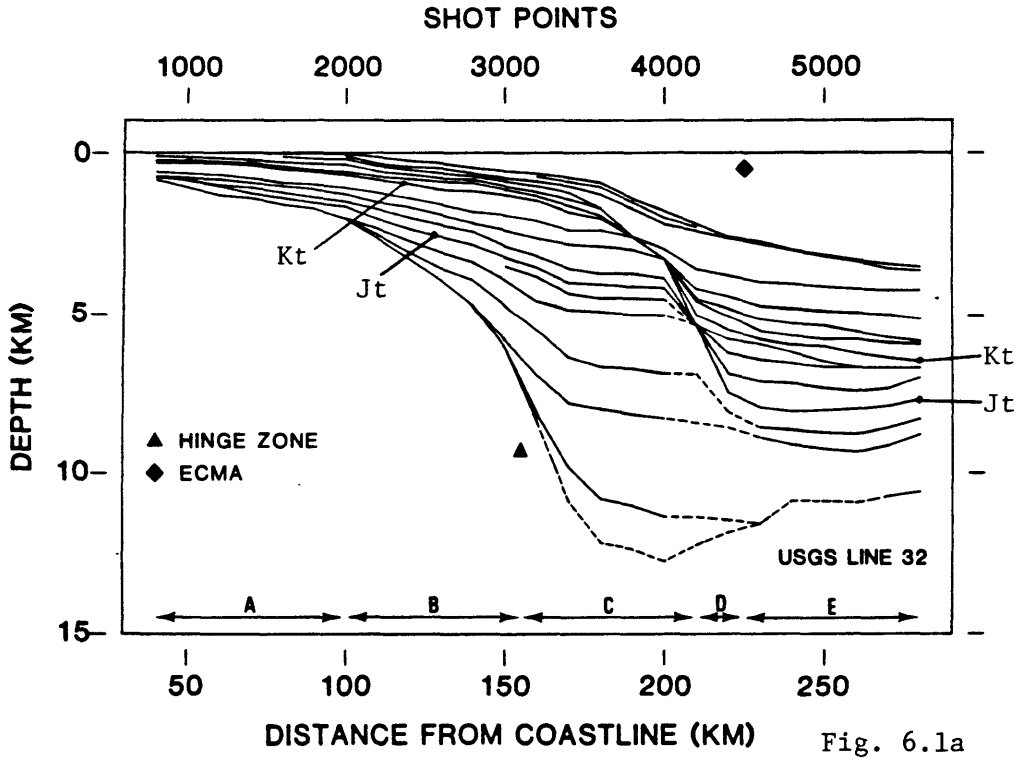

Fig. 6.1a

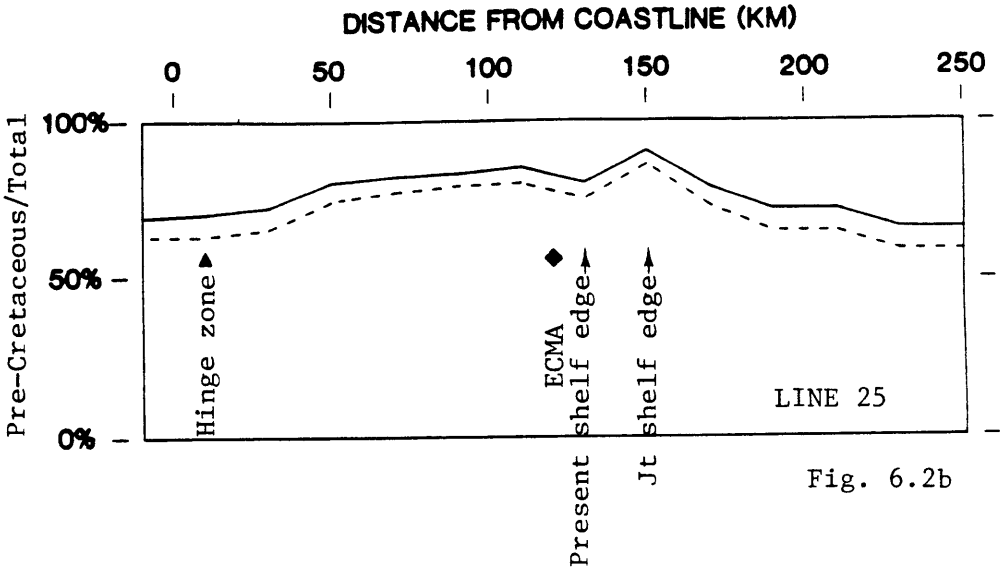

Fig. 6.2b

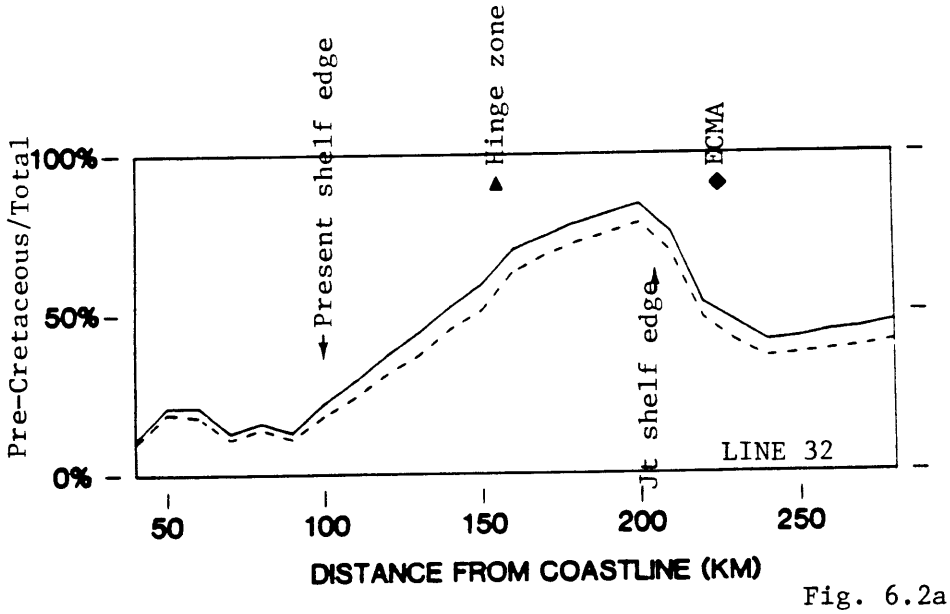

Fig. 6.2a

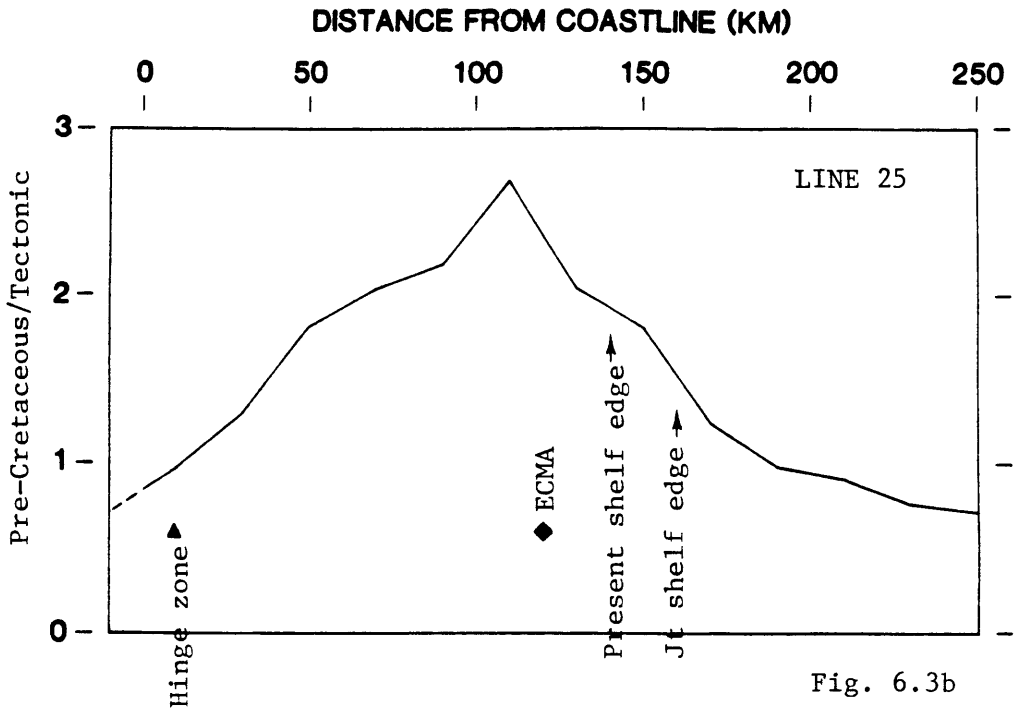

Fig. 6.3b

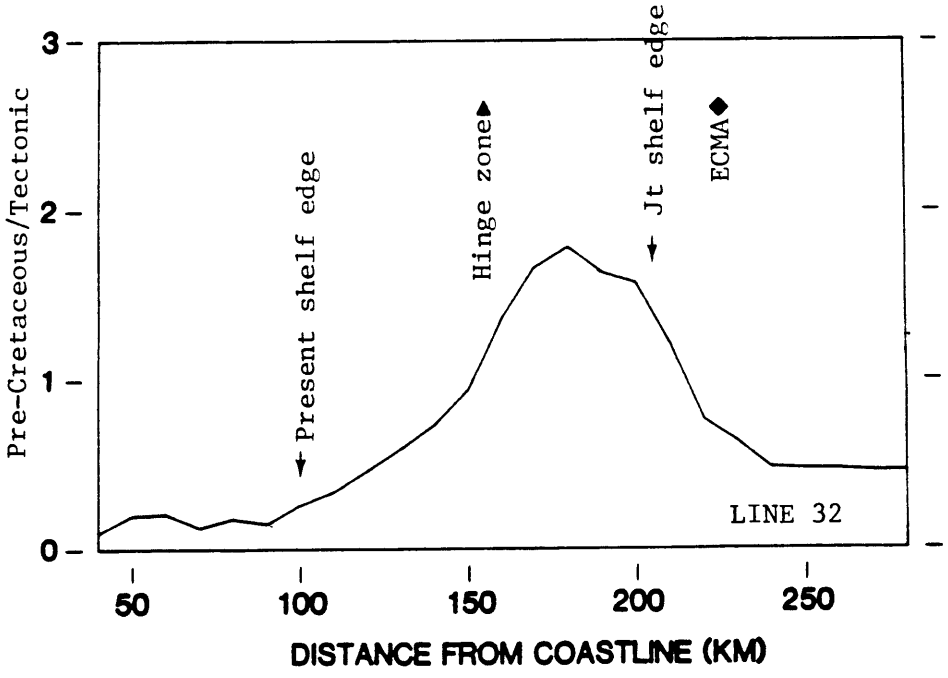

Fig. 6.3a

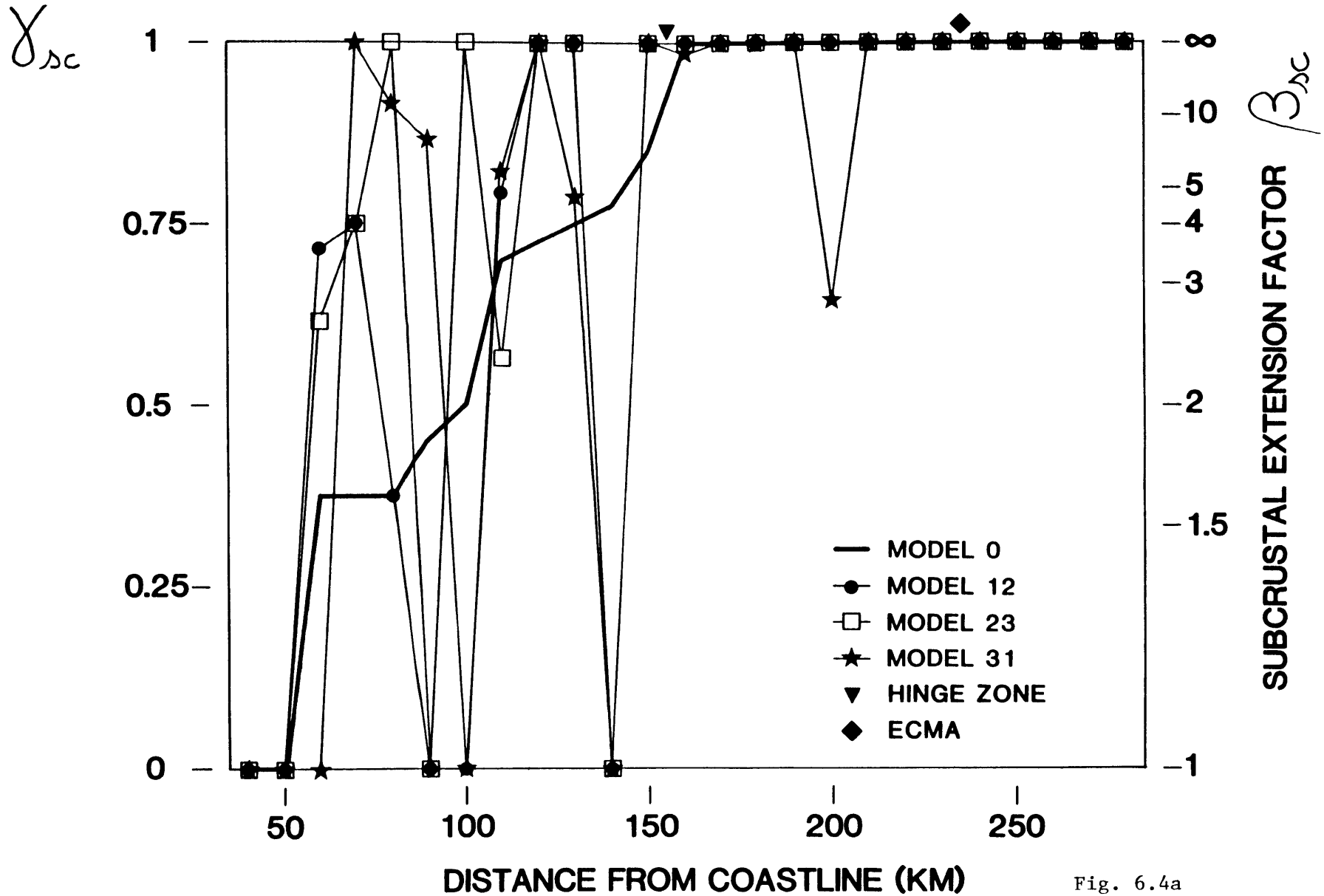
γ_{sc}
1
0.75
0.5
0.25
0
50
100
150
200
250
DISTANCE FROM COASTLINE (KM)
∞
10
5
4
3
2
1.5
1
β_{sc}
SUBCRUSTAL EXTENSION FACTOR
MODEL 0
MODEL 12
MODEL 23
MODEL 31
HINGE ZONE
ECMA

Fig. 6.4a

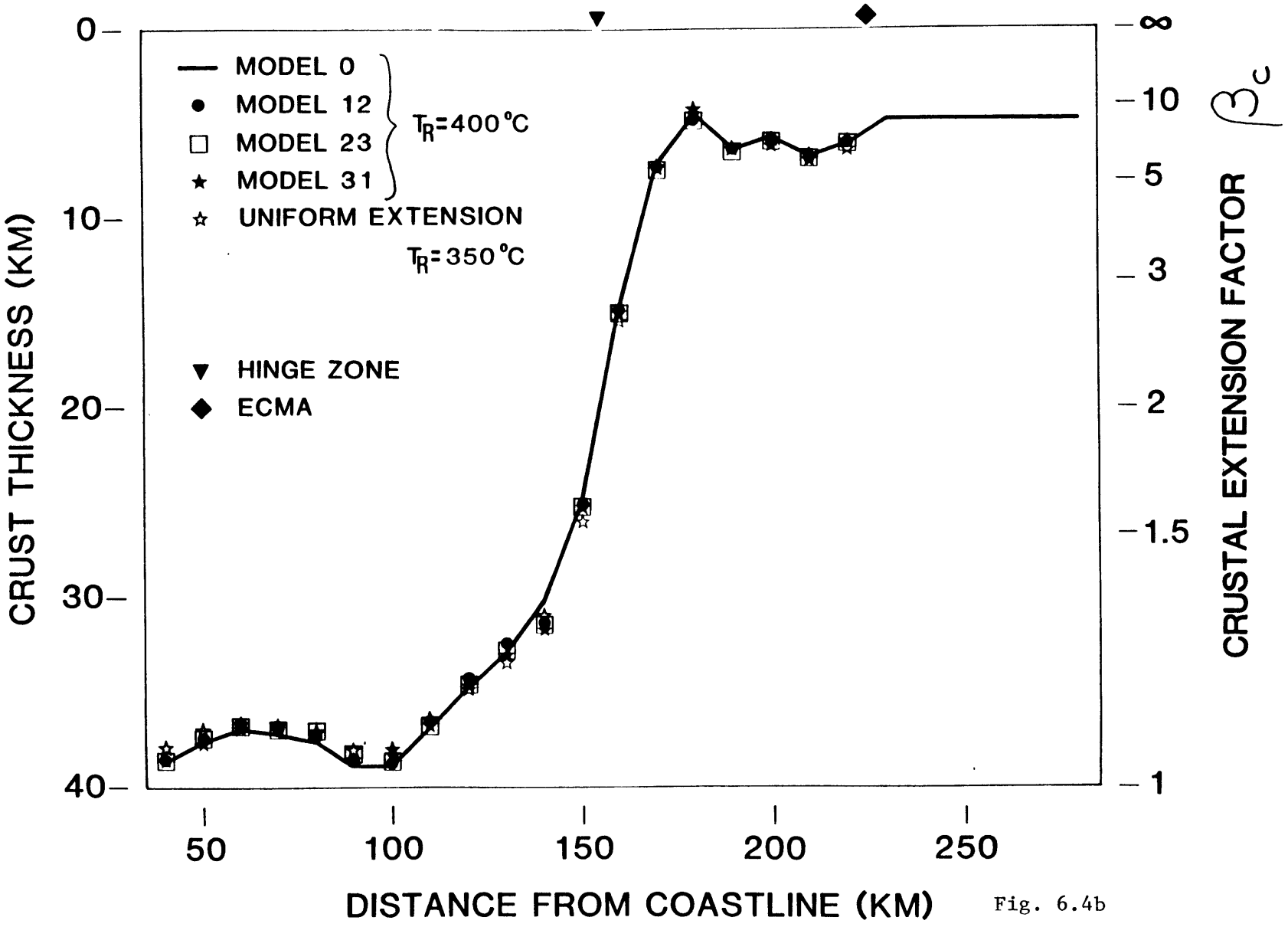
MODEL 0
MODEL 12
MODEL 23
MODEL 31
T_R=400°C
UNIFORM EXTENSION
T_R=350°C
HINGE ZONE
ECMA
CRUST THICKNESS (KM)
0
10
20
30
40
CRUSTAL EXTENSION FACTOR
β_c
∞
10
5
3
2
1.5
1
50
100
150
200
250
DISTANCE FROM COASTLINE (KM)

Fig. 6.4b

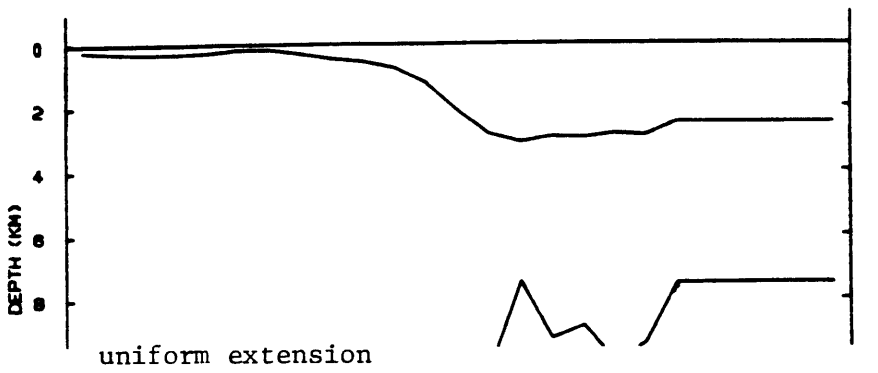
0
2
4
6
8
DEPTH (KM)
uniform extension

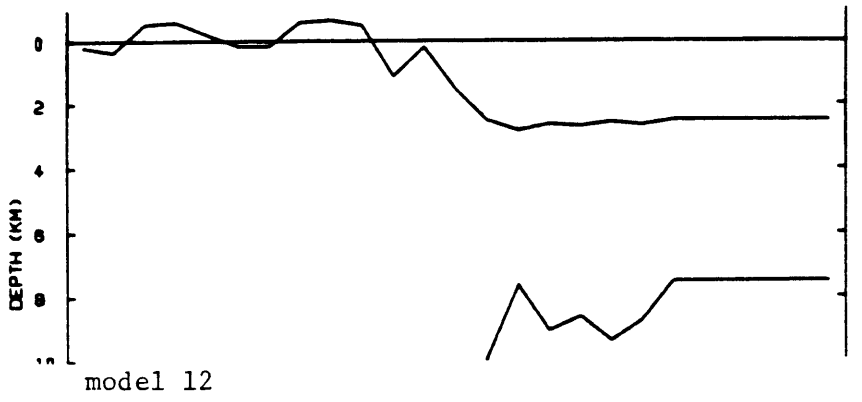
0
2
4
6
8
DEPTH (KM)
model 12

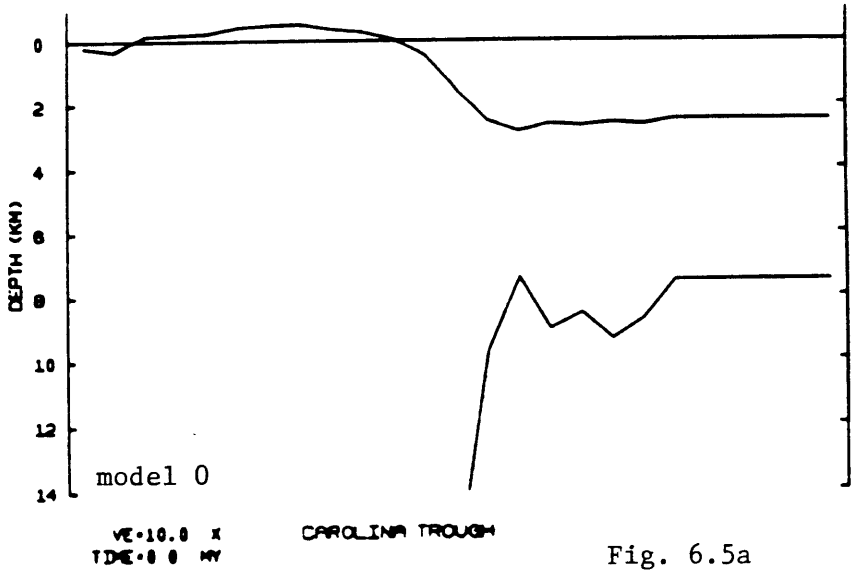
0
2
4
6
8
10
12
14
DEPTH (KM)
model 0
VE=10.0 X
TIME=0.0 MY
CAROLINA TROUGH

Fig. 6.5a

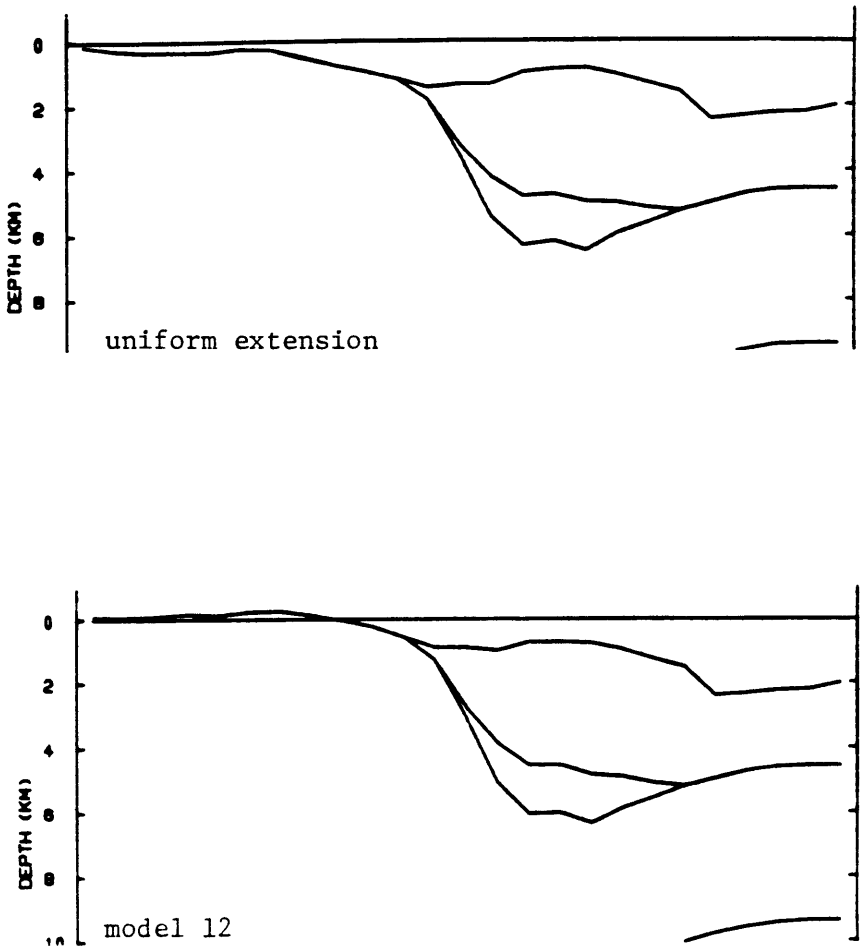
0
2
4
6
8
DEPTH (KM)
uniform extension
0
2
4
6
8
DEPTH (KM)
model 12
0
2
4
6
8
10
12
14
DEPTH (KM)
model 0
VE=10.0 X
TIME=0.0 MY
CAROLINA TROUGH

Fig. 6.5b

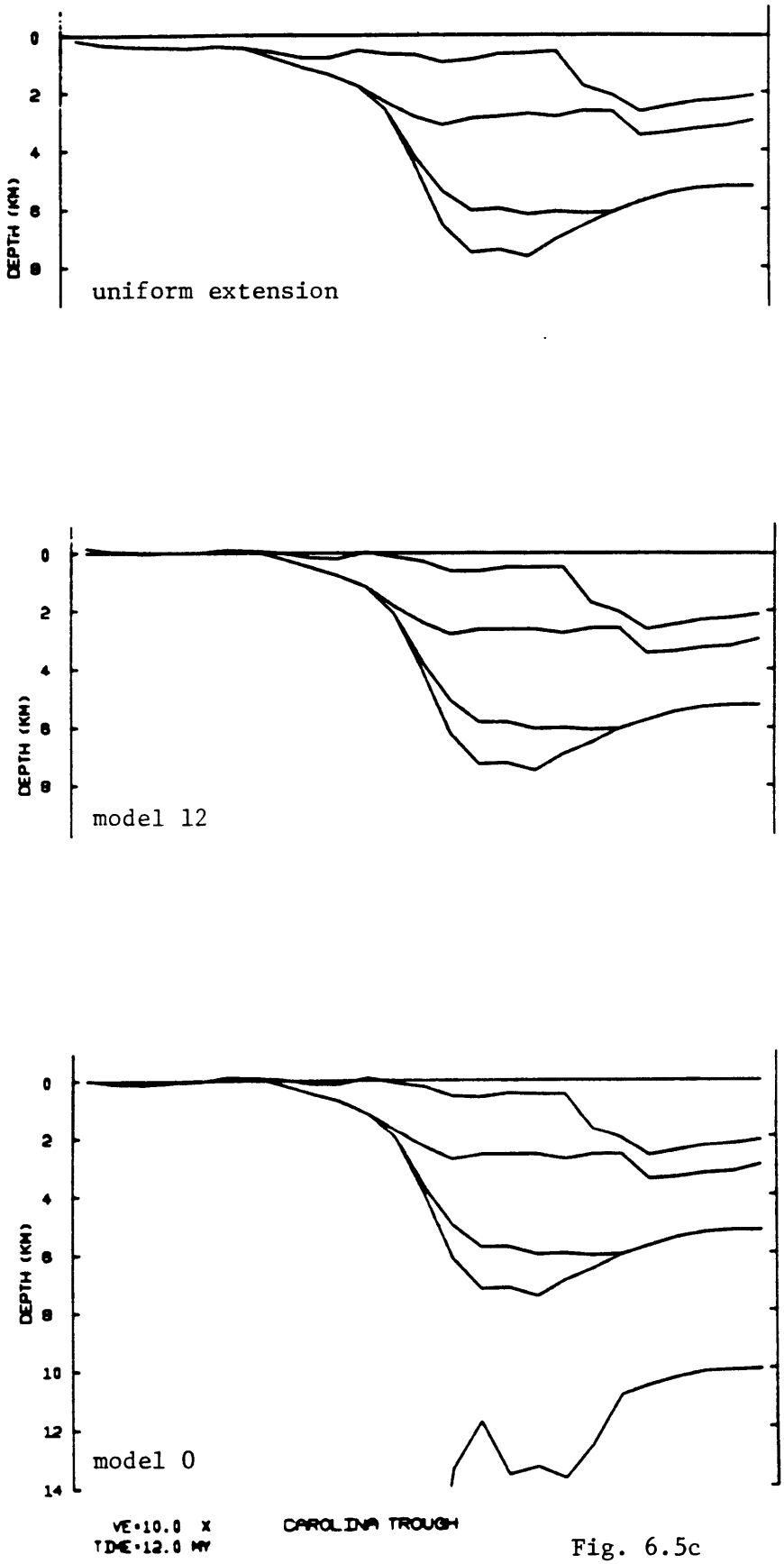
DEPTH (KM)
0
2
4
6
8
uniform extension
DEPTH (KM)
0
2
4
6
8
model 12
DEPTH (KM)
0
2
4
6
8
10
12
14
model 0
VE•10.0 X
TIME•12.0 MY
CAROLINA TROUGH

Fig. 6.5c

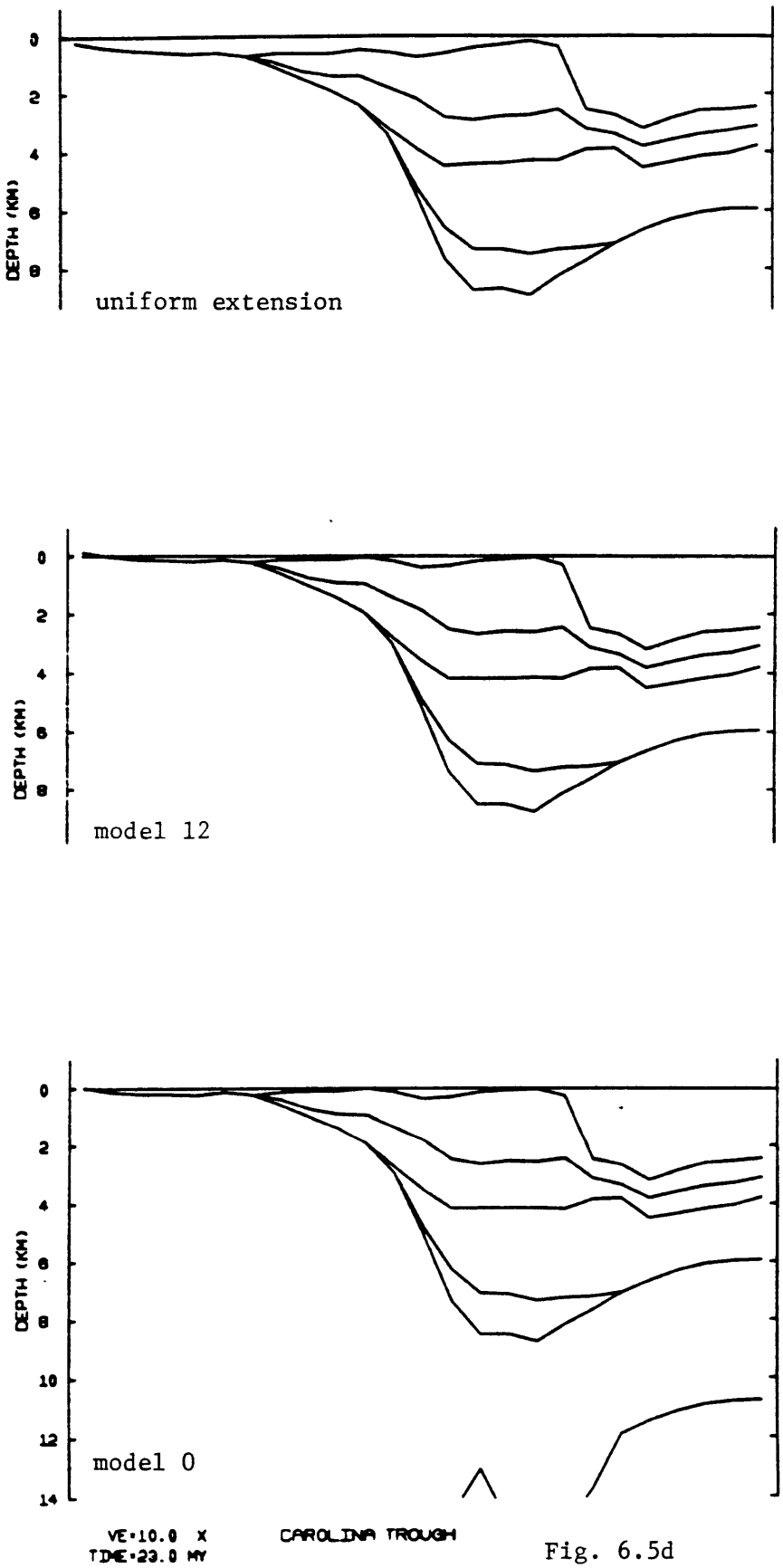
DEPTH (KM)
0
2
4
6
8
uniform extension
DEPTH (KM)
0
2
4
6
8
model 12
DEPTH (KM)
0
2
4
6
8
10
12
14
model 0
VE=10.0 X
TIME=23.0 MY
CAROLINA TROUGH

Fig. 6.5d

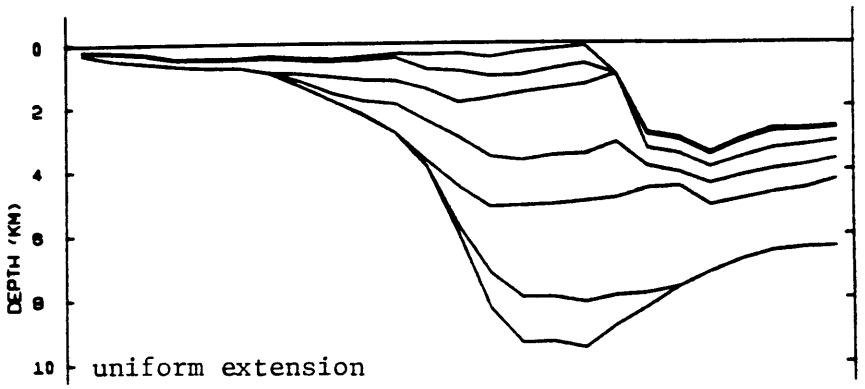
0
2
4
6
8
10
DEPTH (KM)
uniform extension

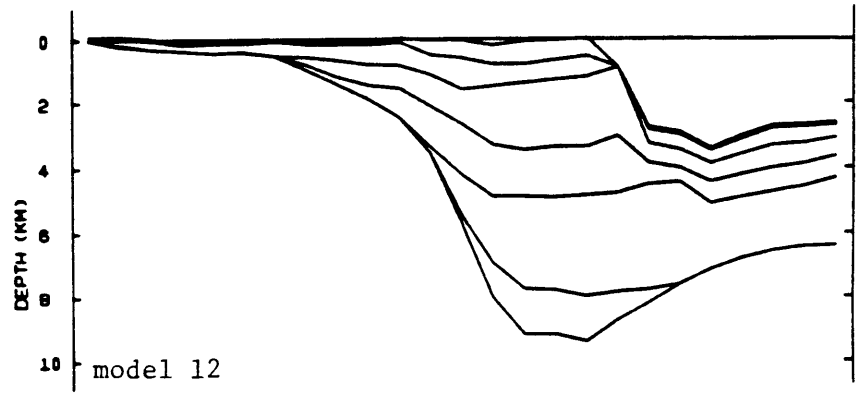
0
2
4
6
8
10
DEPTH (KM)
model 12

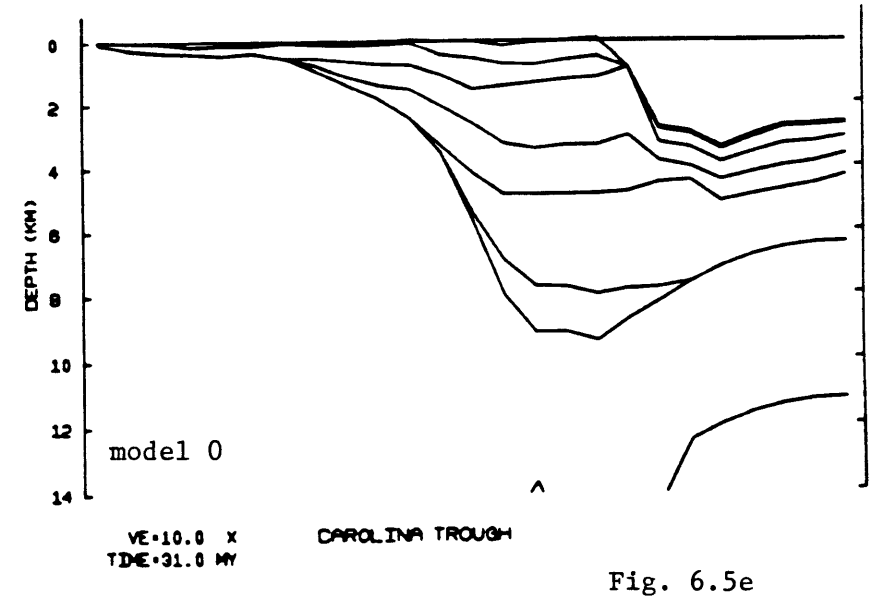
0
2
4
6
8
10
12
14
DEPTH (KM)
model 0
VE=10.0 X
TIME=31.0 MY
CAROLINA TROUGH

Fig. 6.5e

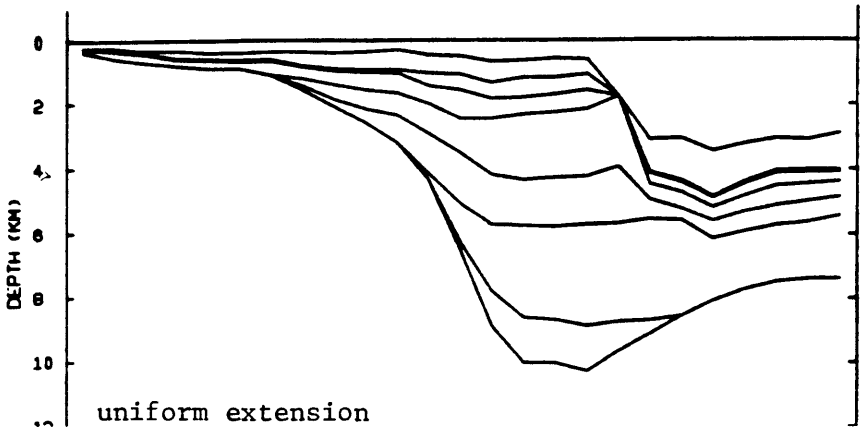
DEPTH (KM)
0
2
4
6
8
10
uniform extension

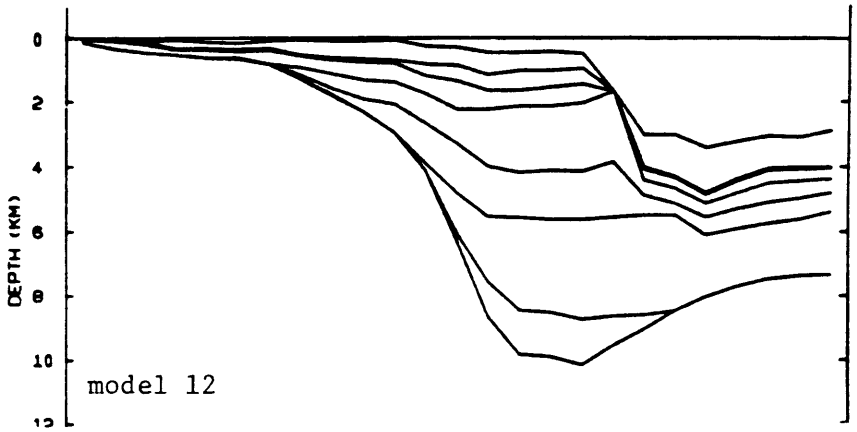
DEPTH (KM)
0
2
4
6
8
10
model 12

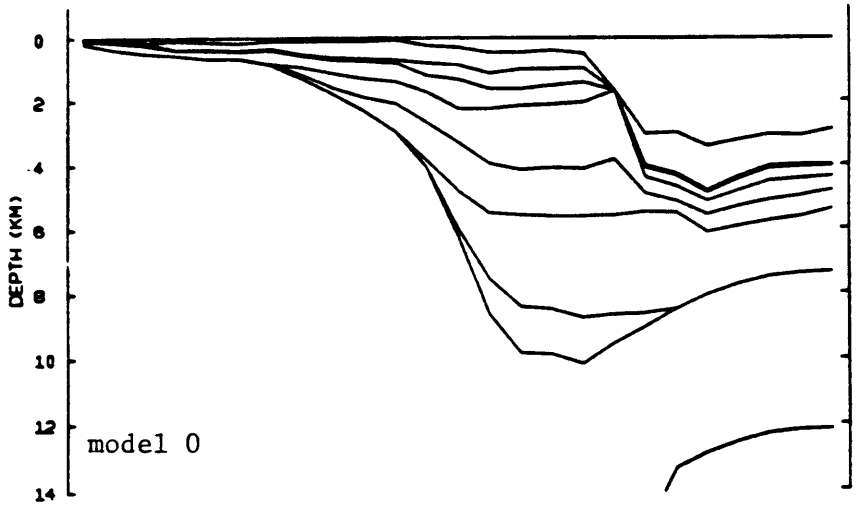
DEPTH (KM)
0
2
4
6
8
10
12
14
model 0
VE=10.0 X
TIME=50.0 MY
CAROLINA TROUGH

Fig. 6.5f

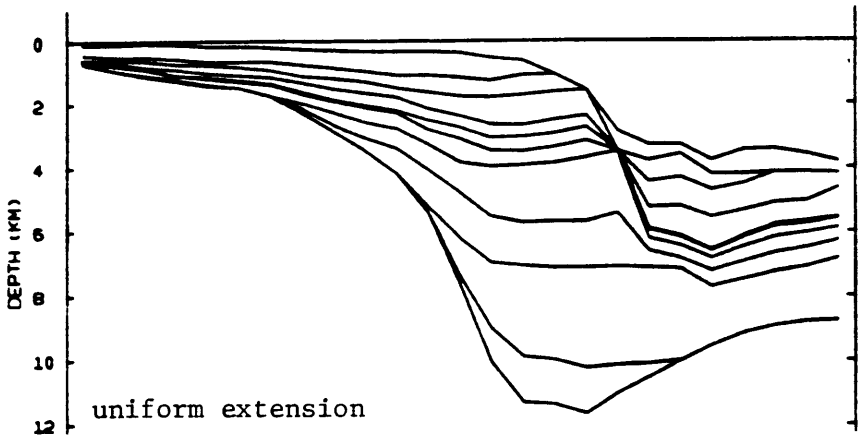
0
2
4
6
8
10
12
DEPTH (KM)
uniform extension

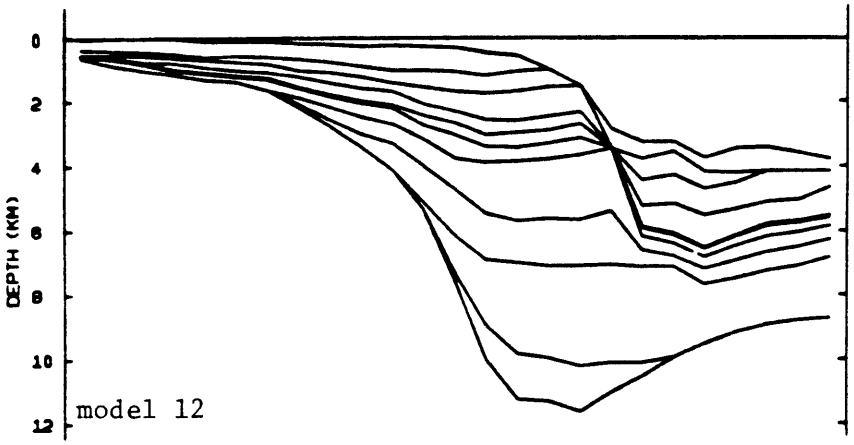
0
2
4
6
8
10
12
DEPTH (KM)
model 12

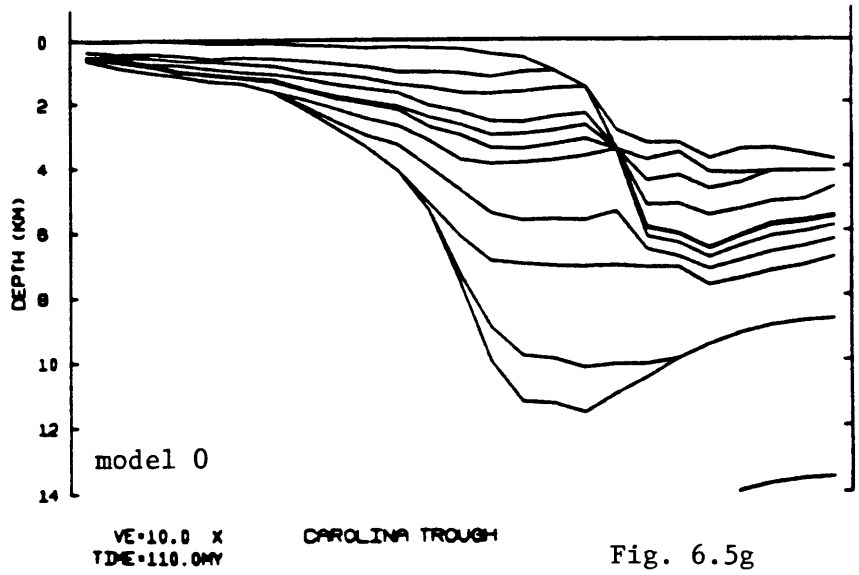
0
2
4
6
8
10
12
14
DEPTH (KM)
model 0
VE=10.0 X
TIME=110.0MY
CAROLINA TROUGH

Fig. 6.5g

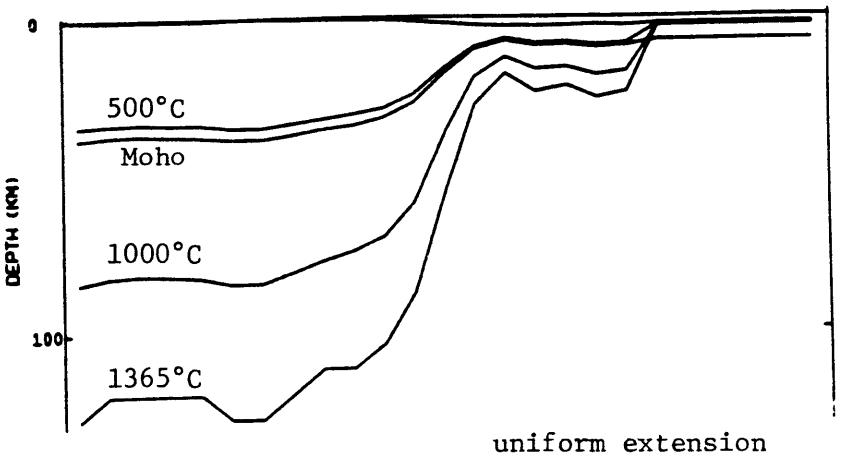

uniform extension

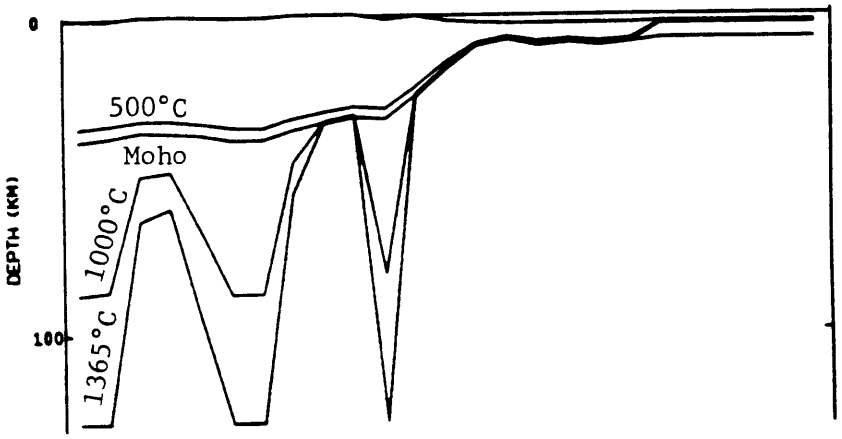

model 12

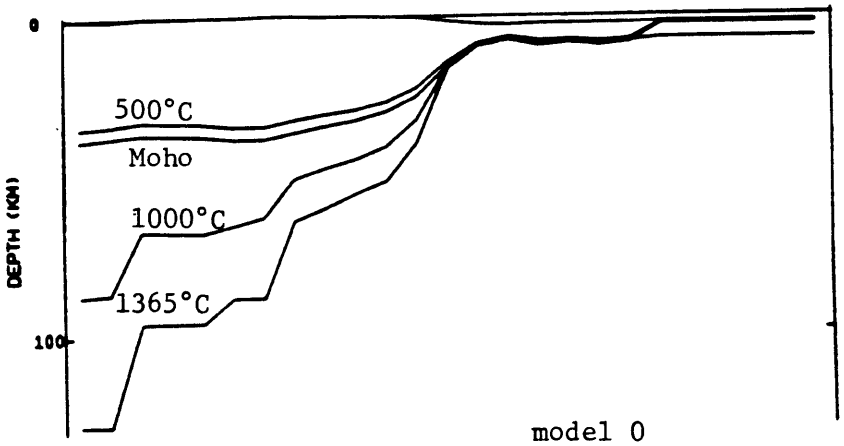

model 0

VE•1.0 x
TIME•0.0 MY

CAROLINA TROUGH

KC30m.0400.RUN10

Fig. 6.6a

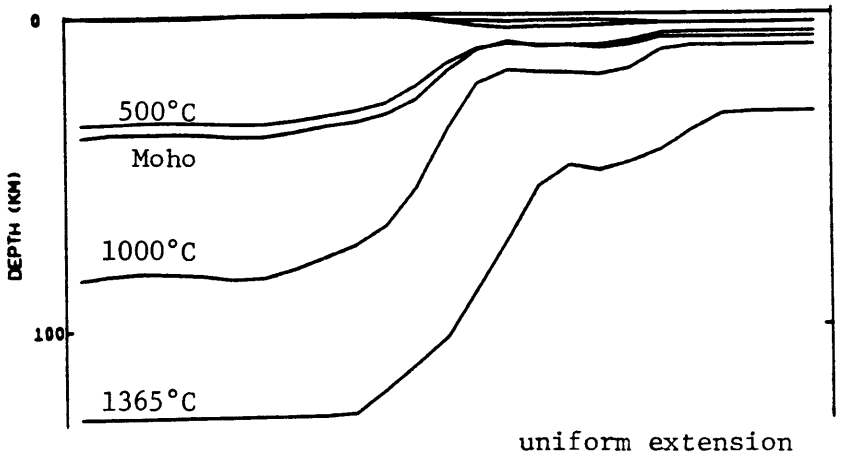

uniform extension

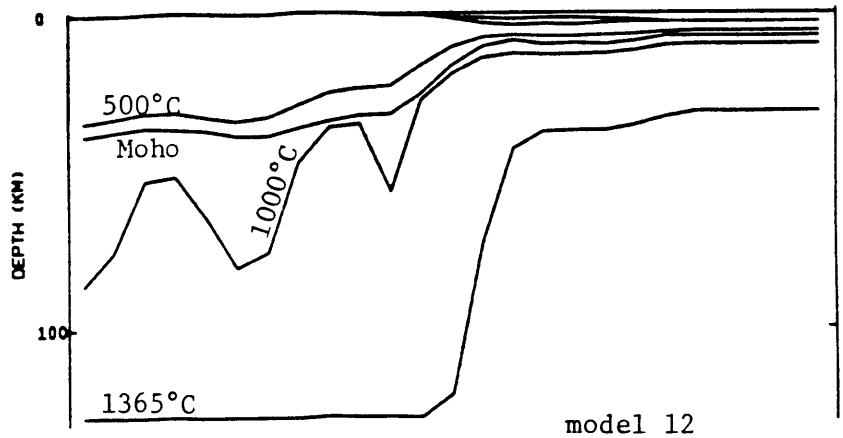

model 12

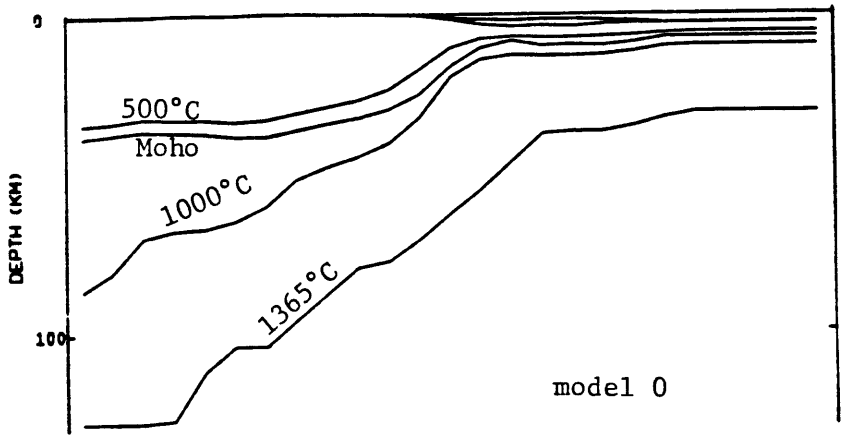

model 0

VE=1.0 X
TIME=1.0 MY

CAROLINA TROUGH

KC30m.0400.RUN10

Fig. 6.6b

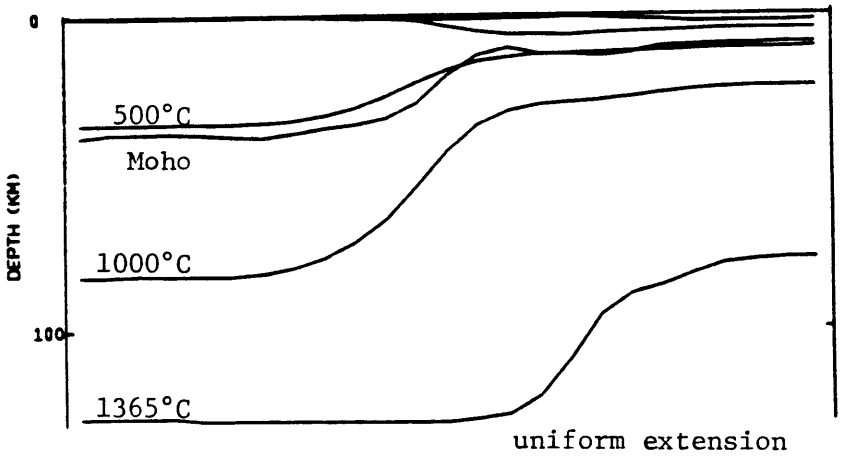

uniform extension

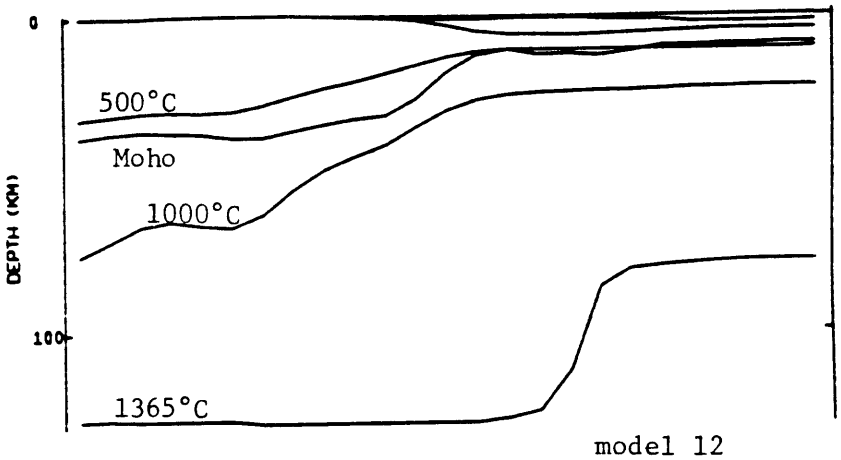

model 12

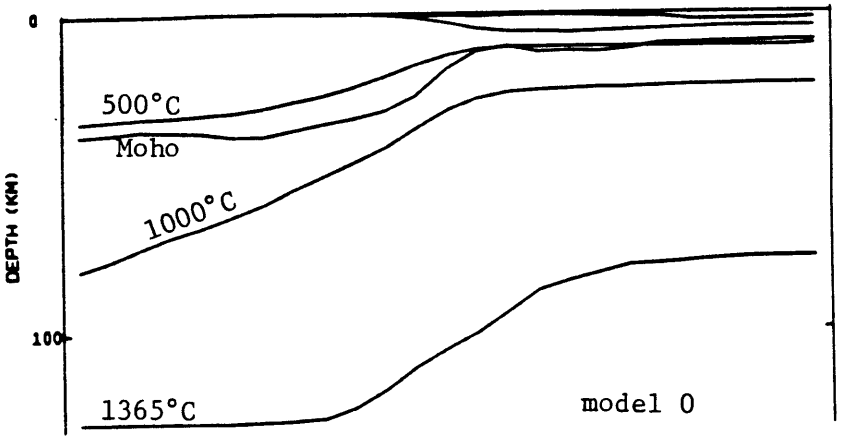

model 0

VE•1.0 X
TIME•0.0 MY

CAROLINA TROUGH

KC30m.0400.RUN10

Fig. 6.6c

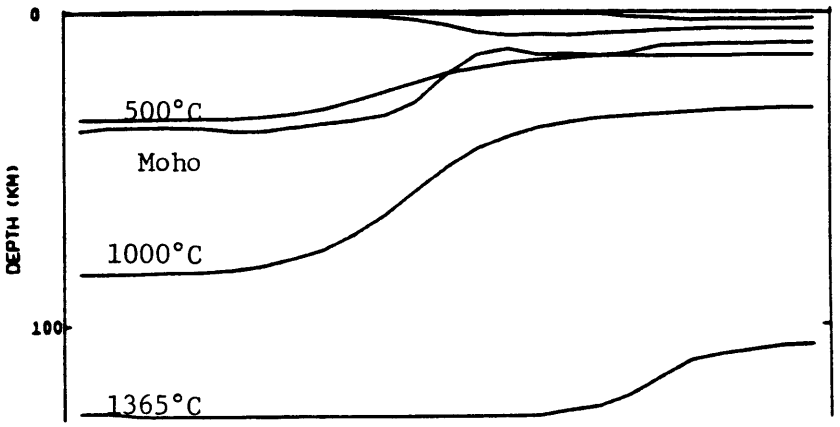

uniform extension

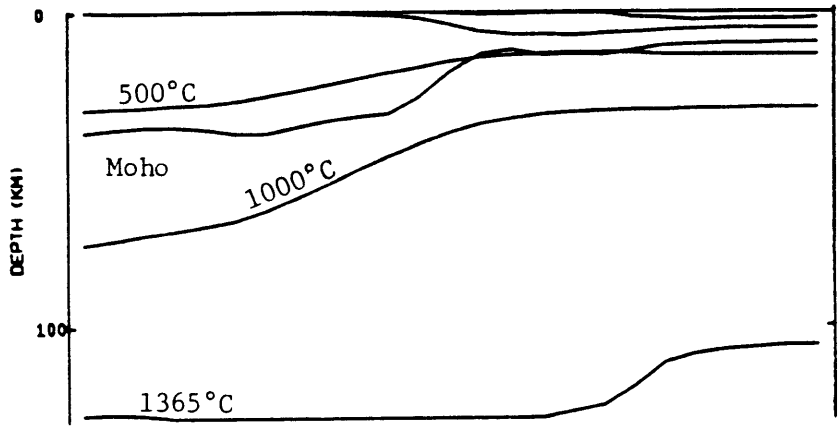

model 12

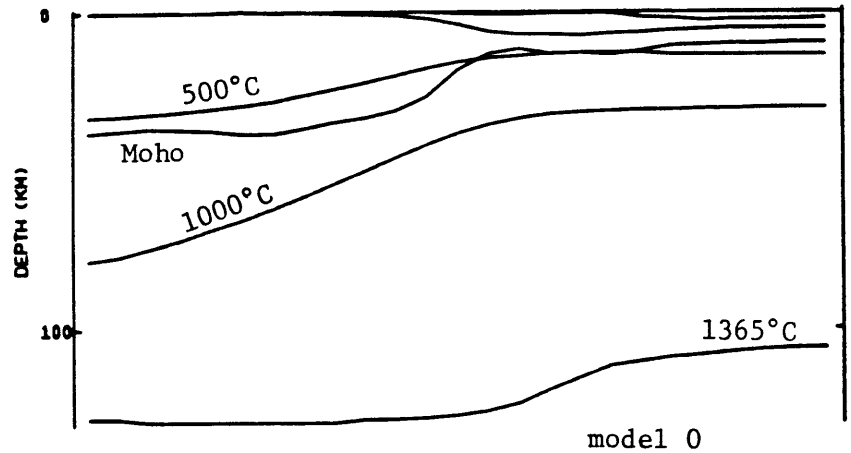

model 0

VE=1.0 X
TIME=12.8 MY

CAROLINA TROUGH

KC30m.0400.RUN10

Fig. 6.6d

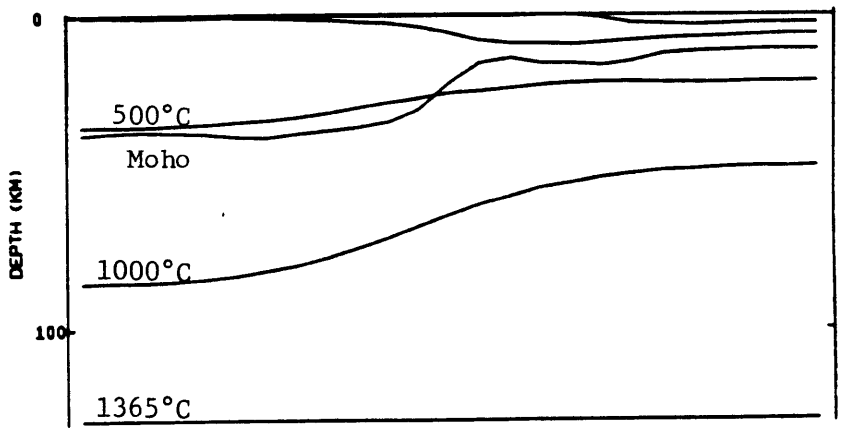

uniform extension

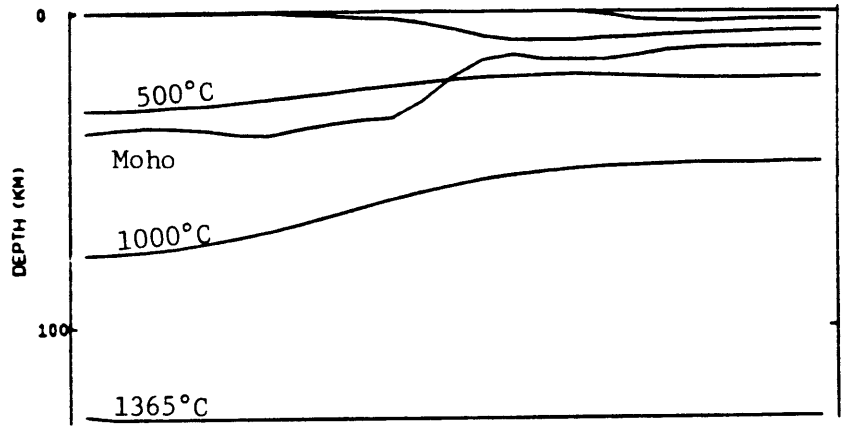

model 12

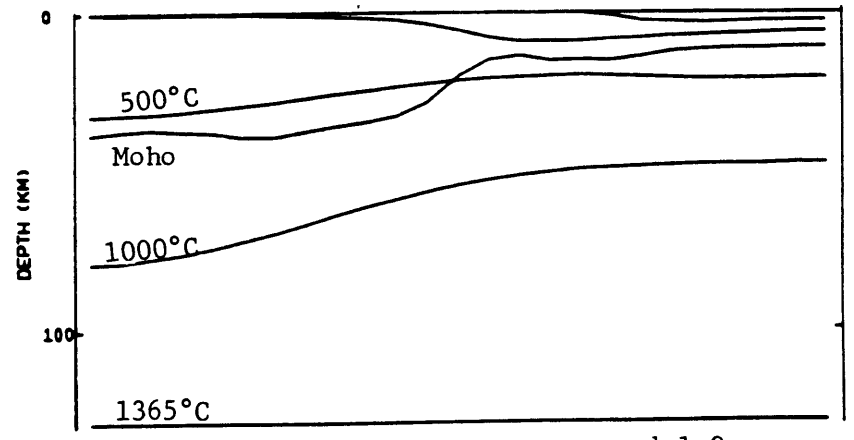

model 0

Fig. 6.6e

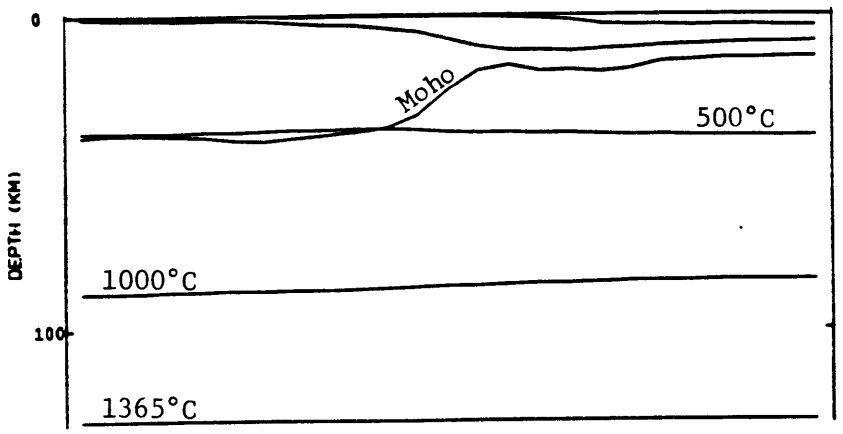

uniform extension

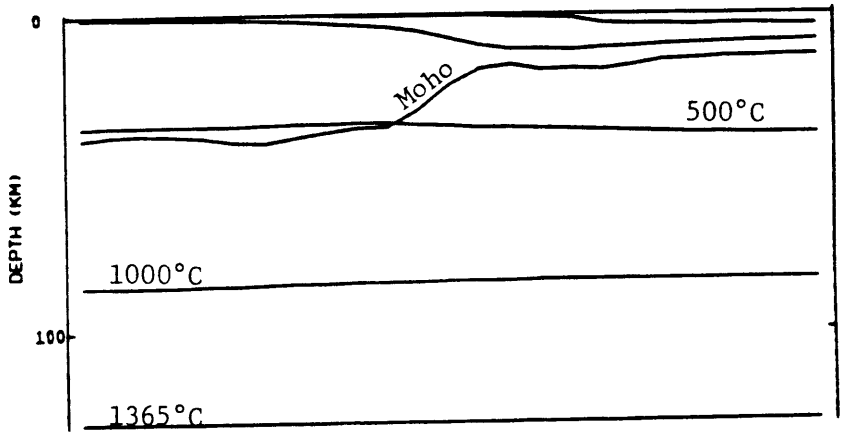

model 12

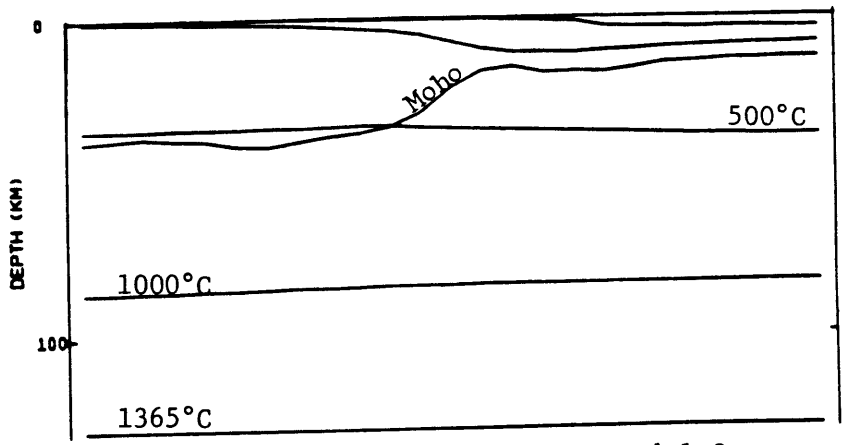

model 0

VE=1.0 X
TIME=110.0MY

CAROLINA TROUGH

KC30m.0400.RUN10

Fig. 6.6f

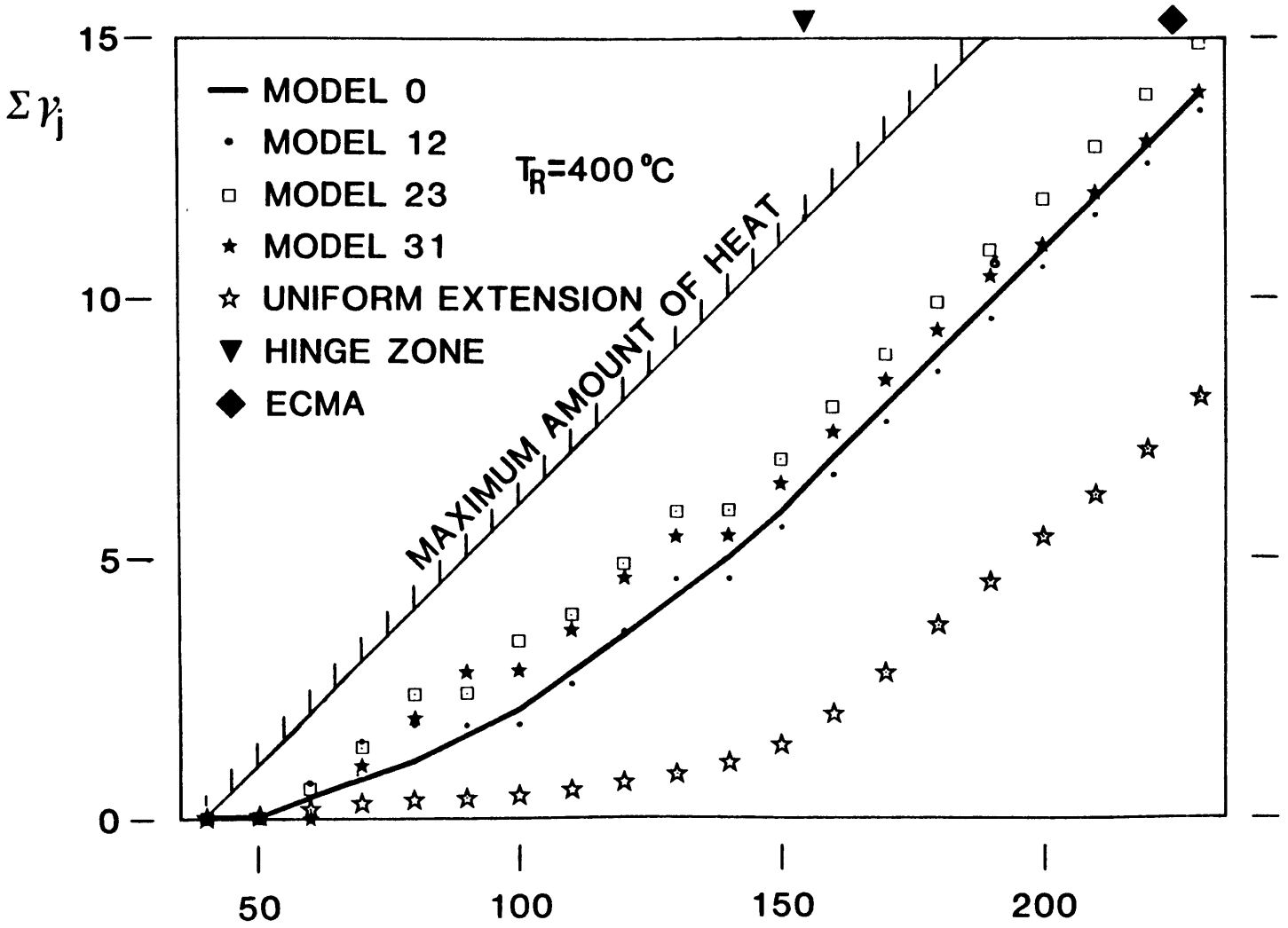
15
10
5
0
$\Sigma \gamma_j$
MODEL 0
MODEL 12
MODEL 23
MODEL 31
UNIFORM EXTENSION
HINGE ZONE
ECMA
T_R=400°C
MAXIMUM AMOUNT OF HEAT
50
100
150
200
DISTANCE FROM COASTLINE (KM)

Fig. 6.7

CHAPTER VII

THERMAL EVOLUTION OF THE CAROLINA TROUGH

When speculation has done its worst,
two and two still make four.

Johnson.

7.1 INTRODUCTION

Our models predict both the subsidence history and the thermal history of the Carolina trough. Previous chapters (4,5,6) evaluated the validity of the subsidence predictions by comparing them with geological inferences. We will now discuss the thermal predictions for which there is no check: the heat associated with rifting has disappeared a long time ago and even present geotherm and degree of sediment hydrocarbon maturation are not known because there is no deep well in the Carolina trough. Since we cannot directly check these predictions, we will try to estimate their error range by looking at the effects of data error and different model assumptions. To simplify this error analysis we will emphasize two types of temperature predictions.

First, a transient geotherm associated with rifting. This geotherm is very dependent on the assumed rifting mechanism or extension model parameters. As discussed before, the major sources of uncertainties on this are uncertainties on the constraining data and model assumptions. The data uncertainties are those on origin time of thermal decay, basement depth and sediments physical properties. The model assumption uncertainties are those in the parameter set up (Appendix A and C), the possibility of non thermal equilibrium before rifting or the possibility of extra subcrustal heat input and the loading response.

Second, an equilibrium geotherm which becomes dominant when the rifting anomaly has decayed. The source of uncertainties in this geotherm are some of our model parameters (such as lithosphere thickness, asthenosphere temperature, crustal radioactive heat generation, conductivities) but also, for the sediment temperatures, the amount of radioactive heat generation within the sediments (Keen and Lewis, 1982).

We will then show standard predictions and the variations one can expect in them depending on these sources of uncertainty.

7.2 CRUSTAL SCALE

7.2.1 Standard results

The standard model is the two dimensional uniform extension model with a relaxation temperature of 350°C (parameters as in Appendix C, table C.1).

The most striking feature is the speed of the evolution after rifting. Initially (Fig. 7.1a) the continental end is close to equilibrium while the oceanic end is extremely hot. Today (175 MY after rifting, Fig. 7.5a) the whole section has reached an equilibrium where the oceanic part is slightly cooler than the continental one. This latter result can be explained by two factors: first the oceanic crust is assumed to produce no radioactive heat in contrast to the continental crust; second, seaward of the hinge zone, the crust, which has a lower conductivity than the mantle, is very thin, therefore heat escapes more easily. Most of the evolution occurs during the first 30 to 50 MY after rifting (Fig. 7.1a, 7.2a, 7.3a) and by 100 MY after rifting (Just before the end of the Cretaceous, Fig. 7.4a) the isotherms are flat, and only little change occurs.

The flexural plate thickness which is controlled by the depth to the 350°C isotherm follows a similar rapid evolution. Initially it varies from 23 km at the landward end to 0 km on oceanic crust. At 25 MY after rifting, (fig. 7.3a) the oceanic plate is already half as thick as the continental one; past 100 MY after rifting plate thickness is uniformly 23 km across the basin (Fig. 7.4a). The lateral variation of plate thickness is therefore important only during the first 50 MY after rifting (therefore until lower Cretaceous only), during which time it depends on the temperature predicted by the extensional model, and past that time the plate thickness could be assumed uniform and depending essentially on the final equilibrium geotherm. There is then a close interaction between the extension model and the loading response only during the first 50 MY after rifting, but this time corresponds to the deposition of a very large proportion of the total sediment load.

We can also get a first order estimate of the importance of the lateral heat flow in respect to the vertical heat flow by measuring the ratio of horizontal to vertical distance between isotherms. If we look at the hinge zone where this effect is the most intense, the horizontal heat flow can be expected to be about 75% of the vertical heat flow immediately after rifting, about 25% 12 MY after rifting, about 10% 31 MY after rifting (top Jurassic) and negligible after 50 MY after rifting (top lower Cretaceous). Therefore a two dimensional model will differ significantly from a one dimensional model only during the first 30 MY after rifting.

This explains why the topography predicted by the two dimensional model with local isostasy (chapter 5) is better than the one predicted by the one dimensional model (chapter 4) before that time and similar to it after that time.

Thermal blanketing by the sediments results in a present basement temperature of more than 150°C in the deepest part of the trough. However, in that part of the basin, the lower conductivity of the sediments is compensated by the thinning of the crust which brings up more conductive mantle; as a result the present isotherms do not upwarp but follow the topographic trend. Earlier, when sediments were not yet so compacted and therefore were less conductive, such an upwarp can be seen (Fig. 7.3a).

7.2.2 Deviation

Assuming local isostasy results in smaller horizontal gradients across the hinge zone and therefore smaller horizontal heat flow (Fig. 7.1c, 7.2c, 7.3c, 7.4c). However these differences are significant only during the first 30 MY after rifting (until end of Jurassic) and negligible thereafter.

Assuming an origin time 200 MYBP instead of 175 MYBP has a longer lasting effect (Fig. 7.1d, 7.2d, 7.3d, 7.4d). The whole section is cooler for the same age before present because this corresponds to later time after rifting. Note the similarity of deep isotherms between similar time after rifting (Fig. 7.2d and 7.3c) even though the sedimentary structure is different. However after the end of the Cretaceous (65 MYBP), the difference is negligible.

The two layer model (Fig. 7.1b, 7.2b, 7.3b, 7.4b) is always similar to the uniform extension at the landward end and over oceanic crust. Initially (Fig. 7.1b) it looks also like the uniform extension model because the major differences are higher temperatures below the crust, which are not shown in this section. This extra heat diffuses into the crust during the first 30 MY (Fig. 7.2b, 7.3b) making the extended continental crust hotter than predicted by uniform extension. From 20 to 50 MY after rifting, the depth to the 400°C isotherm in the two layer model is equivalent to the depth to the 350°C isotherm in the uniform extension model: this explains why we had to increase the relaxation temperature by 50°C in order to maintain an equivalent loading response. Subsequent to

50 MY after rifting, the difference between two layer and uniform extension becomes less significant and by 110 MY after rifting (end of Cretaceous) it is negligible.

The two extreme uniform extension models which incorporate data error (as mentioned in Chapter 5, section 5.2.2), lead to a considerably different early temperature structure between the hinge zone and the ECMA (Fig. 7.1e, 7.2e, 7.3e and 7.1f, 7.2f, 7.3f). By 110 MY after rifting (end of Cretaceous, Fig. 7.4e and 7.4f) the remaining differences are negligible and essentially due to an unrealistic topography seaward of the ECMA.

7.3 SEDIMENTS

7.3.1 Introduction

One of the major applications of this type of modeling is to predict the temperature history of sediment and therefore their degree of hydrocarbon maturation (Royden et al., 1980). Hydrocarbon maturation can be evaluated by the C parameter defined as (Royden et al., 1980):

$$C(t_o) = \ln \int_o^{t_o} 2^{T(t)/10}\, dt$$

where: t_o is the time at which maturation is evaluated and T(t) is the temperature (°C) of the considered sediments at time t (MY). Oil generation occurs when $10<C<16$ while gas generation takes place when $16<C<20$.

We will evaluate the thermal history of the sediments in two different ways: first we will look at the temperature evolution of the sediments deposited at one fixed location along line 32; second we will look at the integrated history of sediment by mapping the isomats (lines of equal C-values) across the basin at different times.

7.3.2 History at SP 3400

SP 3400 was chosen because it is one of the deepest part of the basin where basement is still reasonably well defined. Moreover subsidence history is already evaluated at that location (Chapters 4 and 5).

a) Standard Results

We will distinguish 3 types of sediment, according to the style of their time-temperature curve (Fig. 7.6).

The "Early" sediments which reach their maximum temperature rapidly after rifting (less than 35 MY) and after that tend to cool off slowly. At SP3400, this corresponds to the sediments deposited before the end of the Callovian (12 MY after rifting). These sediments were buried sufficiently fast after rifting to be affected by the transient high rifting heat flux; they reach their present degree of hydrocarbon maturation at a time close to the one when they reach maximum temperature, therefore very early in their history (less than 40 MY after rifting).

The "Late" sediments for which temperature increased constantly since deposition until today. They correspond to sediments deposited after Kimmeridgian (23 MY after rifting). These sediments were deposited at a time when the initial heat had already decayed and, more important, were probably not sufficiently buried to be much affected by the remaining heat anomaly until it was gone. As a result, their temperature evolution seems more related to their burial rate and to the equilibrium geotherm. Their degree of maturation evolved slowly through time.

The "Intermediate" sediments for which temperature increases very fast after rifting and then stabilizes until today. They correspond to sediments deposited in Oxfordian and Kimmeridgian time (between 12 and 23 MY after rifting). The C=10 isomat is at present located between the "Early" and "Intermediate" sediments. While the C=16 isomat is associated only with the very "Early" sediments.

b) Deviation

Assuming local isostasy (Fig. 7.7) affects only the "Early" sediments whose maximum temperature are slightly smaller (up to 10°C less) and reached slightly later after rifting (up to 10 MY later). Today's temperature structure is within 5°C of the standard model. The isomats are barely affected. There is then very little variation due to the difference in loading response because the thermal difference at crustal scale is localized around the hinge zone and short lived (It disappears within 30 MY after rifting).

Assuming an origin time 200 MYBP (Fig. 7.8) instead of 175 MYBP affects only the Early sediment which becomes of intermediate type because they now arrive and are buried longer after rifting. As a result their maximum temperatures are smaller (up to 30°C less) and they are reached

around the same age (around the end of the Jurassic) as in the standard model. Today's temperature structure is also within 5°C of the standard model. The C=10 isomat is not very different from the standard model but the C=16 disappears: the earliest sediments which are assumed to be up to 25 MY older are paradoxically less mature because they are buried later after rifting.

The two layer model (Fig. 7.9) does not affect the intermediate or late sediments, nor does it affect the early sediment past 100 MY after rifting. (For all these cases the maximum temperature differences are about 5°C). The main difference is that the early sediment reaches a higher maximum temperature (up to 25°C higher) sooner (up to 15 MY sooner). As a result the C=10 isomat remains the same today but tends to be reached sooner (up to 10 MY sooner) by most early sediments; the C=16 isomat includes the PRU in contrast to the uniform extension model.

In order to evaluate the error range on the standard model due to data uncertainty, we will simply compare the results obtained with the two extreme data sets with each other (Fig. 7.11 and 7.12). The extreme set corresponding to maximum extension shows much higher temperatures than the one corresponding to minimum extension. This temperature difference appears very large and affects all sediments up to the late sediments where differences can still reach 20°C. The comparison for the synrift sediments is biased by the fact that each model assumed them to be at different sub-bottom depths. As a result the difference in the maximum temperature reached by the synrift sediment varies from 40°C for the youngest (assumed at about the same depth) to be 270°C for the oldest (assumed at very different depth). The post rift early sediments do not suffer from that depth bias but still can have their maximum temperature varying by as much as 40°C (top Bathonian). The present day temperature structure is the same in both cases (at same depth). The C=10 isomat is at the same stratigraphic level today but it is reached at very different times by different sediments (up to 35 MY difference from synrift up to top Bathonian; up to 100 MY for the top Callovian). The synrift and earliest post rift sediment of the maximum extension case reach C values from 16 to more than 20 in contrast to the minimum extension case where 16 is not even reached.

Assuming a high value of radioactive heat generation for the sediment matrix ($5.0\ 10^{-13}$ cal cm^{-3} s^{-1}, Fig. 7.10) changes the two layer model predictions (as in Fig. 7.9) in a very different way from all those discussed above. From 0 to 10 MY after rifting there is no significant difference. But after that the difference increases with time instead of decaying and the sediment ends up being 30°C hotter today. Also, all sediments are affected. The C=10 present isomat is raised in the stratigraphic column and includes the Kimmeridgian while the C=16 isomat is barely modified. We expect this effect to be a maximum error range because we assumed a high value for the heat generation. Because this source of error affects very much the present temperature predictions (Fig. 7.13), it could be easily constrained by temperature well data.

7.3.3 Maturation profiles

The same maturation calculations as shown at SP 3400 can be done at any location along line 32. We can therefore map the isomat at different times along the profiles. We will discuss the results at two times: 31 MY after rifting (top Jurassic) and 175 MY after rifting (present).

a) End of Jurassic

Most models (Fig. 7.14) agree on the position of the C=10 isomat above the top Bathonian in the center of the basin and below it seaward of the Jurassic shelf. There are however two models which differ from that: the uniform extension model with the extreme data set corresponding to minimal extension (Fig. 7.14f) and the uniform extension model which assumes an origin time 200 MYBP (Fig. 7.14d); in both cases the C=10 isomat is much below the standard prediction.

The degree of maturation of the synrift sediments varies from oil mature to overmature depending on model assumptions and data errors. Every model is different; from least mature to most mature we have: flexural uniform extension with minimal extension data set (Fig. 7.14f), local uniform extension with origin time 200 MYBP (Fig. 7.14d), local uniform extension (Fig. 7.14c), flexural uniform extension (Fig. 7.14a), two layer (Fig. 7.14b), two layer with radioactive sediment (Fig. 7.14-g) and flexural uniform extension with maximum extension data set (Fig. 7.14-e).

b) Present

All models agree on a C=10 isomat above the top Callovian (Fig. 7.15) except the model where radioactive sediments are assumed which puts that isomat above the Kimmeridgian (Fig. 7.15-g).

The degree of maturation of the synrift and earliest postrift sediment is totally model dependent and in the same order as it was at the end of the Jurassic.

A similar study supposed to represent a neighboring area locates peak oil generation as high as within the Lower Cretaceous under the present shelf edge (Watts and Thorne, 1984). This is higher than our estimate and other estimates for the Baltimore Canyon trough (Sawyer, 1982; Sawyer et al. 1982b). Because many differences are involved between this approach and ours: different model assumptions and parameters, sediment properties and stratigraphy, it is difficult to assign these different results to a particular cause. However, two points can be made.

First the alternate model stratigraphy, which is more representative of the Baltimore Canyon, shows a present and Cretaceous shelf edge above the Jurassic shelf edge. In our model that part of the Cretaceous shelf edge which has been removed by Cenozoic erosion is ignored. We can then wonder if the corresponding sediment didn't help the sediments underneath them to mature more than we predicted by burying them temporarily. To further answer this question a good estimation of the amount eroded would be necessary.

Second this alternate model shows that the isomat depths are sensitive to the sediment properties. This is not so clear in our results because the extreme cases we studied are not extreme in all respects. Taking for instance the extreme data set which corresponds to maximum extension, therefore, one would expect, to maximum heat input and to shallowest peak oil generation, implies us to assume lightest, therefore most porous sediment; but this in turn implies that these sediments are poorer conductors and therefore impede the propagation of heat upward, hence the chance of shallow maturation.

To go beyond these hypothetical remarks would require information on the temperature history predicted by Watts' and Thorne's (1984) models. However this suggests that the error range that we evaluated may not be conservative in terms of maturation predictions, even though it seemed conservative in terms of subsidence.

7.4 CONCLUSIONS

It appears very helpful to distinguish between the early (less than 30 MY after rifting) thermal history dominated by the transient geotherm associated with rifting from the late (more than 60 MY after rifting) thermal history dominated by the equilibrium geotherm. The dominant causes of error in the early thermal history are the data and origin time uncertainties; uncertainties in subcrustal extension are a smaller source of error while the most transient source of error is the uncertainty on loading response mechanism. A cause of error in the equilibrium geotherm is the uncertainty in the radioactive heat generated by the sediments which can raise the temperatures significantly.

Following the same line of thought for the thermal evolution of the sediments it appears useful to distinguish (1) the early sediments, which are defined as those sufficiently buried during the early thermal history to be affected by it, from (2) the late sediments, which were not very much buried before the late thermal history.

The early sediments temperature history is controlled by the whole thermal history, but the early temperatures are sensitive to rifting mechanism uncertainties. These uncertainties are those in the loading response, the origin time of thermal decay, the initial heat input (or subcrustal "extension") and the data. Among these, the data uncertainties (basement depth and sediment properties) are those with the larger effect. The predictions which are affected include the timing and values of maximum temperatures reached by the early sediments. The past and present degree of maturation of these sediments is essentially determined by the early thermal history during which the highest temperatures are reached. It is therefore sensitive to rifting mechanism uncertainties which would be reduced by better constraint on origin time, basement depth, sediment properties and early paleogeography. Because maturation is integrative, the transient error induced by loading response uncertainties is negligible. In any case, the synrift and earliest postrift sediments are at least mature and the major effect of the uncertainties is to place them is the overmature zone.

The late sediments temperature history is essentially controlled by the equilibrium geotherm and their burial history. We looked at only one source of uncertainty in the equilibrium geotherm; : the amount of radioactive heat generation within the sediments, but very likely other causes would have a similar effect. This affects all sediments and increasingly so as time passes. Well data would very well constrain both this burial history and the equilibrium geotherm, therefore the degree of maturation of these late sediments.

The present C = 10 isomat, located in the intermediate sediments, appears to be sensitive to the equilibrium geotherm and not to rifting mechanism. However if one wants to determine the past position of this isomat, rifting mechanism has to be considered, and here again the most critical causes of error are the uncertainties in origin time, basement depth and sediments properties.

Figure Captions

Fig. 7.1. Crustal thermal prediction at the end of rifting. Figures are labeled in MY after end of rifting. In all these models the sediments are assumed to produce no heat by radioactivity.

7.1a: standard model: uniform extension, T_R = 350°C, end of rifting 175 MYBP

7.1b: two layer model 0, T_R = 400°C, end of rifting 175 MYBP

7.1c: uniform extension, local isostasy, end of rifting 175 MYBP

7.1d: uniform extension, local isostasy, end of rifting 200 MYBP: this figure corresponds then to 200 MYBP instead of 175 MYBP for the others

7.1e: uniform extension, T_R = 350°C, end of rifting 175 MYBP. Maximal extension data set

7.1f: uniform extension, T_R = 350°C, end of rifting 175 MYBP. Minimal extension data set

Fig. 7.2. Crustal thermal prediction after deposition of synrift sediment. Same conventions as Fig. 7.1.

7.1a-7.1f: correspond to 174 MYBP and Fig. 7.1d to 175 MYBP.

Fig. 7.3. Crustal thermal prediction at the End of the Jurassic (144 MYBP)

Fig. 7.4. Crustal thermal prediction at the End of the Cretaceous (65 MYBP)

Fig. 7.5. Present time crustal thermal prediction

Fig. 7.6. Sediments time-temperature history at SP 3400 along line 32 - standard model.

Fig. 7.7. Sediments time-temperature history at SP 3400 along line 32 - uniform extension, local isostasy and 175 MYBP origin time.

Fig. 7.8. Sediments time-temperature history at SP 3400 along line 32 - uniform extension, local isostasy and 200 MY origin time.

Fig. 7.9. Sediments time-temperature history at SP 3400 along line 32 - two layer model 0 , T_R = 400°C, origin time 175 MYBP, no sediment heat.

Fig. 7.10. Sediments time-temperature history at SP 3400 along line 32 - same model as Fig. 7.9 except that sediment matrix is given as radioactive heat generation of 5.0 10^{-13} cal cm^{-3} s^{-1}.

Fig. 7.11. Sediments time-temperature history at SP 3400 along line 32. Same model as on Fig. 7.6 but for extreme data set corresponding to maximum extension.

Fig. 7.12. Sediments time-temperature history at SP 3400 along line 32. Same model as on Fig. 7.6 but for extreme data set corresponding to minimum extension.

Fig. 7.13. Predicted present sediment temperature
Horizontal scale: 40 to 280 km from coastline
7.13a: uniform extension model, T_R = 350°C (standard model)
7.13b: two layer model 0, T_R = 400°C, with radioactive sediment (matrix heat generation: 5×10^{-13} cal cm^{-3} s^{-1}.

Fig. 7.14. Degree of maturation of sediment by the end of the Jurassic (144 MYBP).
7.14a-f: correspond to same model as in Fig. 7.1.
7.14g: same as 13b but with sediment matrix heat generation of 5×10^{-13} cal cm^{-3} s^{-1}.

Fig. 7.15. Present degree of maturation of sediments. Same conventions as Fig. 7.14.

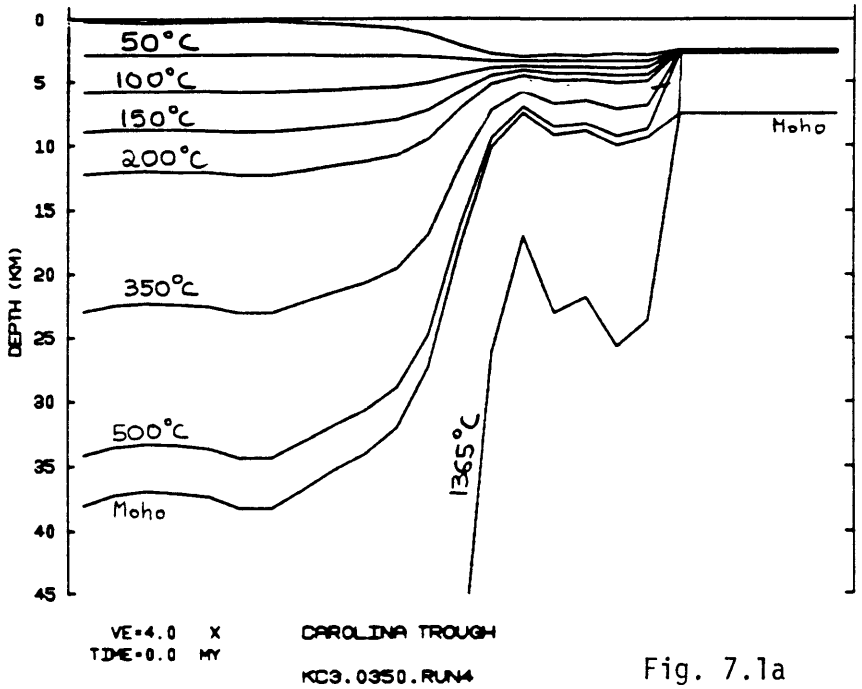

Fig. 7.1a

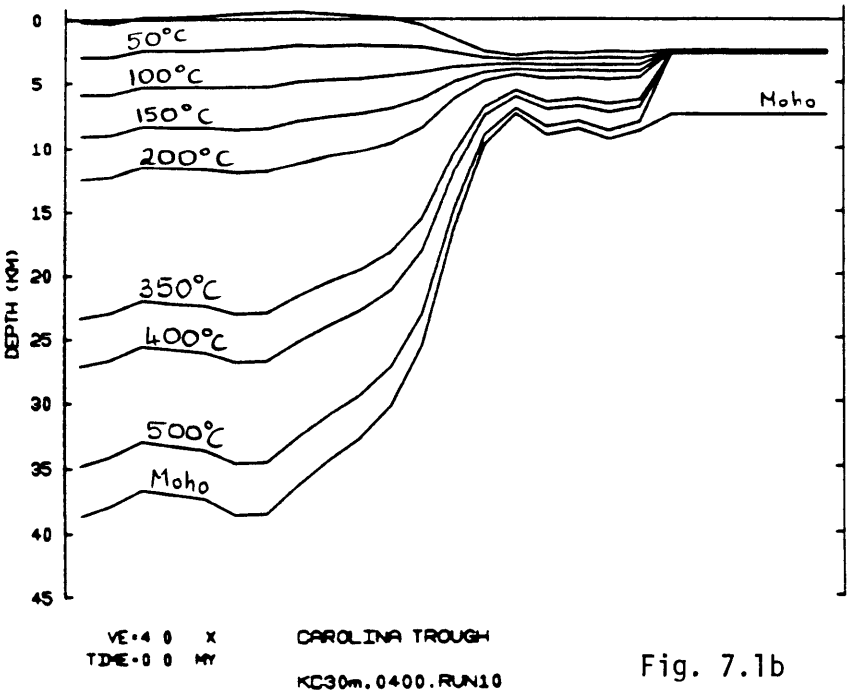

Fig. 7.1b

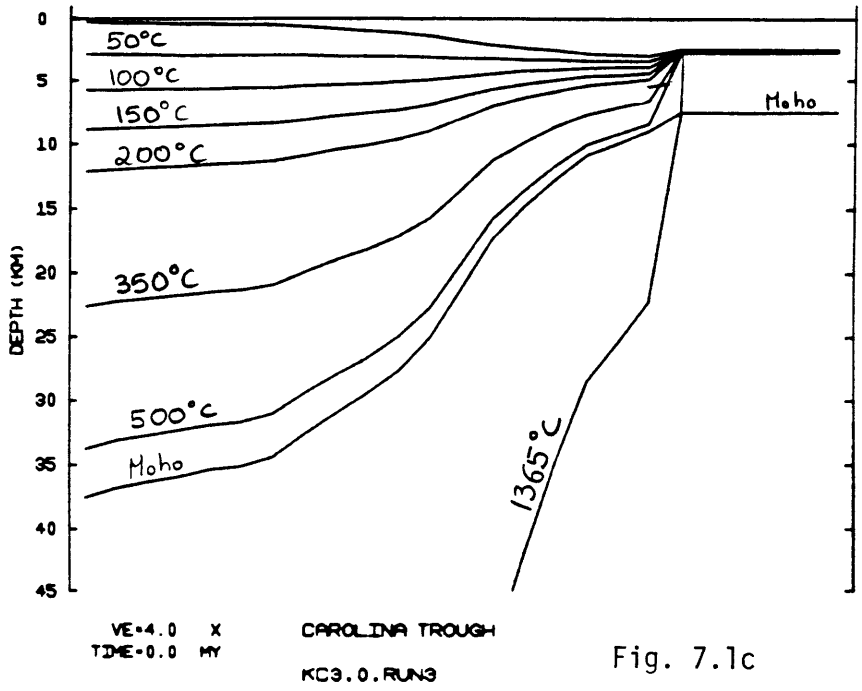

Fig. 7.1c

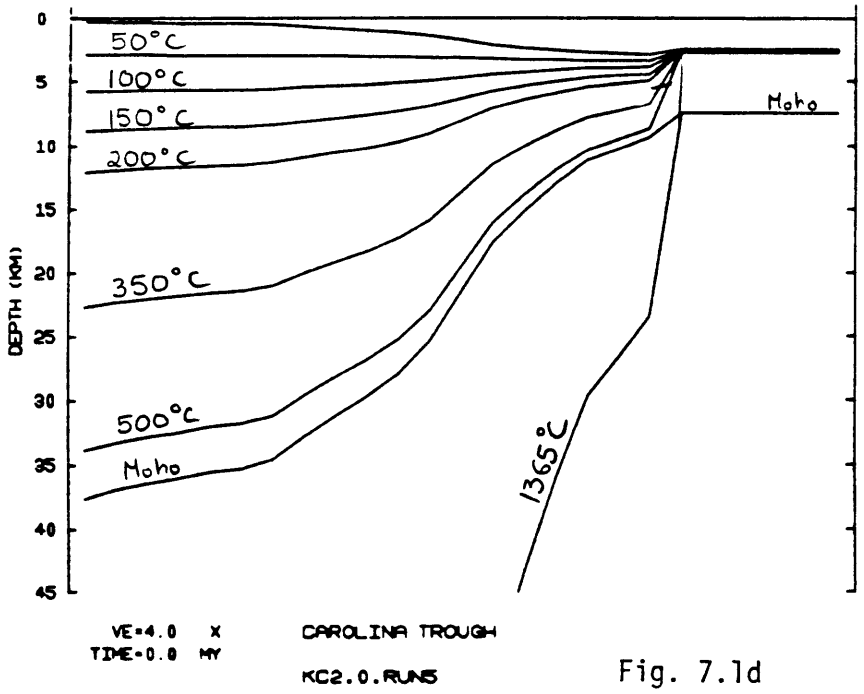

Fig. 7.1d

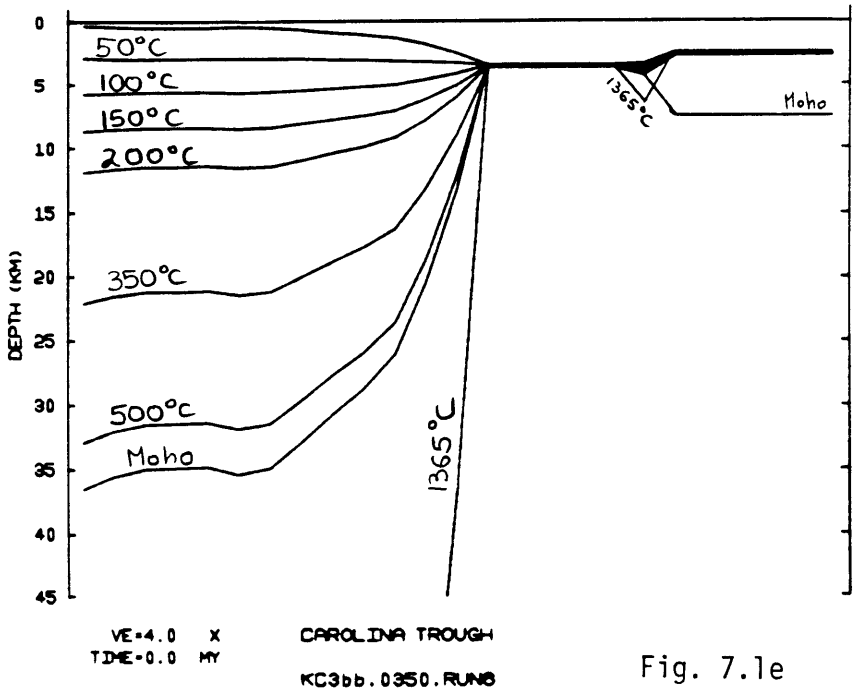

Fig. 7.1e

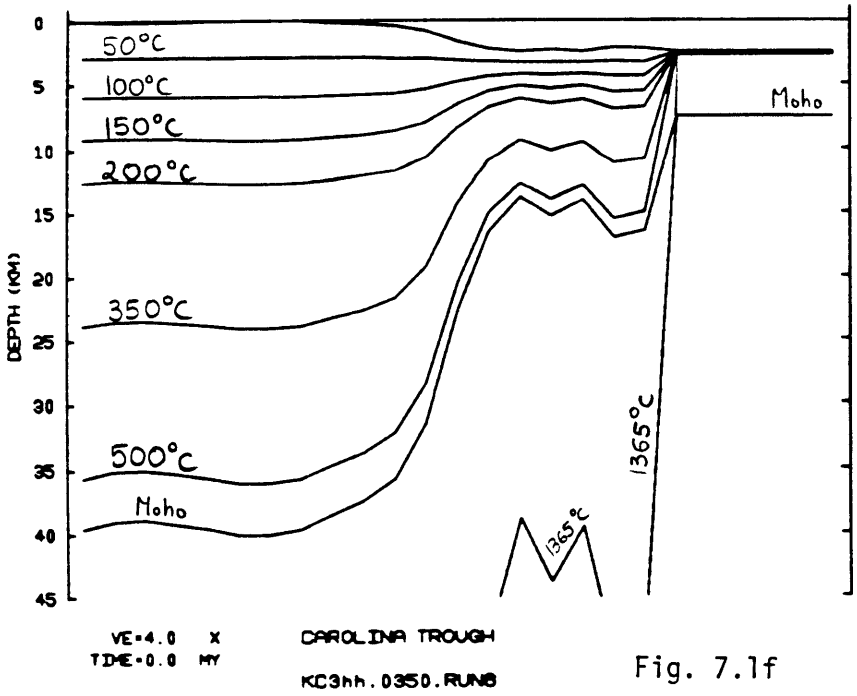

Fig. 7.1f

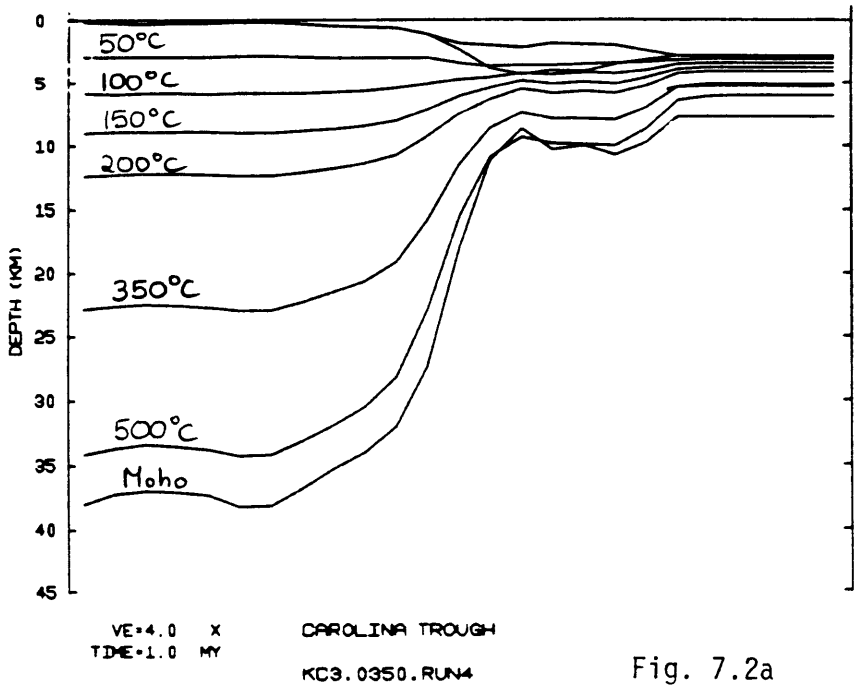

Fig. 7.2a

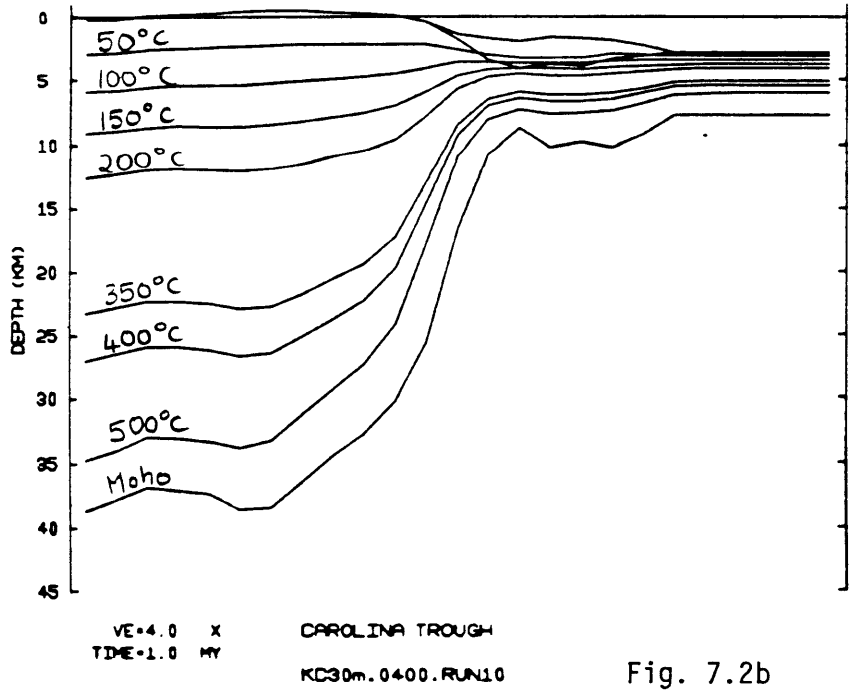

Fig. 7.2b

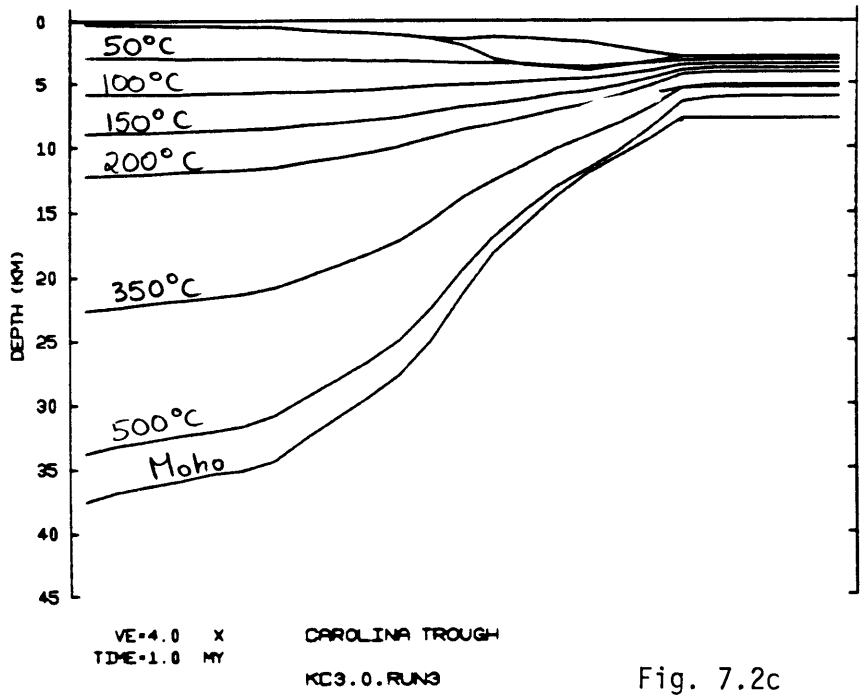

Fig. 7.2c

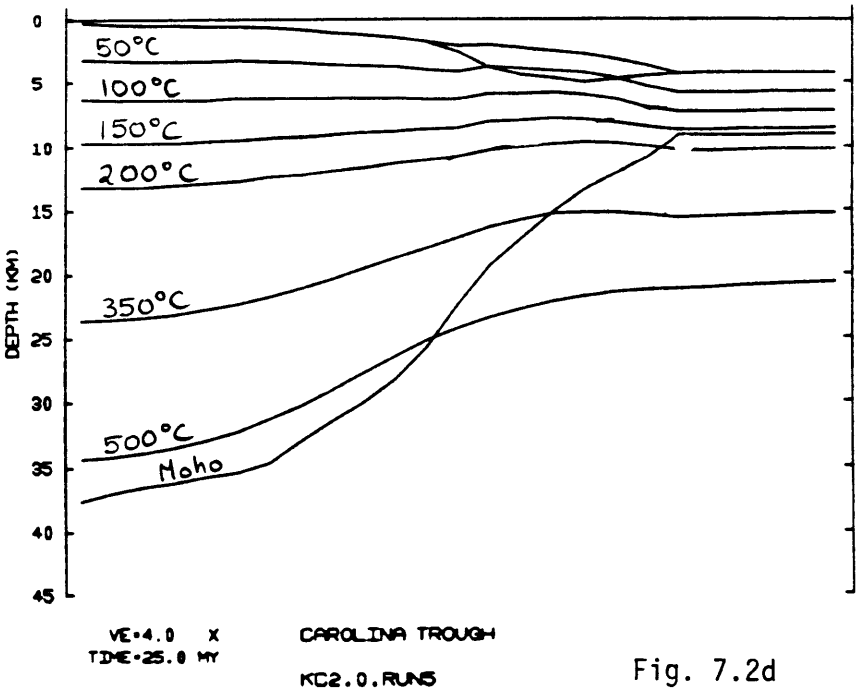

Fig. 7.2d

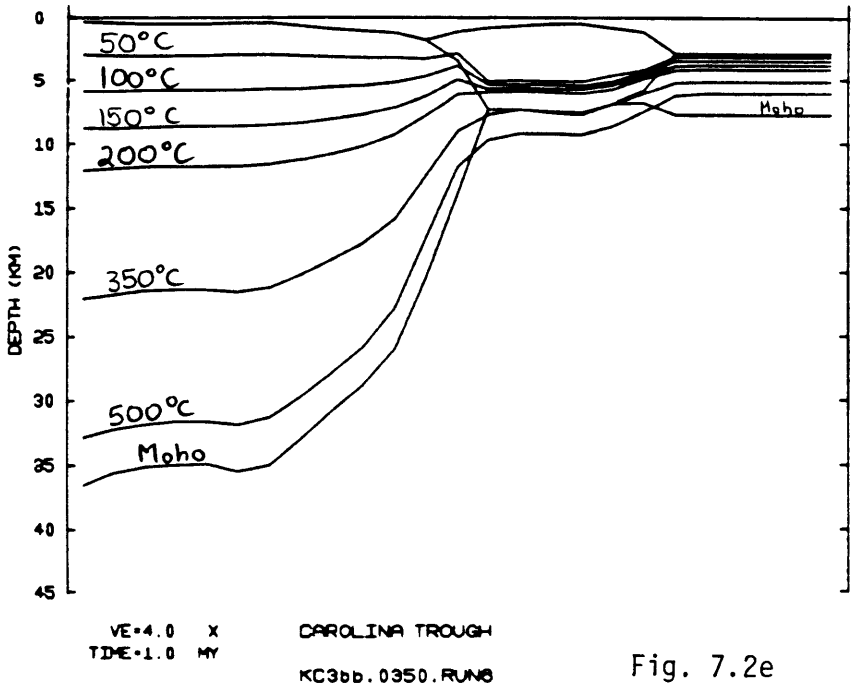

Fig. 7.2e

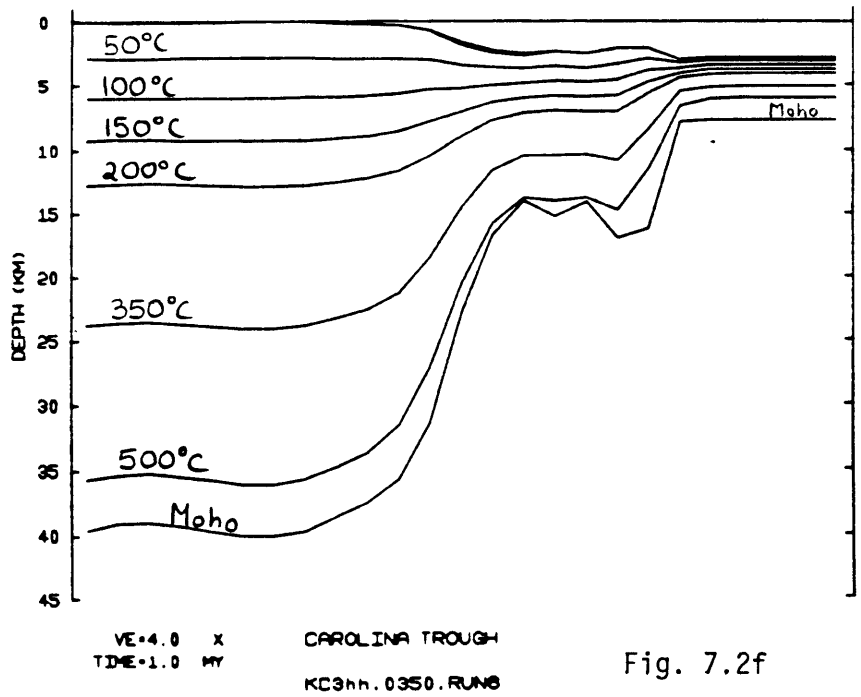

Fig. 7.2f

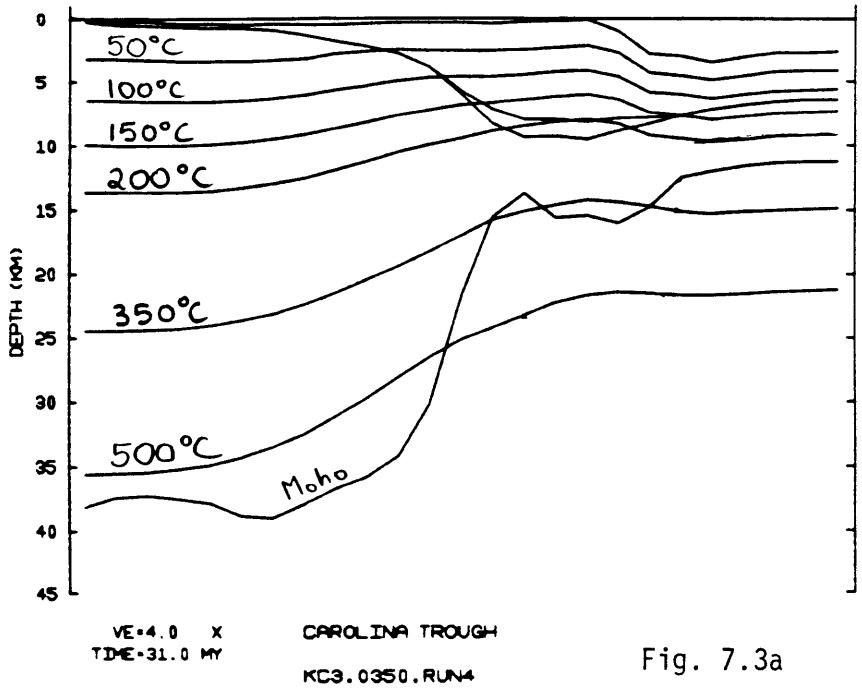

Fig. 7.3a

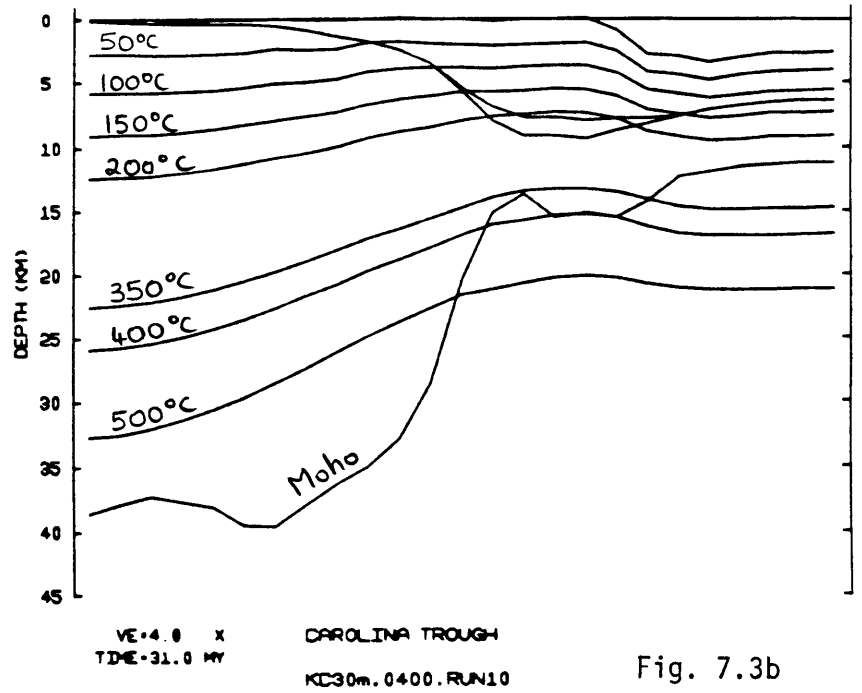

Fig. 7.3b

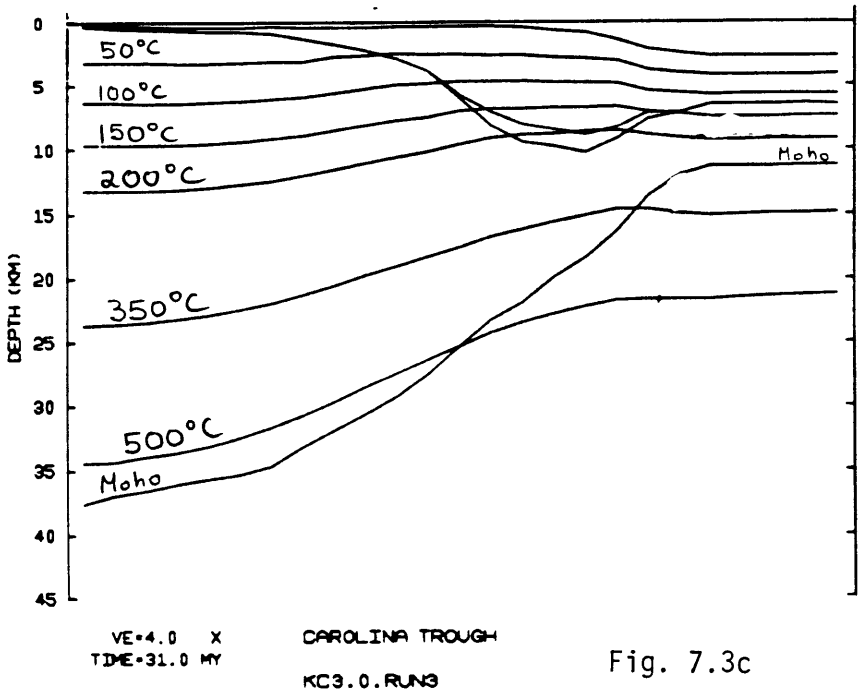

Fig. 7.3c

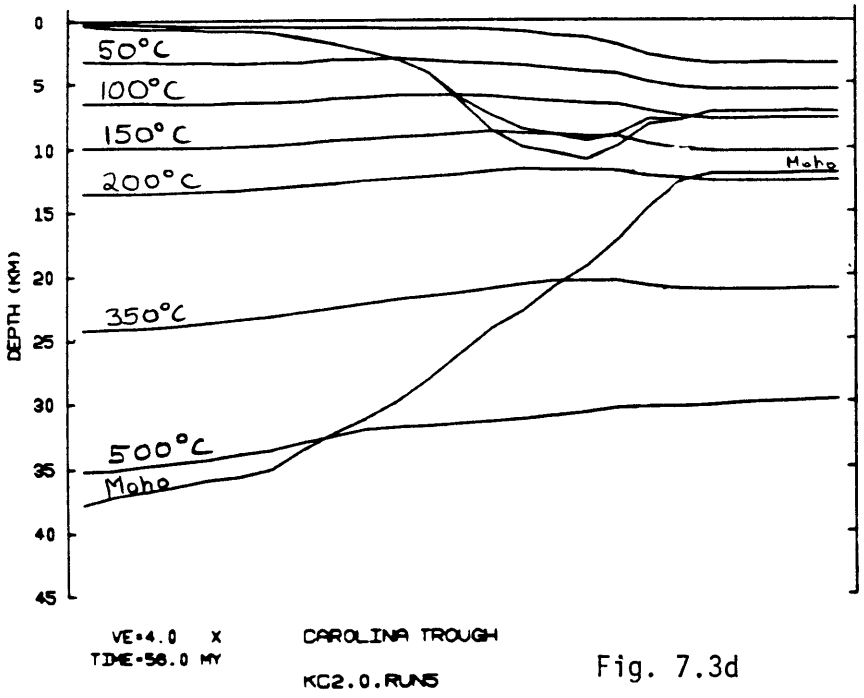

Fig. 7.3d

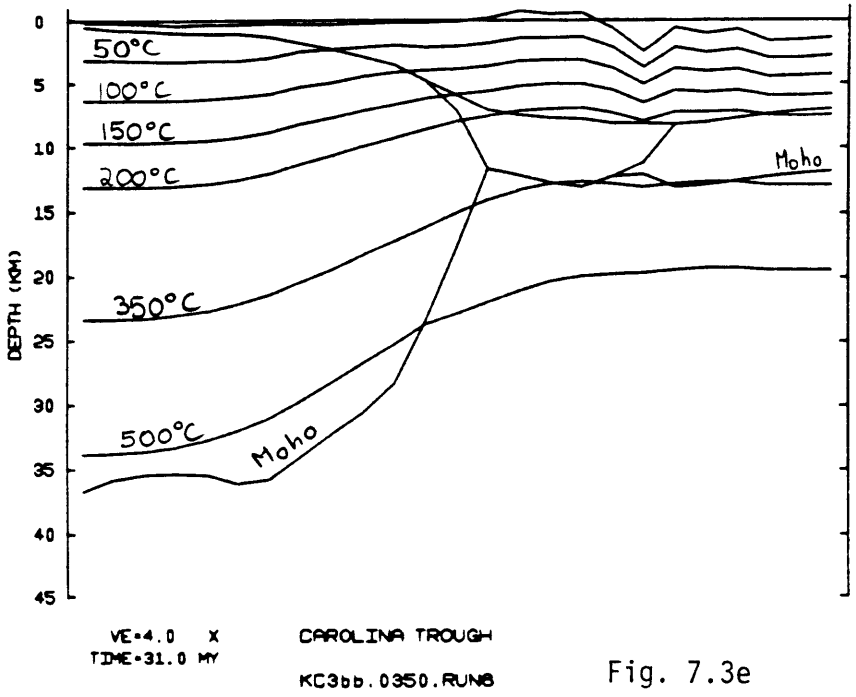

Fig. 7.3e

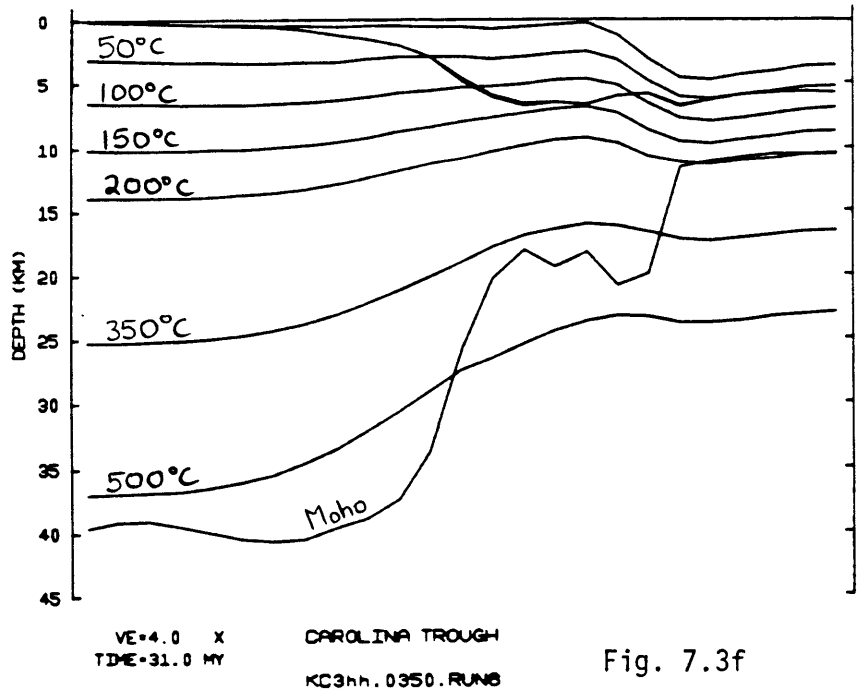

Fig. 7.3f

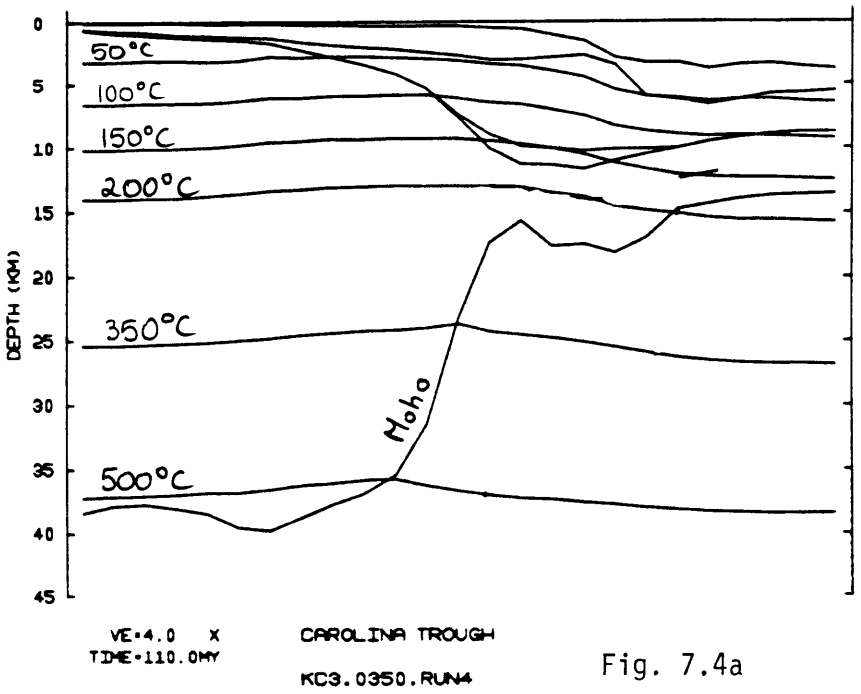

Fig. 7.4a

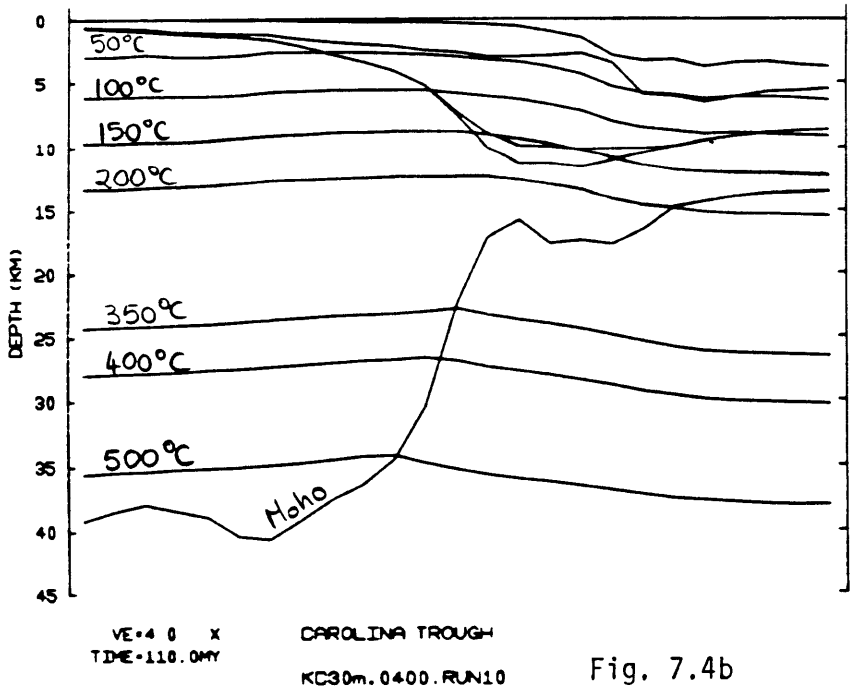

Fig. 7.4b

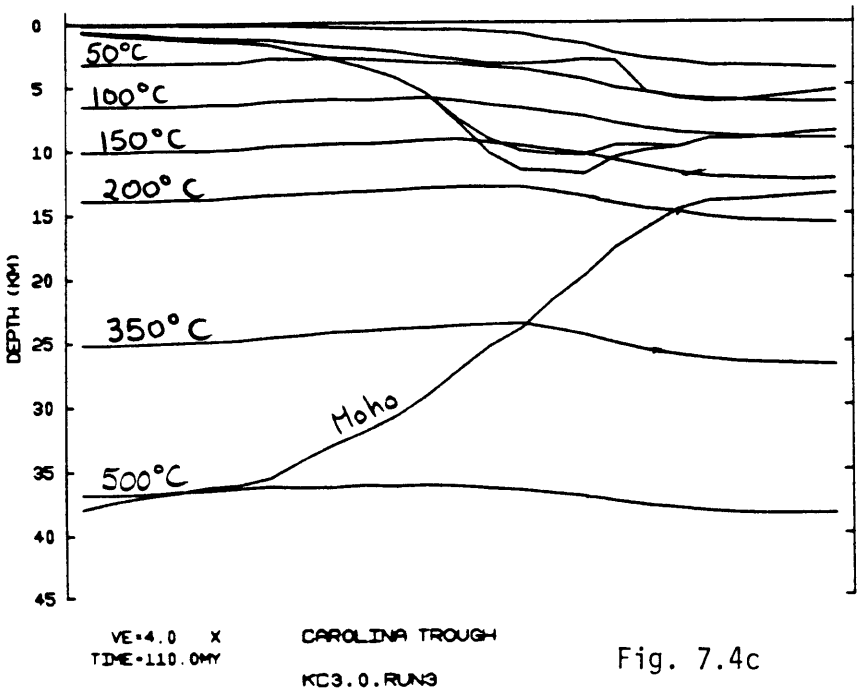

Fig. 7.4c

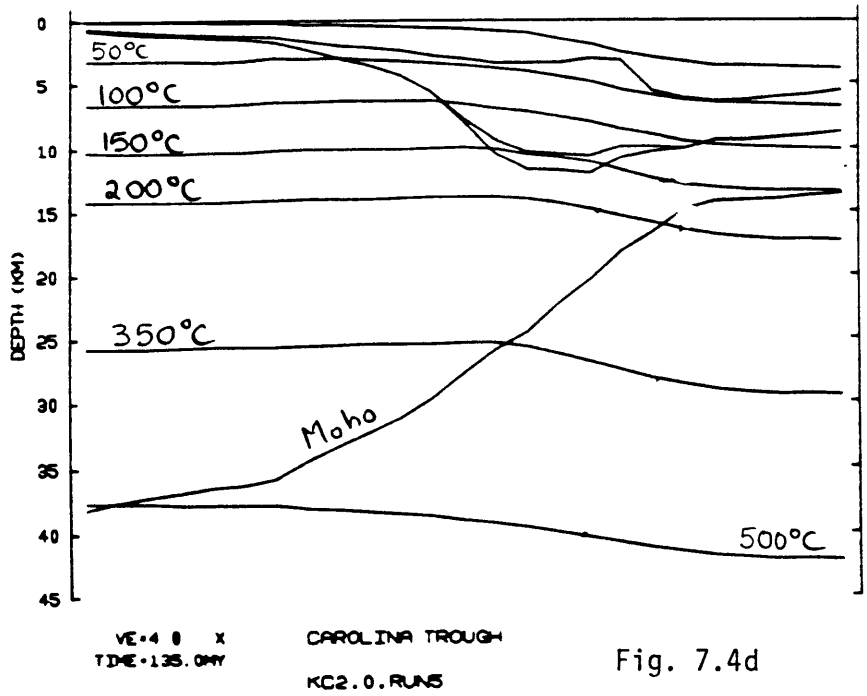

Fig. 7.4d

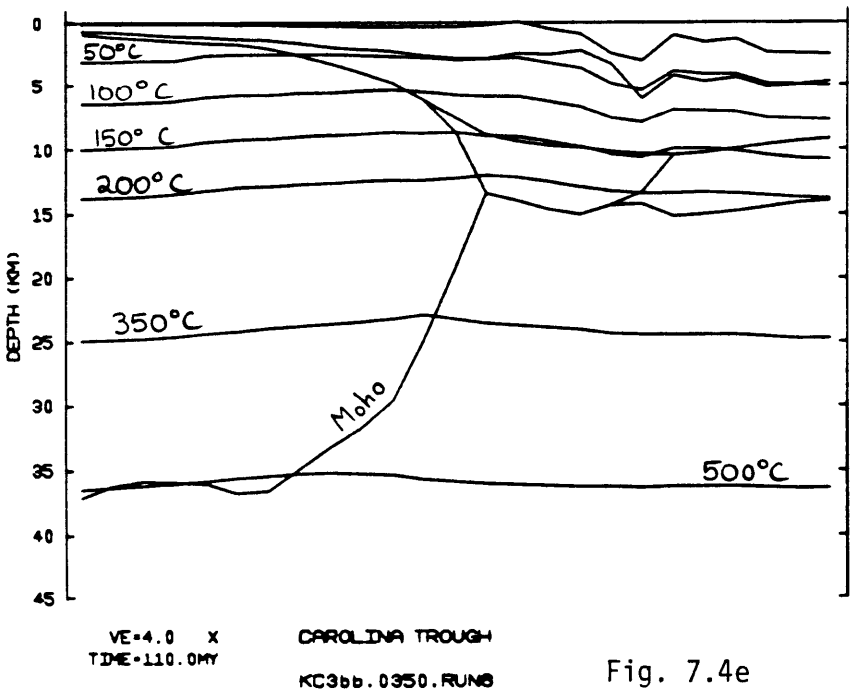

Fig. 7.4e

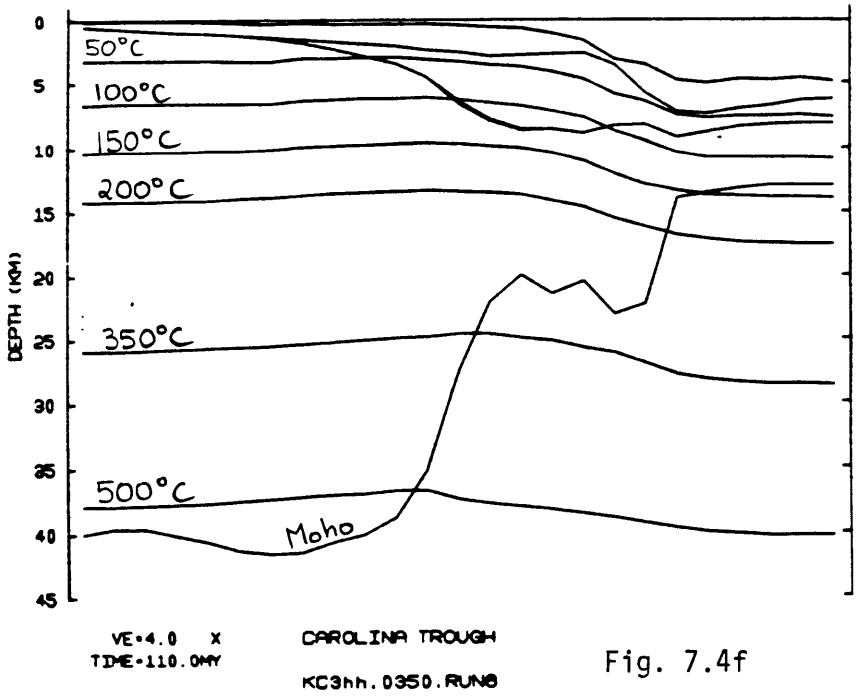

Fig. 7.4f

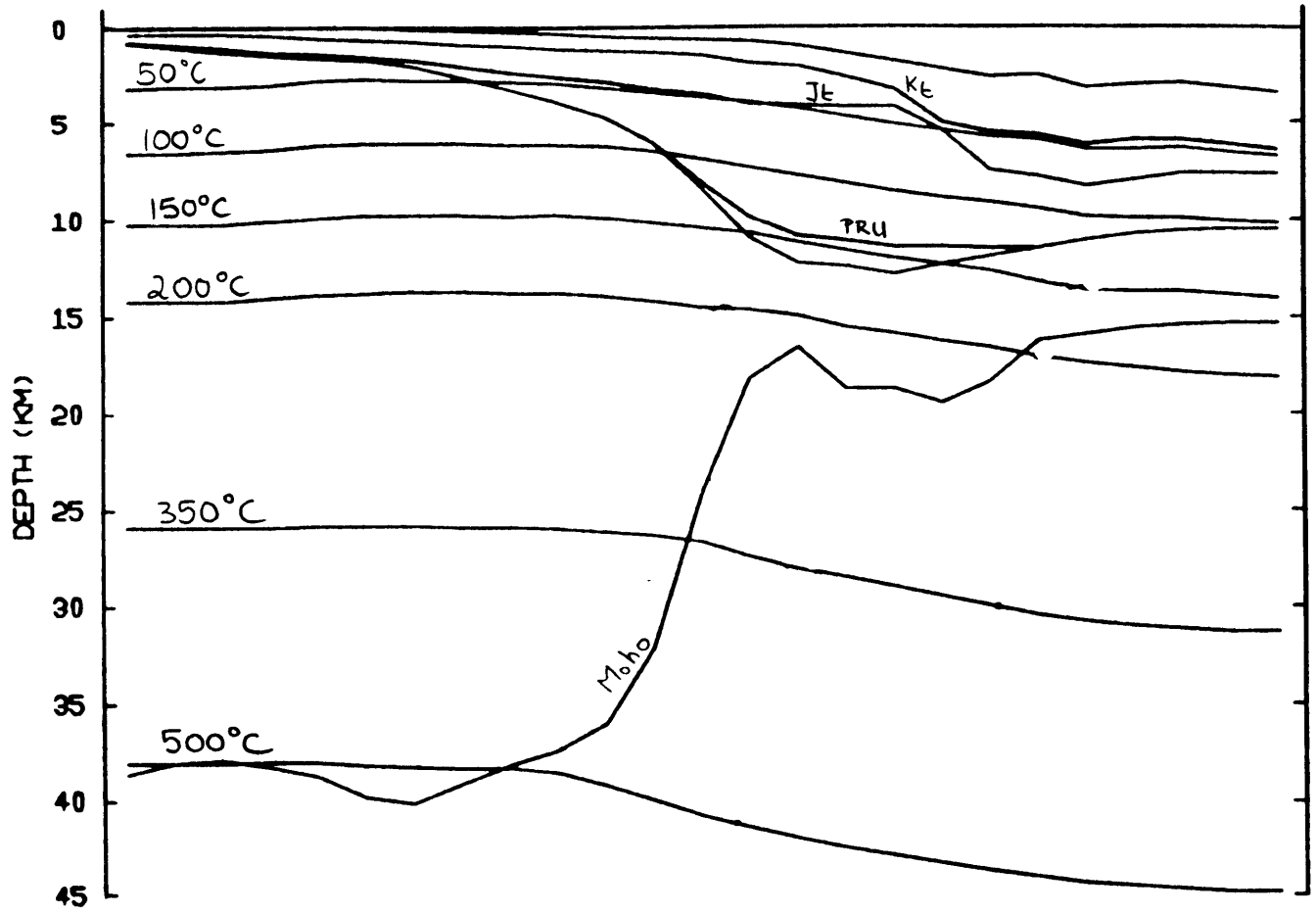
0
5
10
15
20
25
30
35
40
45
DEPTH (KM)
50°C
100°C
150°C
200°C
350°C
500°C
Jt
Kt
TRU
Moho
VE=4.0 X
TIME=175.0MY
CAROLINA TROUGH
KC3.0350.RUN4

Fig. 7.5a

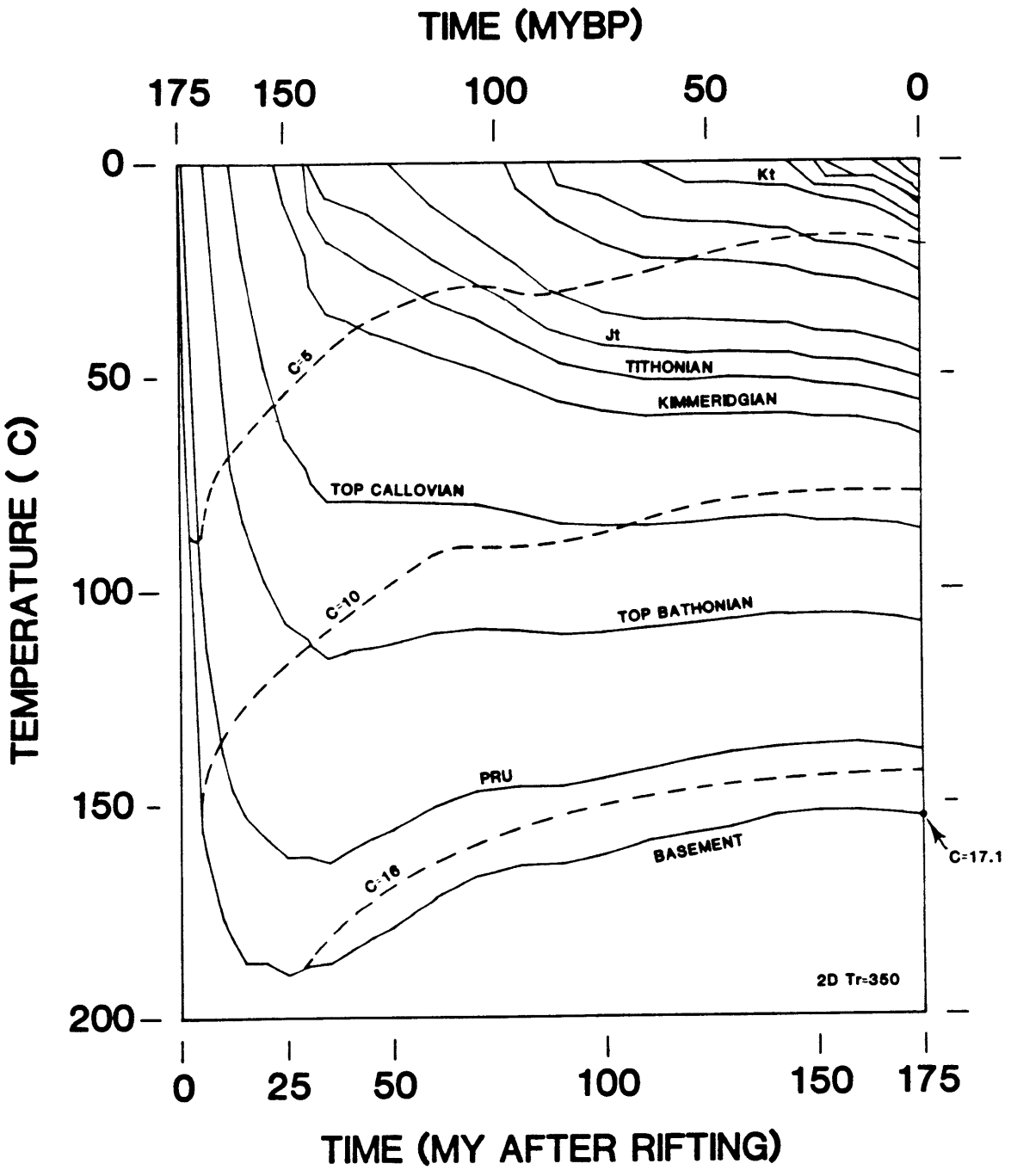
TIME (MYBP)
175
150
100
50
0
0
50
100
150
200
TEMPERATURE (C)
Kt
Jt
TITHONIAN
KIMMERIDGIAN
TOP CALLOVIAN
TOP BATHONIAN
PRU
BASEMENT
C=5
C=10
C=16
C=17.1
2D Tr=350
0
25
50
100
150
175
TIME (MY AFTER RIFTING)

Fig. 7.6

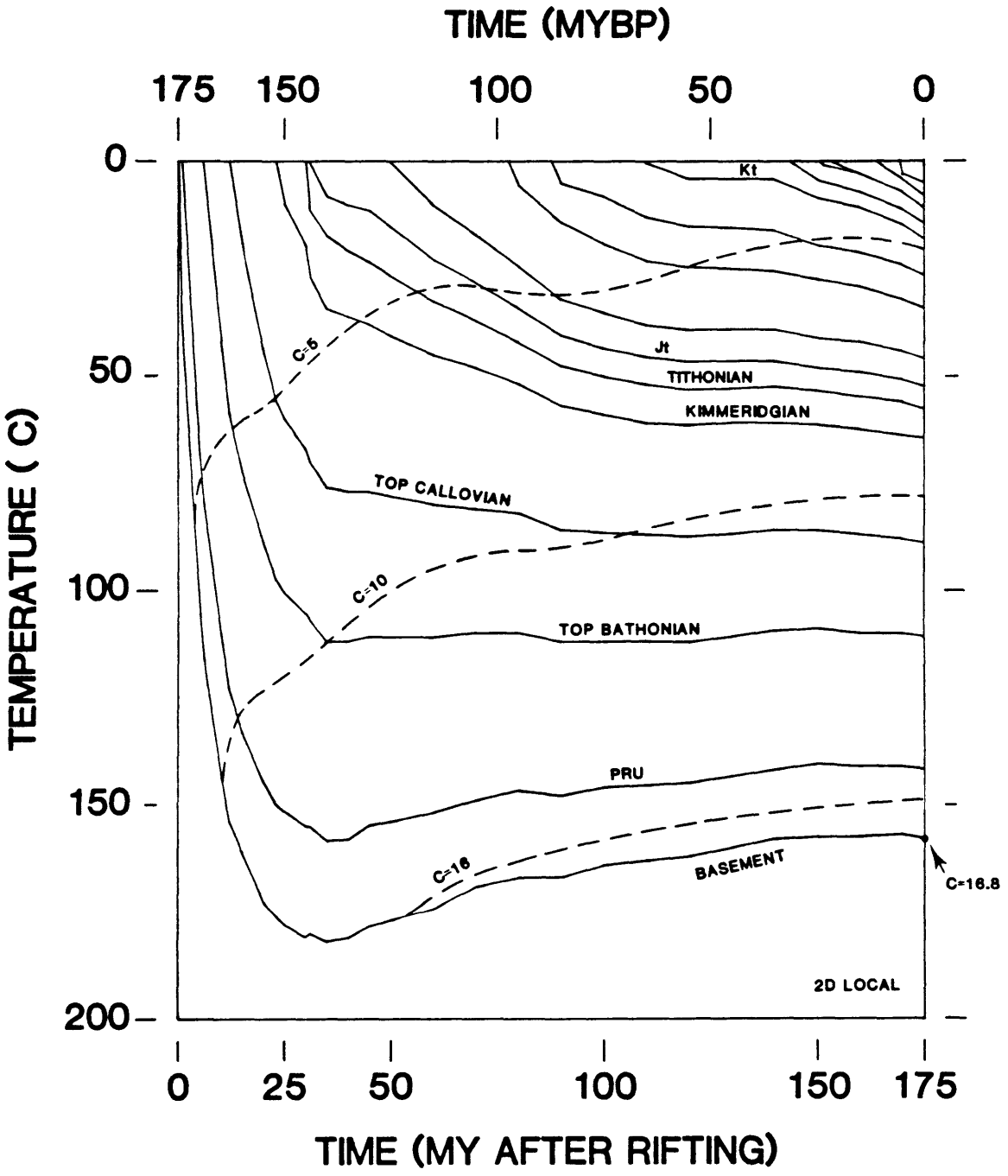
TIME (MYBP)
175
150
100
50
0
0
50
100
150
200
TEMPERATURE (C)
Kt
Jt
TITHONIAN
KIMMERIDGIAN
TOP CALLOVIAN
TOP BATHONIAN
PRU
BASEMENT
C=5
C=10
C=16
C=16.8
2D LOCAL
0
25
50
100
150
175
TIME (MY AFTER RIFTING)

Fig. 7.7

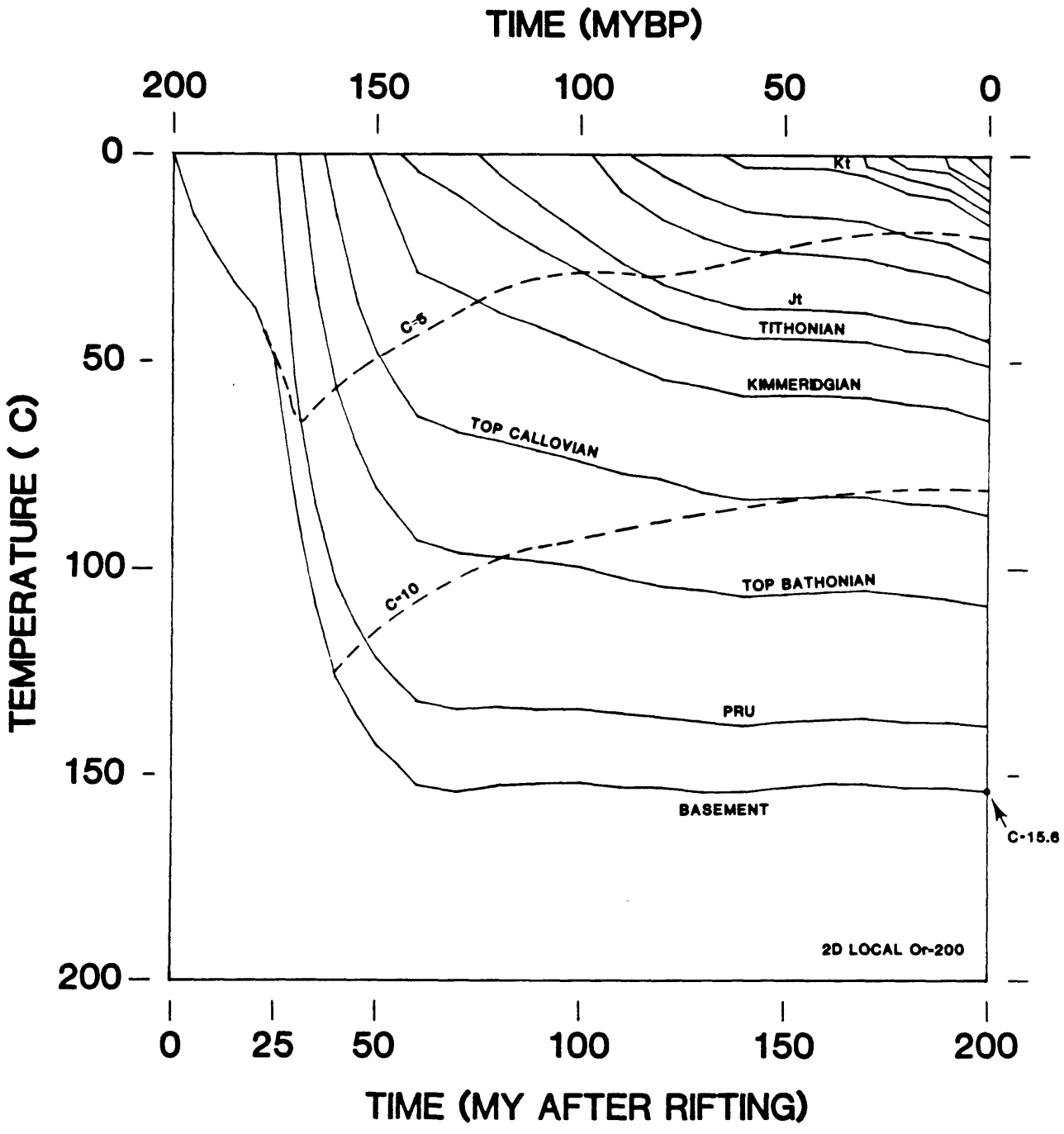
TIME (MYBP)
200
150
100
50
0
0
50
100
150
200
TEMPERATURE (C)
Kt
Jt
TITHONIAN
KIMMERIDGIAN
TOP CALLOVIAN
TOP BATHONIAN
PRU
BASEMENT
C-5
C-10
C-15.6
2D LOCAL Or-200
0
25
50
100
150
200
TIME (MY AFTER RIFTING)

Fig. 7.8

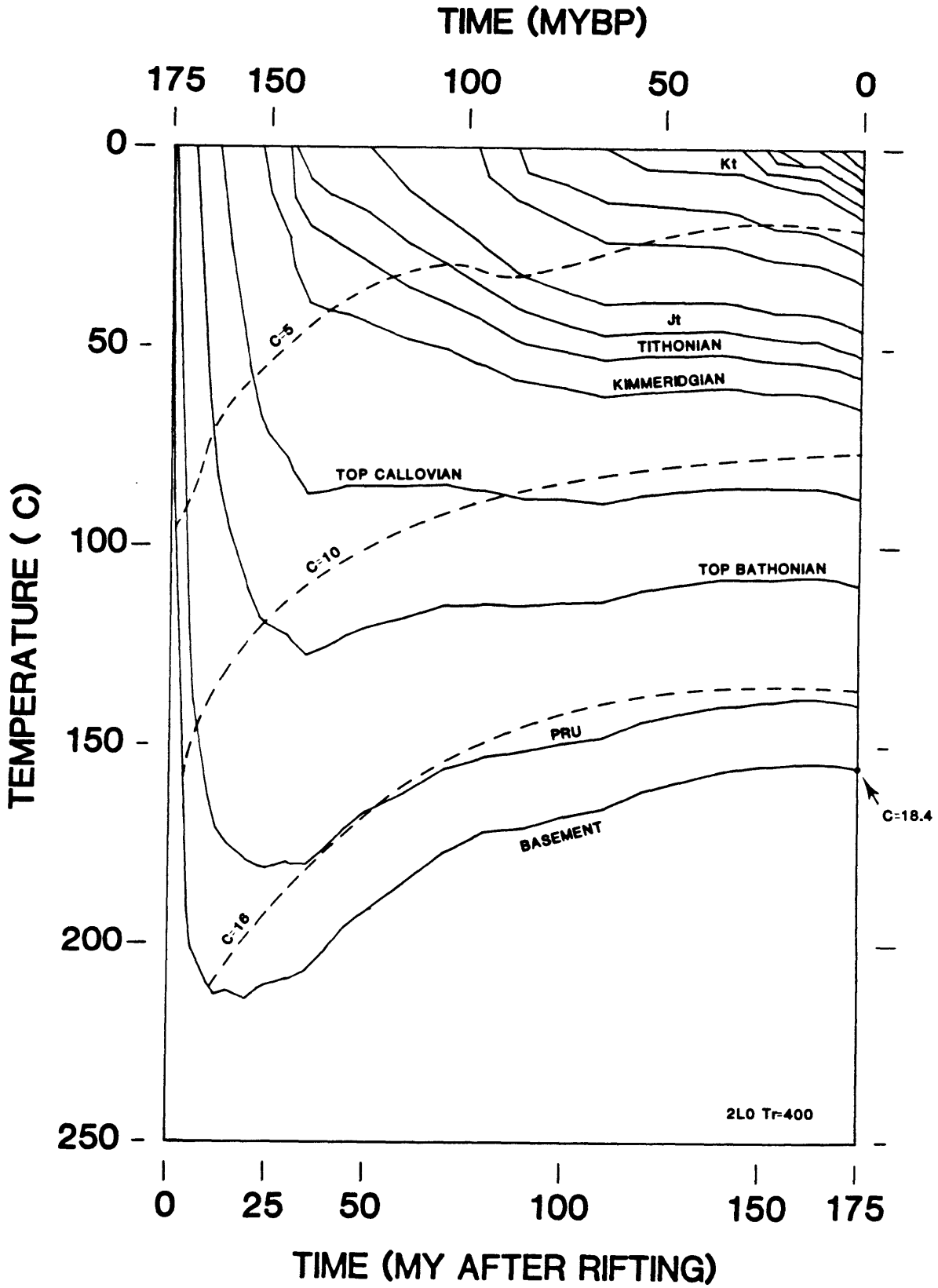
TIME (MYBP)
175
150
100
50
0
TEMPERATURE (C)
0
50
100
150
200
250
Kt
Jt
TITHONIAN
KIMMERIDGIAN
TOP CALLOVIAN
TOP BATHONIAN
PRU
BASEMENT
C=5
C=10
C=16
C=18.4
2L0 Tr=400
0
25
50
100
150
175
TIME (MY AFTER RIFTING)

Fig. 7.9

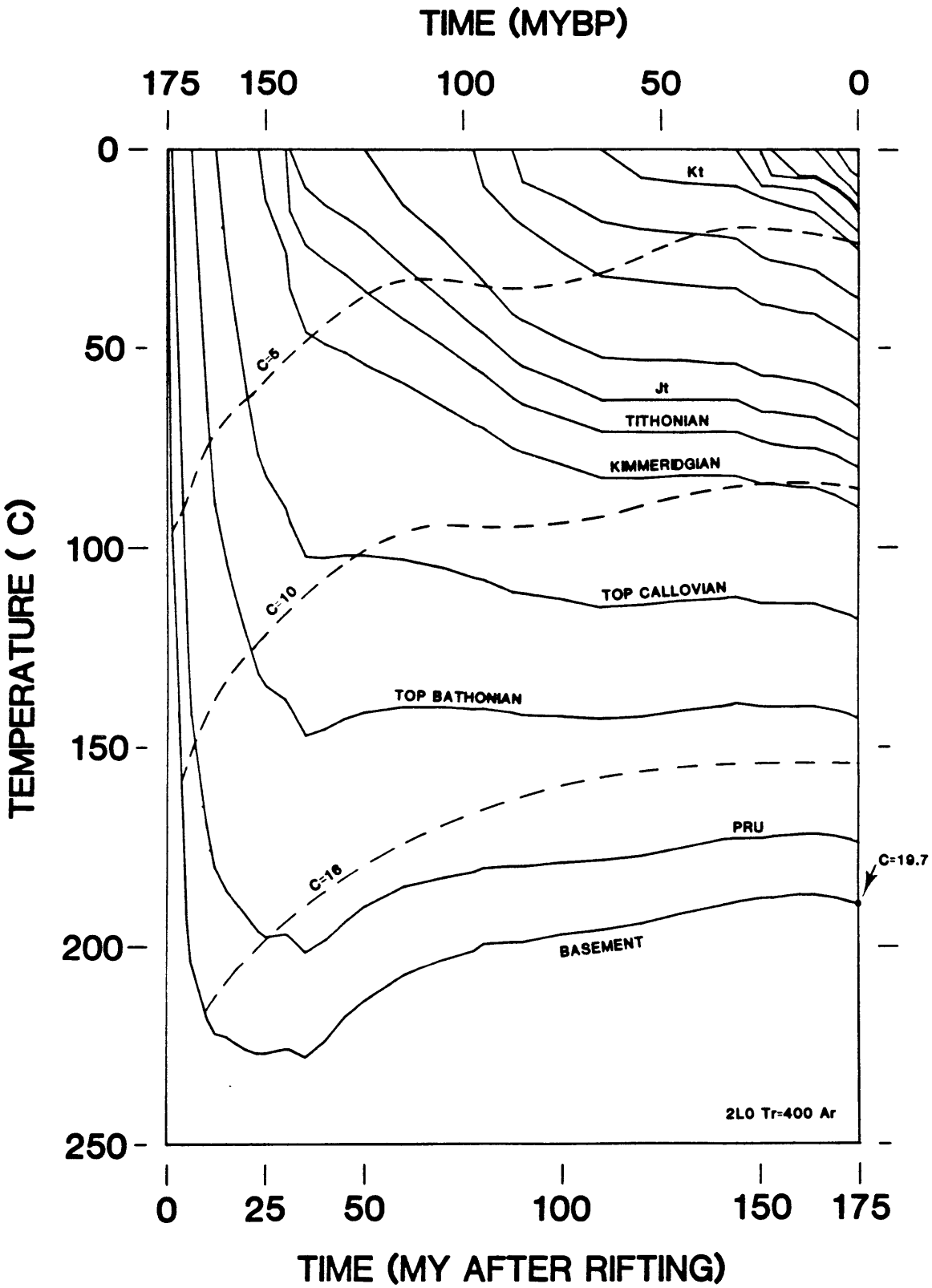
TIME (MYBP)
175
150
100
50
0
0
50
100
150
200
250
TEMPERATURE (C)
Kt
Jt
TITHONIAN
KIMMERIDGIAN
TOP CALLOVIAN
TOP BATHONIAN
PRU
BASEMENT
C=5
C=10
C=16
C=19.7
2L0 Tr=400 Ar
0
25
50
100
150
175
TIME (MY AFTER RIFTING)

Fig. 7.10

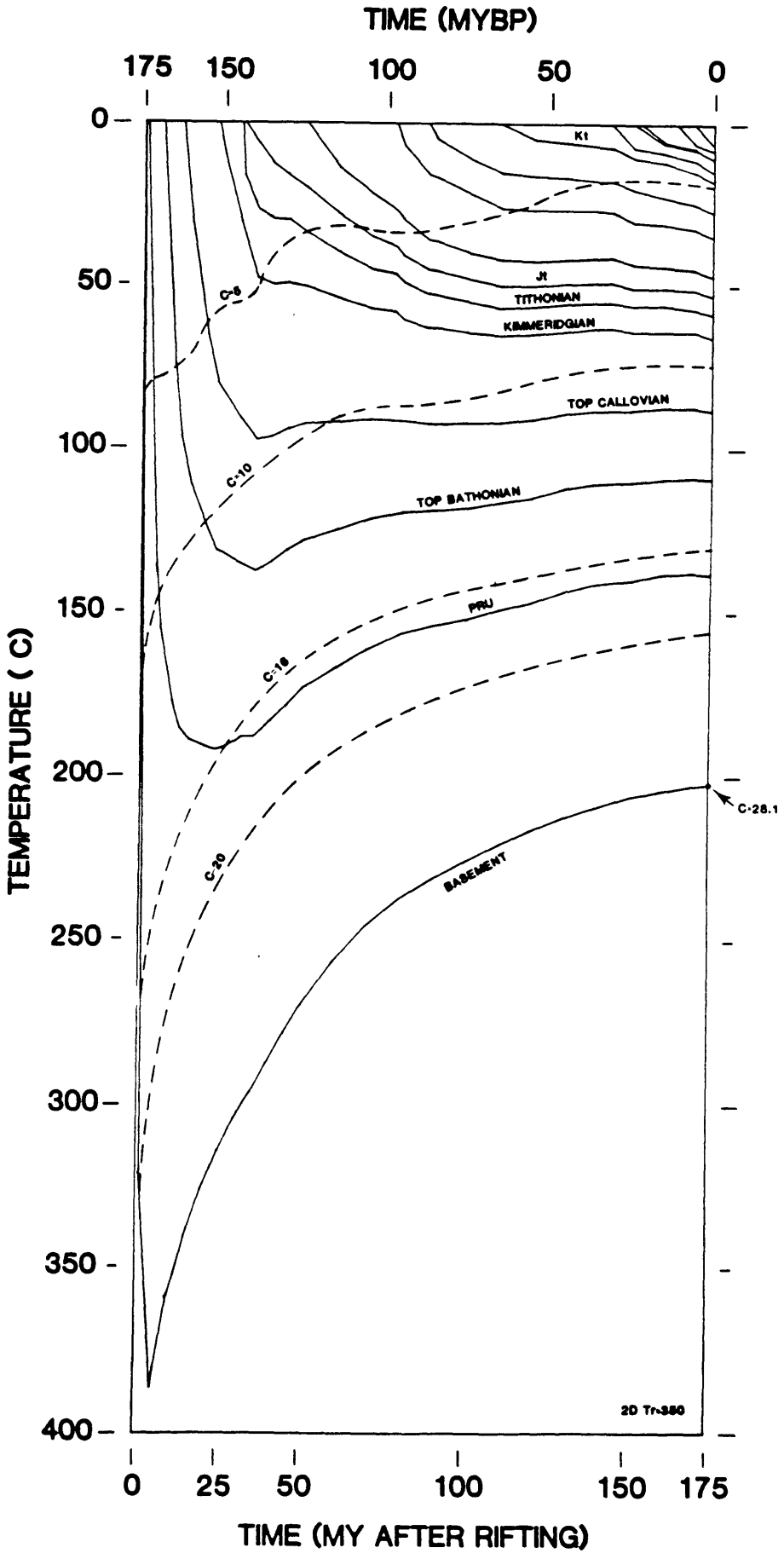
TIME (MYBP)
175
150
100
50
0
0
50
100
150
200
250
300
350
400
TEMPERATURE (C)
K1
Jt
TITHONIAN
KIMMERIDGIAN
TOP CALLOVIAN
TOP BATHONIAN
PRJ
BASEMENT
C-5
C-10
C-15
C-20
C-28.1
2D Tr-350
0
25
50
100
150
175
TIME (MY AFTER RIFTING)

Fig. 7.11

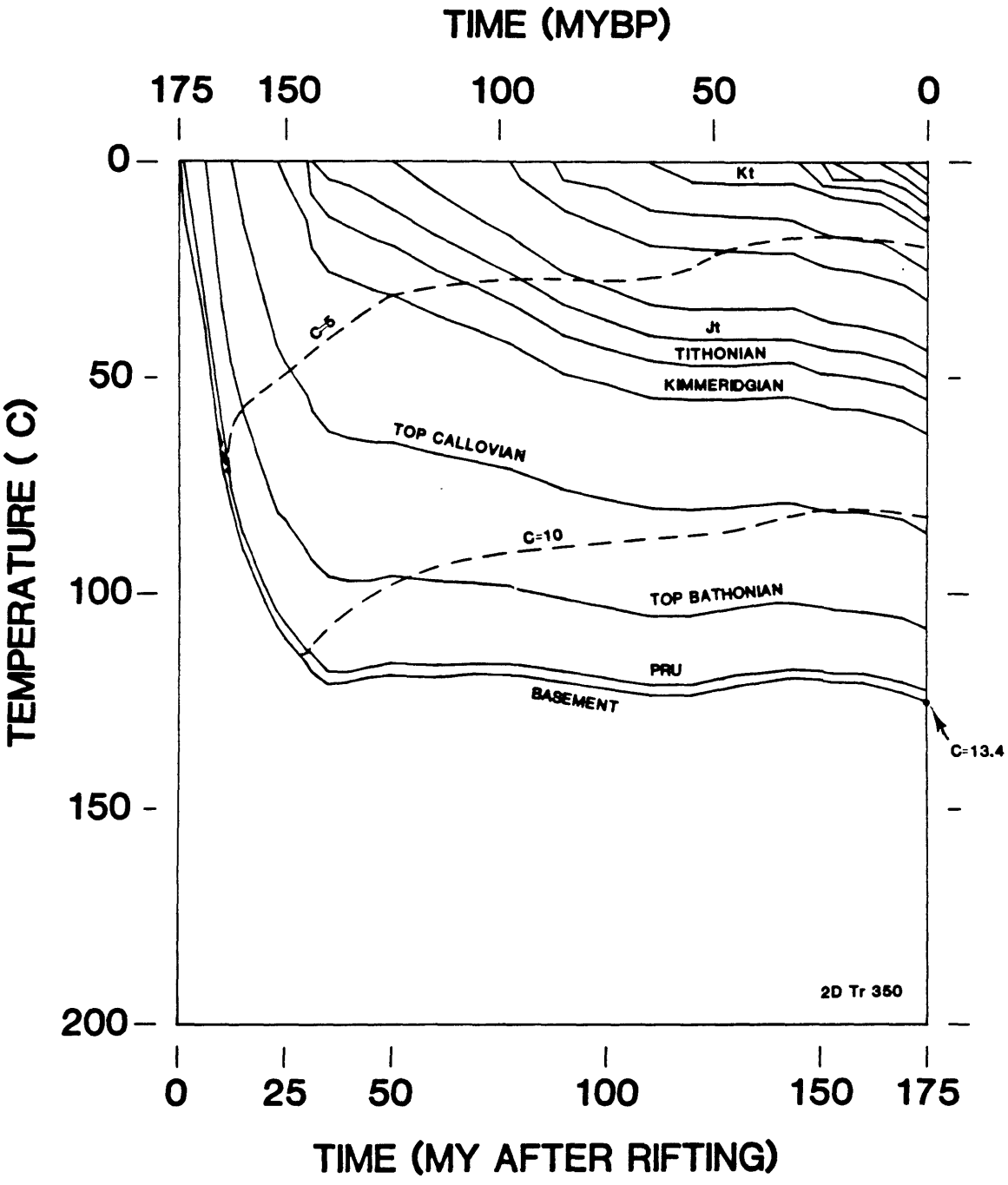
TIME (MYBP)
175
150
100
50
0
0
50
100
150
200
TEMPERATURE (C)
Kt
Jt
TITHONIAN
KIMMERIDGIAN
TOP CALLOVIAN
TOP BATHONIAN
PRU
BASEMENT
C=5
C=10
C=13.4
2D Tr 350
0
25
50
100
150
175
TIME (MY AFTER RIFTING)

Fig. 7.12

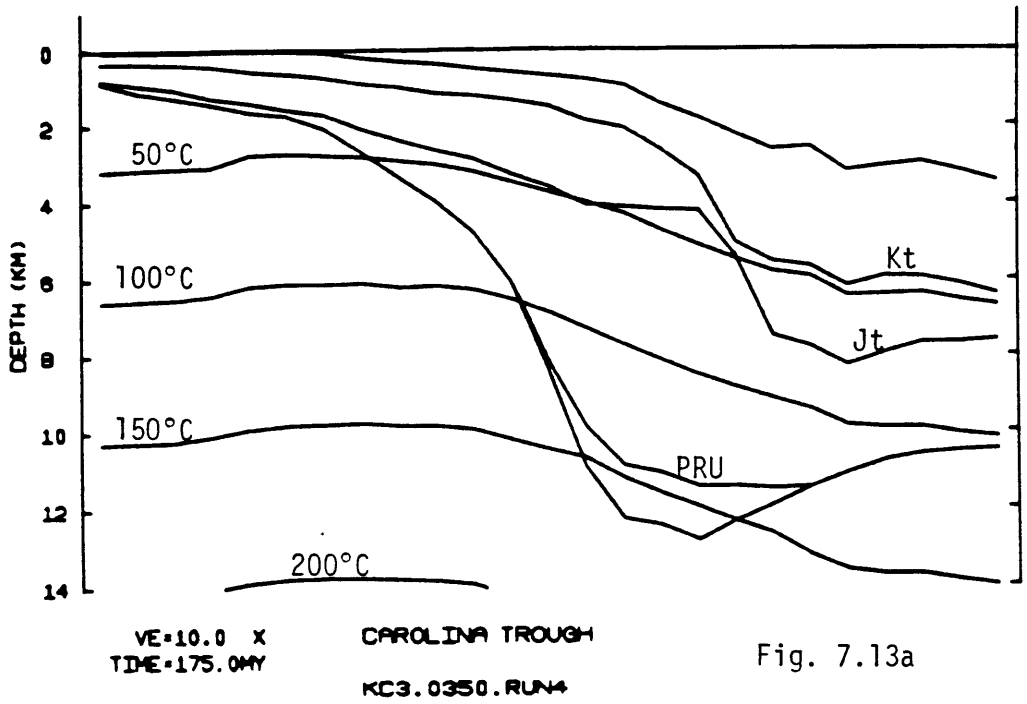

Fig. 7.13a

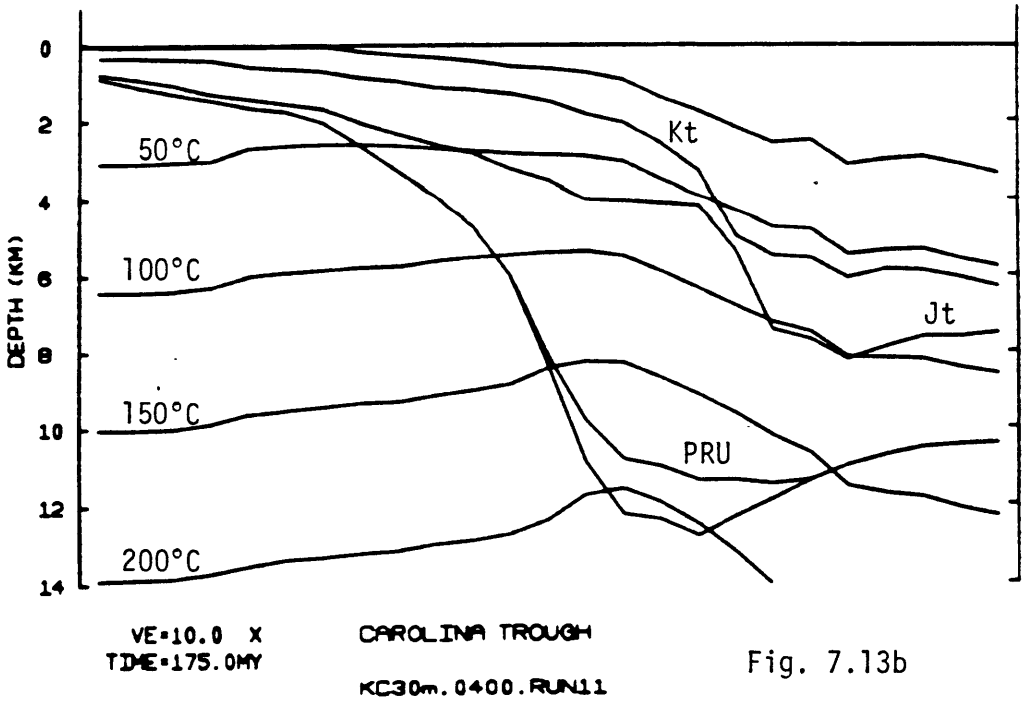

Fig. 7.13b

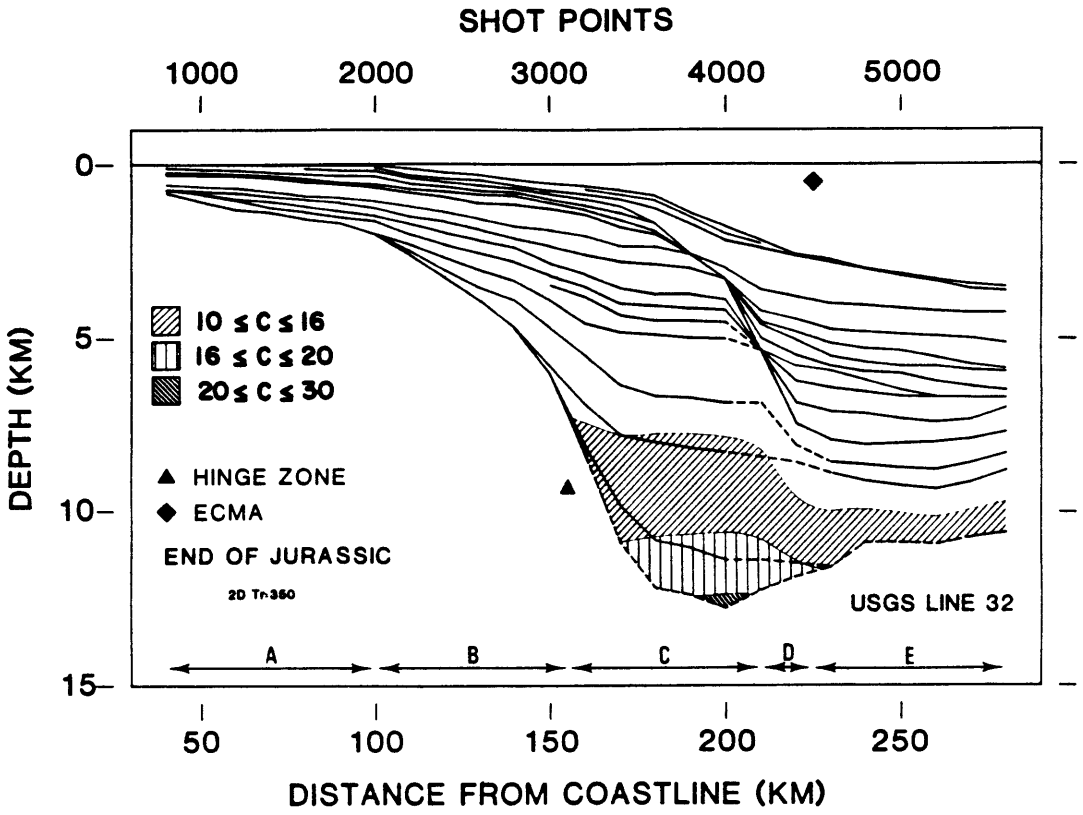

Fig. 7.14a

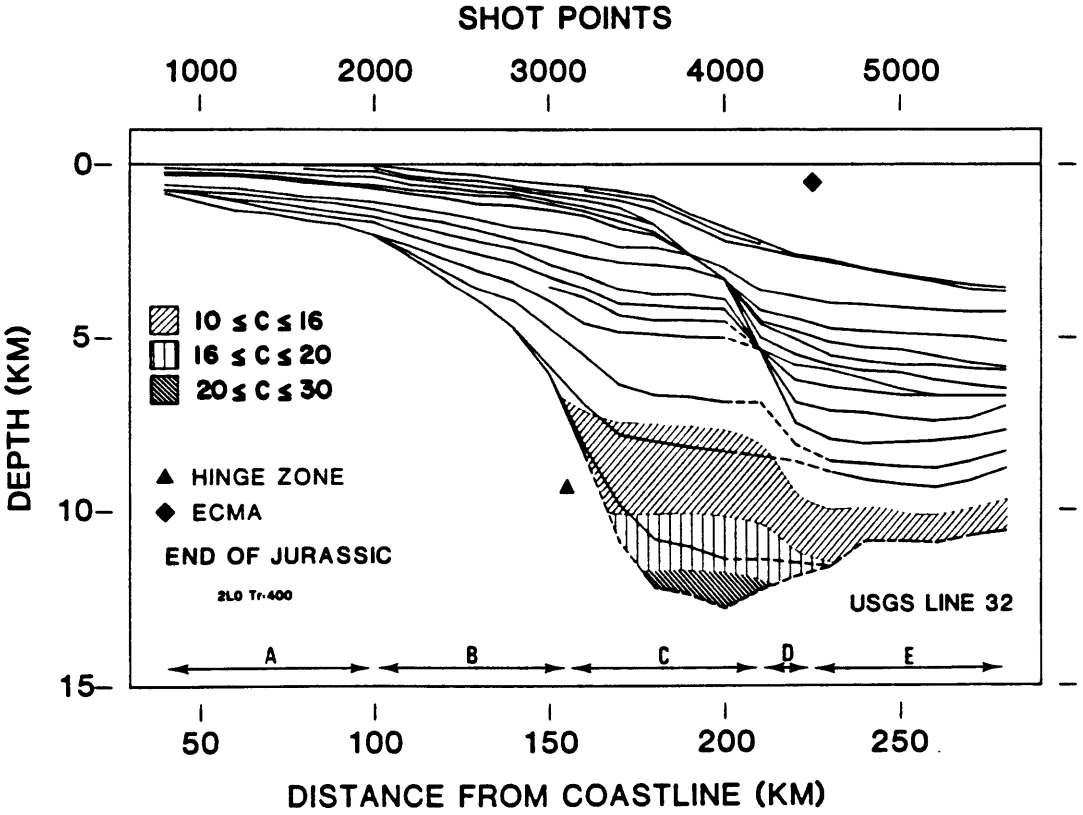

Fig. 7.14b

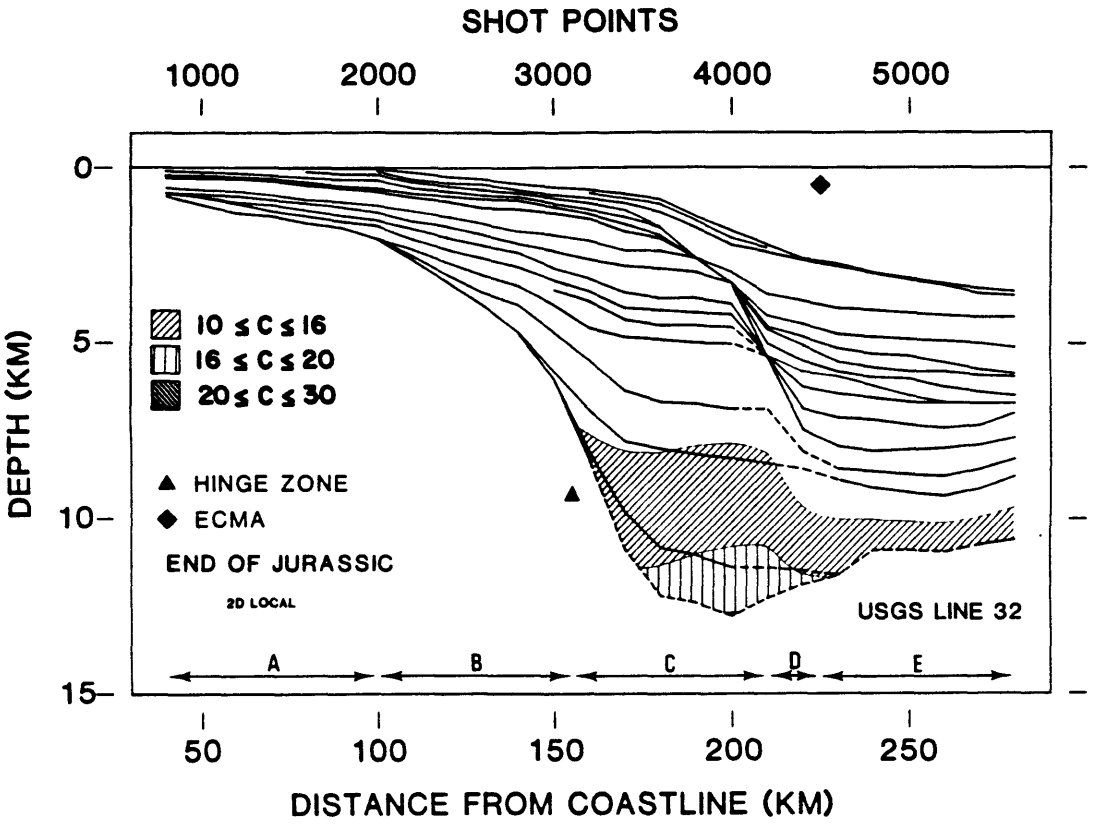

Fig. 7.14c

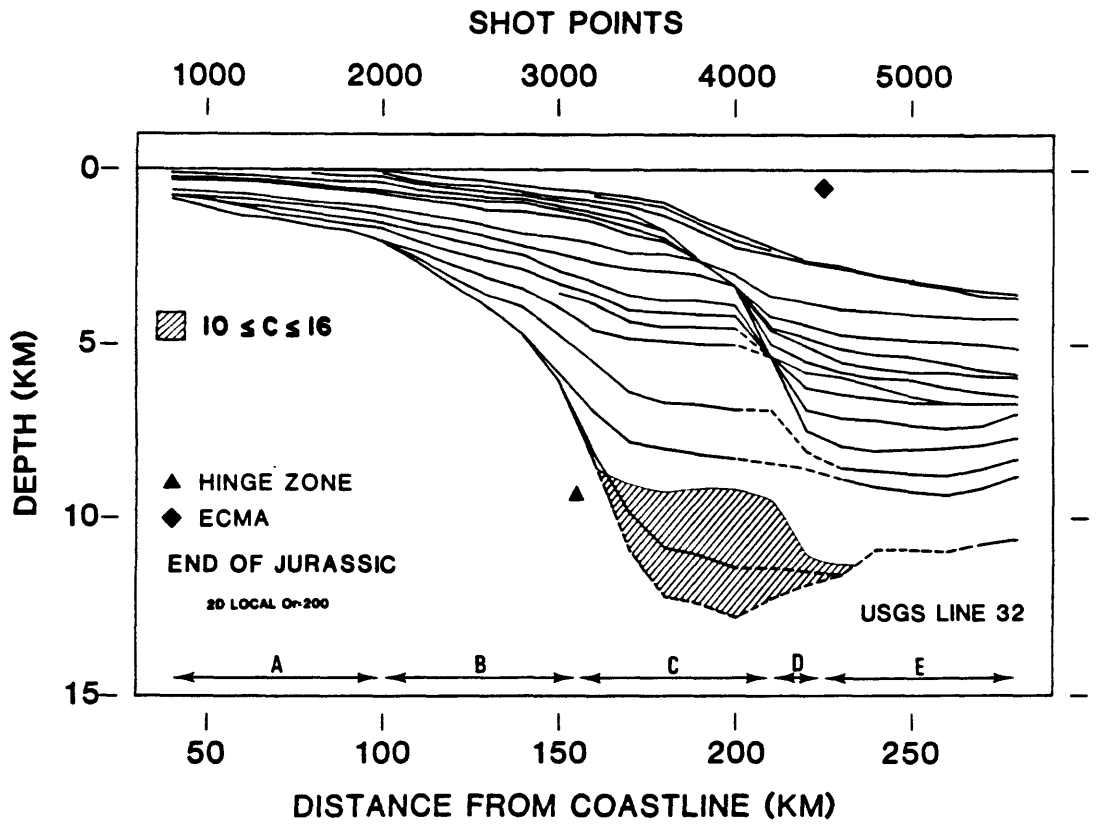

Fig.7.14d

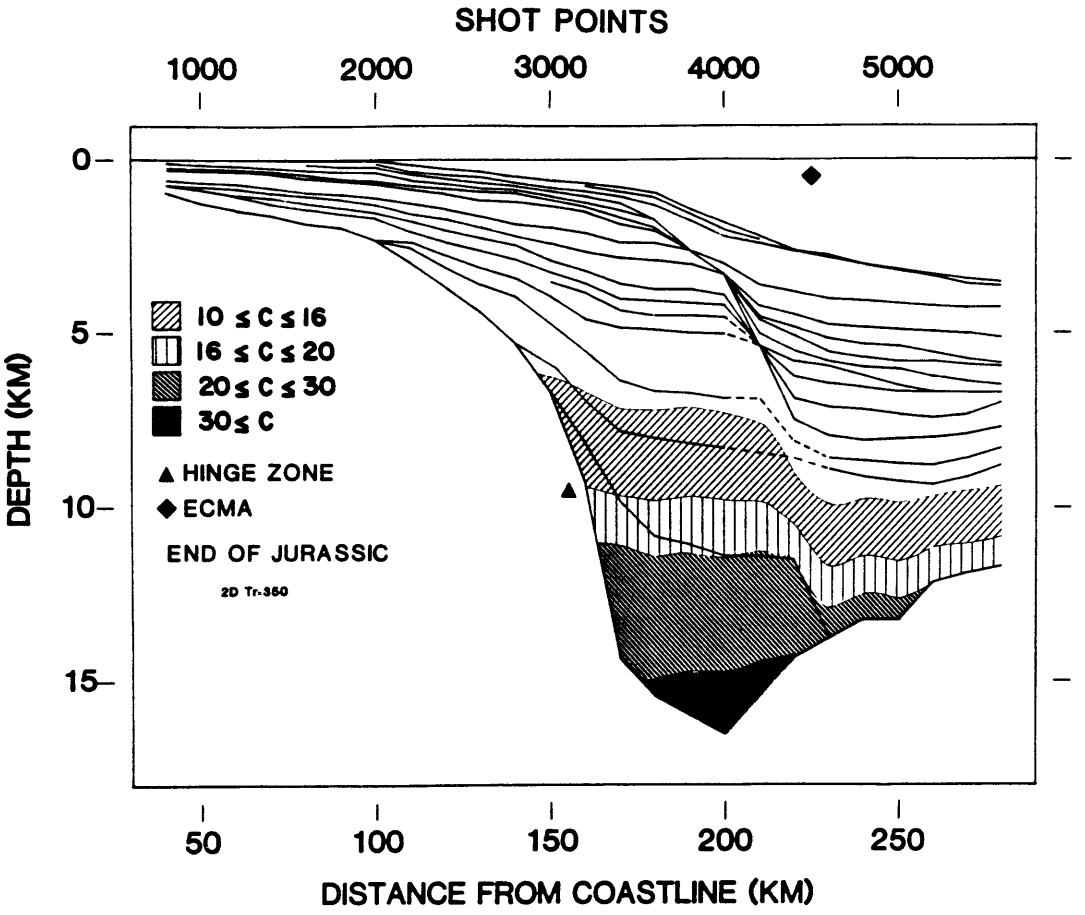

Fig. 7.14e

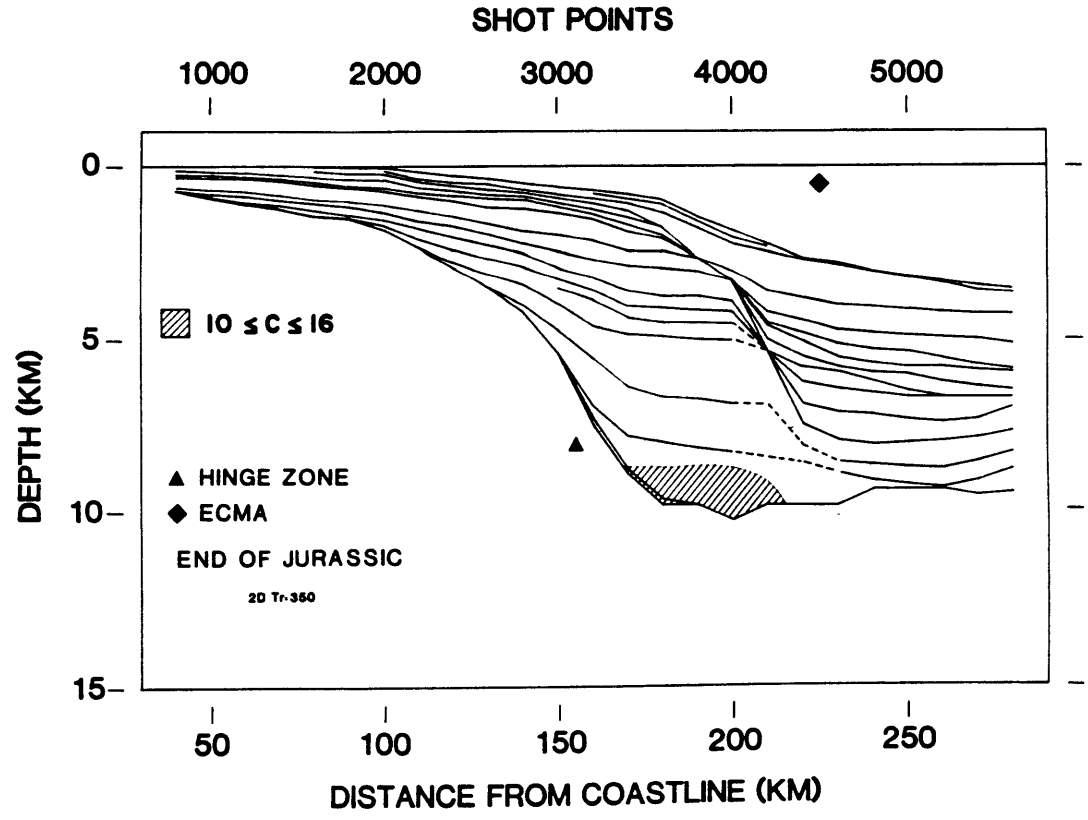

Fig. 7.14f

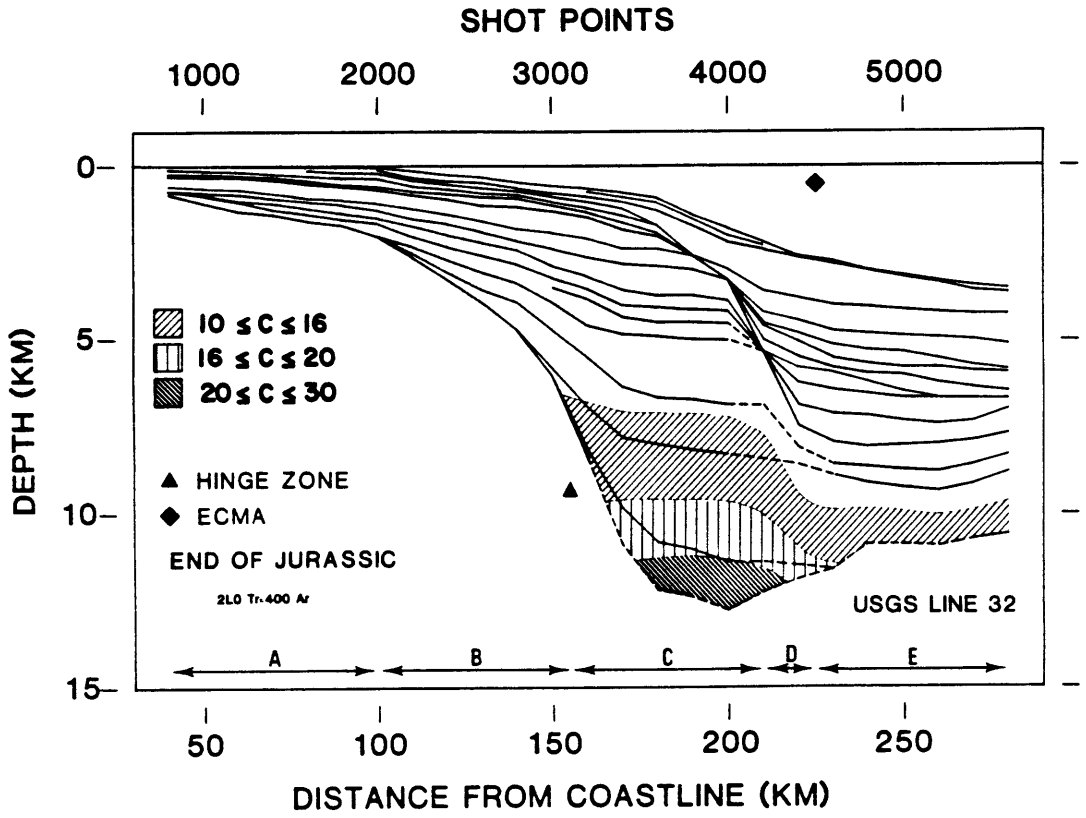
SHOT POINTS
1000
2000
3000
4000
5000
0
5
10
15
DEPTH (KM)
10 ≤ C ≤ 16
16 ≤ C ≤ 20
20 ≤ C ≤ 30
▲ HINGE ZONE
◆ ECMA
END OF JURASSIC
2L0 Tr-400 Ar
USGS LINE 32
A
B
C
D
E
50
100
150
200
250
DISTANCE FROM COASTLINE (KM)

Fig. 7.14g

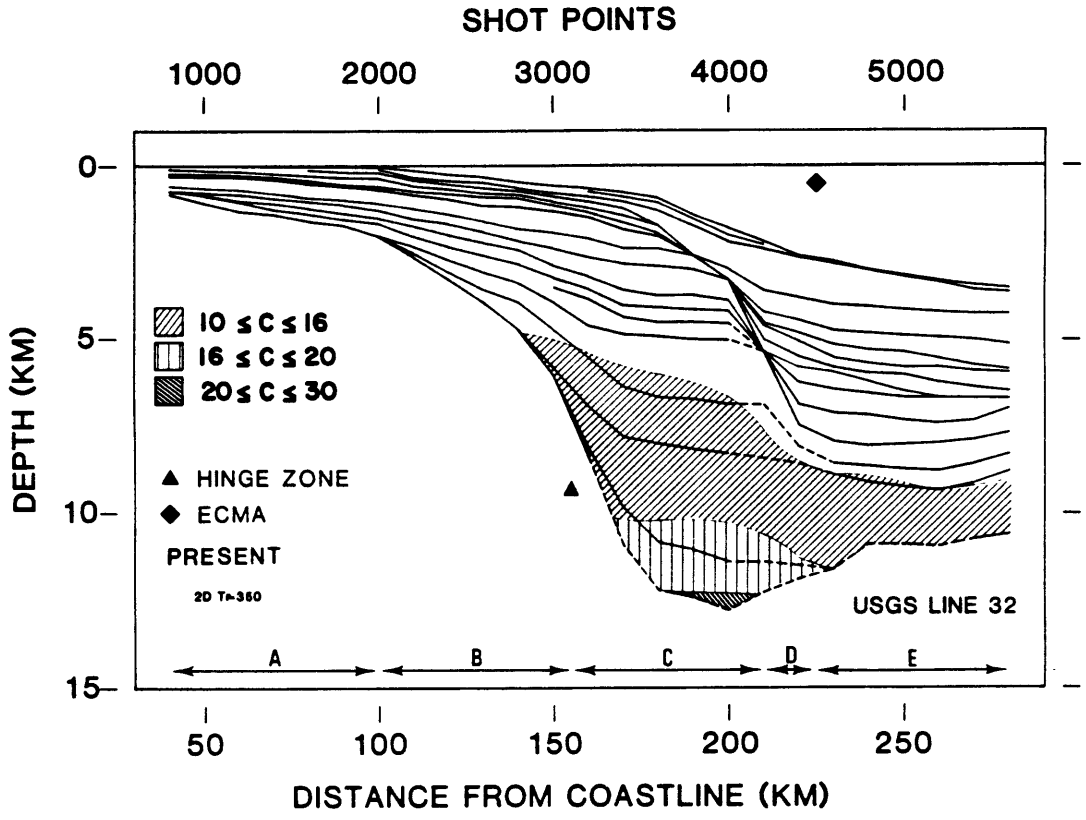

Fig. 7.15a

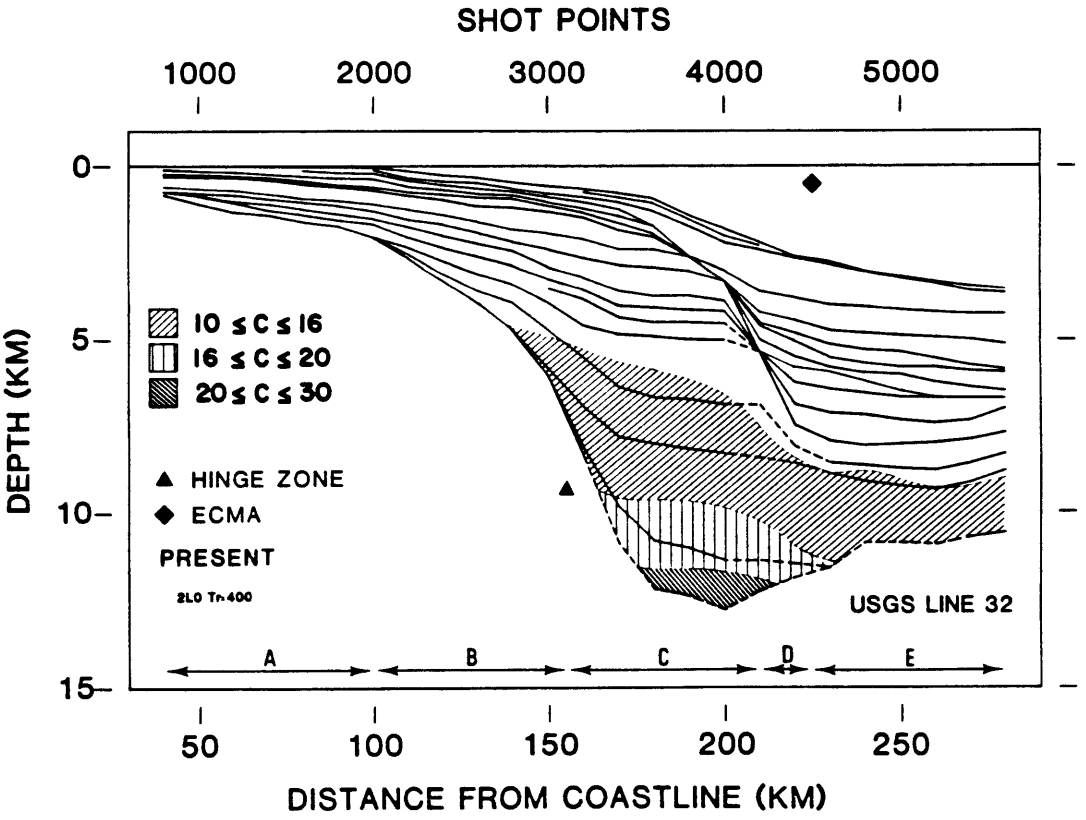

Fig. 7.15b

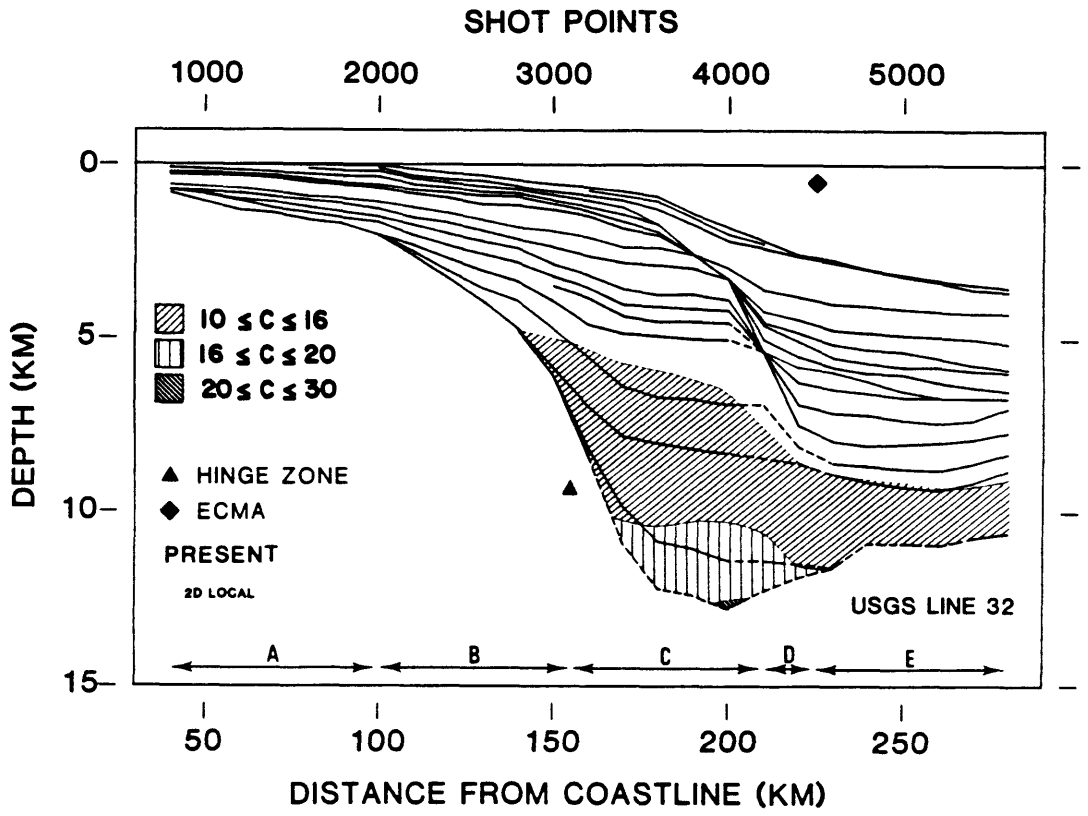

Fig. 7.15c

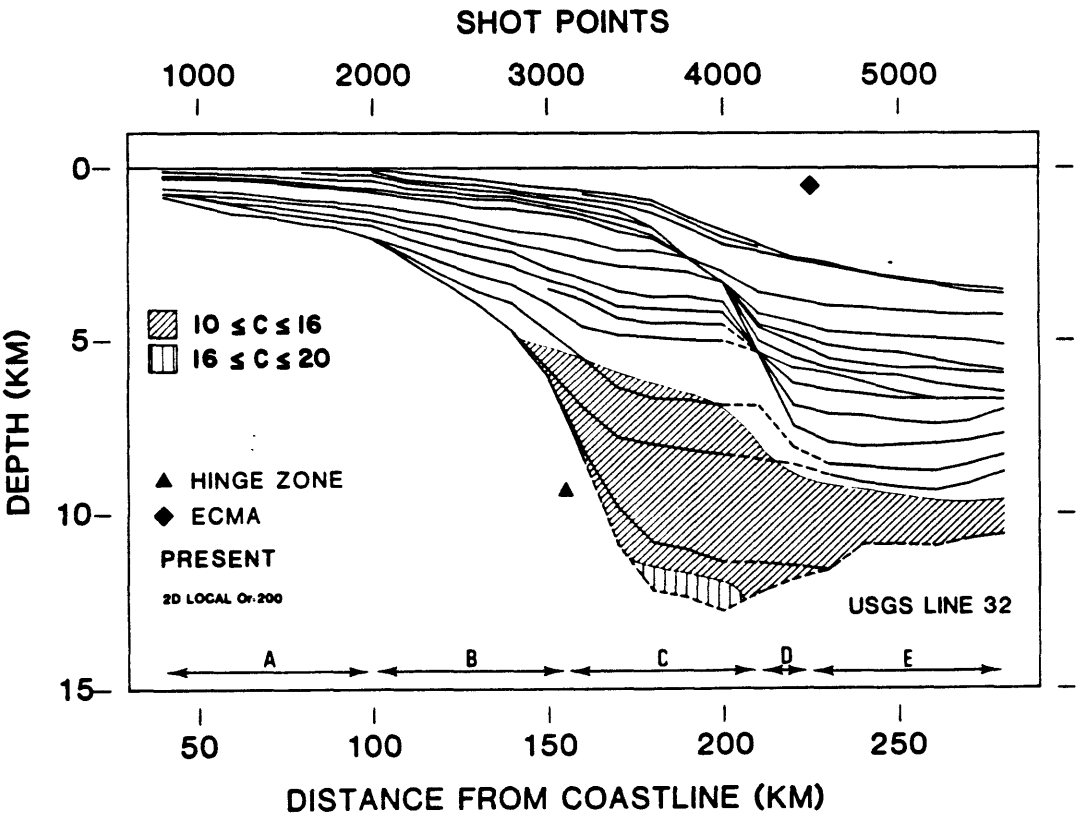

Fig. 7.15d

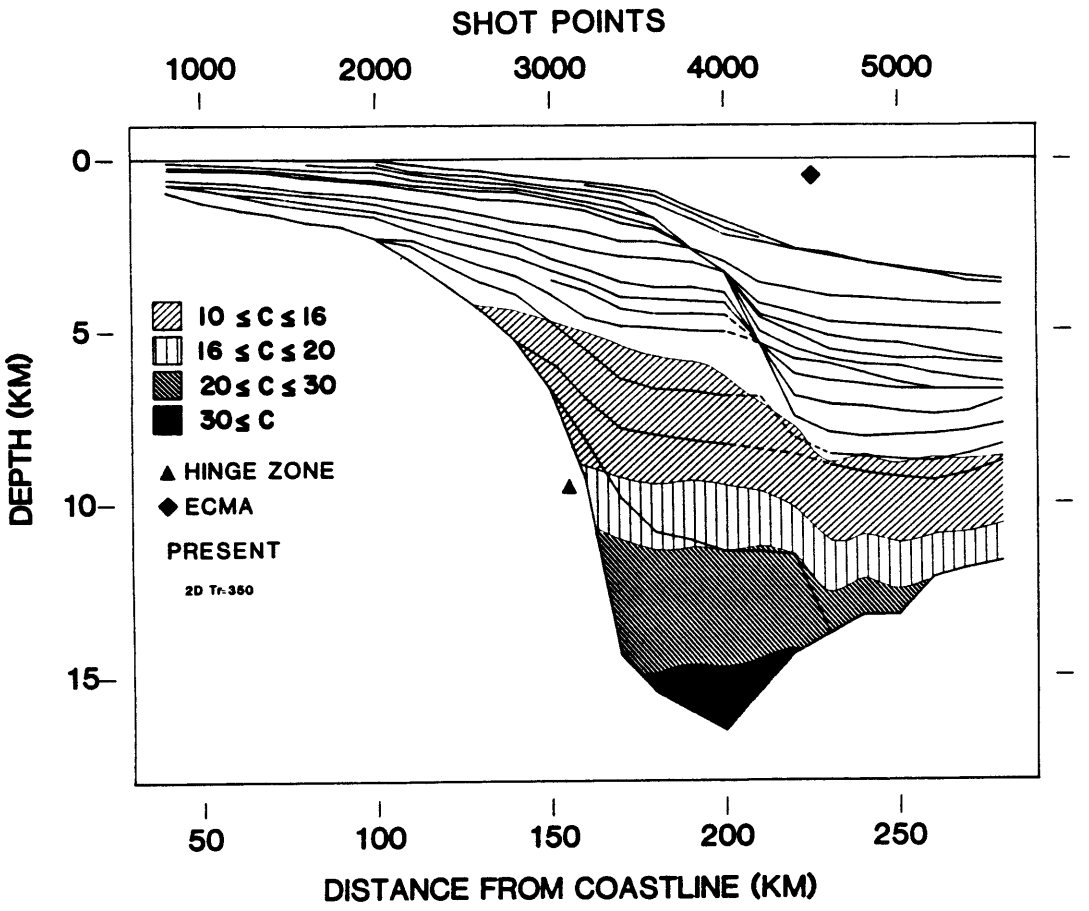

Fig. 7.15e

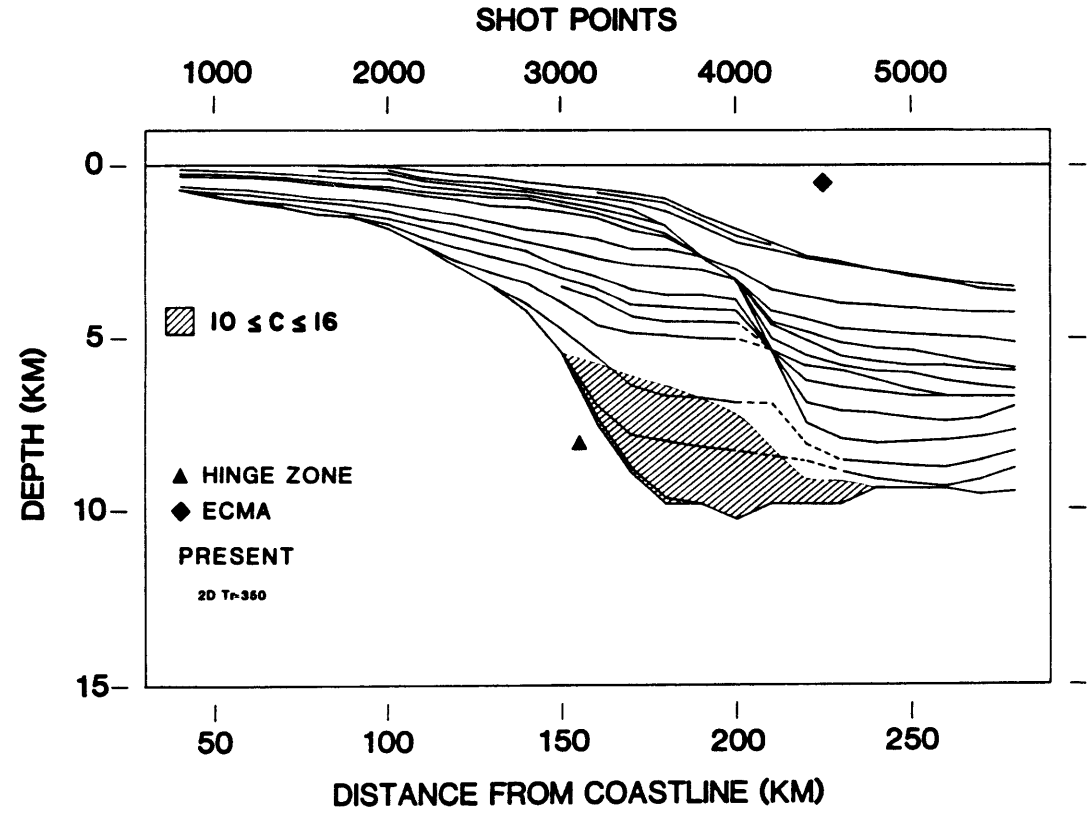

Fig. 7.15f

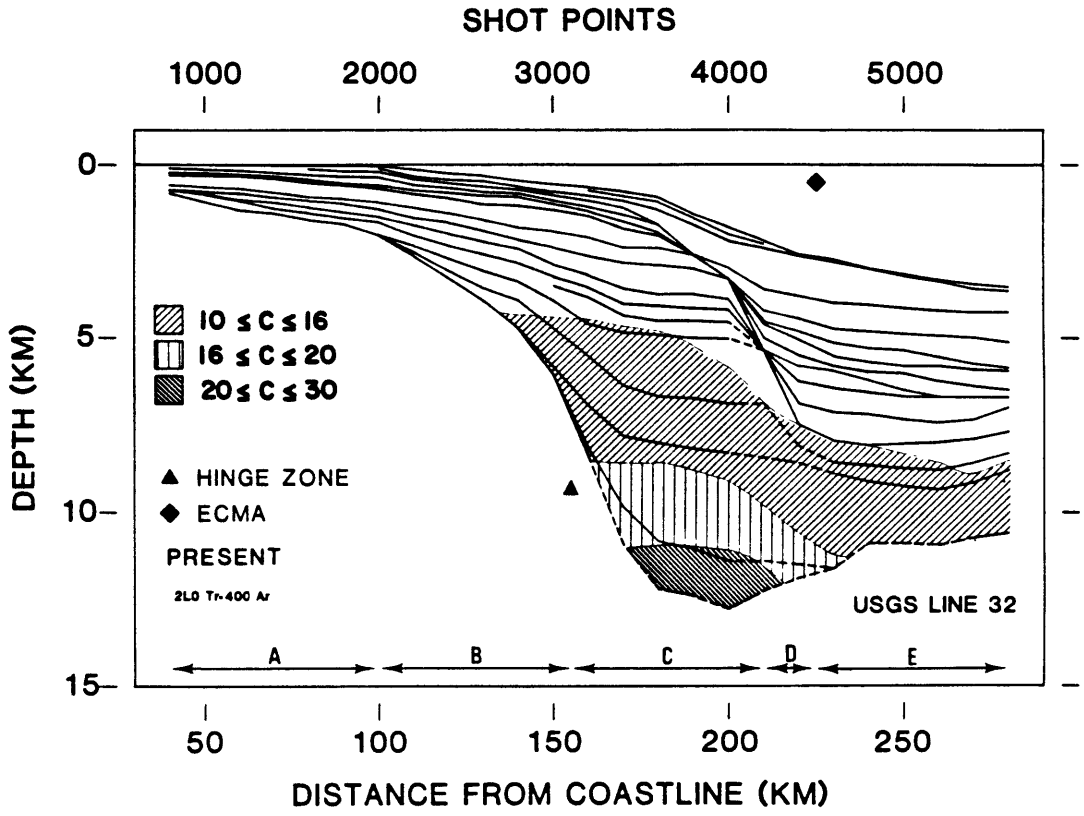
SHOT POINTS
1000
2000
3000
4000
5000
0
5
10
15
DEPTH (KM)
10 ≤ C ≤ 16
16 ≤ C ≤ 20
20 ≤ C ≤ 30
HINGE ZONE
ECMA
PRESENT
USGS LINE 32
A
B
C
D
E
50
100
150
200
250
DISTANCE FROM COASTLINE (KM)

Fig. 7.15g

CHAPTER VIII

CONCLUSIONS

We are not certain, we are never certain.
if we were we could reach some conclusion, and
we could, at last, make others take us seriously

A. Camus, La Chute

8.1 GENERAL CONCLUSIONS

As far as modeling is concerned, applying different models to the same basin has taught us that as the model becomes more sophisticated, and hopefully closer to reality, it also becomes more dynamic. By that we mean that an assumption on one part of the model affects another part of it. For instance, abandoning local isostasy for flexural compensation couples the loading response with the thermal state predicted by the extension model. Likewise, two dimensionality in the loading response as well as in heat propagation, couples the evolution in one location with the one in neighboring locations. If this results in a more realistic approach, the price paid is that through such a dynamic system, error in one model assumption or in data at one location will propagate through the whole system. Conversely decoupling all the elements of the modeling will contain errors and help sort out different effects which remain separated, but the price paid is realism: as we saw, a local estimate of subcrustal extension (or of local amount of initial heat) for instance, doesn't seem to have much significance, unless it is derived from direct thermal measurement, but then again one of the properties of thermal measurement is that they do integrate a lot of regional factors.

As far as the data are concerned, the Carolina trough represents rather typically the characteristics of an old and deeply filled basin. Because it is old, the rifting heat has disappeared and therefore has to be very indirectly estimated by early paleogeographic considerations. Because it contains a thick sedimentary sequence, the basement depth and the oldest sediment are not well known, and the loading response assumptions bear heavily on the tectonic models. In addition to these sources of uncertainties the absence of any deep well within this particular basin adds uncertainties in the sediment properties.

The rifting mechanism can be represented by two functions: the amount of crustal and subcrustal extension along strike. The amount of crustal extension, which is sensitive to loading response assumption and basement depth and sediment properties uncertainties, is poorly constrained in the deepest part of the basin while the amount of subcrustal extension, which depends on the paleogeography of the not well known oldest sediments, is also poorly constrained on most of the basin. As a result the range of rifting conditions cannot be narrowly defined.

In terms of subsidence, the question arises of what level accuracy is required. If one is satisfied with predictions accurate to within 1 km, the one dimensional uniform extension model seems largely sufficient. However if one wants accuracy within, say, 300m, many factors have to be better constrained: loading response mechanism, initial heat input, basement depth, sediment properties, origin time of thermal decay and amounts of erosions. As a rule the degree of complexity seems to grow exponentially with increasing accuracy. Because the largest uncertainties are in the early predictions, constraints on the early conditions would be the most effective, and the best way of testing the validity of models, such as those we presented, is to concentrate on these early predictions, which when controlling data are available, raise most problems (Royden et al., 1983).

In terms of thermal evolution, it appears useful to distinguish between early history (less than 30 MY after rifting) which is dominated by the transient geotherm associated with rifting mechanism and late history (more than 60 MY after rifting) which is dominated by the equilibrium geotherm. Because in an old and thick basin, the rifting mechanism is not very well constrained, the early thermal history shows a large uncertainty range. However one can expect a better control on it in a young basin where heat flow data should provide a strong constraint. The cause of uncertainties on the late history seems easier to constrain through well temperature, heat flow and sediment radioactivity data.

In terms of sediment thermal evolution and degree of maturation it appears important to distinguish the early sediments from the late sediments. The early sediments are those which were not only deposited but also sufficiently buried during the early thermal history so as to be affected by it. The late sediments, were not sufficiently buried before most of the heat related to rifting had disappeared and which consequently are essentially affected by the equilibrium geotherm. On one hand, in an old thick basin the early sediment thermal evolution seems sensitive to errors in the rifting mechanism. However in such a basin, these sediments are most likely to have reached a high degree of maturation anyway and the uncertainty concerns how overmature they could be. In a young basin, the evaluation of the rifting mechanism would be more critical, but heat flow data should provide a good contraint on it. On the other hand, the thermal evolution of late sediment, which concerns only old basins, is more easily evaluated by well data and easily extrapolated backward in time: this is at least one point on which old basins are simpler than young ones because steady state conditions are more easily constrained than transient ones. However, we notice that in the Carolina trough it is only the oldest late sediments which have had a chance to have reached oil maturity.

8.2 SPECIFIC CONCLUSIONS

Local isostasy appears incompatible with gravity data and predicts unrealistic early stratigraphy. Introducing a flexural response to the sedimentary load solves these two problems reasonably.

The inferred small water depth landward of the hinge zone during the Jurassic cannot be accounted for by uniform extension with local isostasy or with flexural response. However introducing extra initial subcrustal heat corrects that problem.

It therefore appears that the two major modifications required to the simple one dimensional uniform extension model are flexural response and non uniform extension. The effect of lateral heat flow and thermal blanketing by the sediments, though significant, are less important, especially once the data uncertainties are considered.

These conclusions are compatible with the ones reached in a similar study on the Nova Scotian margin which did not consider the effect of data uncertainties (Beaumont et al., 1982).

8.3 TECHNIQUES

The one dimensional model is attractive because it allows to get first order predictions and to set up the parameter at very small computational cost. It also is the easiest to constrain and allows to separate easily the different components of a prediction. It then seems a good candidate for a first appraisal of a basin where little is known. However it is unlikely to fully account for the data.

The two dimensional model accounts better for the data but at a high computational cost. Considering that the main source of improvement is the introduction of flexural response, it seems that a good compromise would be a one dimensional model for the thermal calculation coupled with flexural response for the load. Such an intermediate model would probably be satisfactory for an old basin where the data uncertainties are as large as or larger than in the Carolina trough. Neglecting lateral heat flow would alter the early predictions only and allow to use analytical formula at very small computational cost. The effect of thermal blanketing could be included in a next step. However if one either studies a young basin where lateral heat flow is still intense or is interested in accurate early thermal prediction across a hinge zone or concentrate in a basin where high quality data are available, a full two dimensional model is likely to yield more realistic predictions.

In any of the three modeling techniques proposed above, non uniform extension appears as a simple alteration of the initial conditions, therefore as an easy modification. However one has to note that the extra degree of freedom brought by subcrustal extension requires extra constraint. This extra constraint can easily be heat flow data in a young basin, but in an old basin there will be little independent check on the postulated extra heat.

8.4 FURTHER WORK

Two types of questions may be asked. First, how valid are the extensional models and should they be further modified? Second, how could the evolution of the Carolina trough be more narrowly defined?

The answer to the first type of question should not be sought in old and thick sedimentary basins for three reasons. First, the constraints on the models are not sufficient. Second, the thermal event has disappeared. Third, the loading response model, which is not well known, propagates its own errors into the tectonic model. It would seem more appropriate to concentrate on young basins where the initial heat has not yet disappeared or on active rifts where most model assumptions about initial conditions are observable.

To learn further about the Carolina trough evolution seems to require data collections because, at present, the uncertainty range remains too large to benefit from further modeling. Basement depth, sediment physical properties, Moho depth, timing of onlaps, paleowaterdepths, erosion amounts, present geotherm, are the most needed information. To widen the cross section that we modeled by completing it with onshore information would also help sort out the effects of flexure and sea level change, since they can be expected to have clearer consequences there. Finally, modeling the conjugate margin, the Senegal basin, may help in better defining the rifting mechanism which these two basins have in common. Since our attempt to do this was hampered by the lack of deep stratigraphy, acquiring seismic data which reach basement may be a needed first step.

References

Anderson, R.N., D. McKenzie and J.G. Sclater, Gravity, bathymetry and convection in the Earth, Earth and Planet. Sci. Lett., 18, 391-407, 1973.

Angelier, J., Analyse quantitative des relations entre deformation horizontale et mouvemant verticaux: l'extension egeenne, la subsidence de la mer de Crete et la surrection de l'arc hellenique, Annales de Geophysique, t. 37, fasc. 2, 327-345, 1981.

Artemjev, M.E., and E.V. Artyushkov, Structure and isostasy of the Baikal rift and the mechanism of rifting, J. Geophys. Res, 76, 1197-1211, 1971.

Artyushkov, E.V., Stresses in the lithosphere caused by crustal thickness inhomogeneities, J. Geophys. Res., 78, 7675-7708, 1973.

Artyushkov, E.V., Physical origin of crustal movements on passive margins, Oceanologica Acta, no. SP, 167-170, 1981.

Ascoli, P., Supplementary Report on Biostratigraphy (Foraminifera and Ostracoda) and depositional environments of the Atlantic COST G-1 well, Georges Bank, from 10,000 to 14,800', Geological Survey of Canada, report no. EPGS-PAL.21-83PA, 1983.

Austin, J.A., E. Uchupi, D.R. Shaughnessy, and R.D. Ballard, Geology of New England Passive Margin, AAPG Bull., 64, No. 4, 501-526, April 1980.

Avedik, F., A.L. Camus, A. Ginsburg, L. Montadert, D.G. Roberts, and R.B. Whitmarsh, A seismic refraction and reflection study of the continent-ocean transition beneath the north Biscay margin, Phil. Trans. R. Soc. Lond., A305, 5-25, 1982.

Ballard, R.D., and E. Uchupi, Triassic rift structure in Gulf of Maine, AAPG Bull., 59, 1041-1072, 1975.

Bally, A.W., D. Bernoulli, G.A. Davis, and L. Montadert, Listric normal faults Oceanologica Acta, no. SP, 87-101, 1981.

Barss, M.S., Bujak, J.P., and Williams, G.L., Palynologic zonation and correlation of sixty-seven wells, eastern Canada; Canada Geological Survey Paper 78-24, 118p, 1979.

Barton, P.J., The relationship between seismic velocity and density in the continental crust - a useful constraint?, Geophys. J. R. S., in press.

Beaumont, C., C.E. Keen, and R. Boutilier, On the evolution of rifted continental margins: comparison of models and observations for the Nova Scotian margin, GJRAS, 70, 667-716, 1982.

Brunet, M.F., and X. LePichon, Subsidence of the Paris Basin, J. Geophys. Res., 87, 8547-8560, 1982.

Buck, W.R., Small scale convection and the evolution of the lithosphere, MIT Ph.D. thesis, 1984.

Burke, K., Development of graben associated with the initial ruptures of the Atlantic Ocean, Tectonophys., 36, 93-112, 1976.

Burke, K., Diverse geology of Atlantic-type continental margins and some possible implications for the U.S. offshore Atlantic, in: Proceedings of the 9th Annual Offshore Technology Conference, vol. 3, 77-84, 1977.

Burke, K., The edges of the ocean - an introduction, Oceanus, 22, no. 3, 2-9, 1979.

Camus, A.L., Elude de la transition continent-ocean sur la marge continentale nord Gascogne a partir des documents enregistres lors de la campagne sismique refraction a deux bateaux IPOD 79, These de 3^{e} cycle, Universite de Paris 6, 1981.

Chenet, P., L. Montadert, H. Gairaud, and D. Roberts, Extension ratio measurements on the Galicia, Portugal, and Northern Biscay Continental Margins: Implications for Evolutionary Models of Passive Continental Margins, in: J.S. Watkins and C.L. Drake, eds., Studies in continental margin geology, AAPG Memoir 34, 703-716, 1982.

Christensen, N.I., and M.H. Salisbury, Structure and constitution of the lower oceanic crust, Rev. Geophys. and Space Phys., 13, no. 1, 57-86, 1975.

Cochran, J., Simple models of diffuse extension and the pre-seafloor spreading development of the continental margin of the northeastern Gulf of Aden, Oceanologica Acta, n°SP, Actes 26^{e} C.G.I., 155-165, 1981.

Cornet, B., A. Traverse, and N.G. McDonald, Fossil spores, pollen, and fishes from Connecticut indicate Early Jurassic age for part of the Newark group, Science, 182, 1243-1247, 1973.

Cornet, B., and A. Traverse, Palynological contributions to the chronology and stratigraphy of the Hartford basin in Connecticut and Massachusetts, Geoscience and Man, 11, 1-33, 1975.

Cousminer, H.L., and W. Manspeizer, Triassic pollen date Moroccan High Atlas and the incipient rifting of Pangea as middle Carnian, Science, 191, 943-945, 1976.

Cousminer, H.L., W.E. Steinkraus, and R.E. Hall, Biostratigraphic restudy documents Triassic/Jurassic section in Georges Bank COST G-2 well, Abstract, AAPG Bull., 68, p. 466, 1984.

De Charpal, O., P. Guennoc, L. Montadert, and D.G. Roberts, Rifting, crustal attenuation and subsidence in the Bay of Biscay, Nature, 275, 706-711, 1978.

Dillon, W.P., C.K. Paull, R.T. Buffler, and J.P. Fail, Structure and development of the Southeast George embayment and Northern Blake Plateau: preliminary analysis, in: J.S. Watkins, L. Montadert, and P.A. Dickerson, eds., Geological and geophysical investigations of continental margins, AAPG Mem. 29, 27-41, 1979.

Dillon, W.P., P. Popenoe, J.A. Grow, K.D. Klitgord, B.A. Swift, C. K. Paull, and K.V. Cashman, Growth faulting and salt diapirism: their relationship and control in the Carolina trough, east North America, in: J.S. Watkins and C.L. Drake, eds., Studies in continental margin geology, AAPG Memoir 34, 21-48, 1982.

Dillon, W.B., C.K. Paull, and L.E. Gilbert, History of the Atlantic continental margin off Florida: the Blake Plateau basin: In C.W. Poag, Ed., Geologic Evolution of the U.S. Atlantic Margin, Van Nostrand Reinhold Co., Stroudsburg, PA, 1985.

Falvey, D.A., The development of continental margins in plate tectonic theory, Australian Petroleum Exploration Assoc. Journal, 14, 95-106, 1974.

Falvey, D.A., and M.F. Middleton, Passive continental margins: evidence for a pre-breakup deep crustal metamorphic subsidence mechanism, Oceanologica Acta, no. SP, 103-114, 1981.

Fitton, J.G., Active versus passive continental rifting: evidence from the West African rift system, Tectonophysics, 94, 473-482, 1983.

Fleitout, L., and C. Froidevaux, Tectonics and topography for a lithosphere containing density heterogeneities, Tectonics, 1, 21-56, 1982.

Fleitout, L., D. Yuen, and C. Froidevaux, Thermomechanical models of lithospheric deformation: application to the tectonics of Western Europe, Annales Geophysicae, in press.

Folger, D.W., W.P. Dillon, J.A. Grow, K.D. Klitgord, and J.S. Schlee, Evolution of the Atlantic continental margin of the U.S., in: M. Talwani, W. Hay, and W.B.F. Ryan, eds., DSDP Results in the Atlantic Ocean Continental Margins and Paleoenvironment, Maurice Ewing Series 3, AGU, 87-108, 1979.

Ginzburg, A., R.B. Whitmarsh, D.G. Roberts, L. Montadert, A. Camus, and F. Avedik, The deep seismic structure of the northern continental margin of the Bay of Biscay, Annales Geophysicae, 3, 499-510, 1985.

Given, M.M., Mesozoic and early Cenozoic geology of offshore Nova Scotia, Bulletin of Canadian Petroleum Geology, 25, 63-91, 1977.

Grow, J.A., Deep structure and evolution of the Baltimore Canyon trough in the vicinity of the COST No. B-3 well. In: P.A. Scholle, Ed., Geological studies of the COST No. B-3 well, U.S. Mid-Atlantic continental slope area, U.S. Geological Survey Circular 833, 117-124, 1980.

Grow, J.A. and R.G. Markl, IPOD-USGS multichannel seismic reflection profile from Cape Hatteras to the Mid-Atlantic Ridge, Geology, 5, 625-630, 1977.

Grow, J.A., C.O. Bowin, and D.R. Hutchinson, The gravity field of the U.S. Atlantic Continental Margin, Tectonophys., 59, 27-52, 1979a.

Grow, J.A., R.E. Mattick, and J.S. Schlee, Multichannel seismic depth sections and interval velocities over outer continental shelf and upper continental slope between Cape Hatteras and Cape Cod, in: J.S. Watkins, L. Montadert, and P.A. Dickerson, eds., Geological and geophysical investigations of continental margins, AAPG Mem. 29, 65-83, 1979b.

Grow, J.A., and R.E. Sheridan, Deep structure and evolution of the continental margin off the eastern U.S., Oceanologica Acta, n°SP, Actes 26e C.G.I., 11-19, 1981.

Grow, J.A., and R.E. Sheridan, Atlantic continental margin of the U.S. in: D-NAG Special Publication 1, GSA, 143-156, 1982.

Harland, W.B., A.V. Cox, P.G. Llewellyn, C.A.G. Pickton, A.G. Smith, and R. Walters, A Geologic Time Scale, Cambridge Univ. Press, 131 pp., 1982.

Heezen, B., The Atlantic continental margin, UMR Journal, no. 1, 5-25, April 1968.

Heezen, B., Atlantic type continental margins, in: Burk, C.A. and C.L. Drake, Eds., The Geology of Continental Margins, Springer Verlag, NY, 13-24, 1974.

Hellinger, S.J., and J.G. Sclater, Some comments on two-layer extensional models for the evolution of sedimentary basins, J. Geophys. Res., 88, 8251-8269, 1983

Hsu, K.J., Isostasy and a theory for the origin of geosynclines, Amer. J. Sci., 256, 305-327, 1958.

Hsu, K.J., Isostasy, crustal thinning, mantle changes and the disappearance of ancient land masses, Amer. J. Sci., 263, 97-109, 1965.

Hutchinson, D.R., J.A. Grow, K.D. Klitgord and B.A. Swift, Deep structure and evolution of the Carolina trough,in: J.S. Watkins and C.L. Drake, eds., Studies in continental margin geology, AAPG Memoir 34, 129-154, 1982.

Hutchinson, D.R., K.D. Klitgord, R.S. Detrick, Rift basins of the Long Island platform, GSA Bull., in press.

Jansa, L.F., and J.A. Wade, Geology of the continental margin off Nova Scotia and Newfoundland, In: W.J.M. Van der Linden and J.A. Wade, Eds., Offshore Geology of Eastern Canada, Geological Survey of Canada Paper 74-30, 51-105, 1975.

Jansa, L.F., J.P. Bujak, and G.L. Williams, Upper Triassic salt deposits of the western North Atlantic, Canadian Journal of Earth Sciences, 17, 547-559, 1980.

James, D.E., T.J. Smith and J.S. Steinhart, Crustal structure of the middle Atlantic states, J. Geophys. Res., 73, 1983-2007, 1968.

Jarvis, G.T. and D. McKenzie, Sedimentary basin formation with finite extension rates, EPSL, 48, 42-52, 1980

Keen, M.J., Possible edge effect to explain magnetic anomalies off the eastern seaboard of the U.S., Nature, 222, 72-74, 1969.

Keen, C.E. , C. Beaumont and R. Boutilier, Preliminary results from a thermo-mechanical model for the evolution of Atlantic-type continental margins, Oceanologica Acta, n°SP, Actes 26e C.G.I., 123-128, 1981.

Keen, C.E. and T. Lewis, Measured radiogenic heat production in sediments from continental margin of Eastern north America: Implications for petroleum generation, AAPG Bull., 66, 1402-1407, 1982.

Kent, P., Vertical tectonics associated with rifting and spreading, Phil. Trans. R. Soc. Lond., A 294, 125-135, 1980.

Klitgord, K.D., and J.C. Behrendt, Basin structure of the U.S. Atlantic margin. In: J.S. Watkins, L. Montadert, P.A. Dickerson, eds., Geological and geophysical investigations of continental margins, AAPG Memoir 29, 85-112, 1979.

Klitgord, K.D., and J.A. Grow, Jurassic seismic stratigraphy and basement structure of western Atlantic magnetic quiet zone, AAPG Bull., 64, no. 10, 1658-1680, 1980.

Klitgord, K.D., W.P. Dillon, and P. Popenoe, Mesozoic tectonics of the Southeastern United States coastal plain and continental margin, in: G.S. Gohn, ed., Studies related to the Charleston, South Carolina, Earthquake of 1886 - Tectonic and seismicity, USGS Professional paper 1313, P1-P15, 1983.

Le Pichon, X. and J.C. Sibuet, Passive margins: A model of formation, J. Geophys. Res., 86, 3708-3720, 1981.

Le Pichon, X., J. Angelier and J.C. Sibuet, Plate boundaries and extensional tectonics, Tectonophys., 81, 239-256, 1982a.

Le Pichon, X., J.C. Sibuet and J. Angelier, Subsidence and stretching, in: J.S. Watkins and C.L. Drake, eds., Studies in continental margin geology, AAPG Memoir 34, 731-742, 1982b.

Manspeizer, W., Rift tectonics inferred from volcanics and clastic structures, in: W. Manspeizer, ed., Field studies of New Jersey geology and guide to field trips: 52nd annual meeting of the New York State Geological Association, Rutgers University, Newark, NJ, 314-351, 1980.

Manspeizer, W., J.H. Puffer, and H.L. Cousminer, Separation of Morocco and eastern North America: a Triassic-Liassic stratigraphic record, Geol. Soc. Am. Bull., 89, 901-920, 1978.

May, P.R., Pattern of Triassic-Jurassic diabase dikes around the North Atlantic in the context of predrift position of the continents, Geol. Soc. Am. Bull., 82, 1285-1292, 1971.

McIver, N.L., Cenozoic and Mesozoic stratigraphy of the Nova Scotia shelf, Canadian Journal of Earth Sciences, 9, 54-70, 1972.

McKenzie, D., Some remarks on the development of sedimentary basins, Earth and Planet. Sci. Lett., 40, 25-32, 1978a.

McKenzie, D.P., Active tectonics of the Alpine-Himalayan belt: the Aegean Sea and surrounding regions, Geophys. J.R. Astron. Soc., 55, 217-254, 1978b.

Morgan, W.J., Hotspots tracks and the early rifting of the Atlantic, Tectonophys., 94, 123-140, 1983.

Mountain, G.S., and B.E. Tucholke, Mesozoic and Cenozoic geology of the U.S. Atlantic continental slope and rise. In: C.W. Poag, Ed., Geologic Evolution of the U.S. Atlantic Margin, Van Nostrand Reinhold, Co., Stroudsburg, PA, 1985.

Mutter, J.C., M. Talwani, and P.L. Stoffa, Origin of seaward-dipping reflectors in oceanic crust off the Norwegian margin by "subaerial sea-floor spreading", Geology, 10, 353-357, 1982.

Nelson, K.D., J.H. McBride, J.A. Arnow, J.E. Oliver, L.D. Brown and S. Kaufman, New COCORP profiling in southeastern United States. Part II: Brunswick and east coast magnetic anomalies, opening of the north-central Atlantic Ocean, Geology, 13, 718-721, 1985.

Olsen, P.E., Triassic and Jurassic formations of the Newark basin, in: W. Manspeizer, ed., Field studies of New Jersey geology and guide to field trips: 52nd annual meeting of the New York State Geological Association, Rutgers University, Newark, NJ, 2-41, 1980.

Olsen, P.E., A.R. McCune, and K.S. Thomson, Correlation of the early Mesozoic Newark supergroup by vertebrates, principally fishes, American Journal of Science, 282, 1-44, 1982.

Parsons, B. and J.G. Sclater, An analysis of the variation of ocean floor bathymetry and heat flow with age, J. Geophys. Res., 82, 803-827, 1977.

Paull, C.K. and W.P. Dillon, Structure stratigraphy and geologic history of Florida-Hatteras shelf and inner Blake Plateau, AAPG Bull., 64, 339-358, 1980.

Pinet, P.R., and P. Popenoe, Shallow seismic stratigraphy and post Albian geologic history of the northern and central Blake Plateau, GSA Bull., 96, 627-638, 1985.

Poag, C.W., Foraminiferal and seismic stragigraphy, paleoenvironments, and depositional cycles in the Georges Bank basin in: P.A. Scholle and C.R. Wenkam, eds., Geological studies of the COST Nos. G-1 and G-2 Wells, U.S. North Atlantic outer continental margin, USGS Circular 861, 43-91, 1982a.

Poag, C.W., Stratigraphic reference section for Georges Bank Basin - Depositional model for New England passive margin, AAPG Bull., 66, 1021-1041, 1982b.

Poag, C.W., Depositional history and stratigraphic reference section for central Baltimore Canyon Trough: In Poag, C.W., ed., Geol. Evolution of United States Atlantic Margin, Van Nostrand-Reinhold, p. 265-292, 1985.

Poag, C.W. and R.E. Hall, Foraminiferal biostratigraphy, paleoecology and sediment accumulation rates. In P.A. Scholle, ed., Geological studies of the COST GE-1 well. United States South Atlantic Outer Continental Shelf area, U.S. Geol. Survey Circ. 800, 49-63, 1979.

Popenoe, P., Cenozoic depositional and structural history of the North Carolina margin from seismic-stratigraphic analyses, In: C.W. Poag, ed., Geologic Evolution of the U.S. Atlantic Margin, Van Nostrand Reinhold, Stroudsburg, PA, U.S.A, 1985.

Proffett, J.M., Cenozoic geology of the Yerington district, Nevada and implications for the nature and origin of Basin and Range faulting, Geol. Soc. Am. Bull., 88, 247-266, 1977.

Royden, L., A simple method for analyzing subsidence and heat flow in extensional basins, in press, 1986.

Royden, L. and C.E. Keen, Rifting process and thermal evolution of the continental margin of eastern Canada determined from subsidence curves, Earth and Planet. Sci. Lett., 51, 343-361, 1980.

Royden, L., J.G. Sclater and R.P. Von Herzen, Continental margin subsidence and heat flow: important parameters in formation of petroleum hydrocarbons, AAPG Bull., 64, 173-187, 1980.

Royden, L., F. Horvath, A. Nagymarosy, and L. Stegena, Evolution of the Pannonian basin system, 2. Subsidence and thermal history, Tectonics, 2, 91-137, 1983.

Salveson, J.O., Variations in the geology of the rift basins - a tectonic model, Preprint presented at Rio Grande rift symposium, 1978.

Sanders, J.E., Late Triassic tectonic history of northeastern United States, American Journal of Science, 261, 501-524, 1963.

Sawyer, D.S., Thermal evolution of the northern U.S. Atlantic continental margin, M.I.T. Ph.D thesis, 1982.

Sawyer, D.S., A. Swift, J.G. Sclater and M.N. Toksoz, Extensional model for the subsidence of the northern United States Atlantic continental margin, Geology, 10, 134-140, 1982a.

Sawyer, D.S., A. Swift, M.N. Toksoz and J.G. Sclater, Thermal evolution of the Georges Bank and Baltimore Canyon basins, in: J.S. Watkins and C.L. Drake, eds., Studies in continental margin geology, AAPG Memoir 34, 743-764, 1982b.

Scheidegger, A.E. and J.A. O'Keefe, On the possibility of the origination of geosynclines by deposition, J. Geophys. R, 72, 6275-6278, 1967.

Schlee, J.S., Seismic stratigraphy of Baltimore Canyon trough, AAPG Bull., 65, 26-53, 1981.

Schlee, J.S., W.P. Dillon, and J.A. Grow, Structure of the continental slope off the Eastern U.S., SEPM Special Publication no. 27, 95-117, 1979.

Schlee, J.S., and L.F. Jansa, The paleoenvironment and development of the eastern North American continental margin, Oc. Acta., no. SP, 71-80, 1981.

Schlee, J.S., and J. Fritsch, Seismic stratigraphy of the Georges Bank complex, offshore New England, in: J.S. Watkins and C.L. Drake, eds., Studies in continental margin geology, AAPG Memoir 34, 223-252, 1982.

Schlee, J.S. and K.D. Klitgord, Georges Bank Basin — A Regional Synthesis, in J.A. Grow and R.E. Sheridan, eds., The Geology of North America: Atlantic Continental Margin of the United States, Geol. Soc. Amer., DNAG series, in press.

Scholle, P.A., and C.E. Wenkam, Studies of the COST G1 and G2 Wells, north Atlantic outer continental shelf area, USGS Circular 861, 1982.

Sclater, J.G., and P.A.F. Christie, Continental stretching: an explanation of the post-Mid-Cretaceous subsidence of the central North Sea basin, J. Geophys. Res., 85, 3711-3739, 1980.

Sclater, J.G., L. Royden, F. Horvath, B.C. Burchfiel, S. Semken and L. Stegena, The formation of the intra-Carpathian basins as determined from subsidence data, Earth and Planet. Sci. Lett., 51, 139-162, 1980.

Sclater, J.G., B. Parsons and C. Jaupart, Oceans and continents: similarities and differences in the mechanisms of heat loss, J. Geophys. Res., 86, 11, 535-11552, 1981.

Scrutton, R.A., The age relationship of igneous activity and continental break-up, Geol. Mag, 110, 227-234, 1973.

Sengor, A.M.C. and K. Burke, Relative timing of rifting and volcanism on earth and its tectonic implications, Geophys. Res. Lett., 5, 419-421, 1978.

Sheridan, R.E., Subsidence of continental margins, Tectonophys., 7, 219-229, 1969.

Sheridan, R.E., J.A. Grow, J.C. Behrendt, and K.C. Bayer, Seismic refraction study of the continental edge off the eastern United States, Tectonophysics, 59, 1-26, 1979.

Sleep, N.H., Thermal effects of the formation of Atlantic continental margins by continental break-up, Geophys. J. RAS, 24, 325-350, 1971.

Sleep, N.H., Crustal thinning on Atlantic Continental Margins: Evidence from older margins, in: D.H. Tarling, and S.K. Runcorn, editors, Implication of Continental Drift to the Earth Sciences, Academic Press, vol. 2, 685-692, 1973.

Smith, T.E., and Noltimier H.C., Paleomagnetism of the Newark trend igneous rocks of the north central Appalachians and the opening of the central Atlantic ocean, Amer. J. Sci., 279, 779-807, 1979.

Steckler, M.S., Uplift and extension at the Gulf of Suez - Indication of induced mantle convection, Nature, 317, 135-139, 1985.

Steckler, M.S., and A.B. Watts, Subsidence of the Atlantic type continental margin off New York, Earth and Planet. Sci. Lett., 41, 1-13, 1978.

Steckler, M.S. and A.B. Watts, The Gulf of Lion: subsidence of a young continental margin, Nature, 287, 425-429, 1980.

Sutter, J.F., and T.E. Smith, $^{40}Ar/^{39}Ar$ ages of diabase intrusions from Newark trend basins in Connecticut and Maryland: initiation of central Atlantic rifting, Amer. J. Sci., 279, 808-831, 1979.

Tapponnier, P., and J. Francheteau, Necking of the lithosphere and the mechanics of slowly accreting plate boundaries, J. Geophys. R, 83, B8, 3955-3970, 1978.

Tucholke, B.E. and G.S. Mountain, Seismic stratigraphy, lithostratigraphy and paleosedimentation patterns in the North American basin, in: M. Talwani, W. Hay, and W.B.F. Ryan, eds., DSDP Results in the Atlantic Ocean Continental Margins and Paleoenvironment, Maurice Ewing Series 3, AGU, 58-86, 1979.

Turcotte, D.L., Haxby, W.F., and J.R. Ockendow, Lithospheric instabilities in: Island Arcs, Deep Sea Trenches and Back-Arc Basins, Maurice Ewing Series, Vol. 1, AGU, 63-69, 1977.

Uchupi, E. and J.A. Austin, The geologic history of the passive margin off New England and the Canadian maritime provinces, Tectonophysics, 59, 53-69, 1979.

Uchupi, E., J.P. Ellis, J.A. Austin, G.H. Keller, and R.O. Ballard, Mesozoic-Cenozoic regressions and the development of the margin off northeastern North America, in: R.A. Scrutton, M. Talwani, eds.; The Ocean Floor, Wiley, 81-96, 1982.

Vail, P.R., R.M. Mitchum, J.R., and S. Thompson, Seismic stratigraphy and global changes of sea level. Part 4: Global cycles of relative changes of sea level, in: C.E. Payton, ed., Seismic stratigraphy - Applications to hydrocarbon exploration, AAPG Memoir 25, 83-97, 1977.

Valentine, P.C., Calcareous nannofossil biostratigraphy and paleoenvironment of the COST Nos G-1 and G-2 wells in the Georges Bank basin. In: P.A. Scholle and C.R. Wenkam, Eds., Studies of the COST G1 and G2 Wells, North Atlantic outer continental shelf area, USGS Circular 861, 34-42, 1982.

Van Houten, F.B., Triassic-Liassic deposits of Morocco and eastern north America: comparison, AAPG Bull., 61, 79-99, 1977.

Van Houten, F.B., West central New Jersey. In: W. Manspeizer, ed., Field studies of New Jersey geology and guide to field trips: 52nd annual meeting of the New York state geological association, Rutgers University, Neward, NJ, 264-277, 1980.

Vogt, P.R., and N.A. Ostenso, Steady state crustal spreading, Nature, 215, 810-817, 1967.

Walcott, R.I., Gravity, flexure, and the growth of sedimentary basins at a continental edge, GSA Bull., 83, 1845-1848, 1972.

Walton H.S, and A.A. Berti, Upper Triassic and lower Jurassic palynology of the Grand Banks area, Palynology, 2, p 235, 1978.

Watremez, P., Flux de chaleur sur le massif Armoricain et sur la marge continentale: essai de modelisation de l'evolution thermique de la marge continentale, These de doctorat de 3eme cycle, Universite de Bretagne Occidentale, 1980

Watts, A.B. and W.B.F. Ryan, Flexure of the lithosphere and continental margin basins, Tectonophysics, 36, 25-44, 1976.

Watts, A.B., and M.S. Steckler, Subsidence and eustasy at the continental margin of Eastern North America, in: M. Talwani, W. Hay, and W.B.F. Ryan, eds., DSDP Results in the Atlantic Ocean Continental Margins and Paleoenvironment, Maurice Ewing Series 3, AGU, 218-234, 1979.

Watts, A.B., J.H. Bodine, and N.M. Ribe, Observation of flexure and the geological evolution of the Pacific ocean basin, Nature, 283, 532-537, 1980.

Watts, A.B., and M.S. Steckler, Subsidence and tectonics of Atlantic type continental margins, Oceanologica Acta, no. SP, 143-153, 1981.

Watts, A.B., G.D. Karner, and M.S. Steckler, Lithospheric flexure and the evolution of sedimentary basins, Phil. Trans. R. Soc. Lond., A305, 249-281, 1982.

Watts, A.B., and J. Thorne, Tectonics, global changes in sea level and their relationship to stratigraphical sequences at the U.S. Atlantic continental margin, Marine and Petroleum Geology, 1, 319-339, 1984.

Wernicke, B.W., and B.C. Burchfiel, Modes of extensional tectonics, J. Struct. Geol., 4, no. 2, 105-115, 1982a.

Wernicke, B., J.E. Spencer, B.C. Burchfiel, and P.L. Guth, Magnitude of crustal extension in the southern Great Basin, Geology, 10, 499-502, 1982b.

Wood, R. and P. Barton, Crustal thinning and subsidence in the North Sea, Nature, 302, 134-136, 1983.

APPENDIXES

Appendix A

THE ONE DIMENSIONAL UNIFORM EXTENSION MODEL

A.1 INTRODUCTION

McKenzie (1978a) studied the evolution of a uniformly stretched block of lithosphere (Fig. A.1). He showed two important causes of subsidence:

1) the isostatic response to the stretching leads to a quick initial subsidence (Fig. A.1b).

2) the temperature distribution in the thinned lithosphere tends to return to equilibrium by cooling which results in long term thermal subsidence due to thermal contraction of the lithosphere (Fig. A.1c).

We review the quantitative implications of this model and show how we set it up.

A.2 THE INITIAL SUBSIDENCE

A.2.1 Stretched continental crust

Following McKenzie (1978a) we assume local isostasy before and after stretching; that allows us to compute the elevation $Z(\beta)$ of a column stretched by an amount β (Fig. A.2b) by comparing it with normal continental crust ($\beta=1$) of elevation $Z(1)$ (Fig. A.2a) (the meaning of the parameters are given in Table A.1):

$$Z(\beta) = \frac{\rho_a-\delta(Z(1))}{\rho_a-\delta(Z(\beta))} Z(1) + \frac{\rho_a h_\ell-\bar{\rho}_c h_c-\bar{\rho}_m(h_\ell-h_c)}{\rho_a-\delta(Z(\beta))} \left(1-\frac{1}{\beta}\right) \qquad \text{(A-1)}$$

This formula is valid for both cases, elevation under sea level ($z>0$) and elevation above sea level ($z<0$), if one defines δ as:

$\delta(Z) = 0$ if $Z<0$

$\delta(Z) = \rho_w$ if $Z>0$

A.2.2 The Oceanic Crust

a) Introduction

The initial conditions at which oceanic crust is created cannot be satisfactorily represented by an infinitely stretched continent. We must then define a specific model for the oceanic part of a continental margin which will have to be isostatically consistent with the extensional model defined for the non-oceanic part and which will have to be reasonably consistent with observations at mid-oceanic ridges.

b) The problem

If we take the stretching model at its limit when $\beta \to \infty$, we obtain a column of pure asthenosphere at depth $Z(\infty)$ (Fig. A.2c):

$$Z(\infty) = \frac{\rho_a - \delta(Z(1))}{\rho_a - \rho_w} Z(1) + \frac{\rho_a h_\ell - \bar{\rho}_c h_c - \bar{\rho}_m (h_\ell - h_c)}{\rho_a - \rho_w} \qquad (A\text{-}2)$$

This depth is what Turcotte et al. (1977) defined as the mantle geoid depth. But a situation in which the asthenosphere would reach its free surface without segregating a crust, is not realistic (Le Pichon and Sibuet, 1981; Le Pichon et al., 1982a). Then, even if the limit of the stretching model for $\beta = \infty$ gives a good description of the oceanic floor thermal evolution (McKenzie, 1978a), that limit case doesn't give a realistic description of the initial subsidence and crust thickness of that oceanic floor. We then need a model for the initial condition of oceanic floor, i.e. a model for a mid oceanic ridge.

c) The mid-oceanic ridge model

The ridge structure can be represented by three figures: the depth of the ridge, dr, the average ridge crustal density, ρ_c' and the ridge crustal thickness, h_c'. (Table A.1).

The corresponding mantle geoid depth is then:

$$Z(\infty) = dr + h_c' \frac{\rho_a - \bar{\rho}_c'}{\rho_a - \rho_w} \qquad (A\text{-}3)$$

A.2.3 The isostatic balance

The overall isostatic balance will require that equation (A-2) and (A-3) yield the same value of the mantle geoid depth $Z(\infty)$. This condition can be written as:

$$\frac{\rho_a - \delta(Z(1))}{\rho_a - \rho_w} Z(1) + \frac{\rho_a h_\ell - \bar{\rho}_c h_c - \bar{\rho}_m (h_\ell - h_c)}{\rho_a - \rho_w} = dr + h_c' \frac{\rho_a - \bar{\rho}_c'}{\rho_a - \rho_w} \qquad (A\text{-}4)$$

and simply means that the density distribution at the mid-oceanic ridge, defined by dr, ρ_c', h_c', ρ_a, ρ_w cannot be chosen independently from the one of the unstretched continent, defined by $Z(1)$, ρ_c, h_c, ρ_m, h_ℓ, ρ_a. We will consider that when we set our parameter values.

A.2.4 The limit between ocean and continent

At this point we have defined two partial models: the one for the continent and stretched continent, the other for the ocean. The question arises where to set the limit between these two models. On the Eastern United States continental margin the edge of the oceanic crust is rather well defined by the ECMA (Keen, 1969; Klitgord and Behrendt, 1979); we then consider stretched continental crust that is located landward of that anomaly and oceanic crust that is located seaward of it.

A.3 THERMAL SUBSIDENCE

The thermal subsidence is given as a function of the time after stretching, t, and of the stretching factor, β (McKenzie, 1978a):

$$S_t(t,\beta) = E_1 \frac{8}{\pi^2} \sum_{m=0}^{\infty} \frac{1}{(2m+1)^3} \frac{\beta}{\pi} \sin[(2m+1)\frac{\pi}{\beta}][1-\exp(-(2m+1)\frac{t}{\tau}] \qquad (A-5)$$

where
$$E_1 = \frac{h_\ell \rho_m(0) \alpha T_a}{\rho_m(0)-\rho_w} \cdot \frac{1}{2} \qquad (A-6)$$

$$\tau = \frac{h^2_\ell}{\pi^2 \kappa} \qquad (A-7)$$

E_1 represents the maximum subsidence of seafloor since

$$S_t\ (t = \infty,\ \beta = \infty) = E_1 \qquad (A-8)$$

and τ is the time constant of lithospheric cooling.

A.4 SETTING OF THE PARAMETERS

A.4.1 Introduction

We will distinguish between 10 primary parameters which have to be chosen from all the others which can be derived from them (Table A.1). We can break these primary parameters into three groups: (1) lithospheric thermal parameters (2) unstretched continental crust parameter (3) mid-oceanic ridge parameters. All these primary parameters have been derived from former work, except the ridge reference and the initial continental elevation, Z(1).

A.4.2 The mid-oceanic ridge model

Many versions of the density distribution at a mid-oceanic ridge have been proposed and the ridge reference used in this study is quite similar to them (Fig. A.3); it is set up so that, assuming that the whole column is initially at temperature Ta for simplicity, the present (175 My after ridge condition) crustal structure be compatible with the one proposed by Hutchinson et al. (1982).

A.4.3 Initial continental structure

The initial continental elevation Z(1) is taken as zero since the unstretched crust of the Carolina coastal plain is close to zero elevation. The isostasy between the mid-oceanic ridge and the unstretched continent constrains the only remaining free parameter $\rho_m(0)$ of equation A to be:

$$\rho_m(0) = 3.31 \text{ g/cm}^3 \qquad \text{(A-9)}$$

which finishes defining the initial continental structure (Fig. A.4).

A.4.4 Initial subsidence

Two cases are distinguished (Fig. A.5):

(1) The column is not oceanic, it is then considered as stretched by a factor β and its elevation is given by relationship (A-1) which, with our parameters becomes:

$$Z_i(\beta) = Z(\infty)\cdot(1-1/\beta) = 3.48\ (1-1/\beta) \text{ km} \qquad \text{(A-10)}$$

where Z_i is expressed in km below sea level.

(2) The column is oceanic, its initial elevation is then

$$Z_i = dr = 2.50 \text{ km} \qquad \text{(A-11)}$$

This value is obviously not obtained by setting $\beta = \infty$ into (A-10).

A.4.5 Thermal subsidence

The thermal diffusivity can be obtained from Parsons and Sclater (1977) for the Atlantic:

$$\frac{h^2}{\kappa} \simeq 650 \text{ MY}, \qquad \text{(A-12)}$$

then from (A-7)

$$\tau = 65.8 \text{ MY} \qquad \text{(A-13)}$$

The constant E_1 is computed from (A-6) and yields a value of 3.93 km which despite our slightly different choice of $\rho_m(0)$ is very close to Parsons and Sclater (1977) value of 3.90 km (their C_3 coefficient).

The thermal subsidence $S_t(t,\beta)$, Eq. (A-5), is a linear formula in $(1-1/\beta)$ for time $t = \infty$ and can be approximated linearly for time τ = 200 MY and t = 175 MY (even though in the model calculation we used the full series for finite times).

$$S_t(\infty, \beta) = 3.93(1-1/\beta) \quad \text{in km} \qquad \text{(A-14)}$$

$$S_t(200,\beta) \simeq 3.77(1-1/\beta) \qquad \text{(A-15)}$$

$$S_t(175,\beta) \simeq 3.69(1-1/\beta) \qquad \text{(A-16)}$$

For the oceanic part we use the same formula where we take $\beta = \infty$, since this limit of the model does represent the thermal evolution of oceanic floor [McKenzie, 1978a].

A.4.6 Tectonic subsidence

The tectonic subsidence is defined as the sum of the initial and thermal subsidence. The elevation of a continental column stretched by a factor β after 200 m.y. can be obtained by summing (A-10) and (A-5):

$$Z_t(t,\beta) = Z_i(\beta) + S_t(t,\beta) \qquad \text{(A-17)}$$

For the oceanic part the elevation becomes:

$$Z_t(t) = dr + S_t\,(t,\infty) \qquad \text{(A-18)}$$

A.4.7 Error range

We will here investigate how constrained our parameters are in order to evaluate the error range in the initial, thermal and load subsidence that is due to the model set up (Table A.2), as opposed to the error range due to uncertainties in the data which is evaluated in the main text. We do not need to evaluate each parameter error but the error on the combined parameters which really control the initial, thermal and load subsidence (LePichon et al., 1982b; Royden, in press).

The initial subsidence is controlled by the parameters $Z(\infty)$ and $Z(1)$. The error on $Z(\infty)$ can be computed through (A-3) if we estimate the error on dr, h'_c, ρ'_c and ρ_a. For a small amount of extension the error in the initial subsidence would be controlled by Z(1) while for a large amount of extension it would be controlled by $Z(\infty)$ (Fig. A.5). Our estimate of the error in dr does not take into account the possibility of very anomalous ridge depth during the early phase of ocean opening (Mutter et al., 1982).

The thermal subsidence is controlled by the parameters E_1 and τ. Neglecting the effect of errors in τ we obtain a range of error based on the Parsons and Sclater (1977) estimate.

The loading subsidence is obtained by (Appendix B)

$$S_{load} = \frac{\bar{\rho}_s - \rho_w}{\rho_a - \rho_w} H \qquad \text{(A-19)}$$

where ρ_s and H are the sediment average density and thickness. The influence of these two parameters is a major contribution to the final error and is investigated in the main text (data errors). We here compute the influence of the choice of ρ_a only. The resulting error is very small, but it must be remembered that a major cause of error that we ignore here, comes from the assumption of local isostasy.

A.5 APPLICATION

A.5.1 Introduction

For each location within the basin we proceed in two steps: (1) we evaluate the stretching factor from the present total subsidence (Fig. A.6). (2) From the stretching factor we can predict crust thickness, subsidence at any time and reconstruct past basin configurations) (Fig. A.7).

A.5.2 Evaluation of the stretching factor β (Fig. A.6)

For each location on non oceanic crust, the present total subsidence (i.e. the present basement depth if zero elevation is assumed before rifting) once corrected for the loading effect of the sediments (local isostatic unloading, as described in Appendix B) yields the present tectonic subsidence from which β can be evaluated using equation (A-17). If the location is on oceanic crust β will not be adjusted but set at infinity and Equation (A-18) will be used instead.

A.5.3 Reconstruction of past configurations (Fig. A.7)

At any given past time the tectonic subsidence can be computed using equation (A-17). If the geological layer corresponding to that time is also identified then the sediment thickness and density can be reconstituted after correcting for compaction. The subsidence due to the load of these sediments is added to the tectonic subsidence to yield the basement depth. The predicted paleowater depth is then obtained by subtracting the reconstituted sediment thickness from the basement depth. A final correction to basement depth and seafloor depth can be made to account for sea level changes.

TABLE A.1

Parameters used in the one dimensional uniform extension model

Parameter	Meaning	Value		Reference
I. Primary parameters				
h_ℓ	Lithospheric thickness (i)	128	km	(1)
τ^*	Time constant (i)	65.8	MY	(1)
Ta	Asthenosphere temperature (i)	1365	°C	(1)
α	Coefficient of thermal expansion (i)	3.1×10^{-5}	$°C^{-1}$	(1)
Z(1)	Initial continental elevation (ii)	0.00	km	(4)
h_c	Crustal thickness (ii)	40	km	(2)
$\bar{\rho}_c$	Average crustal density (ii)	2.876	g/cm^3	(2)
dr	Ridge depth (iii)	2.5	km	(3)
h'_c	Ridge crustal thickness (iii)	5.0	km	(4)
$\bar{\rho}'_c$	Average ridge crustal density (iii)	2.75	g/cm^3	(4)
II. Derived parameters				
$\rho_m(0)$	Density of mantle material at 0°C	3.308	g/cm^3	(4)
$\bar{\rho}_m$	Average mantle density (*)	3.216	g/cm^3	(4)
ρ_a	Asthenospheric density	3.168	g/cm^3	(4)
$Z(\infty)$	Mantle geoid depth	3.478	km	(4)
Tr	Moho temperature (*)	427	°C	(4)
$\bar{T}m$	Average mantle temperature (*)	896	°C	(4)
E_1	Maximum seafloor subsidence	3.932	km	(4)

(1) Parsons and Sclater, 1977
(2) Hutchinson et al., 1982
(3) Anderson et al., 1973
(4) Estimated in this paper.
(*) For unstretched continental crust

(i) lithosphere thermal parameters
(ii) unstretched continental crust parameters
(iii) mid-ocean ridge parameter

TABLE A.2

Estimate of the uncertainty on the model set up

Parameter X	Absolute error ΔX	Relative error ΔX/X	Reference
ρ_a	0.03 g/cm^3	1%	(3)
$\overline{\rho}'_c$	0.03 g/cm^3	1%	(3)
h'_c	1 km	20%	(3)
dr	0.5 km	20%	(2)
Z(1)	0.2 km		(3)
Z(∞)	0.8 km	23%	(4)
E_1	0.3 km	10%	(1)
τ	10 MY	15%	(1)
Initial subsidence $\beta<1.2$	0.2 km		(4)
Initial subsidence $\beta>1.2$		23%	(4)
Thermal subsidence		10%	(4)
Loading subsidence		1%	(4)

(1) Parsons and Sclater, 1977
(2) Anderson et al., 1973
(3) Our estimate
(4) Computed

Figure Captions

Fig. A.1. McKenzie's [1978a] stretching model.

A.1a: Unstretched continent. The thermal equilibrium geotherm is assumed linear.

A.1b: The lithosphere is instantaneously extended by a factor β. The isostatic compensation causes both an initial subsidence Si and an upwelling of the asthenosphere.

A.1c: The thermal state returns to normal: the lithosphere thickens and the crust subsides thermally by an amount S_t.

Fig. A.2. Isostasy and stretching.

A.2a: Unstretched continent of elevation Z(1).

A.2b: Continent stretched by an amount β. The new elevation is $Z(\beta)$. The initial subsidence is $S_i = Z(\beta)-Z(1)$. The asthenosphere has upwelled.

A.2c: Limiting case when $\beta=\infty$. The elevation $Z(\infty)$ is the mantle geoid depth. This case is not realistic and must be replaced by d.

A.2d: A mid-oceanic ridge defined by its depth dr, its crust average density ρ_c' and its crust thickness h_c'.

Fig. A.3. Proposed mid-oceanic ridge structure.

(1) Christensen and Salisbury (1975).

(2) Turcotte *et al.* (1977).

(3) LePichon and Sibuet (1981).

(4) LePichon *et al.* (1982b).

(5) Cochran (1981).

(6) Keen *et al.* (1981).

(7) Our reference: the whole column is assumed at temperature T_a = 1365°C and the crust is defined so that when its temperature comes back to an average of 150°C it fits the oceanic crust proposed in the gravity model by Hutchinson *et al.* (1982).

Fig. A.4. Assumed temperature and density distribution of the unstretched continental crust of the Carolina trough.

Fig. A.5. Subsidence as a function of γ in the 1-D model.

$\gamma = 1 - 1/\beta$

S_i = initial subsidence

S_t = thermal subsidence

$S_i + S_t$ = tectonic subsidence

Shaded area = error range due to the set up

Note that the two cases; ocean and stretched continent are considered separately; as a result a highly stretched continental crust could subside more than oceanic crust; the question remains to know up to what point the continental crust can be stretched before it breaks.

Fig. A.6. Flow chart: estimate of stretching factor.

Fig. A.7. Flow chart: reconstruction at a given time.

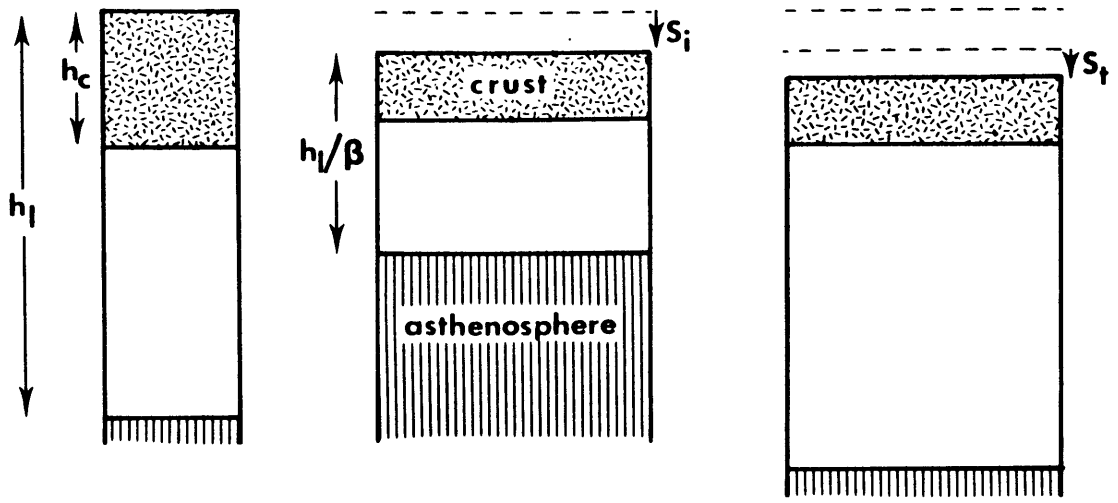

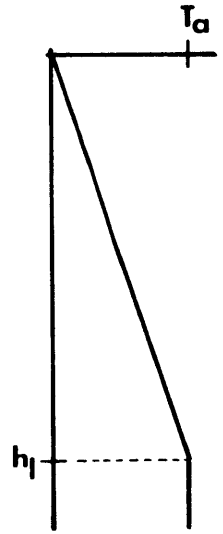

Fig. A.1a

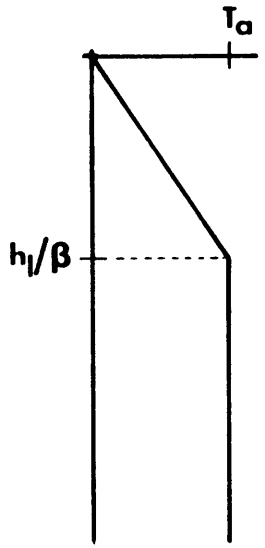

Fig. A.1b

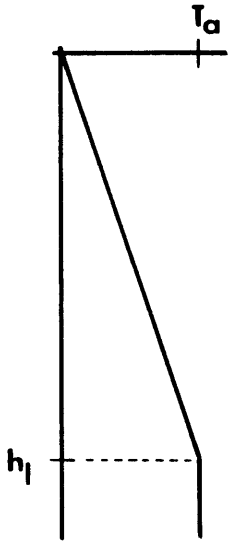

Fig. A.1c

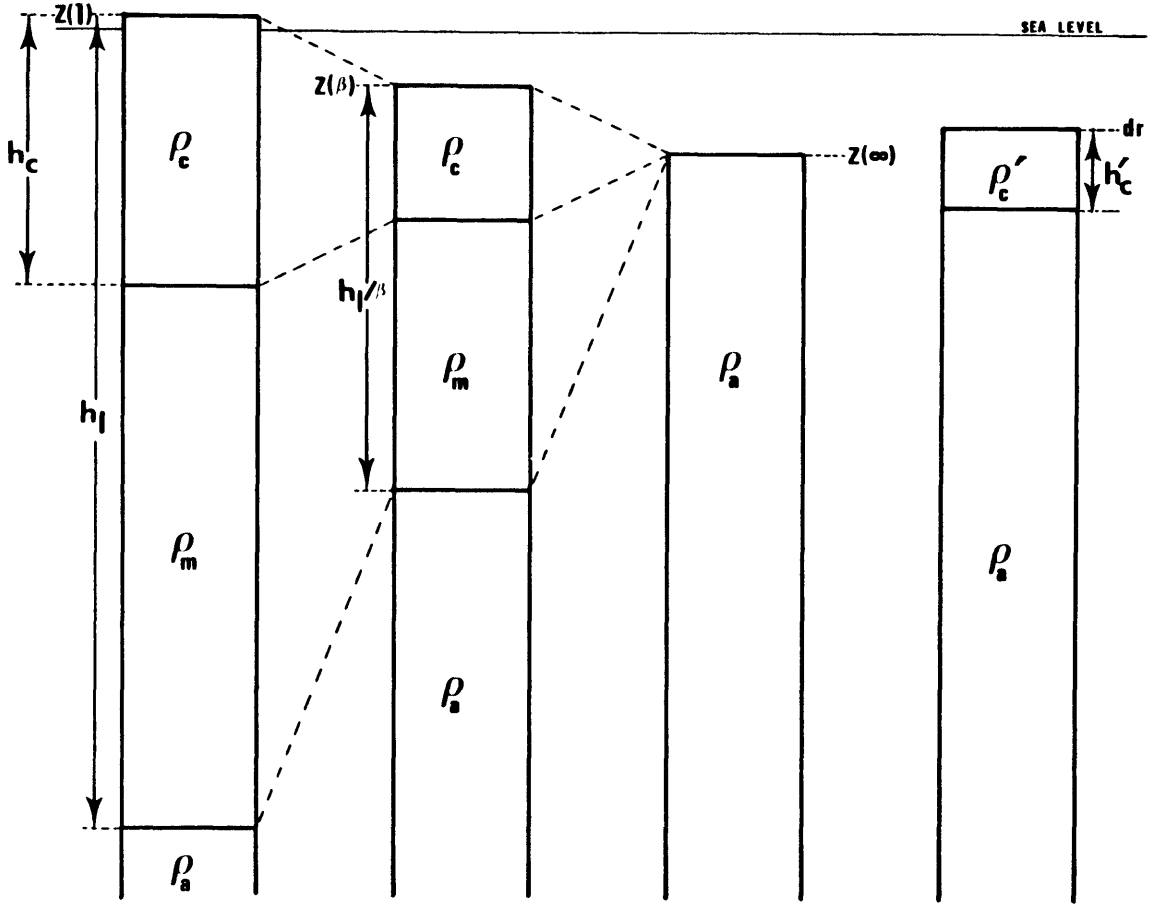

Fig. A.2a Fig. A.2b Fig. A.2c Fig. A.2d

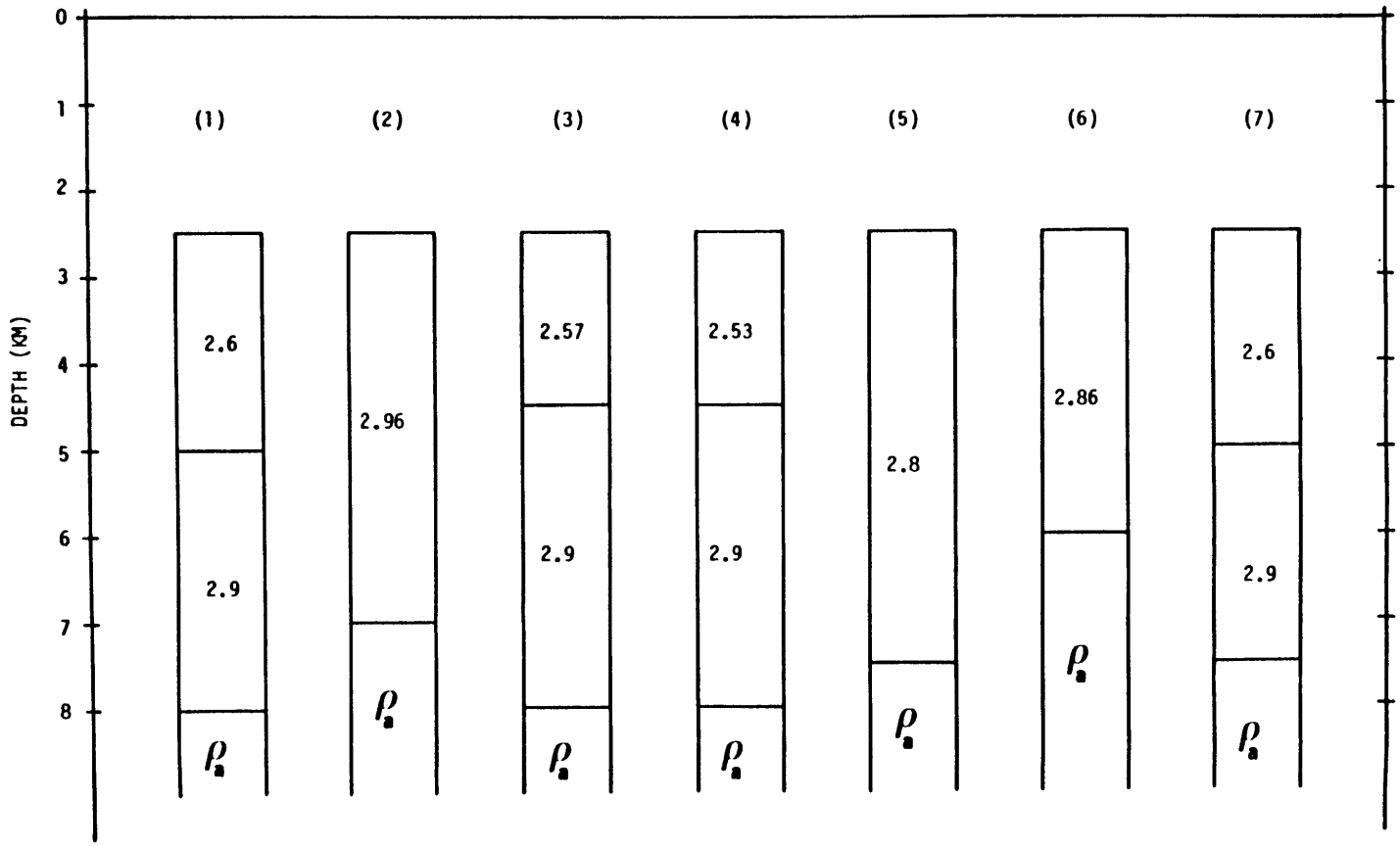

Fig. A.3

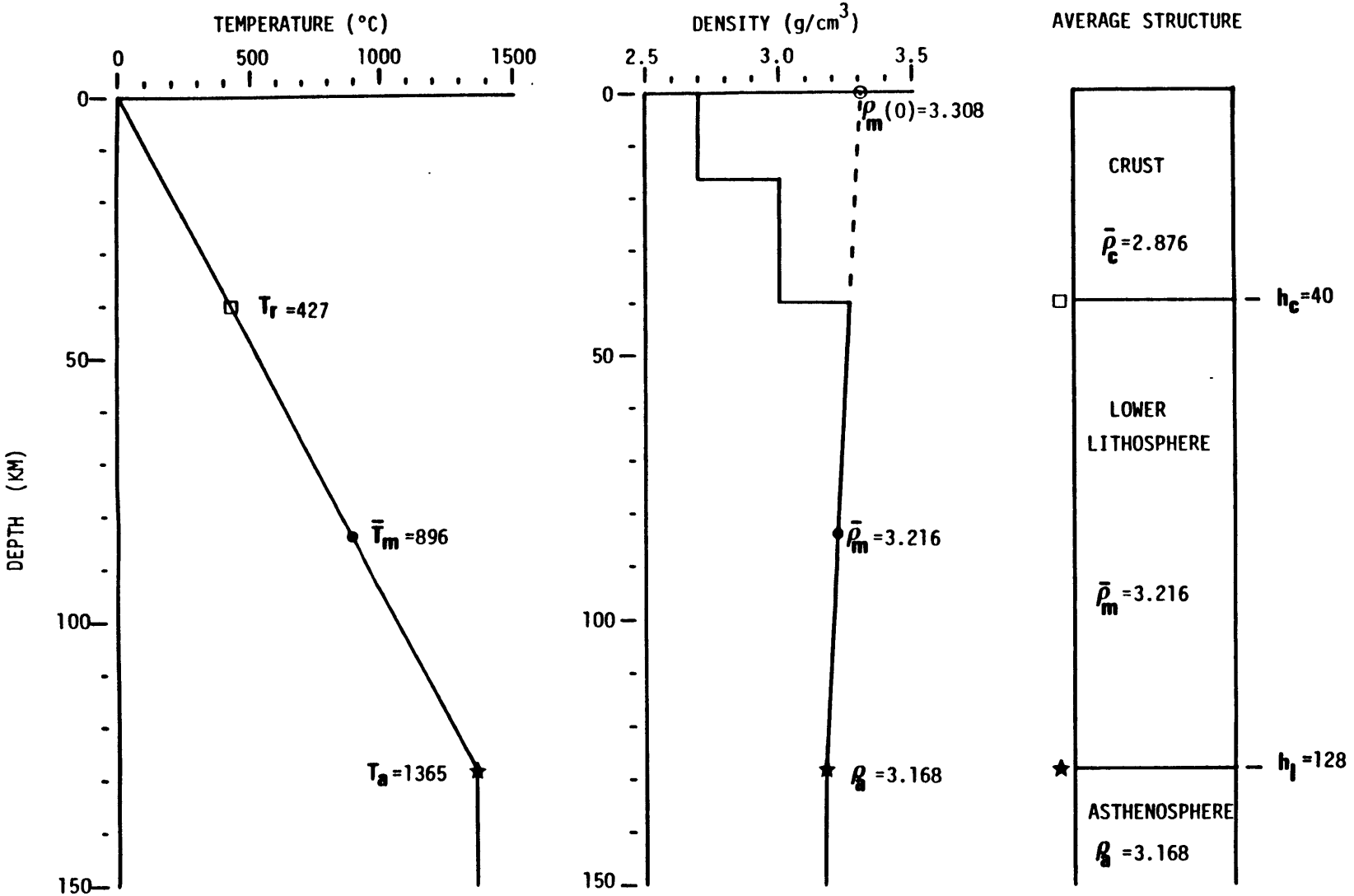
TEMPERATURE (°C)
0
500
1000
1500
DEPTH (KM)
0
50
100
150
T_r =427
$\bar{T}_m$ =896
T_a =1365
DENSITY (g/cm^3)
2.5
3.0
3.5
$\rho_m(0)$=3.308
$\bar{\rho}_m$=3.216
ρ_a =3.168
AVERAGE STRUCTURE
CRUST
$\bar{\rho}_c$=2.876
h_c=40
LOWER
LITHOSPHERE
$\bar{\rho}_m$=3.216
h_l =128
ASTHENOSPHERE
ρ_a =3.168

Fig. A.4

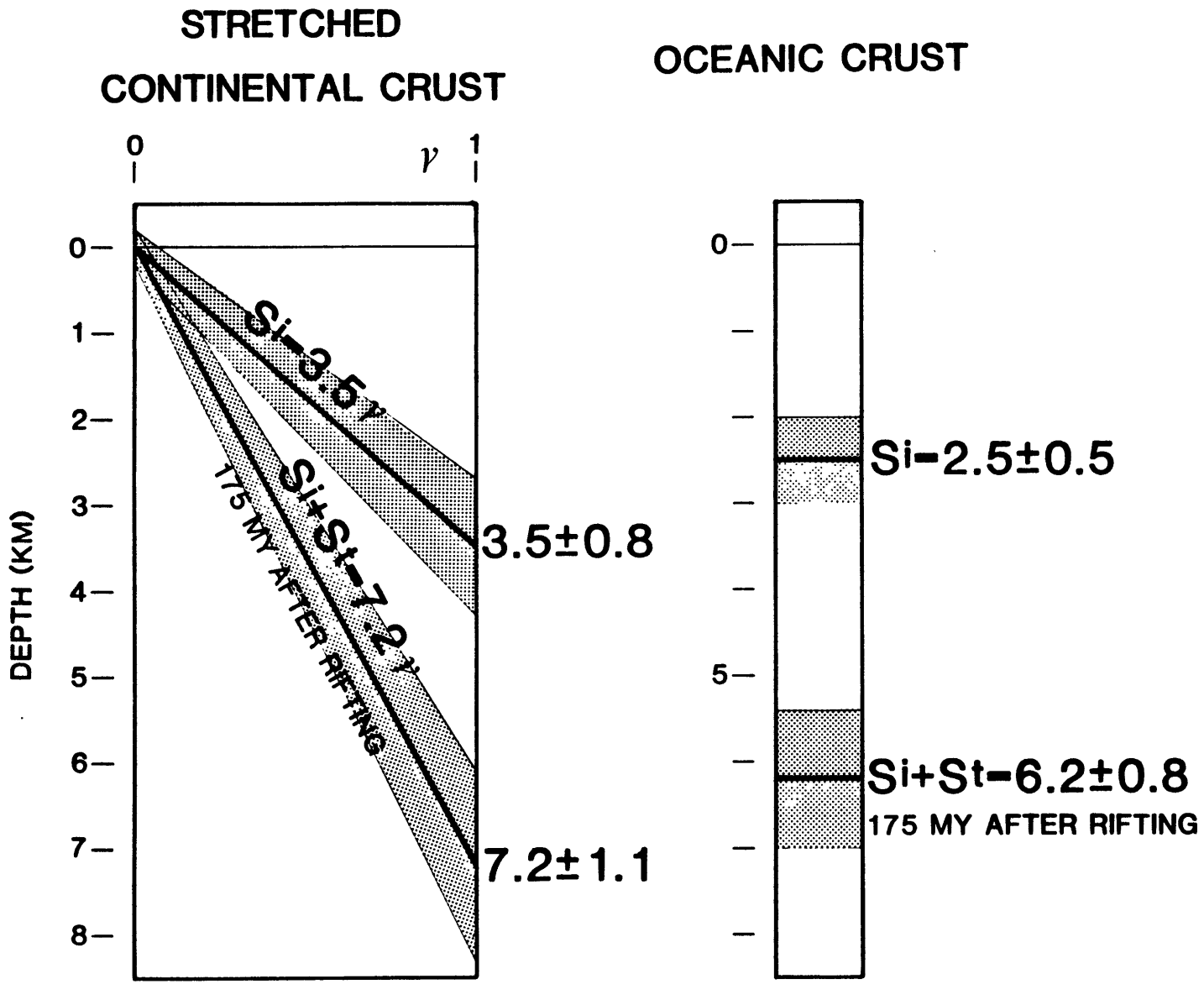
STRETCHED
CONTINENTAL CRUST
OCEANIC CRUST
0
γ
1
DEPTH (KM)
0
1
2
3
4
5
6
7
8
Si-2.5γ
Si+St-7.2γ
175 MY AFTER RIFTING
3.5±0.8
7.2±1.1
Si-2.5±0.5
Si+St-6.2±0.8
175 MY AFTER RIFTING

Fig. A.5

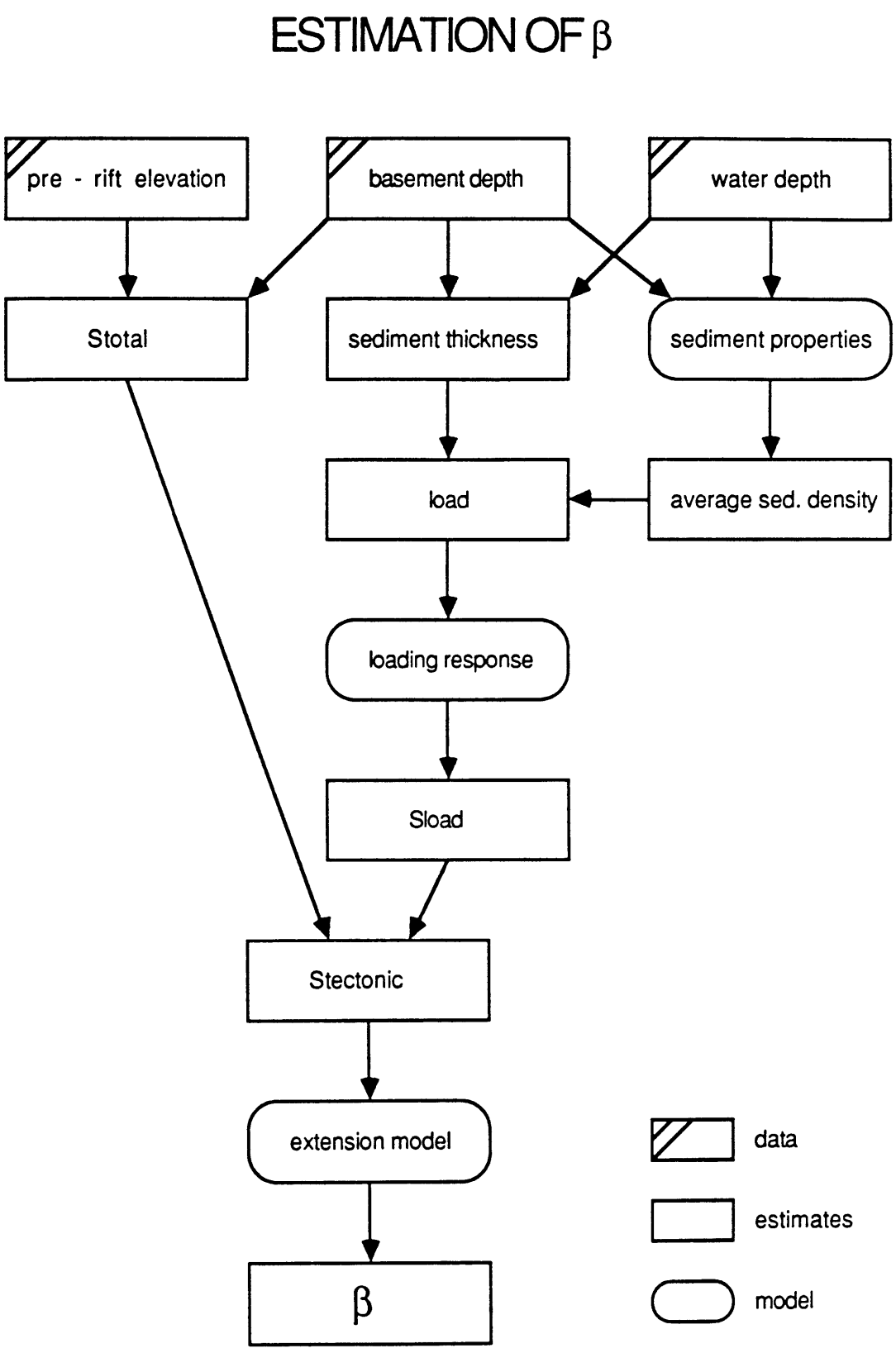
ESTIMATION OF β
pre - rift elevation
basement depth
water depth
Stotal
sediment thickness
sediment properties
load
average sed. density
loading response
Sload
Stectonic
extension model
β
data
estimates
model

Fig. A.6

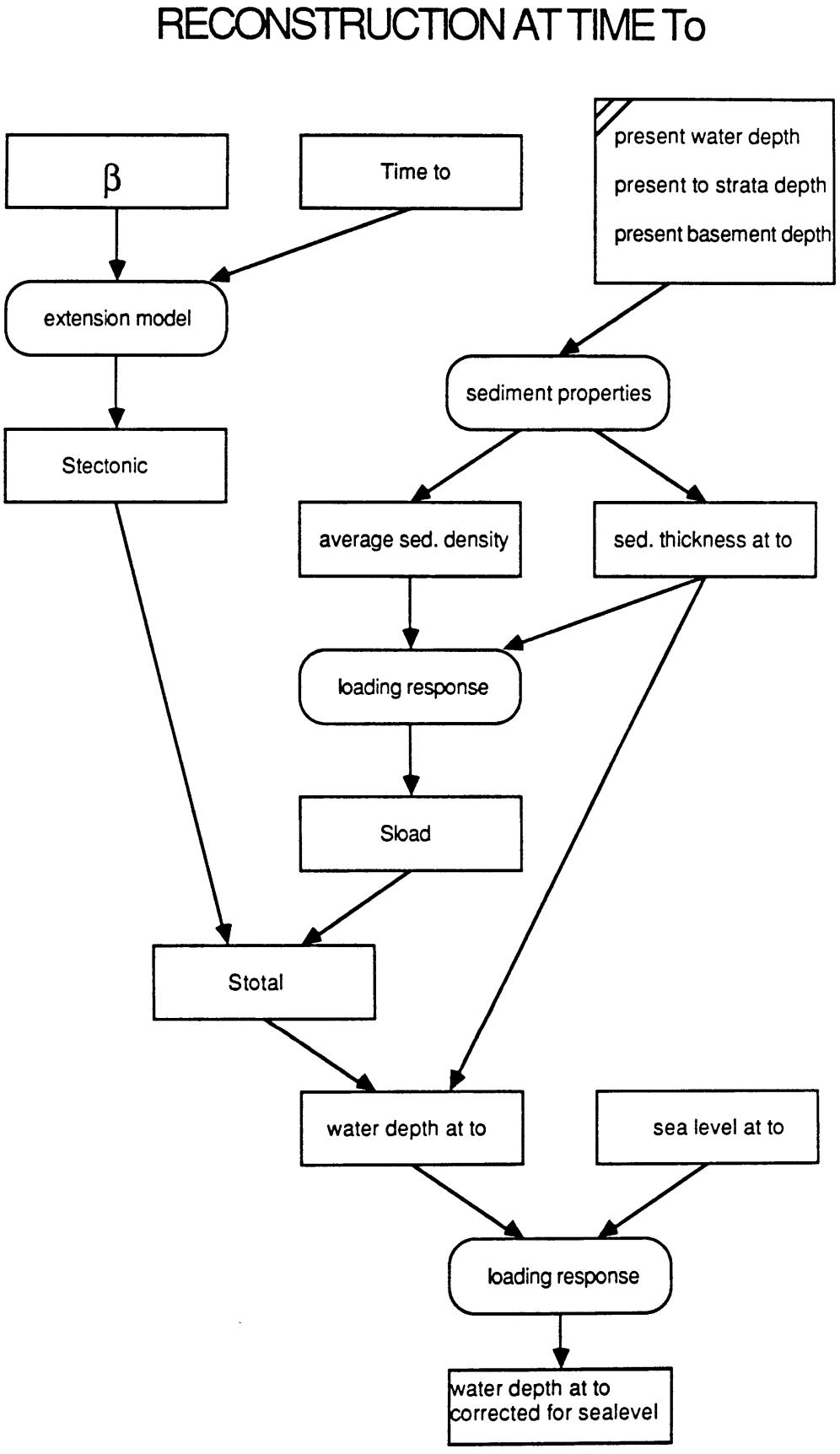
RECONSTRUCTION AT TIME To
β
Time to
present water depth
present to strata depth
present basement depth
extension model
sediment properties
Stectonic
average sed. density
sed. thickness at to
loading response
Sload
Stotal
water depth at to
sea level at to
loading response
water depth at to
corrected for sealevel

Fig. A.7

Appendix B

SUBSIDENCE DUE TO SEDIMENT LOADING

Assuming local isostasy, the effect of a sedimentary cover of average density ρ_s and thickness H, can be estimated by balancing the sediment covered column with an uncovered one (Fig. B.1; variable meaning in Table B.1). If the top of the sediment is under water the resulting effect is:

$$Sload = \frac{\bar{\rho}_s - \rho_w}{\rho_a - \rho_w} \cdot H$$

If the top of the sediment is above water, depending on whether Zb^* or Zw is given, the formula becomes either

$$Sload = \frac{\bar{\rho}_s}{\rho_a} \cdot H - \frac{\rho_w}{\rho_a} \cdot Zb^*$$

or

$$Sload = \frac{\bar{\rho}_s - \rho_w}{\rho_a - \rho_w} H - \frac{\rho_w}{\rho_a - \rho_w} Z_w$$

We want to stress here that the density which comes into these equations is the density at the depth of compensation, thus the asthenosphere density. If the sediment compaction is represented by an exponential law such as:

$$\phi(z) = \phi(0) \cdot e^{-cz}$$

then:

$$\bar{\rho}_s = \rho_r - (\rho_r - \rho_w) \cdot \phi(0) \cdot \frac{1 - e^{-CH}}{C \cdot H}$$

TABLE B.1

Variable Meaning

Zw:	seafloor depth (top of sediment depth)
Zb:	loaded basement depth
Zb^*:	unloaded basement depth
H:	sediment thickness
ρ_s:	average density of the sediments
ρ_w:	density of seawater
ρ_a:	density of the asthenosphere
ρ_r:	density of the sediment matrix
$\phi(Z)$:	porosity of the sediments at subbottom depth Z
C:	coefficient of decay of porosity versus depth
S_{load}:	part of the subsidence due to the sediment load

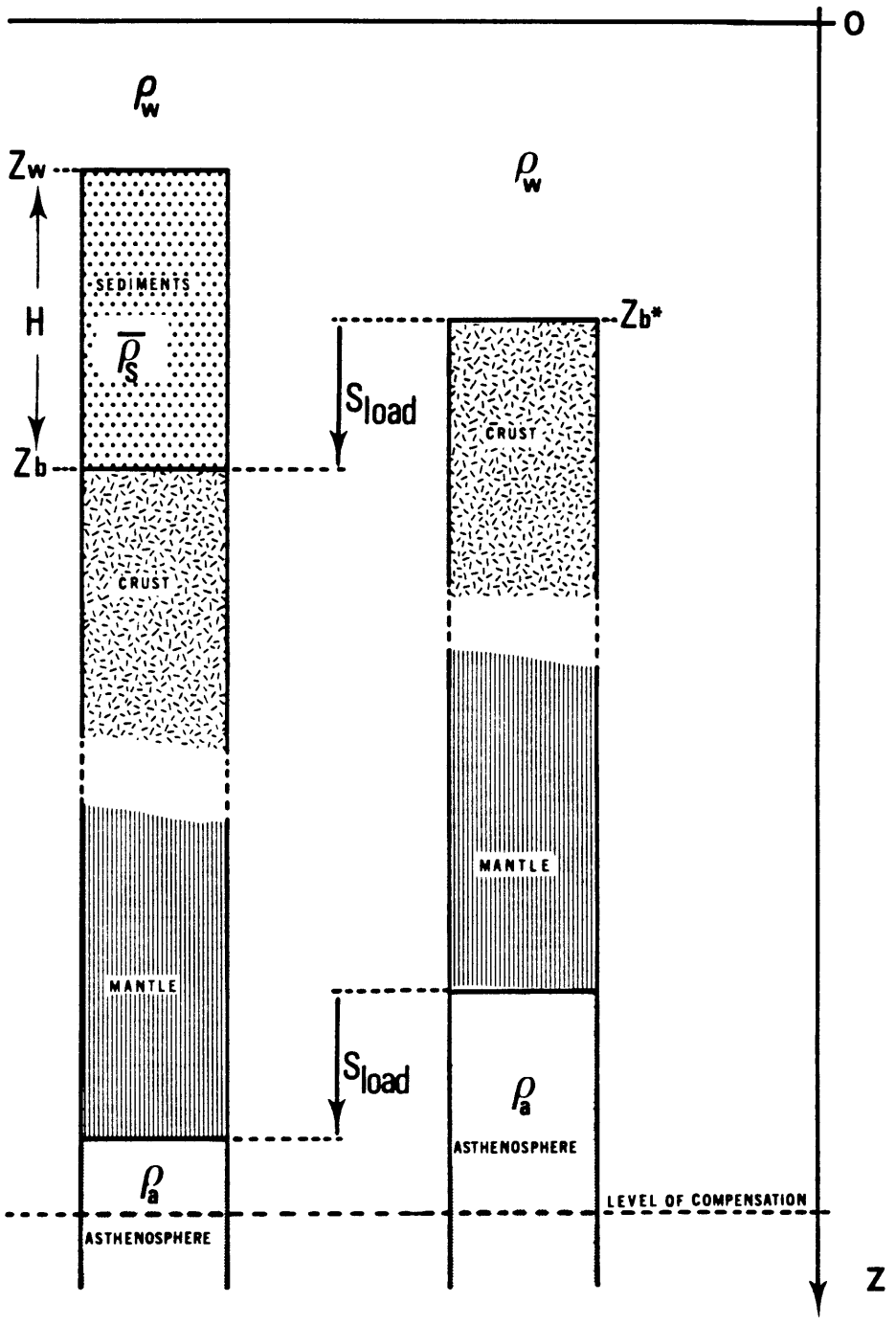

Fig. B.1 : Balancing loaded and unloaded basement

APPENDIX C

THE TWO DIMENSIONAL UNIFORM EXTENSION MODEL

C.1 INTRODUCTION

The initial subsidence is treated as in the case of the 1-D model (Appendix A) but for the thermal subsidence, McKenzie's (1978a) analytical formulae are replaced by a two dimensional finite difference simulation developed by Sawyer (1982). Also, the flexibility of the numerical model allows us to substitute a more realistic geotherm, like those proposed by Sclater et al. (1981) (Fig. C.1), to the simple linear geotherm proposed by McKenzie (1978a). This results in a slightly different setting of the parameters (Table C.1, Fig. C.1).

C.2 THE GEOTHERM

In the crust the radioactive heat generation, A, is assumed exponentially distributed:

$$A(Z) = A_o\, e^{-Z/D} \qquad \text{(C-1)}$$

In the mantle there are no heat sources.

In the asthenosphere, the temperature is constant.

The resulting geotherm has seven degrees of freedom and can be expressed as a function of h_ℓ, h_c, k_ℓ, k_c, A_o, D and Q_o for instance:

$$T(Z) = \frac{Q_o - A_o D}{k_c} Z + \frac{A_o D^2}{k_c} (1 - e^{-Z/D}) \quad \text{if } 0 \leq Z \leq h_c \qquad \text{(C-2)}$$

$$T(Z) = T_r + \frac{Z - h_c}{k_\ell} Q_r \quad \text{if } h_c \leq Z \leq h_\ell \qquad \text{(C-3)}$$

$$T(Z) = T_r + \frac{h_\ell - h_c}{k_\ell} Q_r = T_a \quad \text{if } h_\ell \leq Z \qquad \text{(C-4)}$$

where:

$$Q_r = A_o D(e^{-h_c/D} - 1) + Q_o \simeq Q_o - A_o D \qquad \text{(C-5)}$$

$$T_r = \frac{Q_o - A_o D}{k_c} h_c + \frac{A_o D^2}{k_c} (1 - e^{-hc/D}) \qquad \text{(C-6)}$$

are respectively the heat flow and temperature at the Moho.

C.3 SETTING THE PARAMETERS

We will distinguish the primary parameters which have to be chosen from all the others which can be derived from them [Table C.1]. h_ℓ, T_a, k_c, k_ℓ, α, Cp, ρ_w can be considered as independent from the studied region and are taken from global former works. The remaining parameters are region dependent and discussed now.

C.3.1 Geotherm for the Carolina trough

Short of better estimates, we took some world averages for D and Q_o which, together with h_ℓ, h_c, k_c, k_ℓ and T_a totally define the geotherm. As a consequence A_o cannot be chosen freely but must satisfy Eq. (C-4) which yields a value [Table C.1] quite in the range reported by Sclater et al. (1981).

The resulting geotherm shown in Fig. C.1 can be described as:

$$T(Z) = 12.3Z + 60.8\ (1-e^{-Z/10}) \quad \text{if } 0<Z<40 \qquad \text{(C-7)}$$

$$T(Z) = 178.5 + 9.3\ Z \quad \text{if } 40<Z<128 \qquad \text{(C-8)}$$

$$T(Z) = 1365 \quad \text{if } 128<Z \qquad \text{(C-9)}$$

where the depth is in km and the temperature in °C.

C.3.2 Structure

hc, $\bar{\rho}c$ are taken to be consistent with Hutchinson et al.'s (1982) gravity model. Since the mid-oceanic ridge parameters ρ_c', h_c' and dr are already fixed (as in Appendix A) the only remaining free parameter of the equation which ensures isostatic balance between the unstretched continent and the mid oceanic ridge, (Eq. A-4, Appendix A) are then $\rho_m(0)$ and Z(1). This results in a sensitive dependency of the elevation Z(1) on the choice of the mantle density, $\rho_m(0)$; since this latter is not very well known, it seems legitimate to use the information we have, mainly the elevation, to constrain the choice of that density. Because the unstretched crust of North Carolina is a region of swamp of very small elevation, we impose Z(1) = 0.000 km which determines $\rho_m(0)$.

C.3.3 Sediments

The sediment porosity, ϕ, varies with depth as:

$$\phi(Z) = \phi(0)e^{-C.Z} \qquad \text{(C-10)}$$

(average and extreme values of $\phi(0)$ and C are taken from Chapter 3) and their thermal conductivity, k, is assumed to depend on ϕ as (Sawyer et al., 1982):

$$k(\phi) = (5.3 - 4.3\phi)\cdot 10^{-3} \text{ cal cm}^{-1}\text{s}^{-1} \text{ °C}^{-1} \qquad \text{(C-11)}$$

C.4 INITIAL SUBSIDENCE

The initial subsidence is again derived from (A-1) (Appendix A) and becomes for the non-oceanic part:

$$Z_i(\beta) = Z(\infty)(1-1/\beta) = 3.44\ (1-1/\beta) \text{ km} \qquad \text{(C-12)}$$

and for the oceanic part:

$$Z_i = dr = 2.5 \text{ km} \qquad \text{(C-13)}$$

C.5 THERMAL SUBSIDENCE: THE SIMULATION

C.5.1 Geometry

The continental margin is modeled by a two-dimensional cross section (Fig. C.2) with the following boundary conditions:

- at the two side boundaries the horizontal heat flow is nought.
- the material originally at the bottom is kept at a constant temperature
  T_a (asthenospheric temperature)
- the top boundary is at the constant temperature of 0°C.

The temperatures are computed on a grid (Fig. C.2). The horizontal spacing Δx = 10 km (or 200 SP) while the vertical spacing, Δz, varies from 1 km in the upper parts up to 8 km in the deep parts where the temperature variations are smaller. The stability condition can be written (Sawyer, 1982):

$$\Delta t < \left(2 \frac{k}{\rho C_p} \left(\frac{1}{\Delta x^2} + \frac{1}{\Delta z^2}\right) + \frac{V}{\Delta z}\right)^{-1} \qquad \text{(C-14)}$$

with our grid size we chose Δt_o = 0.5 MY in the coarsest grid (Δz = 8 km, deepest points). In the finest grid (where Δz = 1 km) $\Delta t = \Delta t_o/64$.

C.5.2 Input

The input parameters fall into 4 categories:

a. the physical parameters (Table C.1)
b. the initial conditions, i.e., the distribution of temperature and density immediately after stretching, which is set up in two parts:
   - the non-oceanic columns are derived from an unstretched continental column by a reduction of β.
   - the oceanic columns which are set up as our reference ridge at temperature T_a.
c. the sedimentation rates to be applied during time; we compute these rates from the seismic line reflector depths, assuming that they are constant between each pair of reflectors. They are corrected for compaction.
d. the relaxation temperature T_R

C.5.3 Implementation

For each time step the program solves the heat equation, computes the new temperature distribution, then adds the sediments required and corrects them for compaction, and finally adjusts the elevations by taking into account the thermal contraction, and the response to the load of the newly deposited sediments.

The lithosphere is considered as an elastic plate over an inviscid fluid. The thickness of the elastic plate is defined by the depth to the isotherm at the relaxation temperature, T_R (Watts et al., 1982; Sawyer, 1982). The plate thickness will then vary both laterally with the temperature structure and through time as the temperatures evolve.

C.5.4 Parameters test

With our choice of parameters, the simulation correctly predicts the subsidence of unloaded oceanic crust (Fig. C.3).

C.6 INVERTING FOR β AND T_R BY ITERATION

First, a value of T_R is chosen. Then, the β factors applied to each non-oceanic column are found through iteration so that the predicted present day water depth fits that observed. For oceanic column, β is set to infinity and the subsidence which is totally determined by the initial mid-oceanic ridge thermal conditions and by the loading of the sediments, cannot be adjusted so as to perfectly a fit as the present day water depth.

Once $\beta(x)$ is found, the present day structure is predicted, and from it gravity can also be predicted and compared with the data. Such a comparison is done for models assuming different values of T_R. The one which gives the best agreement is then retained. This process is summarized in Fig. C.4.

TABLE C.1

Parameters used in the two dimensional extension model

I. Primary parameters

Parameter	Meaning	Value	Reference
h_ℓ	initial lithospheric thickness	128 km	(2)
Ta	temperature of the asthenosphere	1365°C	(2)
Q_0	surface heat flow	1.1×10^{-6} cal cm^{-2} s^{-1}	(1)
D	depth constant of radioelement repartition	10 km	(1)
k_c	conductivity of the crust	0.006 cal cm^{-1} $°C^{-1}$ s^{-1}	(1)
k_ℓ	conductivity of the mantle	0.008 cal cm^{-1} $°C^{-1}$ s^{-1}	(1)
α	thermal expansion of the crust and mantle	3.1×10^{-5} $°C^{-1}$	(2)
C_p	heat capacity of rocks	0.3 cal g^{-1} $°C^{-1}$	(2)
Z(1)	initial continental elevation	0.000 km	(3)
h_c	initial continental crust thickness	40 km	(4)
ρ_c	average continental crust density	2.876 g/cm^3	(4)
dr	ridge depth	2.5 km	(7)
h_c'	ridge crustal thickness	5.0 km	(3)
ρ_c'	average ridge crust density	2.75 g/cm^3	(3)
$\phi(0)$	porosity of sediment at sea bottom	55%	(5)
C	coefficient of decay of porosity versus depth	0.43 km^{-1}	(5)
ρ_r	density of sediment matrix	2.7 g/cm^3	(5)
ρ_w	seawater density	1.03 g/cm^3	
$k(\phi)$	thermal conductivity of sediments of porosity ϕ	cal cm^{-1} s^{-1} $°C^{-1}$	(5)
σ	Poisson's ratio	0.25	
E	Young's modulus	$6.6\ 10^{10}$ Pa	(6)

II. Derived parameters

A_0	radioactive heat generation	3.65×10^{-13} cal cm^{-3} s^{-1}	(3)
Tr	temperature at the Moho	549°C	(3)
Tm	average mantle temperature	957°C	(3)
Qr	heat flux at the Moho	7.41×10^{-7} cal cm^{-2} s^{-1}	(3)
$\rho_m(0)$	mantle density at T = 0°C	3.29 g/cm^3	(3)
ρ_m	average mantle density	3.19 g/cm^3	(3)
ρ_ℓ	average lithospheric density	3.09 g/cm^3	(3)
ρ_a	asthenospheric density	3.15 g/cm^3	(3)
$Z(\infty)$	mantle geoid depth	3.444 km	(3)

(1) Sclater et al., 1981
(2) Parsons and Sclater, 1977
(3) This paper
(4) Hutchinson et al., 1982
(5) Sawyer et al., 1982b
(6) Stein et al., 1979
(7) Anderson et al., 19

FIGURE CAPTIONS

Fig. C.1: Temperature and density distribution of the unstretched continental crust for the two dimensional model compared with the ones for the one dimensional model (Appendix A).

Fig. C.2: Grid used in the simulation. Seafloor, basement and moho are outlined in dashed line.

Fig. C.3: Comparison of the simulation predicted oceanic subsidence with Parson's and Sclater's (1977) relationship which, for the Atlantic, is:

$t \leq 30$ MY $\quad d = 2500 + 350\sqrt{t}$

$t \geq 30$ MY $\quad d = 6400 - 3200\, e^{-t/65.8}$

(t = time in MY, d = depth in m)

The difference between the two estimates is at most 75 m.

Fig. C.4: Flow chart explaining how β and T_R are inverted. The dashed arrow represents iterative feedback in the parameter estimations, the solid arrow direct computation.

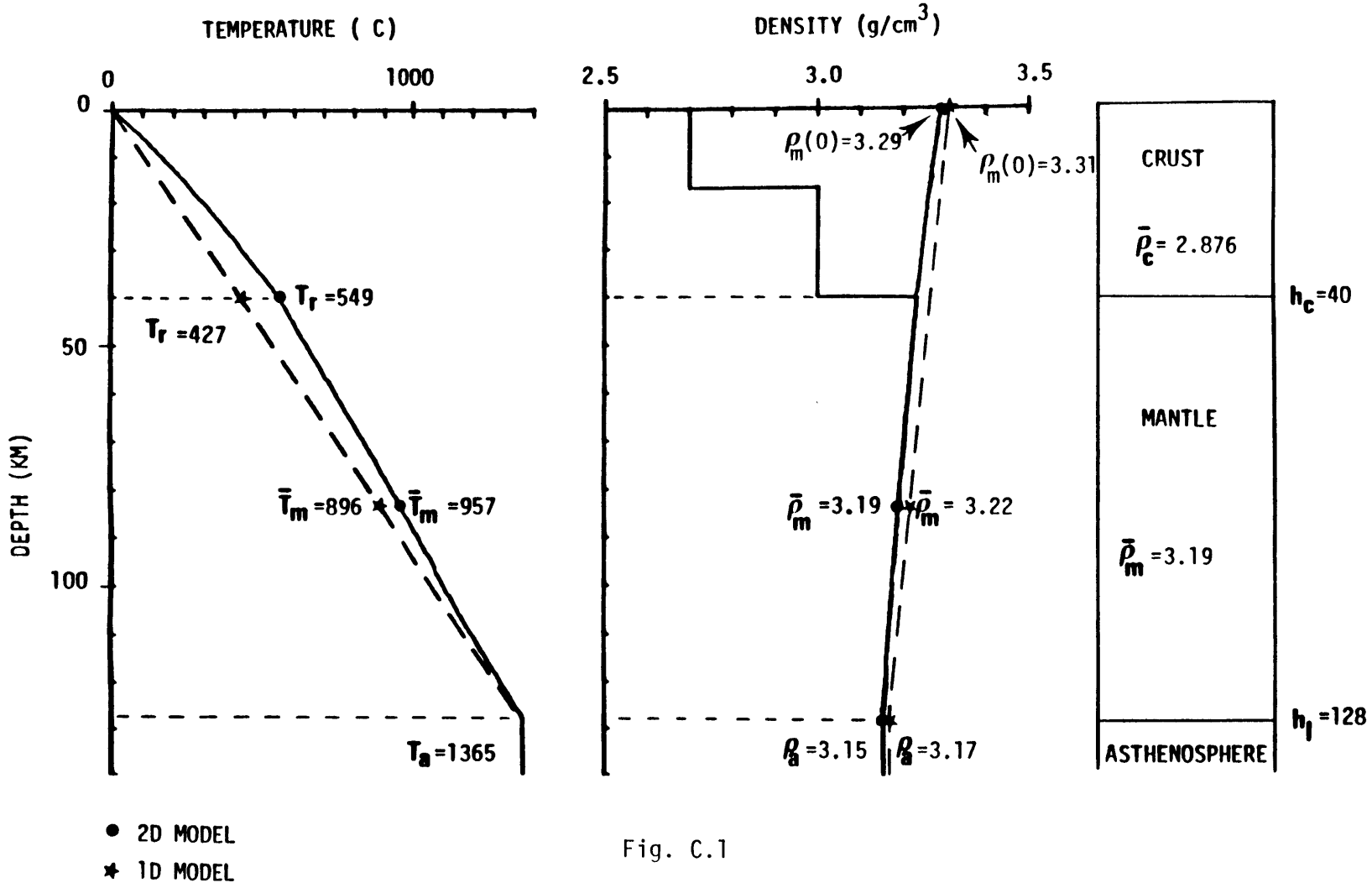
TEMPERATURE (C)
0
1000
0
50
100
DEPTH (KM)
T_r =549
T_r =427
$\bar{T}_m$ =896
$\bar{T}_m$ =957
T_a =1365
DENSITY (g/cm^3)
2.5
3.0
3.5
$\rho_m(0)$=3.29
$\rho_m(0)$=3.31
$\bar{\rho}_m$ =3.19
$\bar{\rho}_m$ = 3.22
ρ_a =3.15
ρ_a =3.17
CRUST
$\bar{\rho}_c$= 2.876
h_c=40
MANTLE
$\bar{\rho}_m$ =3.19
h_l =128
ASTHENOSPHERE
● 2D MODEL
✱ 1D MODEL

Fig. C.1

TOP BOUNDARY CONDITION: T=0 C

SIDE BOUNDARY CONDITION:HEAT FLOW = 0

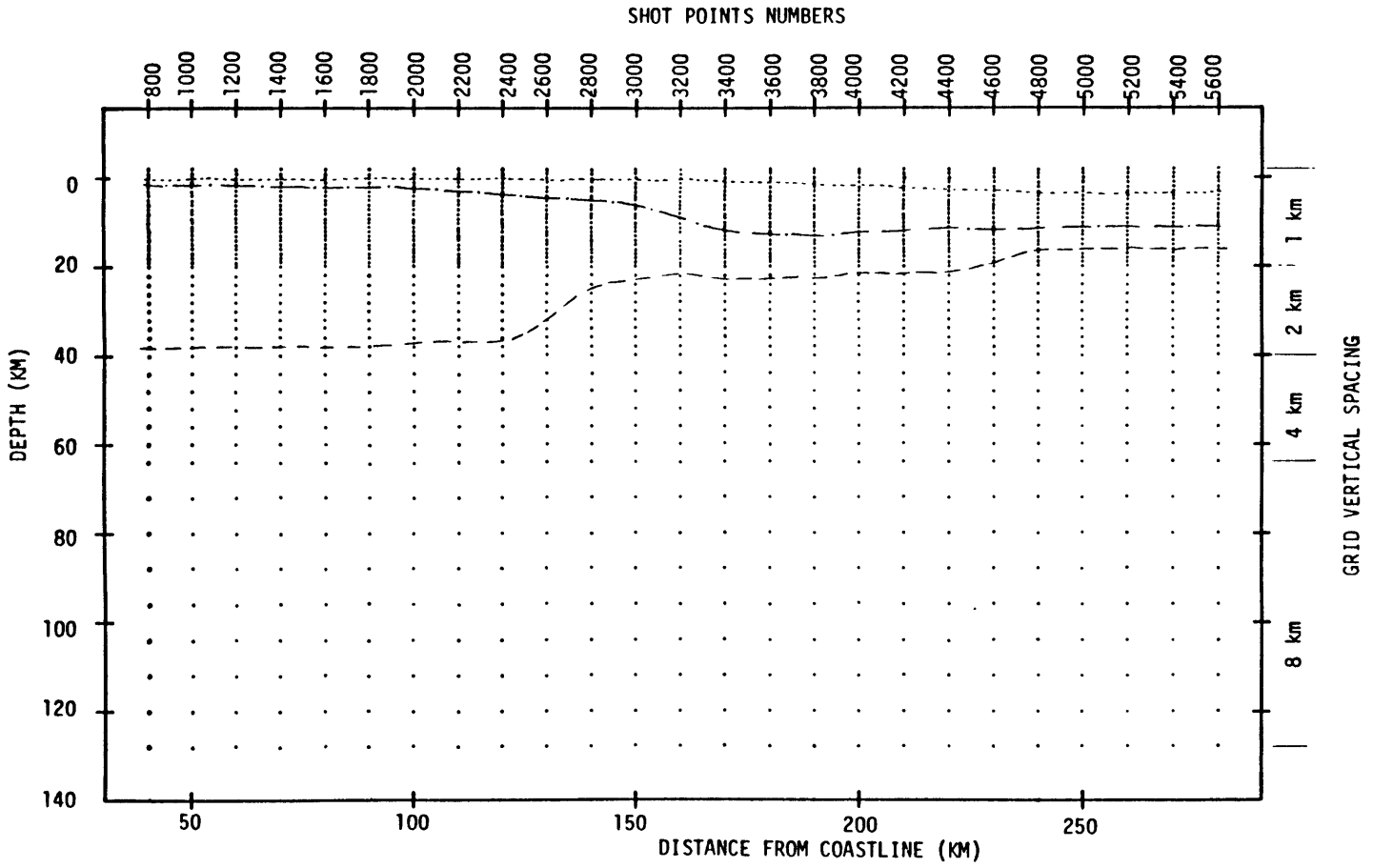

SIDE BOUNDARY CONDITION:HEAT FLOW = 0

BOTTOM BOUNDARY CONDITION:THE MATERIAL ORIGINALLY AT BOTTOM REMAINS AT T_a

Fig. C.2

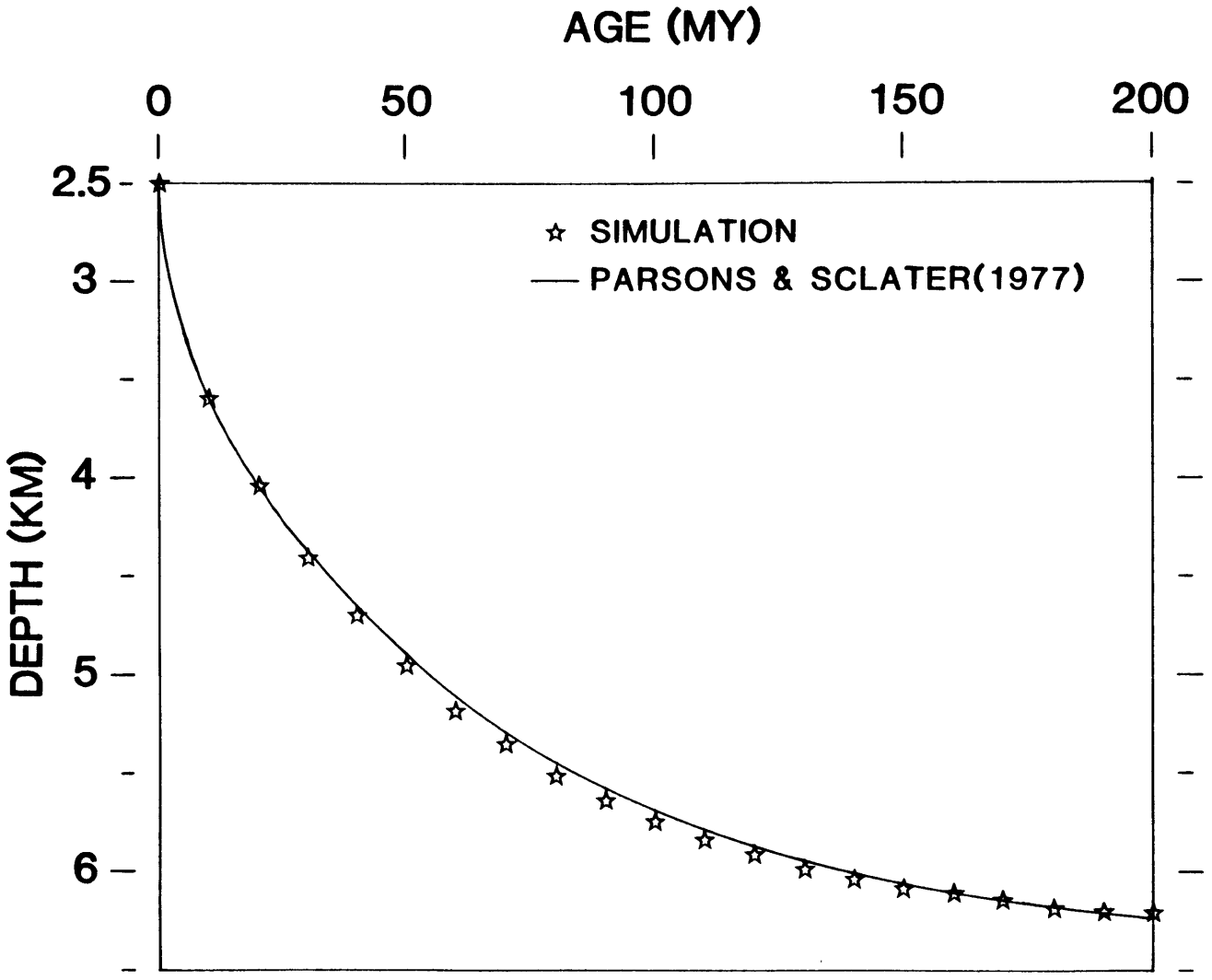
AGE (MY)
0
50
100
150
200
2.5
3
4
5
6
DEPTH (KM)
SIMULATION
PARSONS & SCLATER(1977)

Fig. C.3

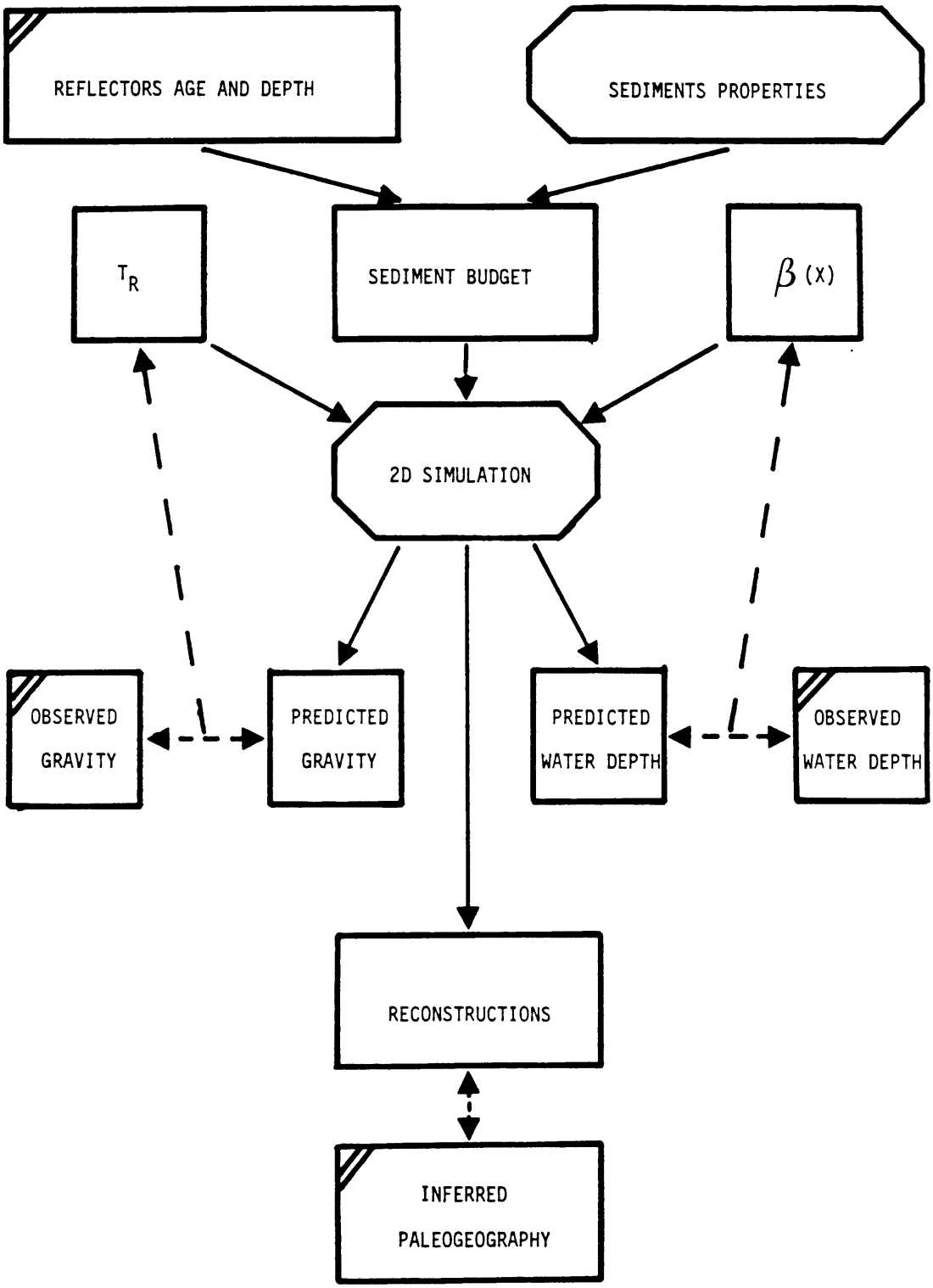
REFLECTORS AGE AND DEPTH
SEDIMENTS PROPERTIES
T_R
SEDIMENT BUDGET
β (X)
2D SIMULATION
OBSERVED GRAVITY
PREDICTED GRAVITY
PREDICTED WATER DEPTH
OBSERVED WATER DEPTH
RECONSTRUCTIONS
INFERRED PALEOGEOGRAPHY

Fig. C.4

Appendix D

THE TWO LAYER TWO DIMENSIONAL EXTENSION MODEL

D.1 INTRODUCTION

Since Sawyer's (1982) finite difference procedures simulate the thermal and tectonic evolution of a basin cross section given its initial condition and sediment input rates, the only alteration brought up by non-uniform extension is in the initial conditions. Two of these conditions are now differently set up: the initial subsidence and the initial temperature distribution.

D.2 INITIAL SUBSIDENCE

The crust being extended by a factor β_c and the subcrustal lithosphere by a factor β_{sc}, the new elevation $Z(\beta_c,\beta_{sc})$ is given by assuming isostatic balance before and after extension (Royden and Keen, 1980; Sclater et al., 1980) (same variables as in Appendix A).

$$Z(\beta_c,\beta_{sc}) = \frac{\rho_a-\delta(Z(1))}{\rho_a-\delta(Z(\beta_c,\beta_{sc}))} Z(1) + \frac{\rho_a\bar{h}_\ell-\rho_c\bar{h}_c-\rho_m(h_\ell-h_c)}{\rho_a-\delta(Z(\beta_c,\beta_{sc}))} (1-1/\beta_c)$$

$$+ \frac{(\bar{\rho}_m-\rho_a)(h_\ell-h_c)}{\rho_a-\delta(Z(\beta_c,\beta_{sc}))} (1/\beta_{sc} - 1/\beta_c) \qquad (D\text{-}1)$$

$$\delta(Z) = 0 \quad \text{if} \quad Z \leq 0$$

$$\delta(Z) = \rho_w \quad \text{if} \quad Z > 0$$

The first two terms are the same as those obtained for uniform extension (Appendix A, Eq. A-1) while the third term represents the correction brought by differential subcrustal extension. This correction allows more initial subsidence if $\beta_{sc}<\beta_c$ and less if $\beta_{sc}>\beta_c$; as expected extra subcrustal heat maintains higher elevations.

D.3 TEMPERATURE STRUCTURE

The geotherm T(Z) after extension can be described as a function of the equilibrium geotherm $T^o(Z)$ as follows:

for $Z \leq h_c/\beta_c$ $\quad T(Z) = T^o(\beta_c \cdot Z)$ (D-2)

for $h_c/\beta_c \leq Z \leq h_c/\beta_c+(h_\ell-h_c)/\beta_{sc}$ $\quad T(Z) = T^o(h_c+\beta_{sc}(Z-h_c/\beta_c))$ (D-3)

for $h_c/\beta_c+(h_\ell-h_c)/\beta_{sc} \leq Z$ $\quad T(Z) = T^o(Z-h_c/\beta_c-(h_\ell-h_c)/\beta_{sc}+h_\ell)$ (D-4)

D.4 PARAMETERS

All the model parameters remain the same as in the uniform extension model (Table C.1; Appendix C).

In one model though, the sediment matrix will be assumed to produce radiogenic heat, contrary to all preceding models where sediment radiogenic heat production is set at zero. In order to estimate the maximum effect of that factor we assumed a high value of heat generation, A_r, for the matrix:

$$A_r = 5.0\ 10^{-13}\ \text{cal cm}^{-3}\ \text{s}^{-1}. \qquad \text{(D-5)}$$